



HAL
open science

Establishment of the apico-basal and medio-lateral axes during the embryogenesis of the brown alga *Saccharina latissima*

Samuel Boscq

► **To cite this version:**

Samuel Boscq. Establishment of the apico-basal and medio-lateral axes during the embryogenesis of the brown alga *Saccharina latissima*. Morphogenesis. Sorbonne Université, 2023. English. NNT : 2023SORUS673 . tel-04621626

HAL Id: tel-04621626

<https://theses.hal.science/tel-04621626v1>

Submitted on 24 Jun 2024

HAL is a multi-disciplinary open access archive for the deposit and dissemination of scientific research documents, whether they are published or not. The documents may come from teaching and research institutions in France or abroad, or from public or private research centers.

L'archive ouverte pluridisciplinaire **HAL**, est destinée au dépôt et à la diffusion de documents scientifiques de niveau recherche, publiés ou non, émanant des établissements d'enseignement et de recherche français ou étrangers, des laboratoires publics ou privés.



CNRS • SORBONNE UNIVERSITÉ
Station Biologique
de Roscoff

Sorbonne Université

École doctorale 515: Complexité du Vivant

UMR8227 (SU - CNRS) Laboratory of Integrative Biology of Marine Models

Team Morphogenesis of MacroAlgae

Establishment of the apico-basal and medio-lateral axes during the embryogenesis of the brown alga *Saccharina latissima*

Philosophiae Doctor (PhD) Thesis

Samuel Boscq

The defense was held on December 21, 2023 in front of the following jury members:

Dr. Chikako Nagasato.....Reviewer
Hokkaido University: Muroran Marine Station

Dr. Kenny Bogaert.....Reviewer
Max Planck Institute for Biology Tübingen

Dr. Alex McDougall.....Jury president
Sorbonne Université: Institut de la Mer de Villefranche

Dr. Philippe Andrey.....Examinator
INRAE-AgroParisTech

Dr. Charlotte Kirchhelle.....Examinator
Laboratoire Reproduction et Développement des Plantes

Dr. Bénédicte CharrierSupervisor
Institut de Génomique Fonctionnelle de Lyon

Abstract

Developmental biology focuses on unraveling the intricate mechanisms governing cell differentiation, pattern establishment, and *in fine* morphogenesis. Brown algae, with their unique evolutionary trajectory diverging from other multicellular lineages, offer a distinctive perspective to uncover novel cellular and molecular mechanisms. The exploration of brown algae developmental processes also holds ecological, economical, and social significance. This thesis delves into the embryogenesis of the brown alga *Saccharina latissima*, providing valuable insights into the regulation of body plan establishment. In addition, this work details the importance of cellular factors, the regulation of pattern development and its response to maternal attachment. The first chapter of the present manuscript sheds light on the roles played by cell wall and cytoskeleton in the establishment of body axes. More precisely, I present that the sequential establishment of the axes is possibly linked to the dynamics of the cell wall, and that the structured layers of cell wall components, including alginates and fucans, exhibit specific spatiotemporal organization during development. Notably, the study provides evidence of the interplay between cytoskeletal elements (filamentous actin), and cell wall composition. The second chapter then explores the role of the maternal tissue in early development of *Saccharina latissima*, revealing the significance of the attachment between the embryo and maternal tissues. The removal of the stalk indeed results in altered developmental patterns, highlighting the influence of maternal signals on the embryo. I also introduce the concept of a maternal unknown message (MUM) that inhibits the transition to Phase II, and present potential candidates for being MUM. The last chapter establishes that the role of the cells of the embryo differs during development. I demonstrate that the basal cell is required for the correct patterning of the embryo while the apical cell is not. In conclusion, these findings are discussed and integrated into an evo-devo approach, comparing developmental processes across brown algal orders, plants and animals. Additionally, I present a model that synthesizes the current knowledge on *Saccharina latissima* embryogenesis. Finally, I address the need for further investigations to better understand the maternal regulation in kelps and their transcriptomic landscape in development.

Résumé

La biologie du développement a pour objectif de comprendre les mécanismes régissant la différenciation cellulaire et la morphogenèse. Les algues brunes, de par leur trajectoire évolutive divergente des autres lignées multicellulaires, offrent une possibilité de découvrir de nouveaux mécanismes cellulaires et moléculaires. L'exploration des processus de développement des algues brunes revêt également une importance écologique, économique et sociale. Au cours de ma thèse je me suis intéressé à l'embryogenèse de l'algue brune *Saccharina latissima*, et plus précisément aux mécanismes de régulation de l'établissement des plans de croissance. Dans ce manuscrit, je détaille l'importance des facteurs cellulaires, de la régulation du patron de développement et de sa réponse à l'attachement au tissu maternel. Le chapitre I démontre d'une part que l'établissement séquentiel des axes est possiblement lié à la dynamique de la paroi et du cytosquelette. D'autre part la structure des couches de composants pariétaux (alginates et fucanes) présentent une organisation spatiotemporelle spécifique au cours du développement. Mes résultats soutiennent notamment l'hypothèse d'une interaction entre les filaments d'actine et la composition de la paroi cellulaire. Dans le chapitre II sont présentés le rôle du tissu maternel dans le développement précoce de *S.latissima*, ainsi que l'importance de l'attachement de l'embryon à ce tissu. Je montre en effet que la suppression du "pédoncule" maternel entraîne des altérations du patron de développement de l'embryon. Par conséquent, j'introduis le concept d'un message maternel non-identifié (MUM) qui empêche la transition précoce en Phase II, et présente des candidats potentiels. Le chapitre III démontre que le rôle des différentes cellules de l'embryon diffère au cours du développement. Plus précisément, la cellule basale est nécessaire à la formation du plan d'organisation de l'embryon, à l'inverse de la cellule apicale. En conclusion, je présente un modèle qui synthétise les connaissances actuelles sur l'embryogenèse de *S.latissima*. L'ensemble des résultats est intégré dans une perspective évolutive comparant les processus de développement à travers les algues brunes, les plantes et les animaux. Finalement, j'aborde des pistes de recherche future visant à élucider la régulation maternelle, et ainsi comprendre les changements transcriptomiques au cours du développement.

Acknowledgments

I would like to first thank the members of my jury: Chikako Nagasato, Kenny Bogaert, Alex McDougall, Charlotte Kirchhelle, and Philippe Andrey for agreeing to read and evaluate the work done during my PhD.

I also want to thank the thesis committee members: Marianne Delarue, Agnès Boutet, and Nathalie Dostatni for the helpful guidance they provided me during these three years.

I would like to sincerely thank Bénédicte Charrier (Ben) without whom nothing would have happened. Thank you for taking me under your wing and teaching me the ways and know-how of science, the MMA way. I owe you the many chances that I had to go to conferences and present my results. While we sometimes have different opinions, I truly think our discussions and debates were fruitful for my personal growth and that of our subject. I also want to thank all the members of the MMA team. Bernard Billoud, for helping me with all the modifications on software analysis to ease the long hours of segmentation and for answering all my questions on statistical matters. Giannis, I owe you a lot for what I learned and experienced in Roscoff, both in the lab and socially. It was a great pleasure to share an office, engage in discussions on how to tackle the understanding of *Saccharina*, share space on the lab benches, and occasionally throw dice together on Sunday afternoons. Sabine, je t'adresse un grand merci pour l'aide immense que tu m'as apportée et les discussions qui ont permis de rendre un peu plus agréables ces longs moments passés sous la hôte que demandait le maintien de la collection de *Saccharine*.

I want to express my gratitude to the interns I had the chance to tutor: Yoann, Roman, Thomas, Tanweer, and Tanguy. I am glad that our paths crossed and that I had the opportunity to introduce you guys to the world of *Saccharina*. Yoann, Roman, Thomas, and Tanweer, I also want to thank you for your assistance with BAM labeling, microdissection, microfluidics, and phytohormone response. It was a pleasure to work with all four of you. Tanguy, as the newest member and soon to be the only PhD student of the MMA team, you are making new history in Lyon! I wish you a fantastic three years ahead.

I also want to extend my gratitude to the individuals I had the privilege to collaborate with. Sophie Le Panse for her extensive TEM work, diligently searching for plasmodesmata in progressively younger organisms. I must express my appreciation to Stéphanie Duterte for her warm welcome at the MRiC platform in Rennes and her assistance in navigating the intricacies of "death-starring" embryos. I want to thank Nino Laübli and Rafaele Attia for the invaluable expertise they provided me regarding microfluidics. Additionally, I am grateful to Nathalie Desban for her advice on improving immunolabeling on moving embryos and to Marina Linardić for inspiring the idea of dissecting embryos using microinjection needles. Lastly, I warmly thank Dan for his tremendous effort and support in helping me complete the life cycle of *Saccharina*.

I also want to sincerely thank Stéphane Égée and Mirjam Czjzek for all the efforts you have spent in supporting me during my PhD, as well as for the engaging discussions we had on science and career pursuits.

I want to express how enjoyable it was to share an office with Aurélien Baud and Lisa Mazéas during our PhD journey, evolving from novice students to fully-fledged scientists. Working alongside friends and caring for each other was a great experience. What a great many laughs over our shared memes.

Of these almost for years spend in Roscoff, not all of my time was spent in the lab. I have moments I hold dear in my memory of the time spend with so many friends. The Roskoloc shared with Jukka and Greg (and Tima when I could see her) felt like my home and second family during the year we spent together. I hope you guys are enjoying life in Iceland!

I also want to express how much fun it was to spend time with many of my friends over these years in Roscoff. I fear I might forget someone if I try to name individuals, but you all need to know that you were fantastic to hang out with and brought so much joy into my life!

I also want to thank my long-time friends from our “frog-faced” conversation for always offering an ear at any time of the day (or night).

J'aimerais également chaleureusement remercier ma famille pour leur soutien sans faille pendant toutes ces années de thèse, leurs conseils avisés ainsi que pour tout leur amour. Ça compte beaucoup, merci à vous

Finally, I want to thank you especially, Louison. Thank you for your wisdom, care, and patience, but also for helping me be a better person. I feel blessed to have met you, and to be able to spend my time with you (hopefully, soon more than the past 4 months). Life without you would be at least half as enjoyable.

Table of contents

1 - Introduction	8
I/ Body plan organization during the development of multicellular organisms	9
A) The evolution and diversity of body plans in eukaryotes	9
B) Establishing the primary axes of multicellular organisms	11
C) Polarity in different models	15
II/ Parental effects	18
A) Parental transcriptomic heredity	18
B) Additional support is provided by parental extra-embryonic tissue.	21
III/ Early embryogenesis of brown algae	23
A) Brown algae are evolutionary divergent pluricellular organisms	23
B) Brown algal models	26
C) Cell Wall in land plants and brown algae	27
D) Functions of the eukaryotic cytoskeleton	32
E) Describing the developmental phases of <i>Saccharina latissima</i>	33
2 - Aim of the study	39
3 - Chapter I	41
The early, elongated embryo of the brown alga <i>Saccharina</i> is surrounded by a corset of alginates that depend on cortical actin filaments.	
4 - Chapter II	67
MUM, a maternal unknown message, inhibits early establishment of the medio-lateral axis in the embryo of the kelp <i>Saccharina latissima</i>	
5 - Chapter III	113
The cell fate of basal and apical cells in <i>Saccharina</i> embryos is different and variable over time	
6 - General Discussion	141
Establishment of the first axes involves the cytoskeleton and the cell wall	142
Connection to maternal tissue is required for establishment of the embryo body plans	145
How MUM signal delays transition from Phase I to Phase II	147
Nature of MUM	149
An evo-devo approach: Shared developmental process in brown algae	151
Conclusion and Perspectives	153
7 - References	157
8 - Annexes	174

Annexe 1: Targeted Laser Ablation in the Embryo of *Saccharina latissima*

Annexe 2: Growth and Labelling of Cell Wall Components of the Brown Alga *Ectocarpus* in Microfluidic Chips

Annexe 3: Cultivation and Imaging of *S. latissima* Embryo Monolayered Cell Sheets Inside Microfluidic Devices

Annexe 4: List of publications.

Annexe 5: List of oral communications and poster in congress and workshops.

1 - Introduction

I/ Body plan organization during the development of multicellular organisms

The formation of body shapes, or morphogenesis, relies on highly controlled processes in multicellular organisms. It constitutes the fundamentals of developmental biology and elaborates on a profoundly interesting subject, since similar shapes can be observed in very distant lineages (e.g., moss, fungi, and algae).

A) The evolution and diversity of body plans in eukaryotes

Body plans are a set of **morphological features** describing the body shape and structure of a given species (Woodger, 1945). Five developmental processes are pivotal in governing the formation of all developmental body plans (Niklas, 2000): 1) Synchronization of cyto- and karyokinesis; 2) Cellular adhesion during divisions; 3) Continuity of cytoplasm; 4) Differentiation between determinate ("closed") and indeterminate ("open") growth in terms of size; 5) Number and spatial orientation of planes of cell division. Combining these fundamental processes results in the emergence of four most elemental body organizations: the unicellular, colonial, siphonous, and multicellular (Figure 1A). While they are unicellular, protists also present axes that structure the organization of their body. In fact, the unicellular cell plan is the most ancient as it was considered for LUCA (Last Universal Common Ancestor) and LECA (Last Eukaryotic Common Ancestor) (Weiss et al., 2016; O'Malley et al., 2019; Niklas and Tiffney, 2022). When cells group within a shared extracellular matrix but lack symplastic junctions they form a colonial body (Niklas and Kutschera, 2009). Siphonous organisms exhibit a tubular cell capable of branching and fusing in diverse patterns, giving rise to a wide array of forms (Verbruggen et al., 2009). Finally, the multicellular body plan is categorized by adjacent cells connected by symplasmic junctions such as plasmodesmata in plants and algae (Franceschi et al., 1993; Aaziz et al., 2001; Terauchi et al., 2015; Kim et al., 2022), septal pores in fungi (Shen et al., 2014), and gap junctions in animals (Shimizu and Stopfer, 2013). Multicellular organisms exhibit one of four fundamental modes of growth in space, namely unbranched filaments, branched filaments, interweaving filaments, and the parenchymatous body plan (Niklas and Kutschera, 2009, Figure 1B). Parenchymatous body plan involves the division of cells in three spatial dimensions and allows the formation of specialized tissues.

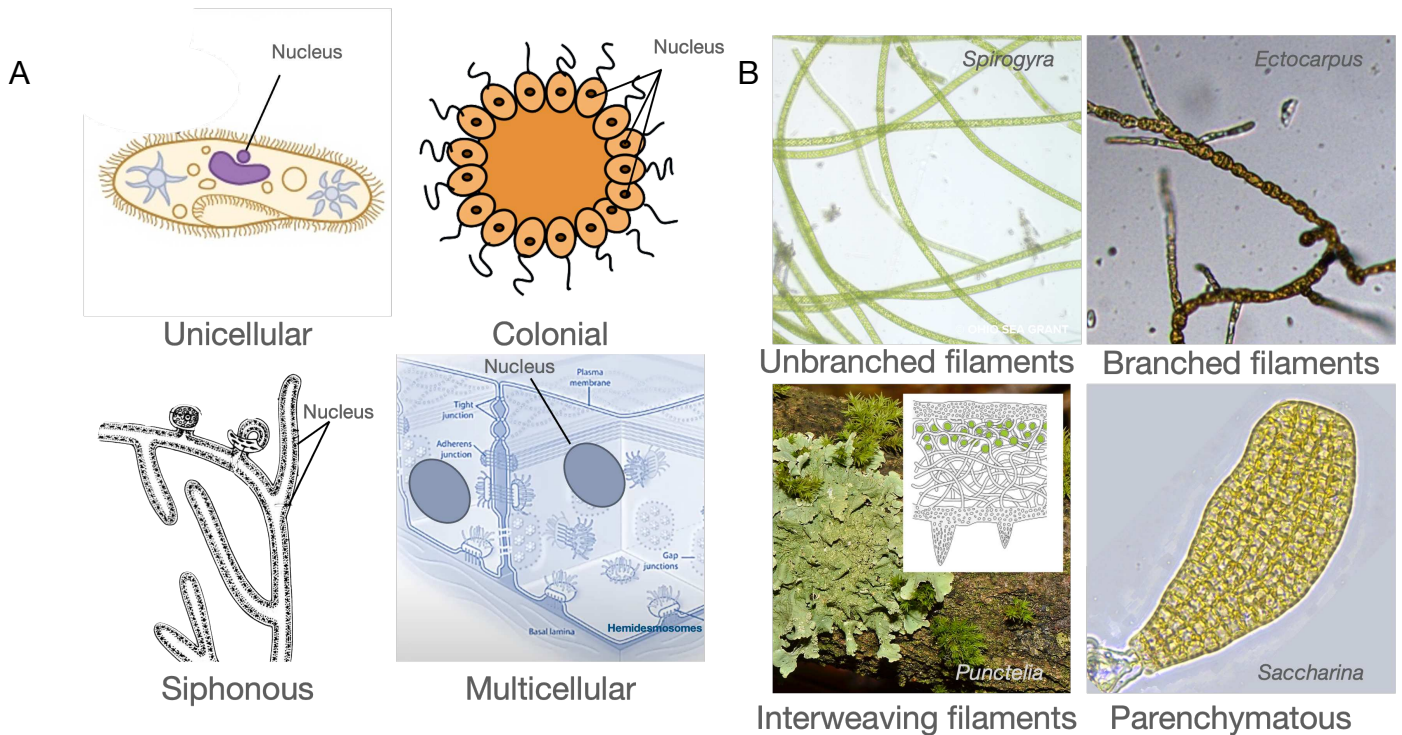


Figure 1: Diversity of body plans in eukaryotes and growth mode of multicellular organisms.

The taxa shown here are not phylogenetically closely related and are used only to illustrate key innovations. The standard model for a unicellular-to-multicellular transition involves a colonial body plan intermediate, a unicellular bottleneck, and an export of fitness from the cellular to the multicellular level of organization.

A) Various body organizations have evolved, namely: unicellular, colonial, siphonous, and multicellular organisms.

B) Different multicellular organizations are described: filamentous unbranched, filamentous branched, filamentous interwoven, filamentous, and parenchymatous.

Complex multicellularity has evolved multiple times independently in eukaryotes (Cock et al., 2010; Baldauf et al., 2013; Niklas and Newman, 2020; Figure 2). Multicellular architectures require the consistent regulation of cell division planes up to the third spatial dimension (3D) to produce structured mature organisms. All of these developmental processes highlight the diversity of morphological processes that organisms undergo to form the main axes that organize their body plan. While embryo geometry and tissue arrangement dynamics can greatly vary from species to species, multicellular eukaryotes present similarities in how the basic geometries are established (Kalinka and Tomancak, 2012). Understanding the similarities and dissimilarities in multicellular development provides a valuable evo-devo perspective. In most multicellular organisms, the body plans can be distilled from one to three body axes (Anlas and Trivedi, 2021). In creating the 3D structure of a multicellular organism, the first step is to set up a primary axis. This axis defines the direction of growth but is not necessarily polarized. After this, most organisms go on to establish further levels of organization and can develop secondary and tertiary axes. In all organisms, **axes** can be defined based on the presence of **molecular gradients** within the embryo (Friml et al., 2003; Shahbazi et al., 2019; Simsek and Özbudak, 2022) or by **morphological asymmetries** (Barthélémy and Caraglio, 2007; Martinez et al., 2016; Deline et al., 2018).

B) Establishing the primary axes of multicellular organisms

The development of walled organisms is mostly defined by **morphological asymmetries**, a feature shared among fungi (Horio and Oakley, 2005), brown algae (Le Bail et al., 2008), and many land plant species, including the plant model *Arabidopsis* (Jeong et al., 2016), rice (Sato et al., 2010), mosses (Sakakibara et al., 2010), and liverworts (Shimamura, 2016).

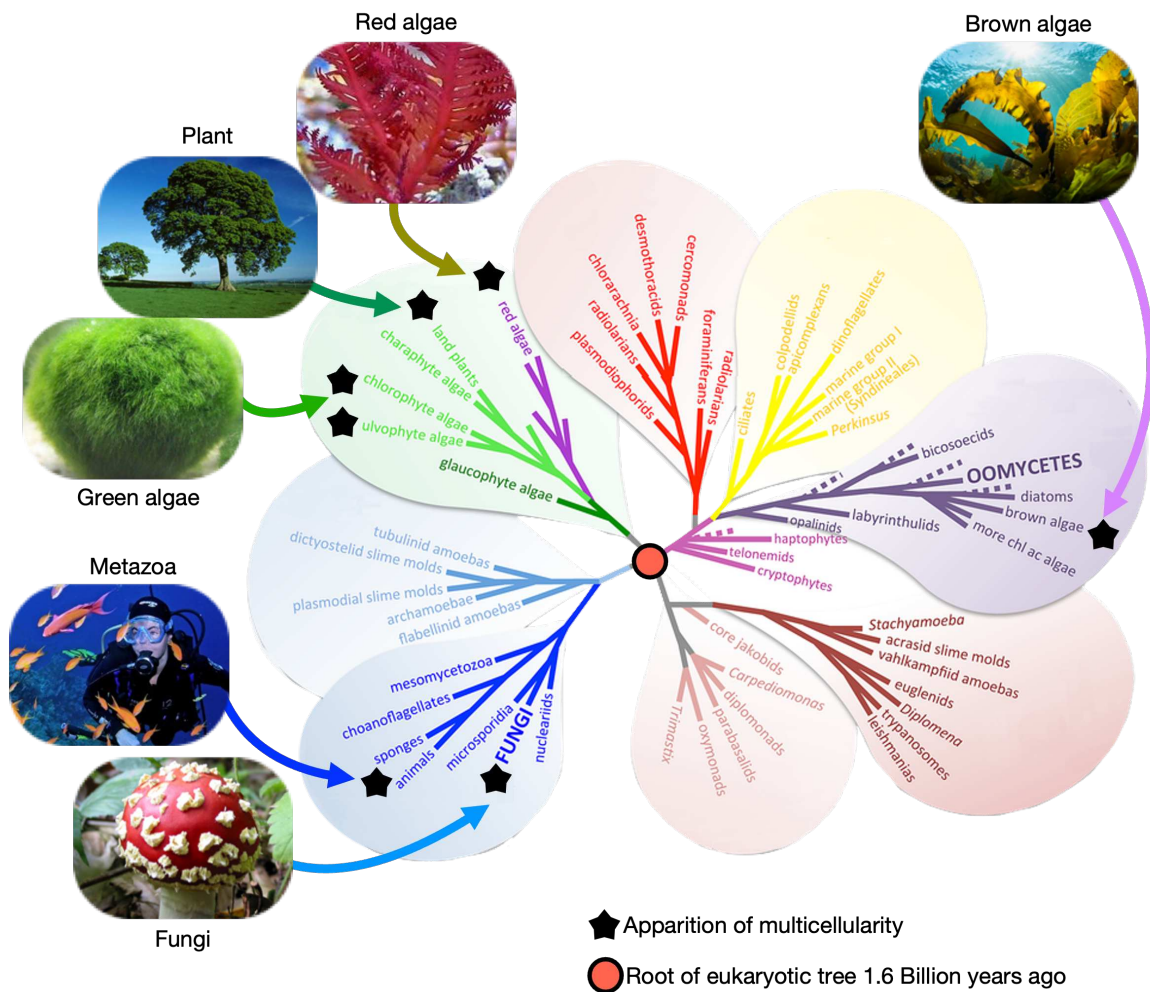


Figure 2: Eukaryotic tree of Life

Adapted from Baldauf et al., 2013, a consensus phylogeny of eukaryotes. The tree shown is an updated version of a previously published consensus phylogeny. Filled stars indicate multicellular groups.

The model plant *Arabidopsis thaliana*'s embryo illustrates a development where the primary axis, named the apical-basal axis, is established through the asymmetric division of the zygote, resulting in a small apical daughter cell and a larger basal daughter cell with a central vacuole (Mansfield and Briarty, 1991). The apical cell generates a spherical proembryo through tangential divisions, forming the secondary axis known as the radial axis (Jürgens 2001), creating an outer protoderm layer and a mass of inner cells (Mansfield and Briarty, 1991). Meanwhile, the basal daughter cell continues to divide horizontally, forming a filamentous suspensor that connects the proembryo to maternal tissues. In the development of seed plants, the apical daughter cell always contributes to at least a part of the embryo, while the basal daughter cell mainly gives rise to extra-embryonic tissues (Wang et al., 2020). Later in development, at the transition stage, the embryo shifts from radial patterning to bilateral patterning, presenting three distinct body axes at the torpedo stage (Lau et al., 2012).

The example described above shares some striking morphological similarities with the early development of the brown algae *Fucus* (Bisgrove and Kropf, 2007). Similarly to plants, the first division is unequal and asymmetrical, generating a large thallus cell and a narrow rhizoid cell (Quatrano, 1978; Bouget et al., 1998). This forms the apical-basal axis, which is the primary axis of the embryo. Then, much like in *Arabidopsis*, during the following stages, elongation is localized only at the rhizoid pole, while the thallus pole establishes a radial axis through both transverse (perpendicular to the primary axis) and longitudinal (parallel to the primary axis) anticlinal divisions (Kropf et al., 1999). The thallus further becomes a parenchymatous tissue, forming a tertiary axis and establishing bilateral symmetry. Later in development, the basal part of the embryo, the rhizoid cells, form the holdfast while the thallus develops a three-dimensional blade and stipe, which persist to the adult stage of *Fucus*. However, unlike *Arabidopsis*, embryos of Fucales start from a spherical homogeneous cell and grow freely outside of the parent organism. In another order of brown algae, the Dictyotales, the zygote undergoes a similar primary axis establishment process, with the exception that the unfertilized egg is not homogeneous but already pre-polarized (Bogaert et al., 2017). The establishment of the primary axis of both Fucales and Dictyotales has been segmented into different serial steps of a process called "axis selection" (Bogaert et

al., 2023). Initially, axis polarization is determined upon fertilization. However, the polarity established is flexible and can be reoriented in response to an environmental cue (e.g., polarized light). The primary axis is permanently established after completion of the "axis formation" (or "axis amplification") step followed by the "axis fixation" step. Afterward, the thallus pole divides through transverse anticlinal divisions, resulting in the elongation of the embryo along the initial axis.

The secondary axis of Dictyotales is established later in development, where the apical half of the embryo widens to develop into a band-shaped thallus, while its lower part generates the rhizome formed of various lateral branches growing horizontally (Fritsch, 1945).

In filamentous organisms, the emergence of a new branch forms a new axis. Additionally, branched filamentous organisms can support the emergence of multiple local repeated polarity axes to form lateral or apical branches (Coudert et al., 2019).

Contrary to walled organisms, metazoans are able to execute cell movement and migration. Animal development studies have mostly focused on genomic and **molecular gradients** to understand how axes are established (Anlas and Trivedi, 2021). Metazoans display diverse body plans characterized by various axes. Some organisms present specified axes upon oogenesis or fertilization. This is the case for hexapods' eggs that are already asymmetrical and present an inherent antero-posterior (A-P) and in some cases a dorso-ventral axis (D-V) even before fertilization (Chipman, 2015). Similarly, most nematodes' zygotes present an antero-posterior axis with distinct distribution of PAR proteins (Geßele et al., 2020). In fact, in many metazoan embryos, a primary axis is defined from oogenesis or the first cleavages following fertilization (Goldstein and Freeman, 1997). These axes are completed later in development with the establishment of additional axes such as proximo-distal (P-D) (Beaven et al., 2022). However, for other metazoans, such as vertebrates, although the previous axes established up to the blastula partially correlate, they do not always align with the final body plan axes (Valentine, 2004; Willmore, 2012). Unlike walled organisms, animal cells are capable of movement inside the tissue (Yamada et al., 2010). As such, to establish their final body plans, some metazoan embryos rely on cell migration and cell sorting, such as invagination

of cell layers and folding in the embryo through a process called gastrulation (Bénazéraf and Pourquié, 2013). All metazoans share genes like Wnt/ β -catenin and T-box genes (Kraus et al., 2016; Bagaeva et al., 2020). These genes have been shown to play a role in establishing primary axes (Technau and Scholz, 2003; Swalla, 2006; Petersen and Reddien, 2009; Turner et al., 2017) and symmetry-breaking events (Loh et al., 2016). They influence sorting, adhesion, and movements of cells during gastrulation (Latinkić et al., 1997; Arnold et al., 2000; Vonica and Gumbiner, 2002; Turner et al., 2014; Pauklin and Vallier, 2015). In vertebrates, uncommitted cells can organize a complete embryonic axis through BMP and Nodal signaling (Xu et al., 2014; Torres-Paz and Retaux, 2021). Following antero-posterior or oral-aboral axis specification, developmental differences increase between the metazoan phylum as embryos of different species establish additional axes increasing the complexity of body organization in the mature organism (Martindale and Hejnal, 2009). However, complementary studies have also tried to elucidate the role of cell regulatory networks to understand the assembly of multicellular ensembles beyond the effect of the genome (Gorfinkiel and Arias, 2021; Steventon et al., 2021).

Additionally, while axes can theoretically be decoupled from polarity, most of the time, axis initiation requires symmetry breaking and the establishment of local polarity in the egg or embryo in order to break the symmetries and form the first axis.

C) Polarity in different models

The large-scale asymmetries observed in multicellular organisms are often tied to initial cellular-scale asymmetries (Li et al., 2010). Most embryos originate from a round cell and need cell symmetry-breaking to establish the axes of the body plans of the adult organism. This initial step is dependent on intrinsic or extrinsic factors (Jan and Jan, 1998). There are two main ways for cells to acquire distinct identities (Bisgrove and Kropf, 2007; Sunchu and Cabernard, 2020): 1) Intrinsic, or cell-autonomous determination, where developmental determinants are differentially partitioned between daughter cells during the division process (Figure 3A). As a result, each daughter cell inherits a different set of cytoplasmic instructions that

guide it toward a unique developmental fate. An example of such mechanisms can be observed in the *Caenorhabditis elegans* zygote, where PAR segregation plays a crucial role in controlling the fates of the daughter cells (Noatynska and Gotta, 2012). 2) Extrinsic, or non-cell-autonomous determination, in which each cell receives unique positional cues either from neighboring cells or from the environment (Figure 3B). An example of this is found in the root and shoot of *Arabidopsis thaliana* (Rishmawi et al., 2014; Fuchs and Lohmann, 2020). Here, asymmetric cell division places daughter cells from the RAM (Root Apical Meristem) or SAM (Shoot Apical Meristem) in different external contexts. Signals from neighboring cells guide these daughter cells to distinct fates. In *Fucus*, environmental cues such as the polarized vector of light result in germination on the opposite direction of the perceived signal, inducing the formation of a rhizoid pole (Bisgrove and Kropf, 2007; Bogaert et al., 2015). Local deposition of cell fate-determining factors, and cell wall loosening combined with realignment of the mitotic apparatus is followed by the first asymmetric cell division (Kropf et al., 1988; Shaw and Quatrano, 1996; Quatrano and Show, 1997).

Diverse factors contributing to asymmetric divisions through one or a combination of these mechanisms have been described in brown algae. They range from asymmetrical distribution of RNA, lipids, sugars, organelles, polarized ionic gradients, mechanical stress, or light perception (Bogaert et al., 2023). This list is far from exhaustive and only aims to represent the diversity of initial factors involved in cell asymmetry. In early development, parental effects play a crucial role in laying the foundation for these mechanisms within the embryo. In the case of *Fucus*, the Ca^{2+} gradient oriented by sperm entry is one of the first cues to establish the primary axis and the first asymmetrical division. However, additional environmental cues, such as light or gravity, can modify the orientation axis of the embryo. In the case of *Saccharina*, the initially spherical egg is polarized by the maternally inherited flagella (Klochkova et al., 2019). After fertilization, the embryo elongates, and the elongation axis follows the polarity axis initially inputted.

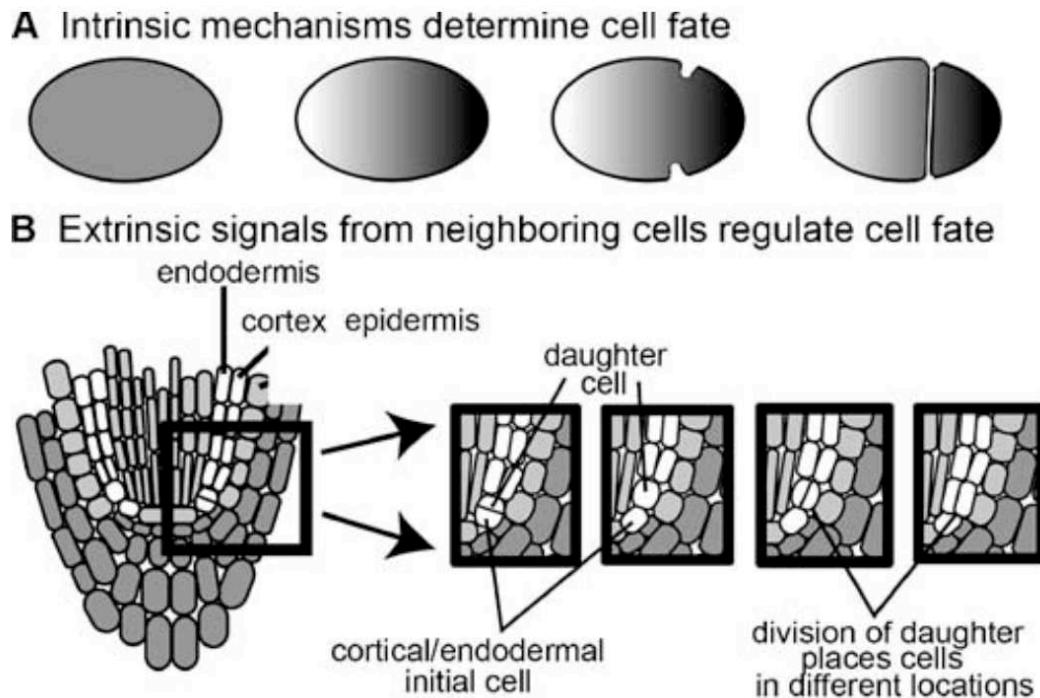


Figure 3: Asymmetric cell divisions generate diverse cell types.

From Bisgrove and Kropf, 2007, these schemes aim to illustrate the two main ways of how asymmetric cell division can create distinct fates:

A) In *C.elegans*: Developmental determinants (gray shading) are segregated to one end of the zygote. When cytokinesis occurs, the daughter cells each inherit cytoplasm that is qualitatively different.

B) In *A.thaliana*: A cortical/endodermal initial cell divides to produce a daughter cell. When the daughter divides, the cell plate is laid down parallel with the longitudinal axis of the root, placing the two new cells in different cell files. Signals from neighboring cells then direct the adoption of either a cortical or an endodermal fate.

II/ Parental effects

In multicellular organisms, parents play a significant role in shaping the development of their embryos. They contribute to embryonic development through various signals, encompassing both genetic and non-genetic factors. Geneticists and evolutionary biologists have long recognized that parental phenotypes can directly impact the phenotype of their offspring (Dickerson, 1947; Cheverud, 1984).

Maternal effects have been described as the causal influence of the maternal genotype or phenotype on the offspring phenotype (Wolf and Wade, 2009). A parallel concept, known as **paternal effects**, describes similar mechanisms in which paternal factors impact the development of the progeny (Rando, 2012; Crean and Bonduriansky, 2014). **Maternal genes** (or **paternal**) encode factors (e.g., protein, RNA) that are present in the oocyte (or sperm) and required for embryonic development (Marlow, 2010; Immler, 2018). In oogamous species, where there is a significant difference in size between male and female gametes, it has been proposed that the maternal contribution is likely more substantial, as it contributes to a larger part of the initial body of the embryo (Breton and Stewart, 2015).

The environment experienced by the mother can affect the offspring in various ways. For example, it can alter the quality of unfertilized eggs or influence the availability of nutrients for the developing embryo (Marshall and Uller, 2007; Li et al., 2021). This complexity adds to the challenge of deciphering how parental effects actually regulate embryogenesis.

A) Parental transcriptomic heredity

In animals, early embryogenesis relies on maternal RNAs stored in the unfertilized egg cell (Tadros and Lipshitz, 2009). A two-step transition occurs in animal systems. For several cell cycles, maternal RNAs regulate post-transcriptionally the development of the embryo while the zygote genome remains silent (Wang et al., 2020). In vertebrates, three maternal pathways interact to determine dorso-ventral patterning at the blastula stage, involving Wnt/ β -catenin, Wnt/ Ca^{++} , and BMP-mediated signaling (Pelegri, 2003). In the nematode *C. elegans*, the PAR genes involved in polarity regulation and the establishment of early body plans are maternally inherited (Bowerman et al., 1997; Robertson and Lin, 2015). This initial

step dependent on maternal RNAs is followed by zygotic genome activation. This crucial shift is described as **maternal to zygotic transition (MTZ)** (Lee et al., 2014; Vastenhouw et al., 2019, Figure 4).

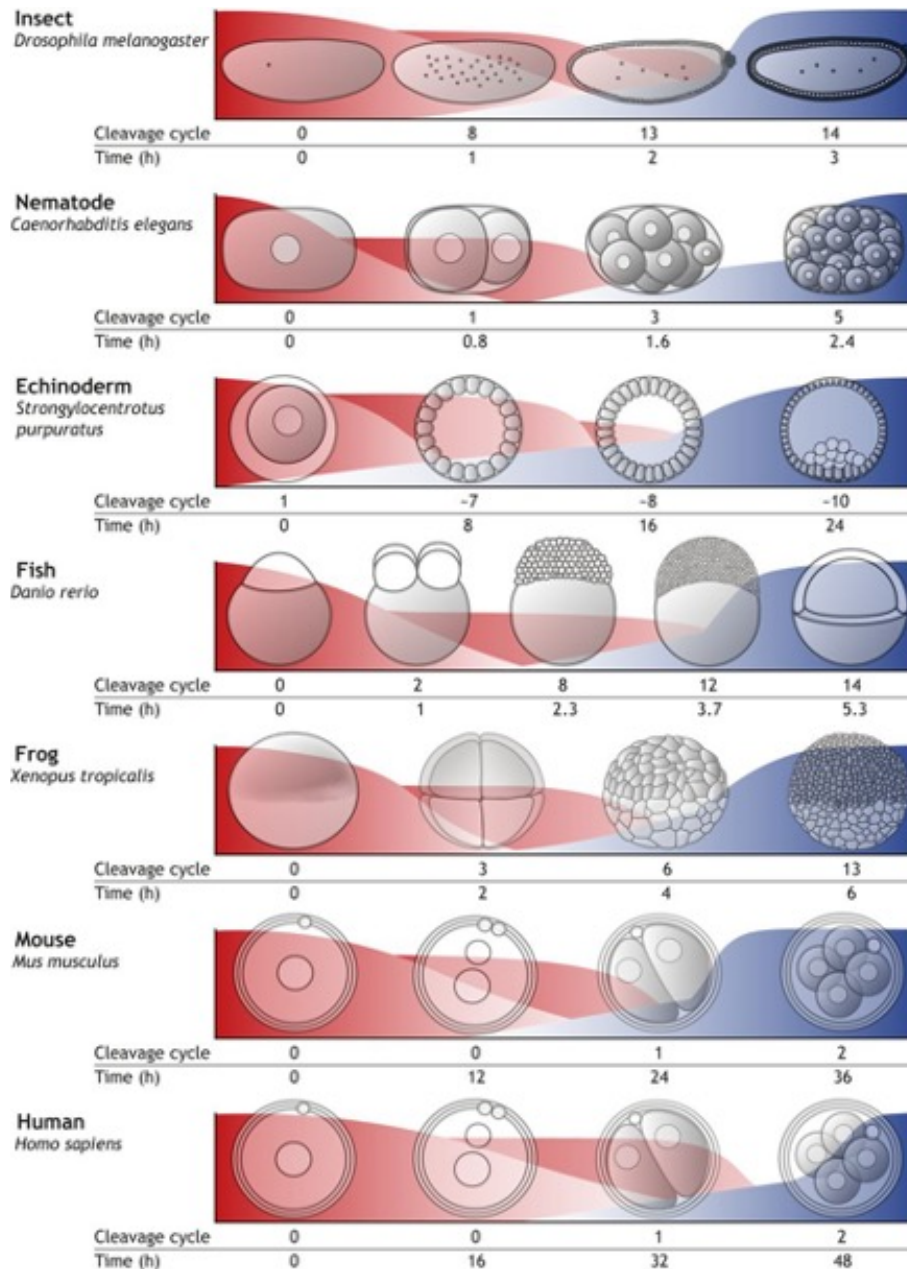


Figure 4 : The maternal-to-zygotic transition (MZZ) in different metazoans.

From Vastenhouw et al., 2019, Schematics depicting embryo MTZ in different species of metazoans. Red curves depict the evolution of maternal transcripts; red gradients represent the timing of the multiple phases of transcript degradation. Blue curve depicts transcription from the zygotic genome; blue gradient represents a gradual increase in the number of genes transcribed during ZGA. Developmental stages are shown for each organism.

In contrast, it was initially believed that no such transition occurs in plant embryos because some genes were transcribed de novo immediately after fertilization (Kawashima and Berger, 2014). However, it has been observed that de novo transcripts only gradually become predominant (Anderson et al., 2017; Shen et al., 2017; Zhao et al., 2019). Thus, **zygote genome activation** (ZGA) is a process that is still considered under parental control (Baroux and Grossniklaus, 2015). Numerous mRNA transcripts inherited from either the mother (**maternal genes**) or the father (**paternal genes**) have been found to impact embryogenesis in both plants and animals.

For example, in *Brassicaceae*, both parents influence embryo development (Ueda and Berger, 2019; Figure 5). The gene SHORT SUSPENSOR (SSP), which encodes a membrane-associated pseudokinase, has its mRNA inherited from the sperm (Bayer et al., 2009). SSP translation activates the YODA MAPK kinase that is necessary for the first asymmetric division. Maternal contributions are crucial for the activation of the YODA MAPK cascade (Zhang et al., 2017). Downstream MAP kinases MPK3/6 phosphorylate the transcription factor WRKY2 in the presence of maternally-derived factors HOMEODOMAIN GLABROUS11/12 (HDG11/12) (Ueda et al., 2017). In the basal land plant species *Marchantia polymorpha* and the uni-algal *Chlamydomonas reinhardtii*, the BELL/KNOX transcriptional regulators, which involve a two-component system of maternal and paternal factors, initiate zygote genome activation (ZGA) (Hisanaga et al., 2021).

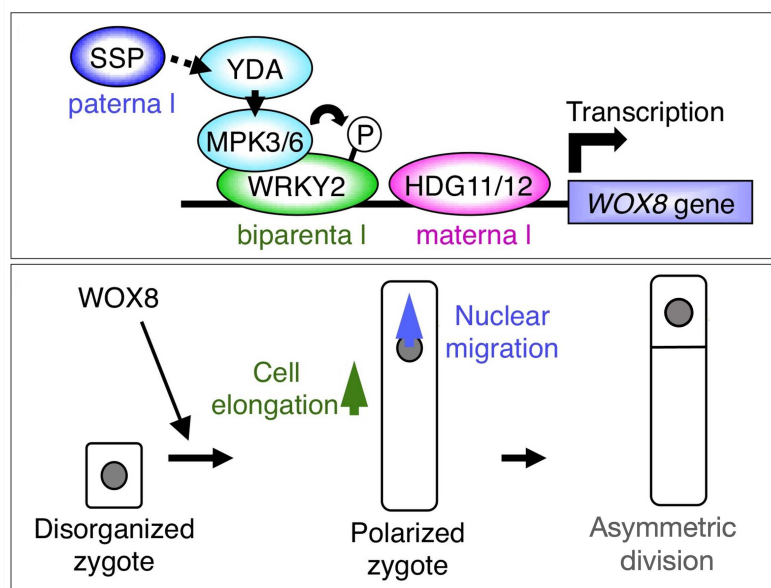


Figure 5: SSP - HDG11/12 pathway and parent attributed pathway in *A. thaliana*.

Adapted from Ueda and Berger, 2019. (Top) Pathway of activation of WOX8. WRKY2 originates from both parents. The paternally-derived SSP triggers the YDA MAP kinase cascade, which in turn phosphorylates WRKY2, activating it. The activated WRKY2, along with the maternally inherited HDG11/12, directly binds to the promoter of WOX8 and initiates its transcription de novo in the zygote. (Bottom) WOX8 contributes to cell elongation and nuclear migration by acting on the cytoskeleton. This is partially responsible for the initial asymmetric division.

B) Additional support is provided by parental extra-embryonic tissue.

Many multicellular organisms develop in partial or direct contact with cells of one of the parent organisms, most commonly the mother. In such cases, in addition to the development of the embryo itself, contact with extra-embryonic tissue provides signaling and mechanical cues. In many species, external input (e.g., mechanical) is actually strictly required for morphogenesis (Li et al., 2008; Sheng and Foley, 2012; Christodoulou et al., 2019). It was functionally demonstrated that coordinated adherence of the insect blastoderm to the vitelline envelope, a structure or shell surrounding the developing embryo, influences tissue movement dynamics during gastrulation (Münster et al., 2019), further highlighting the importance of embryonic-extraembryonic interactions in early patterning processes. Conversely, in metazoans, including *Nematostella*, *Xenopus*, zebrafish, mouse, and human, isolated groups of embryonic stem cells harbor the capacity to self-organize into a

rudimentary body plan with at least a primary axis independently from any extra-embryonic tissue (Anlas and Trivedi, 2021). Thus, while development relies partially on the extracellular matrix (ECM) and inherited parental genetic material, embryo cells in animals exhibit a degree of self-sufficiency to establish the primary axis away from external factors. In the context of plants, the suspensor, except for the uppermost cell, is considered extra-embryonic and serves to connect the embryo to the maternal seed tissue (Wang et al., 2020). Interestingly, 3D growth of plant embryos can be initiated by auxin produced in the extra-embryonic cells and PIN-7 mediated response in the apical cell of the embryo (Yoshida et al., 2014; Robert et al., 2018; Karami et al., 2023). In fact, once the suspensor differentiation is initiated in the basal cell, the suspensor itself seems to become a source of auxin (Robert et al., 2015).



Figure 6: Kelp forests form one of the richest biotopes.

Kelp forests harbor a rich biodiversity. Different types of kelp forests exist, ranging from the towering underwater forest of *Macrocystis* (top) to the covering canopy of *Digitata* (bottom). Brown algae additionally present a major interest as a cultivated crop for food, feed, and industry (right).

III/ Early embryogenesis of brown algae

A) Brown algae are evolutionary divergent pluricellular organisms

Brown algae (or Phaeophyceae) have major ecological relevance. Underwater kelp forests are one of the biotopes harboring the richest diversity (Piñeiro-Corbeira et al., 2022; Eger et al., 2023; Figure 6). Kelps, or Laminariales, are among the largest marine organisms to exist (Cribb, 1954). They thrive mostly in temperate and cold waters or in deep waters of some tropical locations (Muth et al., 2019; Assis et al., 2020; Figure 7). Moreover, they present great economic interests for food, feed, and industry (nutritional value, gels, biofuel, medicinal, and other usages) (Barbier et al., 2019; Lähteenmäki-Uutela et al., 2021). Brown algae belong to the Stramenopiles, a supergroup of Eukaryotes that belongs to the TSAR (Telonemia, Stramenopiles, Alveolates, Rhizaria) lineage (Burki et al., 2007; Strassert et al., 2019; Burki et al., 2020). Brown algae diverged and evolved independently from the other lineages for more than a billion years (Kawai et al., 2015; Figure 2). Brown algae evolved as multicellular organisms around 250 million years ago (Silberfeld et al., 2010), relatively recently compared to other groups of multicellular organisms (King et al., 2008). There are over 2100 species of brown algae described and classified in 21 orders (Reviere et al., 2007; Guiry and Guiry, 2023; Figure 8). Possibly due to their recent acquisition of multicellularity, brown algae display a vast diversity of body plans and life cycles (Charrier et al., 2012; Bogaert et al., 2013; Heesch et al., 2021). Molecular studies have shown that brown algae consist of two main clades resulting from an early divergence event (Bringloe et al., 2020). First, a large clade of four orders known as SSDO (coined from Sphacelariales, Syringodermatales, Dictyotales, and Onslowiales). Second, a more extensive large radiation of all other brown algae referred to as the brown algal crown radiation (BACR) (de Reviere and Rousseau, 1999). The last common ancestor of all BACR has been presented as a heteromorphic photosynthetic organism with intercalary pseudo-parenchymatous growth (Silberfeld et al., 2010).

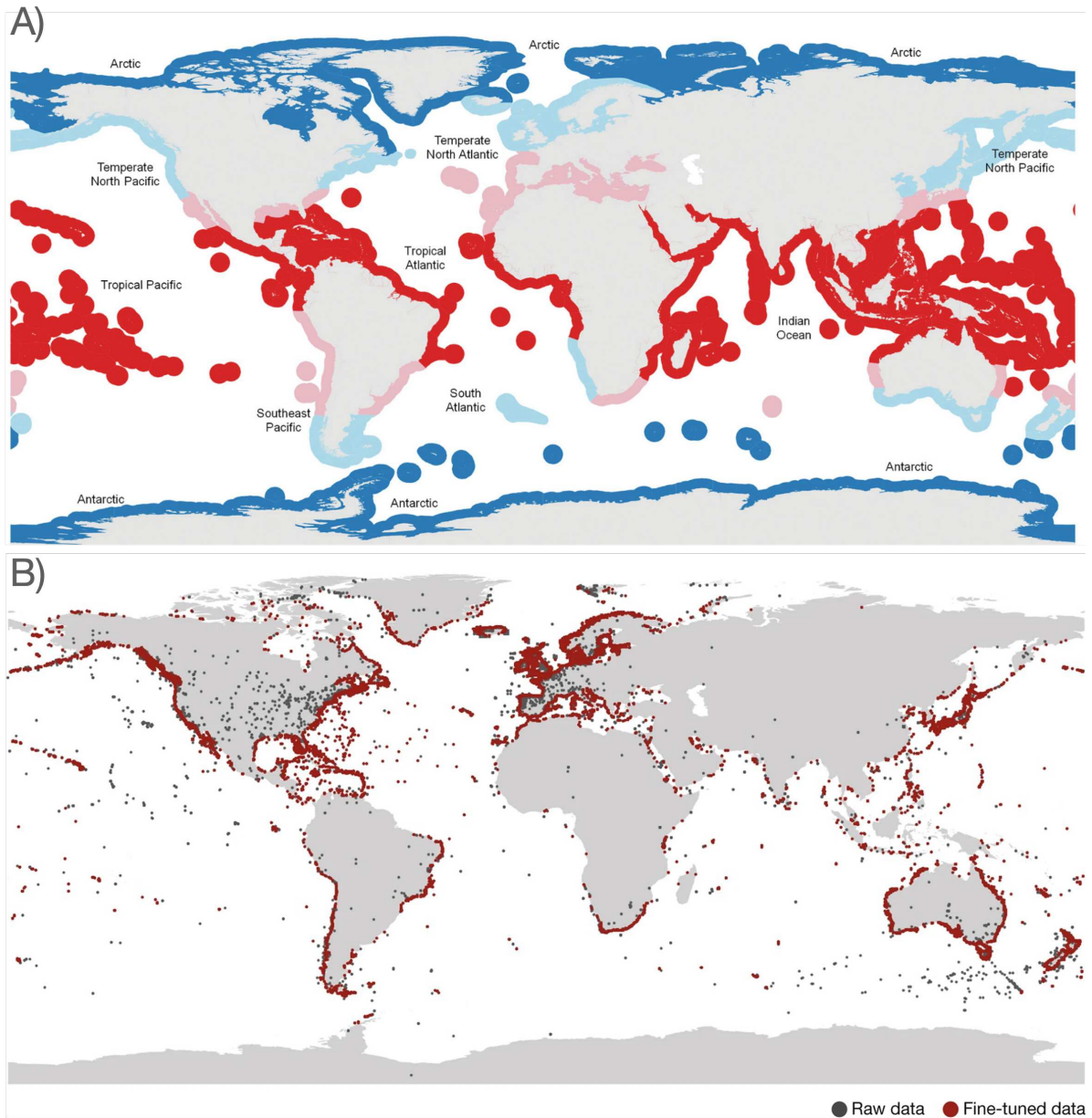


Figure 7: Geographic repartition of brown algae in global waters

A) Biogeographic subdivisions of marine biodiversity. From Bringloe et al., 2020. Dark blue = Arctic; light blue = cold-temperate; pink = warm-temperate; red = tropical. B) Global dataset of marine forest species of brown macroalgae. Adapted from Assis et al., 2020. Included orders: Fucales, Laminariales, and Tilopteridales. Red and gray circles depict raw and corrected data, respectively.

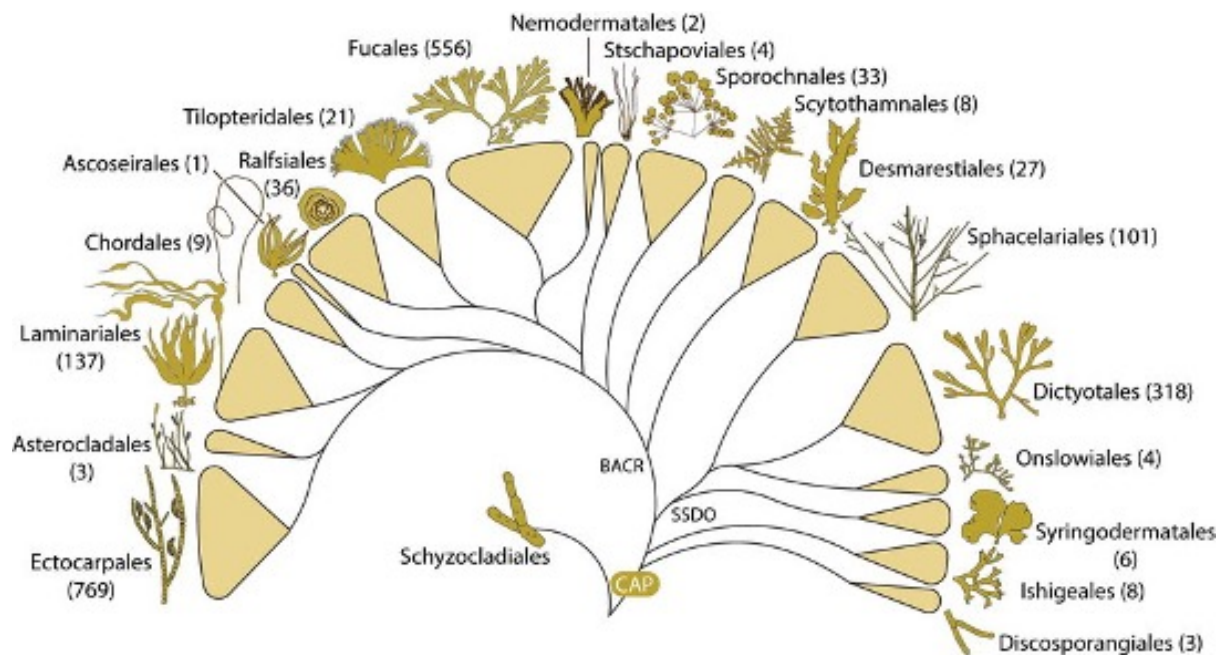


Figure 8: Phylogeny of the brown algal orders.

From Bringloe et al., 2020, Phylogeny of the brown algal orders based on 12 markers. In brackets are the numbers of species within each order according to AlgaeBase (Guiry and Guiry, 2023). CAP: common ancestor of Phaeophyceae; SSDO: Sphacelariales, Syringodermatales, Dictyotales, Onslowiales clade; BACR: brown algal crown radiation.

Due to their independent evolution, other commonly studied model organisms in the realms of plants, animals, fungi, or other algae offer only limited relevance to understand developmental processes in brown algae (Coelho and Cock, 2020). Additionally, it is crucial to challenge much of the existing knowledge from other organisms when studying Phaeophyceae. As a result of this divergent evolutionary trajectory, they display many novel cellular and molecular mechanisms. To cite a few, they present distinctive cell wall structures (Deniaud-Bouët et al., 2017; Charrier et al., 2019), new storage polysaccharides (e.g., laminarin) (Myklestad and Granum, 2009), or different pigments involved in photosynthesis (Anderson et al., 1978; Büchel, 2019).

Despite these differences at the molecular level, brown algae adhere to similar mechanical sets of rules involved in growth. The combination of these two features— i) the diversity at the molecular level and ii) the adherence to the same mechanical rules as all organisms on earth— makes brown algae particularly interesting to study.

B) Brown algal models

Four main model orders have shaped brown algal studies (Coelho and Cock, 2020). The Fucales order, including species like *Sargassum* or *Fucus*, while it may take several years to complete its life cycle, has been an important part of brown algae research, particularly in growth and development (Hurd, 1920; Novotny and Forman, 1975). Studies in ***Fucus*** have provided great insights into apical-basal pattern formation (Bouget et al., 1998), polarization, and axis formation (Bogaert et al., 2015).

Dictyota has recently emerged as a new experimental model for studying early embryogenesis in brown algae (Bogaert et al., 2016). It offers practical advantages compared to *Fucus*, such as a two-month short life cycle or tunable sporogenesis release (Bogaert et al., 2013). Research on *Dictyota dichotoma* has provided insights into cell polarization processes and the potential role of auxins in brown algae.

A relatively simple, filamentous morphology and a small genome have made ***Ectocarpus*** a valuable model (Charrier et al., 2008; Coelho et al., 2020). *Ectocarpus* has been used as a model to answer a broad range of biological questions, but the model organism has gained significant attention due to the development of genomic and genetic tools. These include the assembly of the complete genome sequence (Cock et al., 2010) and the exploration of various molecular tools, such as RNAi methodology (Macaisne et al., 2017), tiling arrays (Cormier et al., 2017), CRISPR-Cas9 genome editing (Badis et al., 2021), and genetic maps (Heesch et al., 2010; Avia et al., 2017). *Ectocarpus* has been instrumental in understanding biological processes in brown algae such as life cycle regulation (Coelho et al., 2011), sex determination (Ahmed et al., 2014), auxin metabolism (Le Bail et al., 2010), and filamentous development (Le Bail et al., 2008; Rabillé et al., 2019).

Increasing interest is being brought to the use of Laminariales as biological models (Zhang et al., 2016). The initial focus was set on ***Saccharina*** in order to develop tools and resources for cultivated crop species, analogous to the use of maize or rice as model terrestrial crop species (Zhang et al., 2017). *Saccharina* has been cultivated for decades, and breeding strategies have been applied to produce high-yield varieties. Genomic resources, including genetic maps (Zhang et al., 2015), the

complete genome sequence (Ye et al., 2015), and CRISPR-Cas9 genome editing (Shen et al., 2023), have been developed, supporting selective breeding efforts. Recently, *Saccharina* is becoming also a model for developmental biology. A detailed description of its developmental phases and its growth in thickness has been published (Theodorou and Charrier, 2023). Depending on regional availability, the focus is currently on two species: *Saccharina latissima* in the Atlantic, and *Saccharina japonica* in the Pacific (WoRMS, 2023).

C) Cell Wall in land plants and brown algae

Land plants, fungi, and algae cells polarize, grow, and divide while being encased in a rigid external frame that is the cell wall. The growth of plant cells is explained by Lockhart's biophysical theory, which involves water uptake (turgor pressure increase) and cell wall yielding (Lockhart, 1965). Cell wall yielding includes the rearrangement of existing wall polymers through stretching and the deposition of new wall material (Takahashi et al., 2006). This process results in cell expansion, and wall extensibility plays a key role in cell growth (Cosgrove, 2016). The evolution of multicellularity has often coincided with the emergence of an extracellular matrix (ECM) (Kloareg et al., 2021). Similarly to land plants, the ECM in brown algae exhibits a layered structure, with ultrastructural variability observed in different cell types (Mazéas et al., 2023). Additionally, the thickness of the ECM can vary, with some cells having thicker outer walls and thinner inner walls, while others have ECMs of more similar thickness (Mariani et al., 1985; Evans and Holligan, 1972). In both plants and brown algae, the basic cell wall structure includes rigid fibrous elements embedded in a gel-like matrix. While both are analogous, the composition of the polysaccharides matrix differs (Cosgrove, 2005; Charrier et al., 2019; Figure 9). In plants, the matrix includes hemicellulose and pectin. Pectin acts as an array in which the network of hemicellulose (cellulose-binding polysaccharides) and cellulose microfibrils are embedded (Pederson et al., 2023).

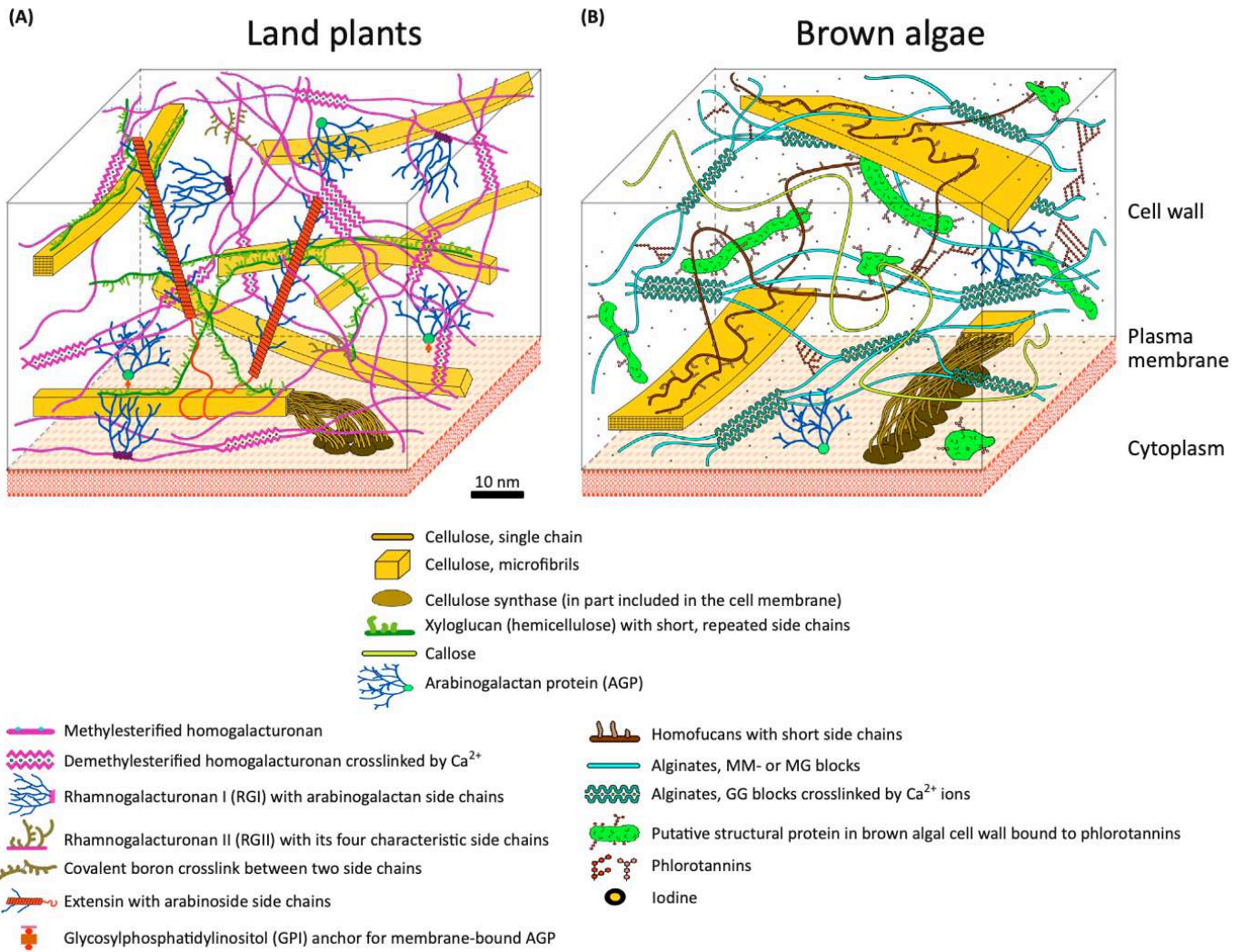


Figure 9: Comparison of cell wall from brown algae and land plants.

In land plants, the cell wall is mainly composed of cellulose microfibrils, hemicellulose chains, and pectin gel networks (A). The cell wall of brown algae remains less well known. It is composed mainly of two components: FCSPs (fucose-containing sulfated polysaccharides) crosslinked with protein and cellulose microfilaments, and alginates networks (B). However, unlike in land plants, cellulose microfilaments are much less abundant as they represent less than 8% of the cell wall dry weight (Charrier et al., 2019).

Brown algae possess an ECM, which is less characterized compared to animals, fungi, and terrestrial plants. Polysaccharides in brown algae are not template-encoded and depend on complex metabolic and trafficking processes (Hoffman et al., 2021). The main polysaccharides in brown algae are made of alginates forming a gel matrix analogous to pectin in plants that interlock fucose-containing sulfated polysaccharides (FCSPs) (Michel et al., 2010; Birkemeyer et al., 2020). The term FCSPs is collectively employed to encompass both fucans and fucoidans. The proportion of matrix or microfibril ECM components varies between plants and brown algae. Typically, plant cell walls consist of 15–40% cellulose, 30–50% pectin, and 20–30% hemicellulose (Cosgrove and Jarvis, 2012). In contrast, in brown algae, the constituents are distributed as 40% alginates, 40% FCSPs, and less than 10% cellulose (Charrier et al., 2019). **Alginates** are linear polymers composed of β -D-mannuronic acid (M) and α -L-guluronic acid (G) (Linardic, 2018). They exhibit different structural organizations based on the arrangement of these monomers (Figure 10A). This arrangement results in various linkages, including M-M, M-G, and G-G. In vitro, a more compact form of alginate is created by G-G linkages, while M-M linkages produce a flatter structure. M-G linkages fall in between these two states in terms of structural assemblage (Mørch et al., 2008). These differences in linkage structures lead to variations in the physical properties of the alginate matrix. Specifically, M-G blocks are more flexible compared to M-M blocks, which are in turn also more flexible than G-G blocks (Smidsrød et al., 1973; Mørch et al., 2008). In both brown algae and plants, the degree of alginate epimerization and pectin esterification can lead to cross-linking, affecting the rigidity of the cell wall. Interaction of alginate chains with calcium ions (Ca^{2+}) results in cross-linking of G in “egg box” junctions, further increasing G-rich alginates' mechanical stiffness (Zhang et al., 2020).

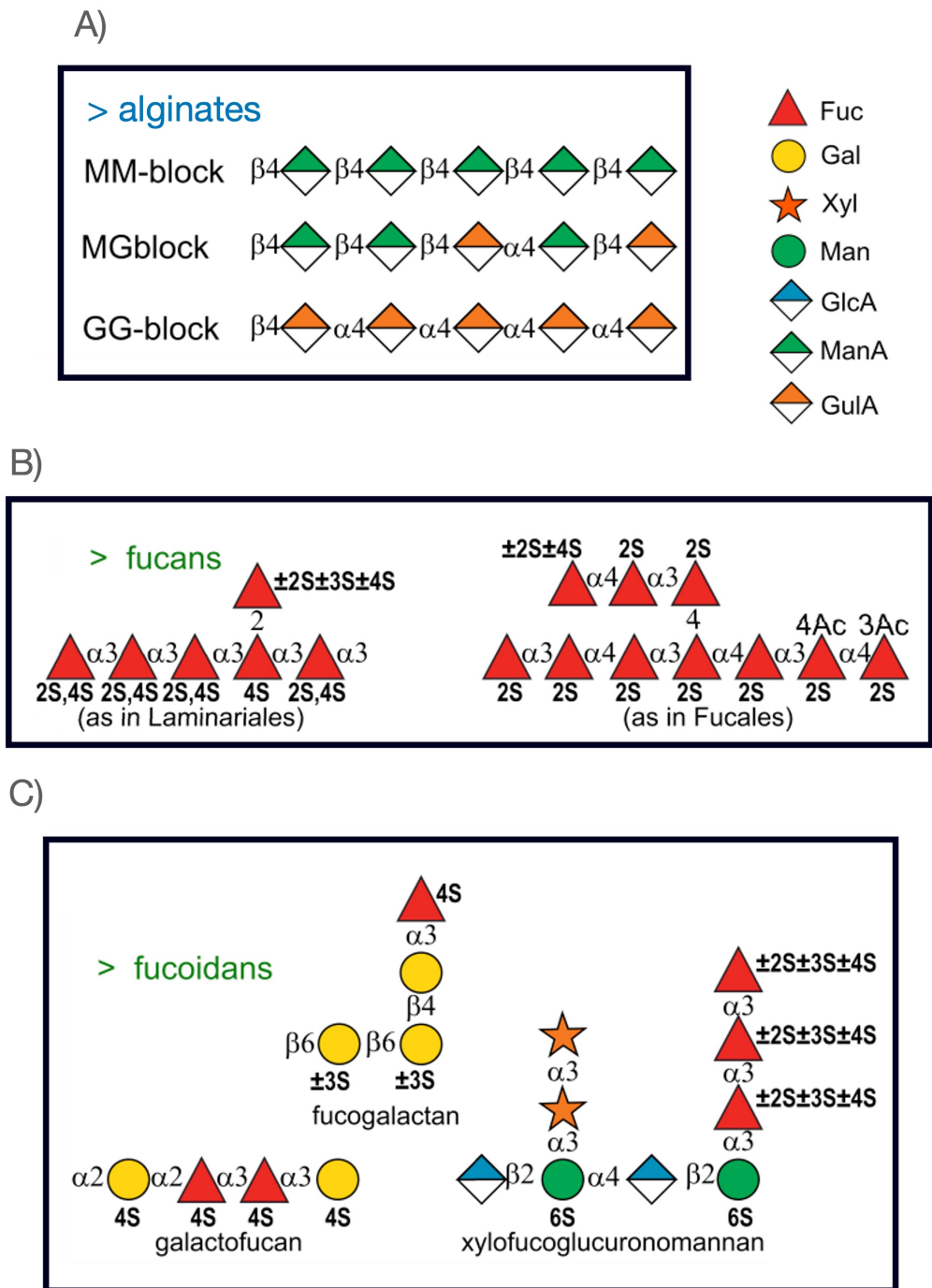


Figure 10: Key structures and composition of both FCSPs and alginates

Examples of typical alginates and FCSP motifs are shown. Structure of Alginates A) Fucans B) and other FCSPs C). Adapted from Mazéas et al., 2023.

In addition to alginates, brown algae contain **FCSPs**, which also vary in structure and composition (Figure 10B). **Fucans** are characterized by their high degree of sulfation and feature a backbone structure primarily composed of sulfated L-fucose residues (Mazéas et al., 2023). These fucans may also exhibit various types of additional branches. On the other hand, fucoidans are a group of polysaccharides known for their structural heterogeneity (Hervé et al., 2016). They consist of diverse backbone structures and may display various branches. Brown algal cell walls also contain significant amounts of proteins, with high diversity (over 900 proteins secreted) (Karyophyllis et al., 2000; West et al., 2021). Various genes involved in cell wall synthesis, composition, and degradation were found in the genome of brown algae and are likely to help tune cell wall structure and properties in response to physiological requirements (Nyval et al., 2003). Yet, only a few enzymes have been experimentally validated. Among them, two known algal MC5Es and an alginate lyase have been validated (Inoue et al., 2018). In *S. japonica*, a recombinant epimerase (SjC5-VI) has been shown to epimerize M to G alternatively (Inoue et al., 2016). In *Ectocarpus* sp., MEP13-C5 is believed to epimerize M-M regions, although its precise function remains unclear (Fischl et al., 2016). MC5Es have been reported to be secreted and directly embedded in the cell wall (Terauchi et al., 2017).

The synthesis of FCSPs likely occurs in the Golgi apparatus (Evans and Callow, 1978). During cytokinesis, Golgi vesicles deliver FCSPs to the site of division. Conversely, the region of synthesis of alginates has not been characterized yet. Antibodies indicate the presence of alginates quite late during the formation of the new cell wall during cytokinesis, inside specific osmiophilic vesicles located very close to the newly formed membrane (Nagasato et al., 2010; Yonamine et al., 2021). As such, it has been proposed that alginates, similarly to cellulose, are synthesized directly at the membrane (Katsaros et al., 2013).

D) Functions of the eukaryotic cytoskeleton

The eukaryotic cytoskeleton is a complex and dynamic network of protein filaments that play a pivotal role in maintaining morphogenesis, cell shape, facilitating intracellular transport, and orchestrating various cellular processes (Wasteneys and Zhang, 2004; Katsaros et al., 2006; Hohmann and Dehghani, 2019; He et al., 2020; Ho-Plagaro et al., 2022). It comprises three main components: **microtubules** (MTs), **actin filaments** (AFs), and intermediate filaments (IFs) (Fletcher and Mullins, 2010). These elements collaborate to ensure structural integrity and functional versatility within the cell. MTs and AFs are polar structures that exhibit dynamic instability, as they can rapidly grow and depolymerize. IFs are apolar, less stiff, and relatively stable components of the cytoskeleton. The organization and functions of the cytoskeleton in various organisms, including animals, plants, and brown algae, reveal interesting differences. In animals, MTs are recognized for their pivotal role in mitosis and intracellular transport, serving as tracks for motor proteins like dynein and kinesin. Additionally, a network of cortical AFs functions in concert with myosin, enabling cellular contractility and generating the forces necessary for cell shape changes (Chugh and Paluch, 2018). IFs provide mechanical support and stability to cells and tissues. In land plants, the MT cytoskeleton is instead organized cortically. The MT network is crucial for perceiving mechanical cues and regulating cell shape and growth direction (Besson and Dumais, 2011; Livanos and Müller, 2019). This is achieved through a mechanical feedback loop (Sampathkumar, 2020; Trinh et al., 2021; Schneider et al., 2022), wherein cortical MTs often align perpendicular to the main growth axis and along the axis of maximal tensile stress (Williamson, 1990; Landrein and Hamant, 2013; Hamant et al., 2019; Chebli et al., 2021). These MTs guide cellulose synthase complexes, contributing to the orientation of CMFs and thereby impacting the physical attributes of the cell wall (Baskin et al., 2004; Paredez et al., 2006; Sampathkumar et al., 2019). While less common, AFs have also been reported to be present cortically in plant cells, within specific structures such as guard cell or pollen tube (Li et al., 2019; Xu and Huang, 2020). In contrast, in brown algal cells, there is a lack of cortical MTs (Katsaros and Galactis, 1992; Motomura, 1994). Instead, much like animals, brown algal cells bear a well-organized cytoskeleton of AFs, including cortical, perinuclear, and endoplasmic

arrays, and possess centriole-bearing centrosomes that serve as microtubule-organizing centers (Katsaros et al., 2006). These centrosomes play a pivotal role in determining the cytokinetic plane after mitosis (Nagasato and Motomura, 2002). In addition, the MTs in brown algae contribute to the establishment of cell polarity, involving changes in the position of the nucleus and potentially influencing cell wall composition (Katsaros et al., 1983; Varvarigos et al., 2005). This organization plays a role in the formation of polar growth patterns and cell wall morphogenesis similar to what is observed in the pollen tube of plants (Karyophyllis et al., 2000; Rabillé et al., 2019; Xu and Huang, 2020). The interaction of MTs with AF arrays has been described in animals (Rodriguez et al., 2003) and plants (Takeuchi et al., 2016). It has been proposed that MTs, being associated with the permanent centrosomes, also have interactions with AFs in brown algae (Goode et al., 2000; Gundersen, 2002). In brown algae, similar to the cortical MT of land plants, the cortical actin network has been observed to perceive wall structure in cells, and similar mechanisms with plant cells (e.g., perception of tensile stress, mediation of wall composition) have been theorized and shown to some extent (Karyophyllis et al., 2000; Theodorou, 2023; Panteris and Pappas, 2023).

E) Describing the developmental phases of *Saccharina latissima*

Despite exhibiting a much lower level of morphological complexity than plants and animals, brown algae, and especially kelp (Laminariales), develop very large bodies, whose organization is based on the establishment of structuring spatial axes. Yet, there is still limited knowledge about the developmental control, cell division activity, and orientation during the formation of 3D body plans in these organisms. The embryo of *Saccharina* begins as a monostromatic structure but eventually undergoes transformation into a complex parenchymatous thallus. Moreover, its embryo remains connected to the maternal structure during this time. Notably, *Saccharina* provides a unique system for studying the formation of body plans because it sequentially transitions from 1D to 2D and finally to 3D growth after approximately 15 days post-fertilization (Theodorou and Charrier, 2023). Despite this, the overall morphology of the embryo remains relatively unchanged until the juvenile stage.

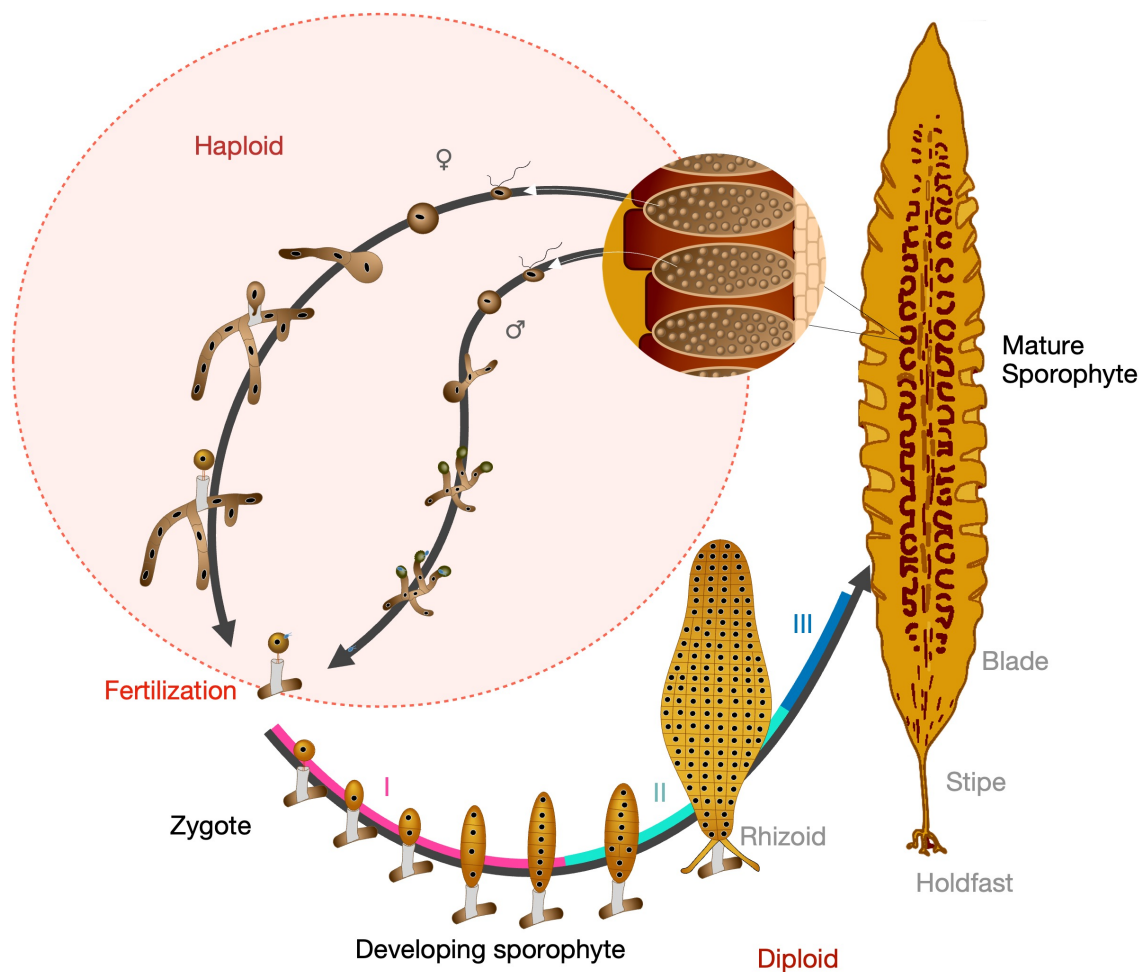


Figure 11: Life cycle of *Saccharina latissima*.

S. latissima presents an alternating life cycle (Vish et al., 2019). Large mature sori produce spores (n) by meiosis in their sporangia (2n). The spores are then liberated into moving water when environmental conditions are favorable (Augyte et al., 2019). Spores then germinate into either male or female gametophytes and grow mainly on sand, rock, or other algae (Klockova et al., 2019). Sexual dimorphism is observed between the male and female gametophytes, as the male presents smaller cells and more branches than the female. Some cells of the female gametophyte will form the oogonium structure from which the egg will be released. In the meantime, the male antherozoids mature and release gametes. After fertilization, the egg remains attached to the female gametophyte. The embryo develops in 6 months into a mature sporophyte.

The gametophyte initiates its growth after the release and germination of the zoospore from the fertile sporophyte (Lüning and Dring, 1975; Figure 11). During this phase, the first cell of the gametophyte, referred to as the "primary cell," begins to form. In the following days, the gametophyte grows vegetatively as a branched filamentous thallus (Cosson et al., 1976). In the case of the female gametophyte, this phase is characterized by a substantial increase in the diameter of the primary cell, often doubling or tripling in size. Conversely, in male gametophytes, this phase is accompanied by limited cell division and a smaller increase in cell size (Lüning, 1981). Notably, this growth phase is not light-dependent, as it occurs under various spectral ranges or darkness. When exposed to blue light or near-ultraviolet light conditions, gametophytes form oogonia (female reproductive structures) or antheridia (male reproductive structures). In contrast, in the absence of this light spectrum, filamentous growth is favored (Lüning and Dring, 1972). Following the development of oogonia, lamoxirene, a sexual pheromone, is produced upon egg release from the oogonium (Lüning and Müller, 1978; Maier and Müller, 1981; Maier et al., 2001). This substance serves the dual purpose of triggering and attracting the release of spermatozoids (Lüning and Müller, 1979). When the mature female gametophyte is ready for egg release, a distinctive bulging of the cell occurs, which marks the future opening site of the oogonium. The process of egg release then begins (Lüning, 1981). Within seconds, the protoplasmic content leaves the oogonium, corresponding to the egg released (Figure 12). The egg remains attached to the oogonium through its flagella (Klochkova et al., 2019). In male gametophytes, a similar release mechanism is initiated by the sexual pheromone, leading to a transversal rupture along the antheridium cap, and ejection of spermatozoids (Maier and Müller, 1981). Within a few minutes, the first freed spermatozoids reach the egg using motility oriented by chemotaxis.

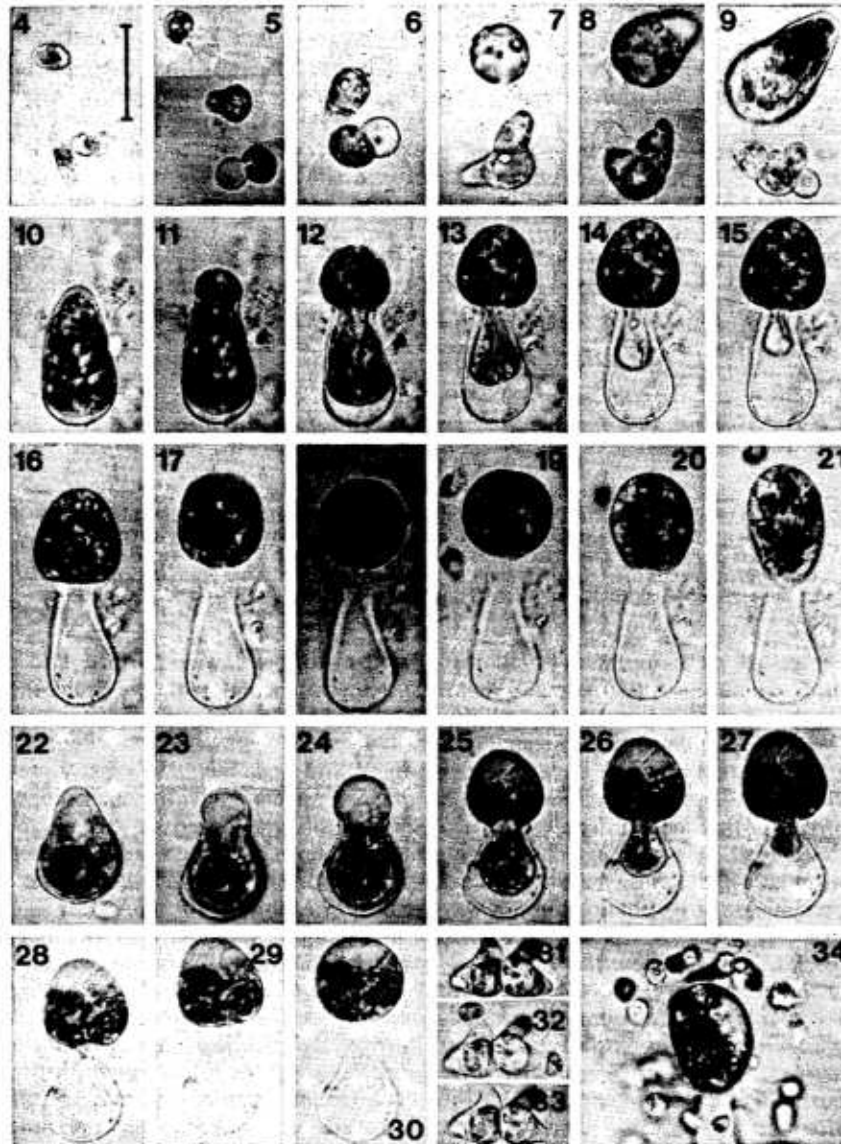


Figure 12: Gamete release in *Saccharina latissima*.

From Lüning 1981, photographs of gametophytes cultured in a 16:8 light-dark regime. Figs 4-9 present the development from zoospore (Fig. 4) to mature gametophyte (Fig. 9). $t = 0$ (Fig. 4); $t = \text{day 1}$ (Fig. 5); $t = \text{day 3}$ (Fig. 6); $t = \text{day 4}$ (Fig. 7); $t = \text{day 5}$ (Fig. 8); $t = \text{day 7}$ (Fig. 9). Figs 10-21 and Figs 22-30 present two series documenting egg release in successive stages, $t = 4 \text{ min}$ before the start of egg release (Figs 10, 22); $t = 0 \text{ s}$ start of egg release; (Figs 11, 23); $t = 5 \text{ s}$ (Figs 12, 24); $t = 10 \text{ s}$ (Figs 13, 25); $t = 20 \text{ s}$ (Figs 14, 26); $t = 30 \text{ s}$ (Figs 15, 27); $t = 45 \text{ s}$ (Figs 16, 28); $t = 2 \text{ min}$ (Figs 17, 29); $t = 3 \text{ min}$ (Figs 18, 30); $t = 7 \text{ min}$ (Fig. 19); $t = 18 \text{ min}$ (Fig. 20); $t = 40 \text{ min}$ (Fig. 21). Figs 31-33 present successive stages of the release of spermatozooids, artificially induced by adding medium from a culture with released eggs. Fig. 34 shows an egg surrounded by spermatozooids. Scale (for all photographs) represents $20 \mu\text{m}$.

The early embryogenesis of *Saccharina* has been recently divided into three main steps (Theodorou and Charrier, 2023) (Figure 13). Phase I initiates the establishment of the primary growth axis, characterized by the initial elongation of the zygote. Although there are instances of eggs undergoing partial elongation in the absence of fertilization, such cases are relatively uncommon, and elongation appears to be induced by fertilization in most cases. During this phase, the embryo grows mainly in one dimension (1D: x-axis) and undergoes a series of transverse anticlinal cell divisions perpendicular to the growth axis, reinforcing the embryo's anisotropic shape. The second growth axis is initiated by the first longitudinal anticlinal cell divisions parallel to the x-axis, transitioning the embryo into Phase II and allowing it to grow along a medio-lateral axis. For about 14-16 days, the embryo keeps developing in two dimensions only (2D: x/y axes) until it reaches about 1000 cells through a succession of both longitudinal anticlinal and transverse anticlinal divisions. As a result, it remains a monolayer cell sheet known as the monostroma. The cells in this phase are still considered 'undifferentiated' due to their cuboid shape, relatively low mitotic activity, and symmetrical division pattern. Emergence of rhizoids at the basal pole often occurs in this step. Finally, the transition to Phase III occurs when mature Phase II embryos initiate tilting of the cell division plane in the z-axis, leading to the embryo growing in three dimensions (3D: x/y/z axes) and thickening. These periclinal cell divisions are parallel to the largest surface of the embryo lamina and are perpendicular to the earlier anticlinal divisions. The detailed understanding of these three steps is essential for unraveling the complexities of 3D tissue formation in brown algae embryogenesis.

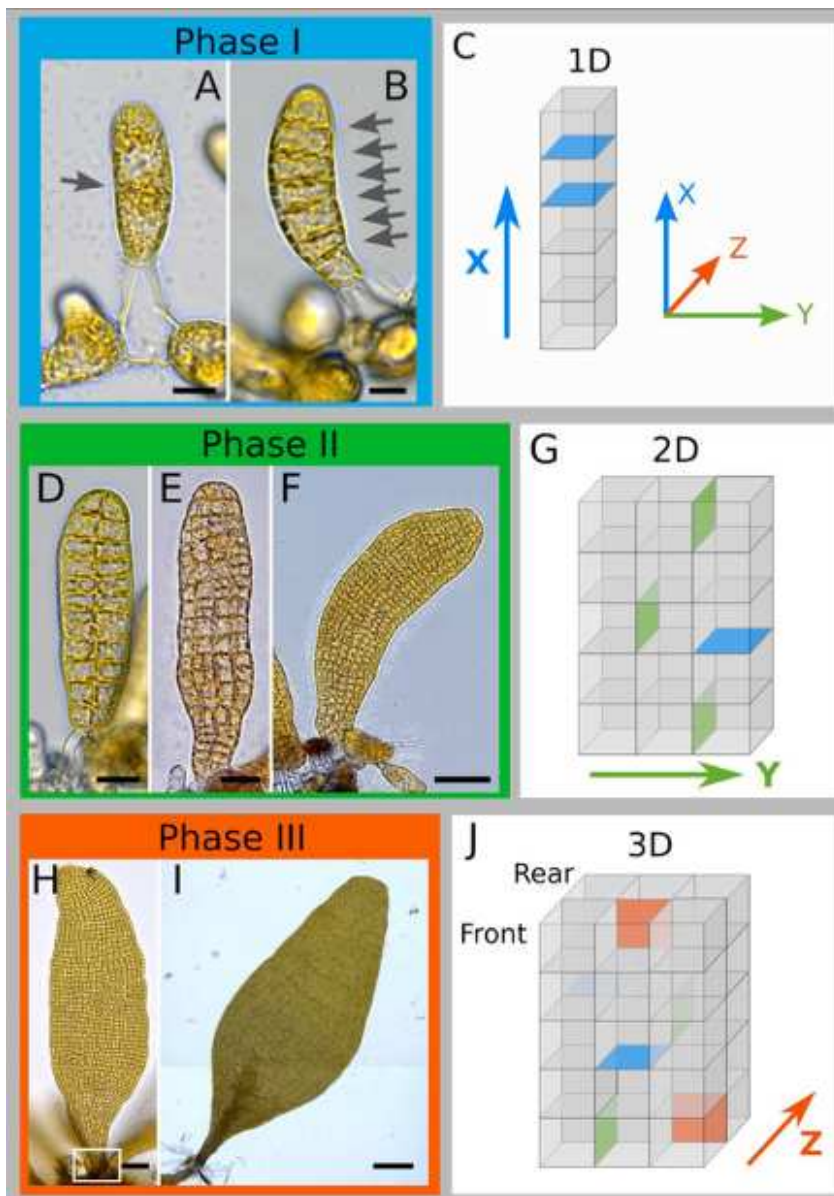


Figure 13: Developmental phases of *Saccharina*

From Theodorou and Charrier, 2023. Top: Bright-field images from developing embryos. Bottom: Schematics indicate the addition of division planes and growth axes. Phase I: (A) Zygote polarization and first unequal division (arrow) 24 hours after zygote polarization (azp). (B) A series of anticlinal divisions (arrows) (60 hours azp). (C) Simplified depiction of cell division during Phase I showing the transverse anticlinal cell division plane and the apico-basal axis (arrow) (x-axis, in blue). Phase II: (D) First longitudinal divisions, 132 hours azp. (E) Advanced stage, 240 hours azp. (F) Last stage of Phase II 324 hours azp. (G) Longitudinal anticlinal (green) along with transverse (blue) divisions, forming a monostroma made of cells aligned in rows and columns (grid). Presence of a secondary growth axis is indicated (y-axis, green arrow). Phase III: (H) First periclinal divisions at the base of the embryo 16 days azp (white box). (I) Further periclinal divisions and addition of cell layers (dark brown region) along the x-axis, 20 days azp. (J) Polystroma during Phase III. Periclinal cell divisions (red) establish a third growth axis (z-axis, arrow) in the developing embryo. Axial system indicated in the lower left corner. Scale bars: 10 μm (A,B); 15 μm (D); 25 μm (E); 70 μm (F); 90 μm (H); 300 μm (I). Representative images from 20 specimens. We designate as the x-axis the first growth axis, then the y- and z- are the second and third growth axes, respectively. Panels D, E, and H show z-projections through Stack focuser on FIJI.

2 - Aim of the study

The evolutionary position of brown algae, being distant from other multicellular organisms, while still following sets of related developmental rules, positions them as an excellent comparative model for gaining insights into the fundamental requirements of multicellular organisms during their development. Among the clade of Pheophyceae, only a limited number of brown algae exhibit developmental processes that maintain a partial connection with the maternal organism. Notably, the Desmarestiales, Sporochnales, Chordales, and Laminariales are four taxonomic groups in which embryonic development occurs in association with maternal cells (Sauvageau, 1918; Kanda, 1938; Fritsch 1954). This unique feature makes brown algae valuable models for investigating the potential impact of maternal regulation on development. The sequential establishment of each body axis makes *Saccharina* a powerful model organism for understanding the regulation and fundamental steps involved in acquiring a 3D body plan. As a result, my PhD project aimed to comprehensively study the establishment of both longitudinal and lateral axes in the kelp *Saccharina latissima* and to identify the underlying determinants. In the following manuscript, I aimed to present a detailed scenario elucidating how kelp embryos acquire and sustain their body plans during the early embryogenetic phases. I addressed the following questions: How do intracellular components contribute to the establishment of body axes? Do other factors determine the formation of these axes? How are the body axes regulated?

Throughout this manuscript, I present some answers to these questions. First, I studied the potential role of the cell wall and cytoskeleton in establishing growth axes. Then, building upon prior observations in the literature, I further explore the impact of embryo attachment to maternal tissue. Finally, I examine the role of individual embryonic cells at the onset of embryogenesis in subsequent embryo development.

By harnessing the distinctive phylogenetic position of *Saccharina* in the tree of life, I aim to draw conclusions that contribute to a deeper understanding of the fundamental principles governing the establishment of body axes.

3 - Chapter I

The early, elongated embryo of the brown alga *Saccharina* is surrounded by a corset of alginates that depend on cortical actin filaments.

Abstract:

This chapter highlights the distribution of cell wall compounds and the localization of actin filaments (AFs) during the development of *Saccharina latissima*. Immunolabeling of cell wall polysaccharides, staining of AFs, and the use of AFs depolymerizing drugs enabled the description of a spatio-temporal pattern of these different cellular factors during the main embryogenesis steps, and elaboration of a model of their potential role in the establishment of the embryo longitudinal axis.

Contribution:

The culture of *Saccharina latissima* organisms used for the study was shared between myself and Roman Milstein, a Master 2 student whom I co-supervised for 6 months (January – June 2022). I adapted the protocol for cell wall immunolabeling (BAMs) on *Saccharina* embryos from the protocol published for *Ectocarpus* in (Rabillé et al., 2019). BAM labeling work was carried out by several members of our team (myself, R. Milstein, A. Le Bail, and S. Chenivresse), while experiments using cytoskeletal drugs were performed by myself and I. Theodorou (former PhD student of the team). Images of actin filaments were acquired by myself and I. Theodorou. I significantly contributed to the results, discussion, and writing presented in the corresponding article.

The early, elongated embryo of the brown alga *Saccharina* is surrounded by a corset of alginates that depends on cortical actin filaments.

Samuel Boscq, Ioannis Theodorou, Roman Milstein, Aude Le Bail, Sabine Chenivresse and Bénédicte Charrier*

Morphogenesis of Macro Algae, UMR8227, CNRS - Sorbonne University, Station Biologique de Roscoff, Place Georges Teissier, 29680 Roscoff, France

* Current address: Morphogenesis of Brown Algae, Institut de Génomique fonctionnelle de Lyon (IGFL), UMR5242, ENSL, CNRS, INRAE, UCBL, 32-34 avenue Tony Garnier, 69007 Lyon, France

Corresponding author:

benedicte.charrier@cnr.fr

Introduction

Embryogenesis of brown algae is characterized by the establishment of different body plans spread out over time. Unlike *Fucus*, whose 3D embryo is formed in three cell divisions, other brown algae such as the parenchymatous kelp *Saccharina* (Laminariales) and the filamentous polystichous alga *Sphacelaria* (Sphacelariales) develop their body axes in sequential steps: first, a unidirectional tissue is formed, which then divides perpendicularly to widen, and finally divides again in the third dimension to thicken.

We have recently described in detail these three steps in the embryogenesis of *Saccharina*, particularly focusing on the transition from 2D to 3D growth, which, in this species, is accompanied by cell differentiation (Theodorou and Charrier, 2023). Initially, after fertilization, the zygote elongates along an axis parallel to the maternal stalk, which is the remaining envelope (cell wall) of the oogonium that stands on the gametophyte filament. Through a series of transverse cell divisions, the zygote generates a monodirectional stack of 8 cells still aligned with the stalk. Subsequently, the cell division plan shifts by 90°, and this first longitudinal cell

division initiates growth in the medio-lateral axis. After a series of alternating transverse and longitudinal cell divisions, forming a monolayered lamina of ~ 1000 cells, the cell division orientation shifts again by 90° (Z-axis), leading to lamina thickening and cell differentiation (Theodorou and Charrier, 2023).

This exceptional series of ordered shifts from 1D growth to 2D and then 3D suggests that important positional cues must operate to guide cell division in such controlled changes of orientation.

Therefore, in this paper, we mapped cell wall components of the embryo from the egg stage to Phase II. The cell wall of brown algae is composed mainly of alginates and fucans embedding cellulose microfibrils present at a lower proportion (Charrier et al., 2019; Deniaud-Bouët et al., 2017; Mazéas et al., 2022). Chains of alginates are composed of different epimers, namely mannuronan acids (M) and guluronan acids (G), usually mixed within the chains as M-M, M-G, or G-G blocks. We used monoclonal antibodies that specifically recognize these blocks. To further characterize the process that controls the specific organization of the cell wall, we also labeled actin filaments (AFs). AFs play two major roles in brown algae. First, an actin plate of AFs is formed at cytokinesis, and depleting it with drugs impairs the completion of cytokinesis (Karyophyllis et al., 2000; Katsaros et al., 2003; Katsaros et al., 2006). Secondly, in some brown algae belonging to the orders Fucales and Sphacelariales, the accumulation of cell wall components was shown to depend on the organization of the cytoskeleton (Hable, 2014; Hable and Kropf, 2005; Hable et al., 2003; Hable et al., 2008; Henry et al., 1996; Katsaros et al., 2003; Muzzy and Hable, 2013).

We then sought to correlate the mapping pattern of different cell wall polysaccharides with the presence of AFs during *Saccharina* embryogenesis and to assess whether these factors may play a role in establishing embryo growth axes.

Results

Alginates and fucans cell wall polysaccharides display different spatio-temporal patterns during the embryogenesis of *Saccharina latissima*

To map alginates and fucans in the embryo of *Saccharina latissima*, we used the monoclonal antibodies produced by Torode et al. (2015; 2016). We observed that while in eggs, the mannuronate-rich alginates (M-M blocks labeled with monoclonal antibody BAM6) were homogeneously displayed on the egg surface (Suppl. Fig. 1A, left), in zygotes, they appeared to be present only in the flanks, with the apex and base devoid of any signal (Fig. 1A). This localization was retained after the zygote divided transversally. A corset of M-M rich alginates was observed at the 2-cell stage and persisted until the 6-8 cell stage, leaving the tip and base of the embryos unlabeled (Fig. 1B-G). Interestingly, this corset disappeared as the embryo switched to Phase II. As mannuronate-rich alginates disappeared progressively from the outer cell wall of the embryos, only transverse cell walls were labeled at the end of Phase (Fig. 1H-K) and transverse and longitudinal cell walls in Phase II embryos (Fig. 1L-O) and beyond (Suppl. Fig. 1A, right). It is noteworthy that in the cell walls within the embryo lamina, the M-M-rich alginates accumulate in the innermost layer, so that two distinct cell walls were observed at each boundary between two cells, separated by a layer of cellulose microfibrils (Fig. 1P). This also seems to be the case in zygotes (Suppl. Fig. 1A). This suggests that M-M rich alginates are present in the most recent cell wall layers, in agreement with reports in *Fucus* embryos (Yonamine et al., 2021).

In summary, M-M-rich alginates were found in all cells except in the apex of embryos. From our experience, *Saccharina* zygotes and embryos do not grow apically but by diffuse growth (not shown). Therefore, the absence of M-M-rich alginates in this specific location raises puzzling questions about their role in *Saccharina* embryogenesis.

The BAM7 antibody, which labels M-G-rich alginates (Torode et al., 2016), did not display the same spatio-temporal pattern as the BAM6 antibody (Suppl. Fig. 1B). In contrast to M-M-rich alginates, M-G-rich alginates covered the fertilized eggs and zygotes homogeneously. After the zygote stage, M-G-rich alginates were no longer detected in the external cell wall and accumulated only in the internal cell walls (Suppl. Fig. 1B).

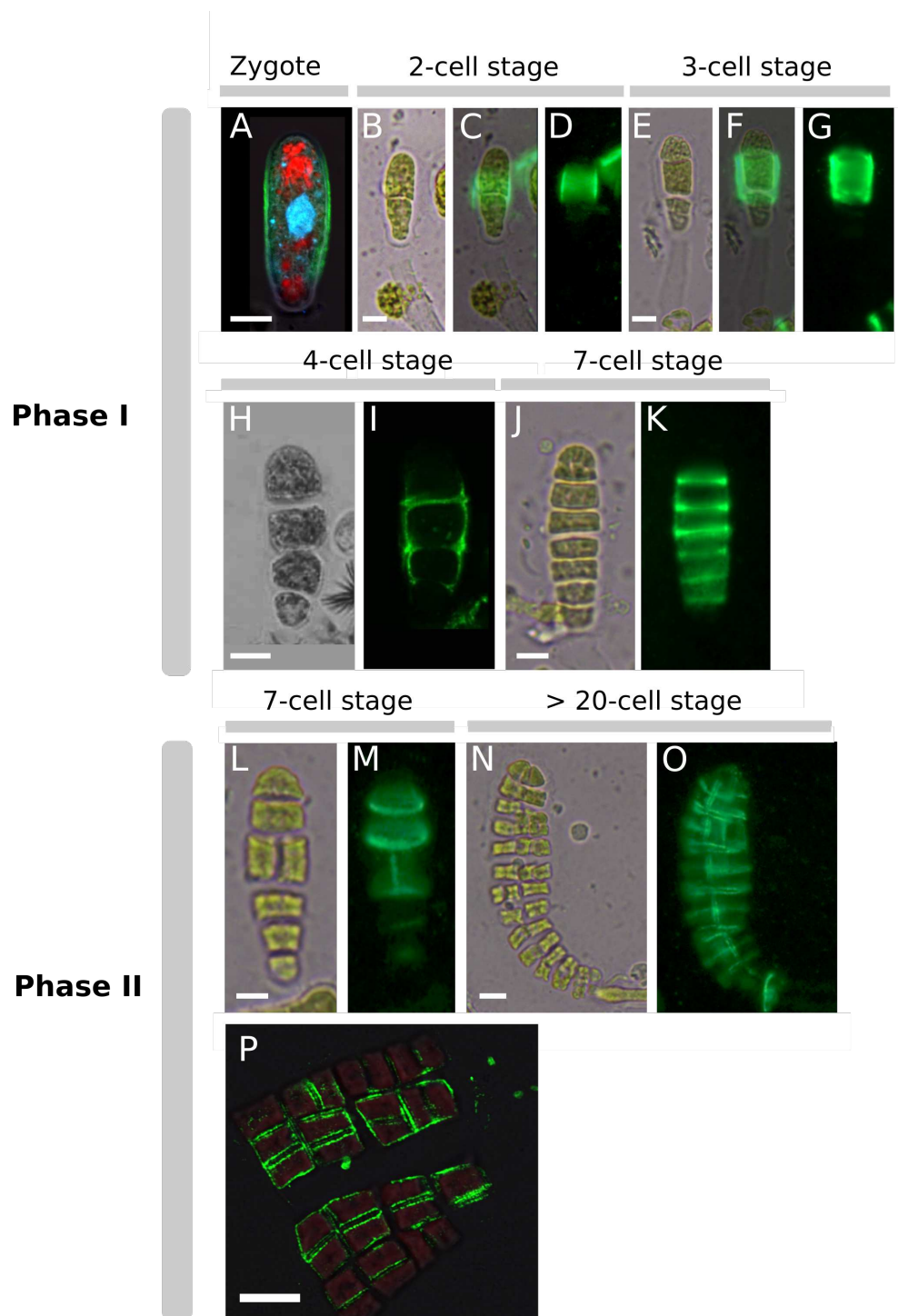


Figure 1: Detection of mannuronate-rich alginates during the development of *Saccharina* embryos. Zygote and embryos up to the >20-cell stages were labelled with the monoclonal antibody BAM6, specific for mannuronate-rich alginates. B,E,H,J,L,M: Bright field image. D,G,K,M,O: epifluorescence of FITC-BAM6 antibody (green signal). C,F: merge. A, H, I and P are confocal images. P is a zoom-in of a Phase II blade showing M-M-rich alginates in the innermost cell wall of each cell (green: FITC; red: chloroplast autofluorescence; blue: Calcofluor; cyan: DAPI). Scale bars = 10µm.

However, in zygotes, as for BAM6, BAM7 epitopes were localized in a more internal layer than the layer rich in cellulose. This feature was conserved at later stages in the internal cell walls (Suppl. Fig. 1B).

Guluronate-rich alginates, labeled by monoclonal antibody BAM10 (Torode et al., 2016), were detected on the surface of embryos from the egg stage to mature Phase II (Suppl. Fig. 1C, right). In comparison, these polysaccharides were barely detected in internal walls, where the signal was much weaker than that of Calcofluor White, which marks cellulose microfibrils (Suppl. Fig. 2C, blue channel).

A similar pattern was found for fucans, which are abundant components of cell walls in most brown algae (Charrier et al., 2019). Using the monoclonal antibody BAM4 (Torode et al., 2015), we observed that sulfated fucans uniformly cover the surface of eggs, zygotes, and embryos until late Phase II at least (Suppl. Fig. 1D). No signal was detected in the internal cell walls of Phase II embryos (Suppl. Fig. 1D). Interestingly, like G-G-rich alginates, sulfated fucans were detected more externally than cellulose (nicely shown in, for example, the zygote in Suppl. Fig. 1C and Phase I and II embryos in Suppl. Fig. 1D).

In contrast to alginate and fucan matrix polysaccharides that seem to be present in specific locations during the development of *Saccharina* embryos, cellulose labeled with Calcofluor White appears to be distributed homogeneously in both the external and all internal cell walls from the egg to the Phase II stages (Suppl. Fig 1A-D).

Actin filaments are localized cortically in Phase I and Phase II embryos

The actin filaments (AFs) were labeled with Rhodamine-phalloidin or Alexa488-phalloidin in fixed embryos. In zygotes, a network of cortical AFs was observed all around newly-formed zygotes (Fig. 2A,B), but this distribution seems to be concentrated mainly on the flanks of elongated zygotes (Fig. 2C,D; yellow arrows). At the cellular level, this cortical location was maintained in the cells of Phase I embryos (Fig. 2E,F) and even more clearly in Phase II, as all the internal sides of the cuboid cells that characterize Phase II were homogeneously labeled (Fig. 2G-J). The cortical localization of AFs is not specific to *Saccharina* embryos as it has been observed in many brown algal cells, particularly when cells are in interphase (Katsaros et al., 2006). Interestingly, a weaker signal was observed at the outward-pointing edges of the embryo (Fig. 2H,J), suggesting that the role of AFs in the cells

of the lamina differs between the inner edges shared by neighboring cells and the outer edge where cells are exposed to the outer cell wall in contact with seawater. The nuclei have no specific configuration in relation to the axis of the embryo and instead have an apparently random position.

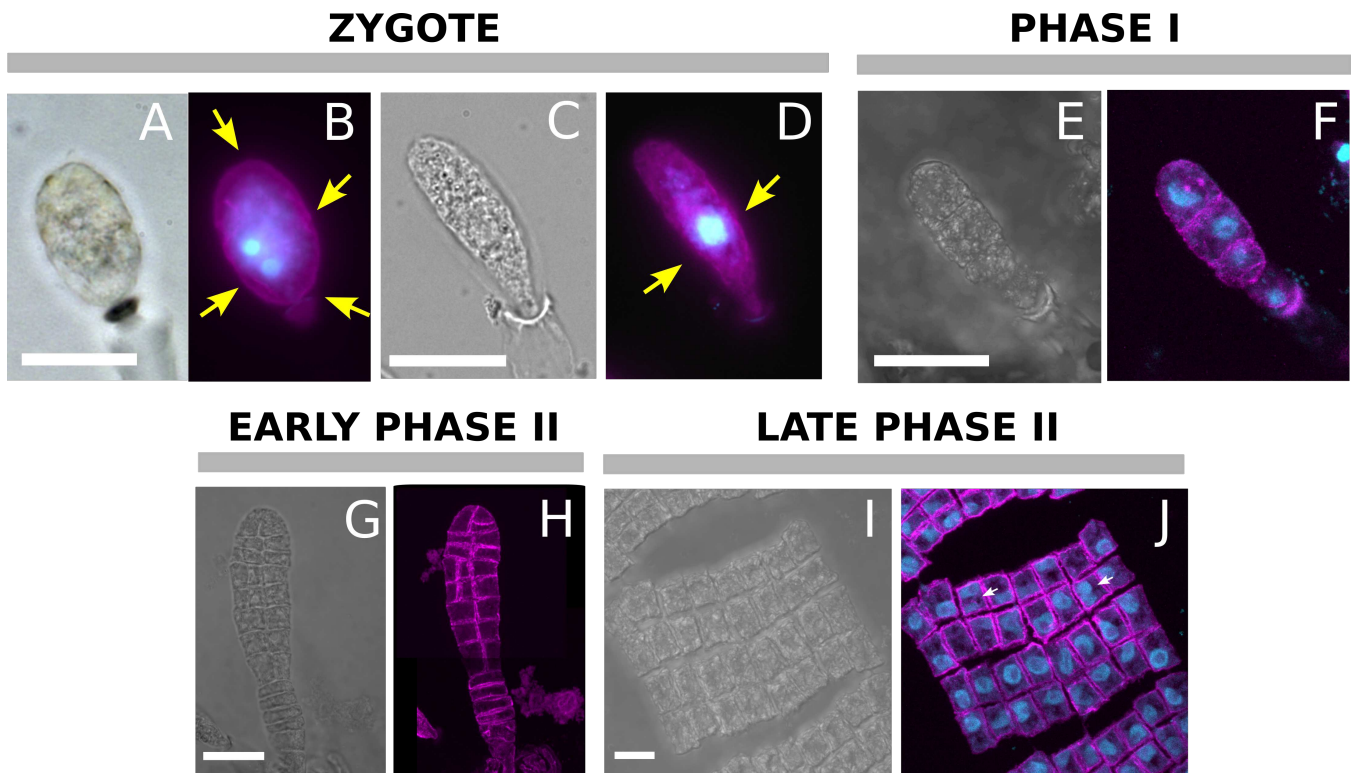


Figure 2: Actin organisation during *Saccharina* embryogenesis. (A,C) Transmission light images of epifluorescence microscopy of specimens shown in B and D; (E,G,I) Transmission light images from confocal microscopy of the specimens F, H, and J in respective order. A and C are maximal projections of Z stacks. (F-G) Maximal projections of confocal Z-stacks. Actin filaments (AF, magenta) in B and D are stained with Phalloidin-Alexa Fluor 488 conjugate and in F, H, and J with Phalloidin-Rhodamine. Nuclei (cyan) were stained with DAPI in images B, D, F, and J. Yellow arrows indicate cortical labeling. All bars are 20 μm .

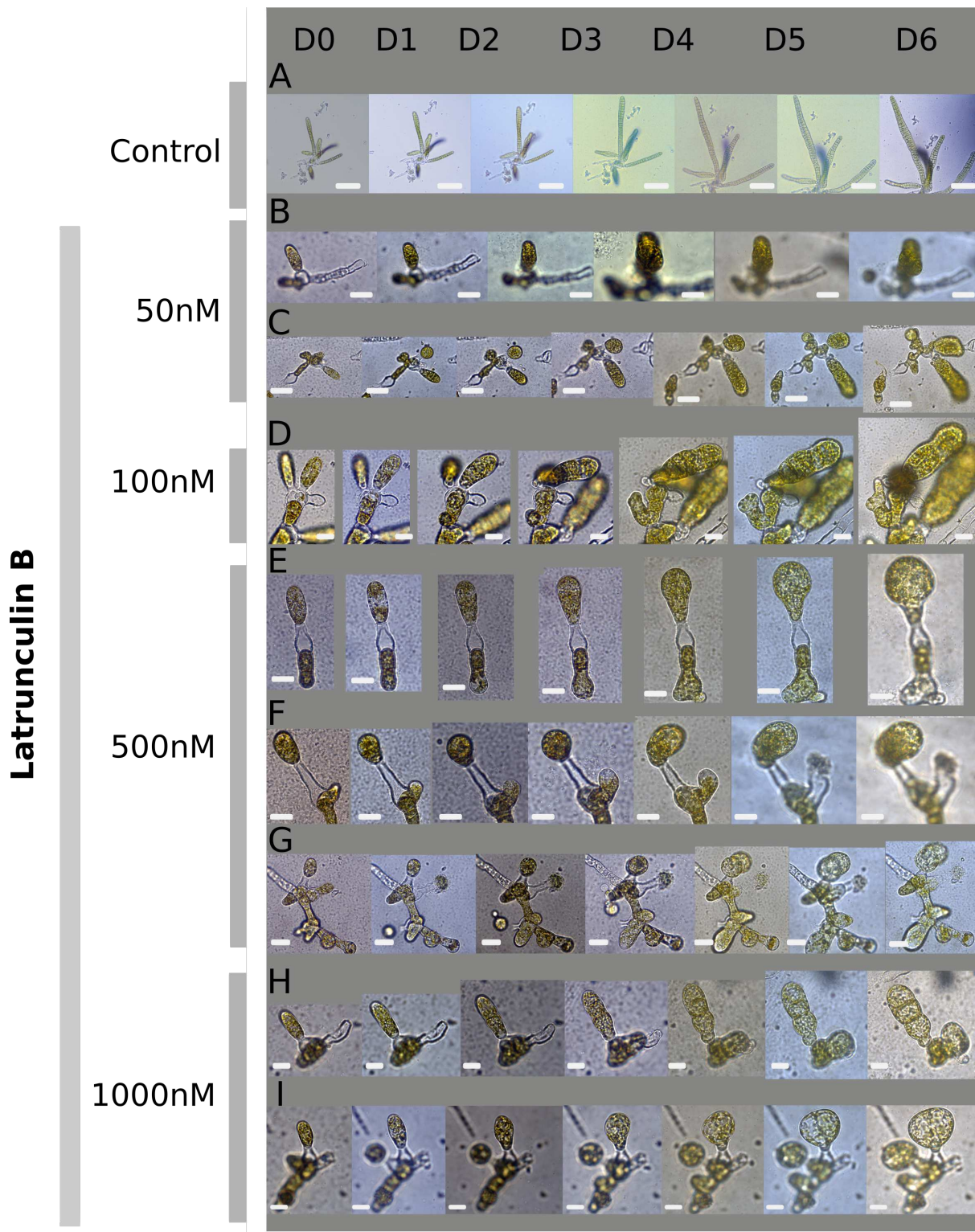


Figure 3: Morphological response of *Saccharina* zygotes to treatment with Latrunculin B.

Zygotes were treated with 50, 100, 500, and 1000 nM of Latrunculin B for 7 days (D0 to D6). A photo is shown for each day after the treatment and in DMSO controls. A, B: 50 nM LatB concentration, C: 100 nM, D-F: 500 nM; G, H: 1 μ M. Scale bars = (A) 200 μ m, (B, C) 20 μ m, (D-I) 10 μ m.

Actin filaments control cell shape

Latrunculin B (LatB) is a drug that binds actin monomers and halts their polymerization into actin filaments (Wakatsuki et al., 2001). Embryos were treated for 7 days with 50, 100, 500, and 1000 nM of LatB in seawater. While control embryos immersed in 1% DMSO showed no malformation (Fig. 3A), LatB-treated embryos displayed abnormal morphologies (Fig. 3). These morphological responses were observed for LatB concentrations as low as 50 nM (Fig. 3B,C), for which eggs and zygotes grew into larger cells compared to the control, and with irregular shapes. The impact of LatB on the morphology of the embryo increased with LatB concentration from 100 nM (Fig. 3D) up to 1 μ M (Fig. 3E-I). Zygotes swelled and grew asymmetrically, generating bumps in all three spatial directions (e.g., Fig. 3B), or a pair of spherical cells parallel to each other in the medio-lateral direction (Fig. 3G). Some returned to an isotropic form, losing their elongated shape and apico-basal axis (Fig. 3E,I). This indicates that AFs are involved in maintaining the elongated shape of the zygote, and in controlling the orientation of divisions during Phase I. However, the effect of LatB on the orientation of cell divisions diminished once the first transverse division occurred, and only cell shape remained impacted (Fig. 3D,H). Eggs, whether recently fertilized or not (spherical cell), can adopt an irregular shape (Fig. 3C).

Actin filaments control the spatio-temporal pattern of mannuronate-rich alginates during *Saccharina* embryogenesis Phase I and Phase II

To assess the role played by actin filaments in the composition of the cell wall, we repeated the labeling experiments on eggs, zygotes, and embryos in the presence of Lat B, which has been shown to impact the formation of the cell wall in brown algae (Hable et al., 2003; Karyophyllis et al., 2000; Katsaros et al., 2003; Katsaros et al., 2006; Nagasato and Motomura, 2009; Varvarigos et al., 2004; Varvarigos et al., 2007).

Eggs, zygotes, and embryos treated with 1 μ M Latrunculin B for 1 week displayed large cells with irregular outlines (Fig. 4). In addition, in these samples, mannuronate-rich (M-M, labeled with BAM6 antibody) alginates accumulated in the apex of zygotes in addition to the flanks (Fig. 4A-F), whereas M-M block-rich alginates were not detected in the apex of control embryos (Fig. 2 and text above).

Labeling of M-M-rich alginates in the tip of the embryos persisted to the 7-cell stage (Fig. 4G-J), where the first apical half of the embryos was homogeneously labeled in addition to the transverse cell walls. Therefore, the "corset" of mannuronate-rich alginates limited to the flanks in the control embryos is transformed into a "sock" in the Latrunculin B-treated embryos.

In Phase II embryos, once longitudinal cell divisions occurred, M-M blocks were observed on the boundary of the blade (Fig. 4M-V). This contrasts with the pattern observed in control embryos, in which the blade boundary was depleted of M-M blocks. The labeling of transverse cell walls in response to Latrunculin B was unchanged (Fig. 4R, T, V). In summary, LatB-mediated depolymerization of AFs resulted in a ubiquitous accumulation of BAM6 epitope in the periphery (outer cell wall) of the egg, zygote, and embryos and in the transverse cell walls within the lamina. Furthermore, the regulation through the embryonic phase was lost, as this pattern was maintained from the egg stage to the advanced Phase II, whereas it differs between Phase I and Phase II in control embryos.

Therefore, AFs play a role in the regulation of mannuronate-rich alginates in the external cell wall, which grows and thickens since the zygotic stage, but not in the formation of the transverse and longitudinal internal cell walls, which are formed by cytokinesis. Remarkably, this regulation of the spatio-temporal accumulation pattern is highly specific for M-M-rich alginates, as no such modification was observed in the presence of Latrunculin B when using BAM7, BAM10, and BAM4 antibodies or Calcofluor White to display the cell wall polysaccharides (Suppl. Fig. 2, compared to Suppl. Fig. 1). However, it is noteworthy that the signal was less finely tuned than in the absence of Latrunculin B, especially for images corresponding to the zygote and early Phase I embryos (Suppl. Fig. 2C). In Phase II embryos, uneven patches of FITC were observed for BAM6 and BAM7 along internal cell walls.

Altogether, this result supports the impairment of M-M-rich alginates localization in LatB-treated embryos.

Interestingly, LatB did not impact the location of cellulose and sulphated fucans, as these cell wall polysaccharides displayed a similar distribution as that described in control conditions (Suppl. Fig. 1). In the presence of LatB, G-G-rich alginates and sulphated fucans still surrounded the zygotes and Phase II embryos (Suppl. Fig. 2D, left). Cellulose microfibrils were similarly present in the external and internal cell

walls as in the control conditions (nicely seen in Suppl. Fig. 2D, for example, Phase I embryos). Therefore, in the early development of *Saccharina latissima* embryo, neither the location of sulphated fucans nor the formation of cellulose microfibrils seem to depend on the AFs network.

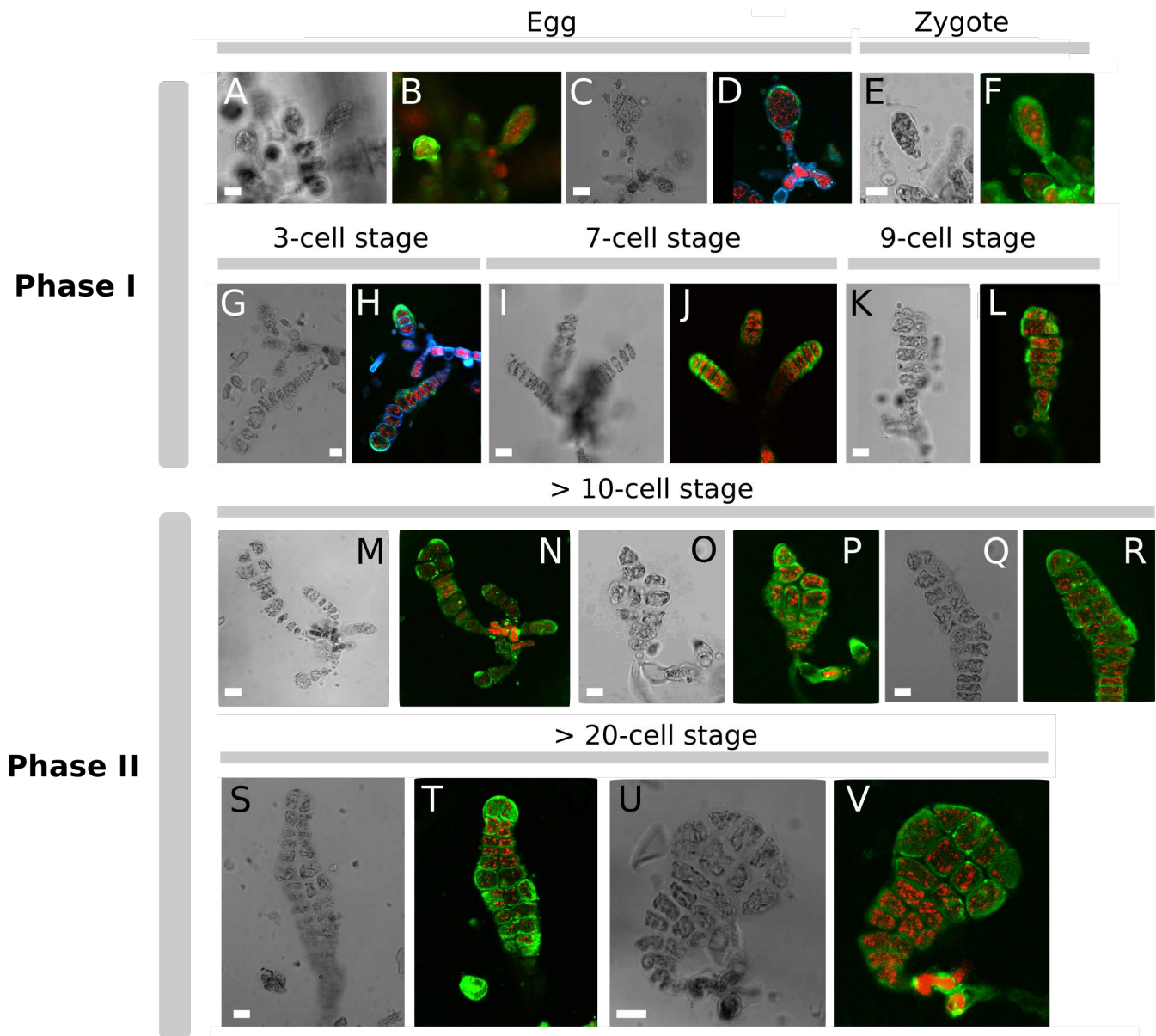


Figure 4: Detection of mannuronate-rich alginates during the development of *Saccharina* embryos treated with Latrunculin B.

Fertilized eggs, zygotes, and embryos were labeled with the monoclonal antibody BAM6 after having been treated with 1 μM Latrunculin B for 7 days. A, C, E, G, I, K, M, O, Q, S, U: Bright field images. B, D, F, H, J, L, N, P, R, T, V: Confocal images of FITC-BAM6 labeling (green: FITC; red: chloroplast autofluorescence; blue: Calcofluor white). Scale bars = 10 μm.

Discussion

We immunolocalized alginates and fucans in the cell wall of *Saccharina* eggs, zygotes, and embryos. We showed that, in contrast to the other cell wall polysaccharides tested in this study, the accumulation pattern of mannuronate-rich alginates coincides in space and time with the establishment of the longitudinal axis of the zygote (Fig. 5). We also showed that AFs are necessary for the zygote to establish or maintain this longitudinal axis (Fig. 5). These results prompt the following question: could mannuronate-rich alginates regulate the formation of the longitudinal axis, and if so, how?

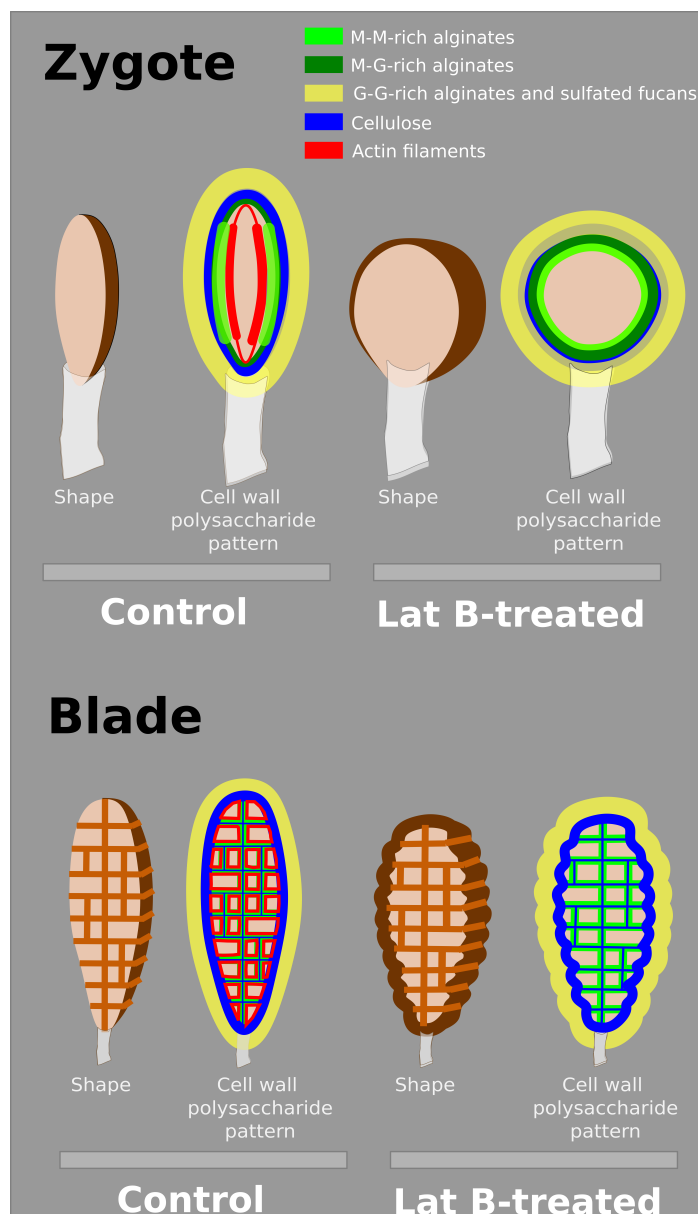


Figure 5: Summary schematics of the localisation pattern of the cell wall polysaccharides in zygotes and Phase II embryos.

Schematics representing the typical shape and localization pattern of cell wall polysaccharides in the zygote (top) and Phase II embryo (bottom) of *Saccharina latissima*, in standard culture conditions (left) or in the presence of Latrunculin B (right). In the Phase II embryo, the M-G-rich alginates are not represented because their pattern is the same as the M-M-rich alginates (green).

There are many different explanations for a molecule no longer being labeled using immunochemistry. This includes processes such as its degradation, changes in its conformation, synthesis, or delivery of another compound obscuring the epitope required to reveal the molecule (Hawes et al., 2009; Vázquez-Gutiérrez and Langton, 2015). Whatever the reasons for the signals appearing and disappearing, our experiments show that polysaccharides fall into two categories in the context of the *Saccharina* embryo. The first category accumulates in the outer cell wall only. In this compartment, polysaccharides like guluronate-rich alginates and sulfated fucans are homogeneously distributed in the most external layer of the cell wall all around the embryo. Their localization pattern does not change from the egg stage to the Phase II embryo. These polysaccharides are a permanent constituent of the thick, external cell wall surrounding the embryo since the egg stage and are weakly detected in the internal cell walls. In brown algae, the cell wall is formed quickly after fertilization (Motomura, 1990; and our observation). In Fucales, the zygote starts forming a fibrous cell wall less than 5 minutes after fertilization (*Fucus vesiculosus*, Pollock, 1970), which is surrounded by a multilayered cell wall thick of ~ 500 nm 4-6h after fertilization (*Pelvetia compressa*, (Bisgrove and Kropf, 2001). Similarly, in Dictyotales, cell wall secretion is detected within 90 seconds after fertilization (*Dictyota dichotoma*, Bogaert et al., 2017b). Thus, many brown algal embryos synthesize an outer envelope very quickly after fertilization. Our results are therefore consistent with this general pattern.

The second category of cell wall polysaccharides accumulates in specific locations, which vary during the growth of the embryo. M-M-rich and M-G-rich alginates were first localized at the surface of the zygote, and then in the internal transverse and longitudinal cell walls of Phase I and Phase II embryos (Fig 1; Suppl. Fig 1A,B). Therefore, their spatial pattern changes with time. Furthermore, and very interestingly, M-M-rich alginates were not detected in the apex of zygotes and Phase I embryos, in contrast to M-G-rich alginates. Instead, they form a corset on the sides of the zygote and up to 8-cell long early embryos, and remarkably, this corset disappears as the embryo continues to grow. Upon fertilization, the egg elongates and preliminary data suggest that the elongation of the *Saccharina* egg is accompanied by a reduction in cell volume (not shown). This suggests the requirement for a mechanism that retracts the flanks inwards for the benefit of the

expansion of the egg along the longitudinal axis. This mechanism was also described in the zygote of *Dictyota*, which elongates less than 90 seconds after fertilization through only a modification of cell shape devoid of growth (Bogaert et al., 2017a). After monitoring and quantifying the growth of the embryos from the egg stage to Phase II, we observed that first, longitudinal cell divisions do not occur until the embryo reaches ~8 cells (Theodorou and Charrier, 2023). Secondly, growth during Phase I is proportionally higher in length than in width (unpublished). While Phase I embryos doubled their length from 30 μm at the egg stage to 60 μm at the 8-cell stage, they had limited growth in width (15 μm at the egg stage vs 20 μm at the 8-cell stage; not shown). Therefore, growth in width is limited both in cell expansion and cell division, and Phase I embryos grow mainly longitudinally. Thus, the corset, which persists until the 8-cell stage in some Phase I embryos, could ensure that cells do not expand laterally. At the end of Phase I, the corset disappears, and the cells begin to divide longitudinally, allowing the embryo to widen. Unfortunately, detailed analysis of the cell wall composition in the elongating zygote of *Dictyota* has not yet been performed, and, while the cellulose layer appears to be homogeneously distributed at the surface of the elongating zygote (Bogaert et al., 2017b), it remains unknown whether alginate epimers accumulate anisotropically along the longitudinal axis.

In *Ectocarpus*, the location of alginates along the sporophytic filament does not correlate with cell differentiation but with the amount of tensile stress at the surface of the cell (Rabillé et al., 2019b).

Furthermore, when probing the cell surface with atomic force microscopy, spherical cells with lower curvatures displayed a stiffer innermost cell wall layer than cylindrical cells with higher curvatures (Rabillé et al., 2019b). In *Saccharina* elongated zygotes, flanks have the lowest meridional and circumferential curvatures. Hence, because the thickness of the external cell wall is similar all around the egg and embryos (TEM observations of transverse and longitudinal section of *Saccharina* zygotes and embryos; not shown), the flanks must experience the highest tensile stress (for rationale, see Lockhart, 1965; Rabillé et al., 2019a). Therefore, the fact that the M-M-rich alginates are positioned in the inner layer of cell walls of *Saccharina* zygotes and in the regions with the lowest curvature resonates with the results obtained in *Ectocarpus*. However, not only M-M-rich, but

also M-G and G-G rich alginates contribute to the cell wall mechanical resistance in *Ectocarpus*, and G-G rich alginates were even shown to contribute to a higher extent. This contrasts with the results obtained in *Saccharina*, where only M-M rich alginates display a specific pattern on the flanks of the zygotes.

In cell-walled organisms, there are several examples of envelopes surrounding the embryo and maintaining its mechanical balance. In *Arabidopsis*, the presence of a transient proteinaceous envelope around the early globular stage embryo has been reported (Harnvanichvech et al., 2023). It is thought to control the outward mechanical forces due to the cell turgor in embryo cells, which the surrounding endosperm cannot control because it deflates at that stage. However, in *Arabidopsis*, and in contrast to *Saccharina*, this control seems to be isotropic as the embryo is almost spherical at that stage. In the free zygote of the brown algae belonging to the order Fucales, alginates are the first polysaccharides to be synthesized on the surface of the fertilized egg (about 8-16 hours post-fertilization, PF), after cellulose 2 hours PF (Torode et al., 2016). They are distributed all around the zygote, which is still spherical at the time. When the rhizoid germinates, M-M-rich alginates concentrate in the thallus cell and disappear from the future rhizoid emergence site, where sulfated fucans in turn accumulate (Torode et al., 2016). Interestingly, it was shown that AFs, in contrast to microtubules, were necessary for maintaining the strength of the cell wall in a Golgi-dependent manner (Bisgrove and Kropf, 2001). These are two examples of embryo envelopes that contribute to the management of the mechanical forces by the embryo. AFs were also shown to play an important role in the formation of the cell wall in the filamentous brown alga *Sphacelaria* (Karyophyllis et al., 2000; Katsaros et al., 2002). In this alga, apical cells treated for 24 hours with cytochalasin B, a drug inhibiting actin polymerization, displayed cellulose microfibrils randomly aligned within a thicker cell wall, while cell shape did not change. Because drug-mediated inhibition of Golgi vesicle trafficking reduced the strength of the cell wall (Bisgrove and Kropf, 2001), it is hypothesized that AFs control cell wall stiffness and composition by controlling vesicle trafficking. However, in *Saccharina*, we showed that the location of M-M-rich alginates in the internal cell walls of the embryo, which results from cytokinesis, was not dependent on the presence of AFs, while it is in the outer cell wall. This suggests that the formation of the two types of cell walls, the external one and the internal ones, is

regulated through different processes. Alginates were shown to be delivered at the new cell plate through ER-derived flat cisternae (Mazéas et al., 2022; Nagasato et al., 2010) under the control of AFs (Katsaros et al., 2013; Nagasato et al., 2010), but how alginates are delivered in thickening cell walls over time is unclear.

Whatever the role of this alginate corset and how AFs could control its formation, it is no less puzzling that it disappears at the end of Phase I. We observed that M-M-rich alginates were located mainly in the innermost layers of both external and internal cell walls. Similar observations were reported in *Ectocarpus* cells by Terauchi et al. (2016) and anticipated by McCully (1965) in *Fucus*. Therefore, mannuronates would be delivered to the plasma membrane before being transformed into guluronates by the mannuronate C5-epimerases (Fischl et al., 2016) that are present in the cell wall (Mazéas et al., 2022). Hence, they would be less represented in the outermost cell wall layers, in agreement with our results. Alternatively, M-M-rich alginates could be degraded by alginate lyases recently identified in brown algae (Inoue and Ojima, 2019; Mazéas et al., 2022).

We have thus highlighted the possibility that an alginate corset contributes to the elongation of the zygote and thus to the establishment of the apico-basal axis of the *Saccharina latissima* embryo. This hypothesis needs to be tested using tools that are more likely to be mechanical, or mutants with a reduced M-M rich alginate composition. In response to what signal this corset forms on the sides of the zygote and how it disappears at the end of Phase I of embryogenesis also remains to be discovered.

Material and methods

Preparation of Saccharina embryos

Embryos were produced from fertilization of female gametophytes as described in Theodorou et al. (2021) and distributed in dishes with a glass bottom (NEST). In short, gametogenesis was induced under white light conditions at 16 $\mu\text{mol photons m}^{-2}\cdot\text{s}^{-1}$, 14:10 light:dark photoperiod, and 13°C using full Provasoli enriched

seawater (PES) (Le Bail and Charrier, 2013; Theodorou et al., 2021). Embryos were kept under white light to develop.

BAM immunolabeling

Immunolocalization was adapted from Rabillé et al. (2019b). Briefly, embryos were fixed with 4% paraformaldehyde (PFA) dissolved in a mixture of water and seawater (NSW) (50:50) for 70 minutes at room temperature (RT). Cells were washed once with NSW:PBS (50:50), then two times with PBS for 10 minutes each, and blocked in PBS with 5% milk for 1 hour at RT. The embryos immunolabeled with BAM 4 were treated with alginate lyase diluted in 50 μ M Tris and 150 μ M NaCl for 1 hour at RT. Alginate lyase was washed three times for 5 minutes with PBS. The embryos were incubated overnight (O/N) at 4°C with the BAMs monoclonal primary antibodies (Torode et al., 2015; Torode et al., 2016) diluted 1/10 in PBS with 5% milk. Antibodies were washed with PBS three times for 5 minutes each. The cells were then incubated O/N at 4°C with the secondary antibody anti-rat conjugated with FITC diluted 1/100 in PBS. Antibodies were washed three times for 10 minutes each with PBS. The embryos were then stained for 30 minutes with 20 μ M of Calcofluor (Fluorescent Brightener 28, Sigma-Aldrich, St. Louis, MI, USA) and washed three times with PBS. Finally, the embryos were mounted in Vectashield (H-1000-10, Vector®, with or without DAPI) and covered with a coverslip.

Labeling of actin filaments

The actin labeling protocol was a modified version of Rabillé et al. (2018). First, the material was prefixed at 300 μ M m-maleimido benzoic acid N-hydroxy succinimide ester (MBS; Sigma-Aldrich®), 0.2% Triton X-100, and 2% dimethyl sulfoxide (DMSO) in MTB for 30 minutes in the dark and at room temperature (RT). Fixation took place without washes for 1 hour and 30 minutes in the dark and at RT. Material was fixed at the same time as the actin labeling with 2% paraformaldehyde (PFA), 0.2% glutaraldehyde (GTA), and 2 U of Rhodamine-conjugated phalloidin (Ph-Rh; R415, Invitrogen™) or Alexa-fluor™ 488 conjugated phalloidin (Ph-Alexa488; A12379, Invitrogen™). After cells were washed with MTB:PBS 1:1, the cell wall was digested with cell wall lysis buffer in 1:1 MTB:PBS and the same composition of enzymes as above with the addition of 5 U Ph-Rh/ Ph-Alexa488 and 0.15% Triton

X-100. The incubation in the modified cell wall lysis buffer took place for 10 minutes in the dark at RT. The extraction step took place with 5% DMSO, 3% Triton X-100, and one of the Phalloidin conjugates (2U) in PBS for 10 minutes in the dark and at RT. The actin filaments were finally stained with 15U of the chosen Phalloidin conjugate in MTB:PBS 1:1, overnight at 4°C in the dark. The nucleus was stained with DAPI and before observation, the material was mounted in Vectashield H-1000-10 (Vector®).

Latrunculin B treatments

Eggs, zygotes, and embryos of 2 to 8 cells were treated with a range of concentrations from 50 nM to 1 µM of Latrunculin B (Sigma Aldrich) or incubated in 0.1% or 1% DMSO (Latrunculin B solvent used here as a control). Their growth was then monitored every day for up to 7 days using bright-field microscopy (DMI8 inverted microscope, Leica Microsystems). Samples treated for 1 week with 1 µM LatB were used for the immunostaining experiments (results shown in Supplementary Figure 2).

Image acquisition

Image data were acquired using the bright-field and epifluorescence microscope DMI8 (Leica Microsystems) equipped with the color camera DMC4500 (Leica Microsystems), Leica EL6000 compact light source, and controlled with LAS X v3.0 (Leica Microsystems). Confocal microscopy was performed using a TCS SP5 AOBS inverted confocal microscope (Leica Microsystems) controlled by the LASAF v2.2.1 software (Leica Microsystems). Data analysis was conducted using FIJI (Schindelin et al., 2012).

Observations of FITC, Calcofluor White, and autofluorescence of the cells were carried out using a TCS SP5 AOBS inverted confocal microscope (Leica Microsystems) with the HCX PL APO CS 20.0x0.70 DRY UV objective. The excitation wavelengths for DAPI/Calcofluor White, FITC, and chloroplasts were 405nm, 488nm, and 496-514nm, respectively. The emission wavelength ranges were 415-469nm for DAPI/Calcofluor White, 415-469nm for FITC, and 661-749nm for chloroplasts. The opening of the pinhole was set to 1AU, and line average and line accumulation were set to 1.

Observation of Rhodamine or Alexa488-phalloidin labeled AFs was carried out using a TCS SP8 AOBS inverted confocal microscope (Leica Microsystems) with the 100X/NA 1.4 objective.

Acknowledgement

S.B was funded by the Region Bretagne (project “Primaxis”, grant number 1749) and Sorbonne University. I.T was funded by an ARED grant from the Bretagne Regional Council (“PUZZLE” Project) and NMBU. We are grateful to MITI CNRS for additional financial support. Part of the work was funded by the European Union (ERC, ALTER e-GROW, project number 101055148). Views and opinions expressed are, however, those of the author(s) only and do not necessarily reflect those of the European Union or the European Research Council Executive Agency. Neither the European Union nor the granting authority can be held responsible for them. For the purpose of open access dissemination, a CC-BY-NC license has been applied by the authors to this document.

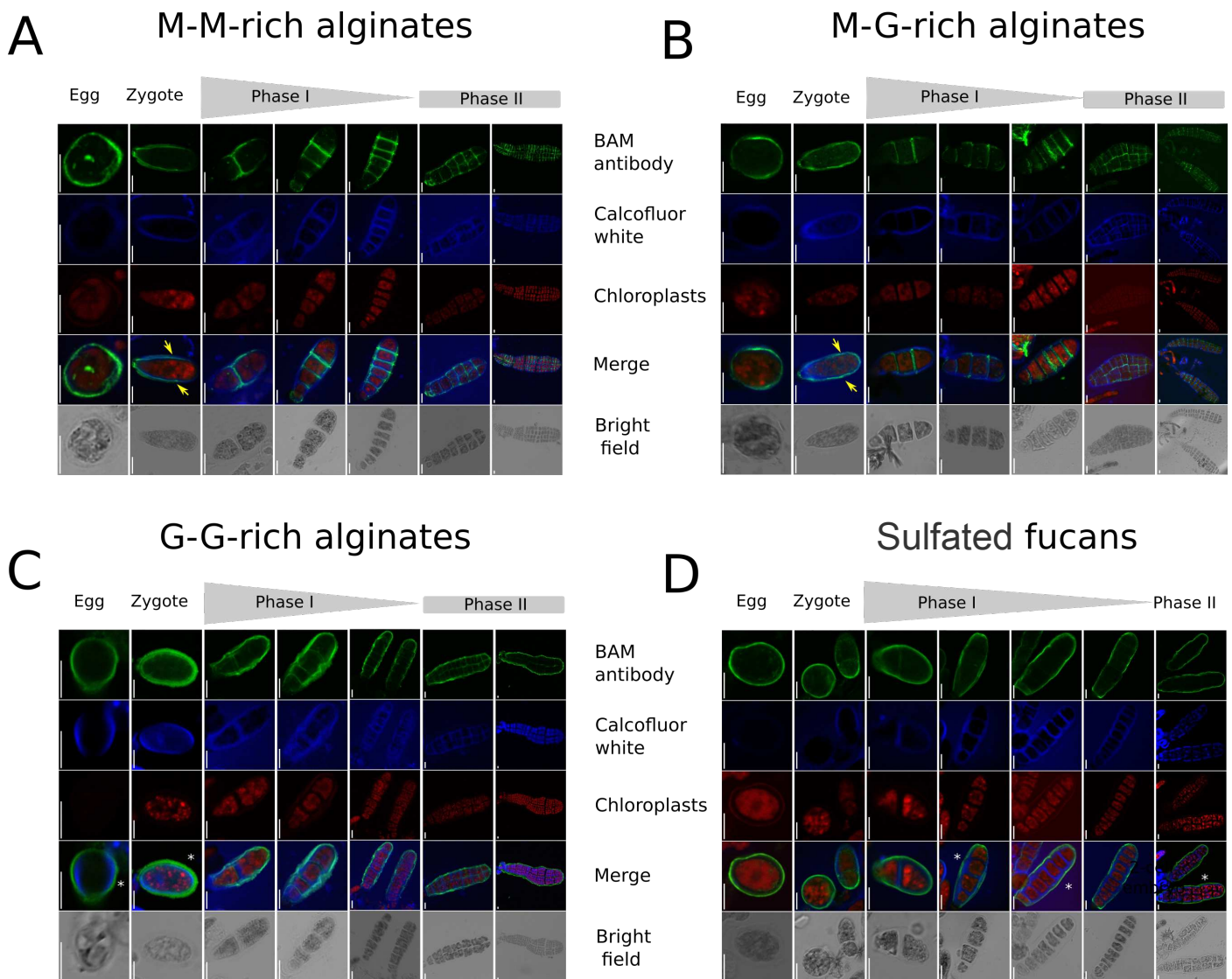
References

- Bisgrove, S. R. and Kropf, D. L.** (2001). Cell wall deposition during morphogenesis in fucoid algae. *Planta* **212**, 648–658.
- Bogaert, K. A., Beeckman, T. and De Clerck, O.** (2017a). Two-step cell polarization in algal zygotes. *Nat Plants* **3**, 16221.
- Bogaert, K. A., Beeckman, T. and De Clerck, O.** (2017b). Egg activation-triggered shape change in the Dictyota dichotoma (Phaeophyceae) zygote is actin–myosin and secretion dependent. *Ann Bot* **120**, 529–538.
- Charrier, B., Rabillé, H. and Billoud, B.** (2019). Gazing at Cell Wall Expansion under a Golden Light. *Trends Plant Sci.* **24**, 130–141.
- Deniaud-Bouët, E., Hardouin, K., Potin, P., Kloareg, B. and Hervé, C.** (2017). A review about brown algal cell walls and fucose-containing sulfated polysaccharides: Cell wall context, biomedical properties and key research challenges. *Carbohydrate Polymers* **175**, 395–408.

- Fischl, R., Bertelsen, K., Gaillard, F., Coelho, S., Michel, G., Klinger, M., Boyen, C., Czjzek, M. and Hervé, C.** (2016). The cell wall active mannuronan C5-epimerases in the model brown alga *Ectocarpus*: from gene context to recombinant protein. *Glycobiology*.
- Hable, W. E.** (2014). Rac1 signaling in the establishment of the fucoid algal body plan. *Front. Plant Sci.* **5**, 690.
- Hable, W. E. and Kropf, D. L.** (2005). The Arp2/3 complex nucleates actin arrays during zygote polarity establishment and growth. *Cell Motility* **61**, 9–20.
- Hable, W. E., Miller, N. R. and Kropf, D. L.** (2003). Polarity establishment requires dynamic actin in fucoid zygotes. *Protoplasma* **221**, 193–204.
- Hable, W. E., Reddy, S. and Julien, L.** (2008). The Rac1 inhibitor, NSC23766, depolarizes adhesive secretion, endomembrane cycling, and tip growth in the fucoid alga, *Silvetia compressa*. *Planta* **227**, 991–1000.
- Harnvanichvech, Y., Borassi, C., Daghma, D. E. S., van der Kooij, H. M., Sprakel, J. and Weijers, D.** (2023). An elastic proteinaceous envelope encapsulates the early Arabidopsis embryo. *Development* dev.201943.
- Hawes, D., Shi, S.-R., Dabbs, D. J., Taylor, C. R. and Cote, R. J.** (2009). Immunohistochemistry. *Modern Surgical Pathology* 48–70.
- Henry, C. A., Jordan, J. R. and Kropf, D. L.** (1996). Localized membrane-wall adhesions in *Pelvetia* zygotes. *Protoplasma* **190**, 39–52.
- Inoue, A. and Ojima, T.** (2019). Functional identification of alginate lyase from the brown alga *Saccharina japonica*. *Sci Rep* **9**, 4937.
- Karyophyllis, D., Katsaros, C., Dimitriadis, I. and Galatis, B.** (2000). F-Actin organization during the cell cycle of *Sphacelaria rigidula* (Phaeophyceae). *European Journal of Phycology* **35**, 25–33.
- Katsaros, C. I., Karyophyllis, D. A. and Galatis, B. D.** (2002). Cortical F-actin underlies cellulose microfibril patterning in brown algal cells. *Phycologia* **41**, 178–183.
- Katsaros, C., Karyophyllis, D. and Galatis, B.** (2003). F-actin cytoskeleton and cell wall morphogenesis in brown algae. *Cell Biology International* **27**, 209–210.
- Katsaros, C., Karyophyllis, D. and Galatis, B.** (2006). Cytoskeleton and morphogenesis in brown algae. *Ann. Bot.* **97**, 679–693.
- Katsaros, C., Nagasato, C., Terauchi, M. and Motomura, T.** (2013). Cytokinesis in brown algae. In *Advances in Algal Cell Biology*, p. 224. Berlin, Boston: De Gruyter.
- Le Bail, A. and Charrier, B.** (2013). Culture Methods and Mutant Generation in the Filamentous Brown Algae *Ectocarpus siliculosus*. In *Plant Organogenesis* (ed. De Smet, I.), pp. 323–332. Humana Press.
- Lockhart, J. A.** (1965). An analysis of irreversible plant cell elongation. *Journal of Theoretical Biology* **8**, 264–275.

- Mazéas, L., Yonamine, R., Barbeyron, T., Henrissat, B., Drula, E., Terrapon, N., Nagasato, C. and Hervé, C.** (2022). Assembly and synthesis of the extracellular matrix in brown algae. *Semin Cell Dev Biol* S1084-9521(22)00071-4.
- McCully, M. E.** (1965). A note on the structure of the cell walls of the brown alga fucus. *Can. J. Bot.* **43**, 1001–1004.
- Motomura, T.** (1990). Ultrastructure of Fertilization in *Laminaria angustata* (Phaeophyta, Laminariales) with Emphasis on the Behavior of Centrioles, Mitochondria and Chloroplasts of the Sperm. *Journal of Phycology* **26**, 80–89.
- Muzzy, R. and Hable, W.** (2013). RAC1 regulates actin arrays during polarity establishment in the brown alga, *Silvetia compressa*. *Developmental Biology* **383**, 28–38.
- Nagasato, C. and Motomura, T.** (2009). Effect of Latrunculin B and Brefeldin a on Cytokinesis in the Brown Alga *Scytosiphon Lomentaria* (scytosiphonales, Phaeophyceae)1. *Journal of Phycology* **45**, 404–412.
- Nagasato, C., Inoue, A., Mizuno, M., Kanazawa, K., Ojima, T., Okuda, K. and Motomura, T.** (2010). Membrane fusion process and assembly of cell wall during cytokinesis in the brown alga, *Silvetia babingtonii* (Fucales, Phaeophyceae). *Planta* **232**, 287–298.
- Pollock, E. G.** (1970). Fertilization in *Fucus*. *Planta* **92**, 85–99.
- Rabillé, H., Koutalianou, M., Charrier, B. and Katsaros, C.** (2018). Actin fluorescent staining in the filamentous brown alga *Ectocarpus siliculosus*. In *Protocols for Macroalgae Research* (ed. Charrier, B., Wichard, T.), and Reddy, C.), pp. 365–379. Boca Raton: Taylor & Francis group, CRC Press.
- Rabillé, H., Billoud, B., Tesson, B., Le Panse, S., Rolland, É. and Charrier, B.** (2019a). The brown algal mode of tip growth: Keeping stress under control. *PLoS Biol.* **17**, e2005258.
- Rabillé, H., Torode, T. A., Tesson, B., Le Bail, A., Billoud, B., Rolland, E., Le Panse, S., Jam, M. and Charrier, B.** (2019b). Alginates along the filament of the brown alga *Ectocarpus* help cells cope with stress. *Sci Rep* **9**, 12956.
- Terauchi, M., Nagasato, C., Inoue, A., Ito, T. and Motomura, T.** (2016). Distribution of alginate and cellulose and regulatory role of calcium in the cell wall of the brown alga *Ectocarpus siliculosus* (Ectocarpales, Phaeophyceae). *Planta* **244**, 361–377.
- Theodorou, I. and Charrier, B.** (2023). The shift to 3D growth during embryogenesis of kelp species, atlas of cell division and differentiation of *Saccharina latissima*. *Development* **150**, dev201519.
- Theodorou, I., Opsahl-Sorteberg, H.-G. and Charrier, B.** (2021). Preparation of Zygotes and Embryos of the Kelp *Saccharina latissima* for Cell Biology Approaches. *Bio-protocol* e4132–e4132.

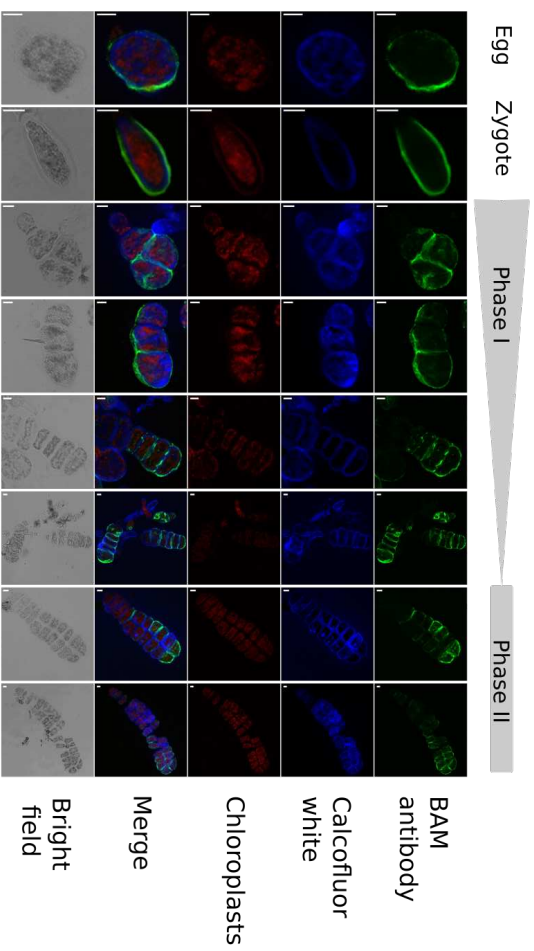
- Torode, T. A., Marcus, S. E., Jam, M., Tonon, T., Blackburn, R. S., Hervé, C. and Knox, J. P.** (2015). Monoclonal Antibodies Directed to Fucoidan Preparations from Brown Algae. *PLOS ONE* **10**, e0118366.
- Torode, T. A., Siméon, A., Marcus, S. E., Jam, M., Le Moigne, M.-A., Duffieux, D., Knox, J. P. and Hervé, C.** (2016). Dynamics of cell wall assembly during early embryogenesis in the brown alga *Fucus*. *J. Exp. Bot.* **67**, 6089–6100.
- Varvarigos, V., Katsaros, C. and Galatis, B.** (2004). Radial F-actin configurations are involved in polarization during protoplast germination and thallus branching of *Macrocystis pyrifera* (Phaeophyceae, Laminariales). *Phycologia* **43**, 693–702.
- Varvarigos, V., Galatis, B. and Katsaros, C.** (2007). Radial endoplasmic reticulum arrays co-localize with radial F-actin in polarizing cells of brown algae. *European Journal of Phycology* **42**, 253–262.
- Vázquez-Gutiérrez, J. L. and Langton, M.** (2015). Current potential and limitations of immunolabeling in cereal grain research. *Trends in Food Science & Technology* **41**, 105–117.
- Wakatsuki, T., Schwab, B., Thompson, N. C. and Elson, E. L.** (2001). Effects of cytochalasin D and latrunculin B on mechanical properties of cells. *Journal of Cell Science* **114**, 1025–1036.
- Yonamine, R., Ichihara, K., Tsuyuzaki, S., Hervé, C., Motomura, T. and Nagasato, C.** (2021). Changes in Cell Wall Structure During Rhizoid Formation of *Silvetia babingtonii* (Fucales, Phaeophyceae) Zygotes. *Journal of Phycology* **57**, 1356–1367.



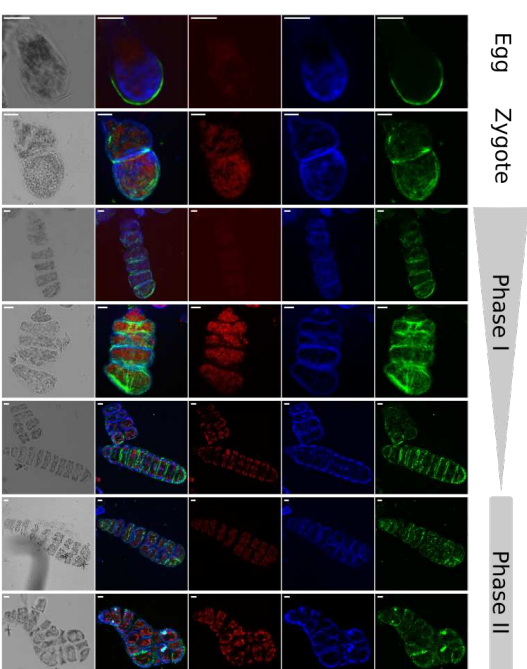
Suppl. Figure 1: Confocal microscopy images of eggs, zygotes, and embryos labelled with BAM6, BAM7, BAM10, and BAM4 antibodies (green) and Calcofluor White (blue).

A) M-M-rich alginates labelled with BAM6; B) M-G-rich alginates labelled with BAM7; C) G-G-rich alginates labelled with BAM10; D) Sulfated fucans labelled with BAM4. Red signal shows the autofluorescence of chloroplasts. Grey: bright field. White asterisk indicates where cellulose is observed more internally than G-G rich alginates or sulfated fucans. Yellow arrows show where cellulose is more external than M-M and M-G-rich alginates. Scale bars: 10 μ m.

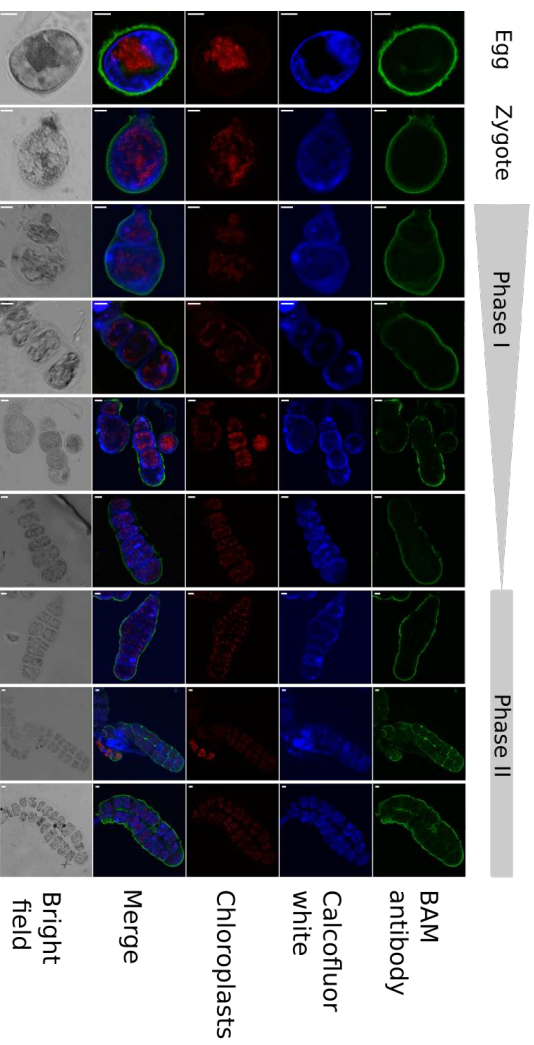
M-M-rich alginates



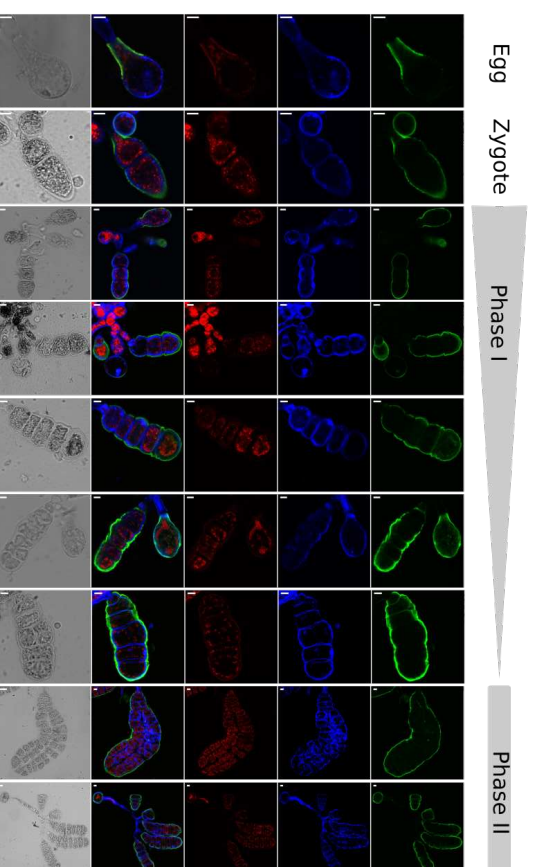
M-G-rich alginates



G-G-rich alginates



Sulfated fucans



Suppl. Figure 2 (previous page): Confocal microscopy images of eggs, zygotes, and embryos treated for one week with Latrunculin B.

A) M-M-rich alginates labelled with BAM6; B) M-G-rich alginates labelled with BAM7; C) G-G-rich alginates labelled with BAM10; D) Sulfated fucans labelled with BAM4. Green: BAM antibodies; Blue: Calcofluor White (cellulose). Red signal shows the autofluorescence of chloroplasts. Grey: bright field. Note that the unfertilized eggs are not labelled because they have no cell wall at that stage. White asterisk indicates where cellulose is observed more internally than G-G rich alginates or sulfated fucans. Scale bars: 10 μ m.

4 - Chapter II

**MUM, a maternal unknown message,
inhibits early establishment of the
medio-lateral axis in the embryo of
the kelp *Saccharina latissima***

Abstract:

This chapter highlights the role of the embryo's connection to its maternal tissue in development. Microdissection techniques enabled the physical separation of the embryo. This revealed the necessity of the attachment up to the 8-cell stage. When disconnected, the embryo loses distinct axes, presenting smaller and rounder cells. We suggest the involvement of a Maternal Unknown Message (MUM) that regulates the division orientation in early brown algae development.

Contribution:

All the organisms used during the experiments were cultured, imaged, and segmented by myself and I. Theodorou. Embryos were sectioned from their gametophyte using a micropipette for which I designed the protocol, based on recommendations provided in 2020 by Marina Linardić (post-doc in S. Braybrook's team). I conducted most of the microdissections to disconnect embryos from their stalk. Over a period of six months (September - February 2022), I taught T. Joemmanbacks, a Master 2 student, in learning how to culture and experiment on *Saccharina latissima*. Tanweer participated in providing additional samples dissected from their stalk. I conducted photo acquisition of all samples. The software to analyze the segments was coded by B. Billoud, and the software results were analyzed by both B. Billoud and myself. With the assistance of S. Le Panse (Roscoff imaging platform Merimage), I performed transmission electron microscopy experiments. I significantly contributed to the results, discussion, and writing presented in the corresponding article.

MUM, a maternal unknown message, inhibits early establishment of the medio-lateral axis in the embryo of the kelp *Saccharina latissima*

Samuel Boscq, Bernard Billoud*, Ioannis Theodorou, Tanweer Joemmanbacks and Bénédicte Charrier*

Morphogenesis of Macro Algae, UMR8227, CNRS - Sorbonne University, Station Biologique de Roscoff, Place Georges Teissier, 29680 Roscoff, France

* Current address: Institut de Génomique fonctionnelle de Lyon (IGFL), UMR5242, ENSL, CNRS, INRAE, UCBL, 32-34 avenue Tony Garnier, 69007 Lyon, France

Corresponding author:

benedicte.charrier@cnrs.fr

Introduction

In all organisms, the establishment of spatial axes during embryonic development serves as the fundamental basis for organizing the developing body. Despite the immense morphological diversity exhibited by eukaryotes, the majority of organisms can still be characterized by three primary body axes (Anlas and Trivedi, 2021). These axes can be defined based on morphological asymmetry (Barthélémy and Caraglio, 2007; Deline et al., 2018; Martinez et al., 2016), or by the presence of molecular gradients within the embryo (Friml et al., 2003; Shahbazi et al., 2019; Simsek and Özbudak, 2022). Symmetry-breaking events are crucial for establishing axes within initially homogeneous states, and this process is the key behind the facilitation of cell differentiation. However, although polarity is often associated with axis establishment, axial determination can occur independently of polarity in certain symmetrical systems (Cove, 2000).

Brown algae (also named Phaeophyceae) have evolved diverse morphologies (Bogaert et al., 2013; Bringloe et al., 2020; Charrier et al., 2012), ranging from small filamentous forms (e.g., order Ectocarpales) to large multilayered parenchymatous

bodies that can reach up to 40 m (e.g., order Laminariales) (Cribb, 1954). They diverged from the ancestors of other extant multicellular organisms at the root of the eukaryotic tree at least 1 billion years ago and emerged as complex multicellular organisms relatively recently, around 250 million years ago (Burki et al., 2020; Kawai et al., 2015). Being evolutionarily distinct from animals, fungi, plants, and other algae, brown algae possess unique biological mechanisms (Charrier et al., 2019; Nagasato et al., 2022; Terauchi et al., 2015). They have evolved diverse complex embryonic patterns. For example, contrary to some land plants and metazoans, which develop inside the maternal tissue, brown algae embryos are usually free-growing. Furthermore, after the initial stages of development, they develop simple morphologies. These two features make them easier to access for imaging and manipulation and consequently, brown algae such as *Fucus*, *Ectocarpus*, and *Dictyota* have become developmental models to study polarized cell growth (Bogaert et al., 2017; Goodner and Quatrano, 1993; Rabillé et al., 2019). Reports on *Fucus* and *Dictyota* have shown that the elongation of oospheres occurs only after fertilization by sperm, but environmental cues such as light can change symmetry, shifting the orientation of the cell before the selection of the axis (Bogaert et al., 2015; Jaffe, 1968).

Unlike these species, no environmental cue such as light polarization has been reported to affect the formation of the body plans in Laminariales. These algae, like those of orders Desmarestiales and Sporochnales, undergo embryogenesis while being physically connected to their maternal tissue (Fig. 1) (Fritsch, 1945; Klochkova et al., 2019; Wiencke and Clayton, 1990). Therefore, they are powerful models for studying the influence of maternal factors on embryogenesis in brown algae. Although detailed studies have shed light on the impact of maternal tissue on the development of animal and land plant embryos, there is limited documentation for brown algae.

In the genus *Saccharina*, a member of the Laminariales group, the egg and developing embryo maintain a connection to the maternal tissue throughout embryogenesis. During the initial stages of development, the *Saccharina* egg cell possesses two anchored flagella that facilitate attachment to the gametangia that has differentiated from the filamentous maternal gametophyte (Fig. 1A) (Klochkova et al., 2019). After karyogamy, these flagella degrade (Fig. 1B), but the zygote firmly

anchors its base to the female gametophyte, potentially through the accumulation of glycoconjugates (Klochkova et al., 2019). In 1936, Kanda (Kanda, 1936) was the first to report the abnormal shapes of embryos that happened to detach from the maternal gametophyte. Recently, the early developmental pattern of the *Saccharina latissima* sporophyte was described in three main steps, corresponding to the establishment of three distinct body plans (Theodorou and Charrier, 2023) (Fig. 1C-E). After fertilization, the zygote elongates, followed by parallel transverse divisions that lead to the development of an 8-cell stack. Both processes — elongation and transverse divisions — establish and maintain the apico-basal axis, respectively (Phase I, Fig. 1C). Subsequently, the embryo undergoes two-dimensional growth, forming the medio-lateral axis, and growth in these two axes, the apico-basal axis on the one hand and the medio-lateral axis on the other hand forms a small cellular monolayered lamina (also named blade) (Phase II, Fig. 1D). The transition to three-dimensional growth and cellular tissue differentiation (Phase III, Fig. 1E) begins once the blade reaches around 800–1000 cells (Theodorou and Charrier, 2023). In this article, we present a detailed analysis of how the maternal gametophyte controls the establishment of the medio-lateral axis in the early development of the *S. latissima* sporophyte. Using microdissection to separate the maternal gametophyte from the sporophytic embryo, we monitored the development of the early embryos over time. Image segmentation followed by quantitative analyses of the morphological traits made it possible to assess the role of the maternal tissue in the control of body plan formation in the very early stages of embryogenesis.

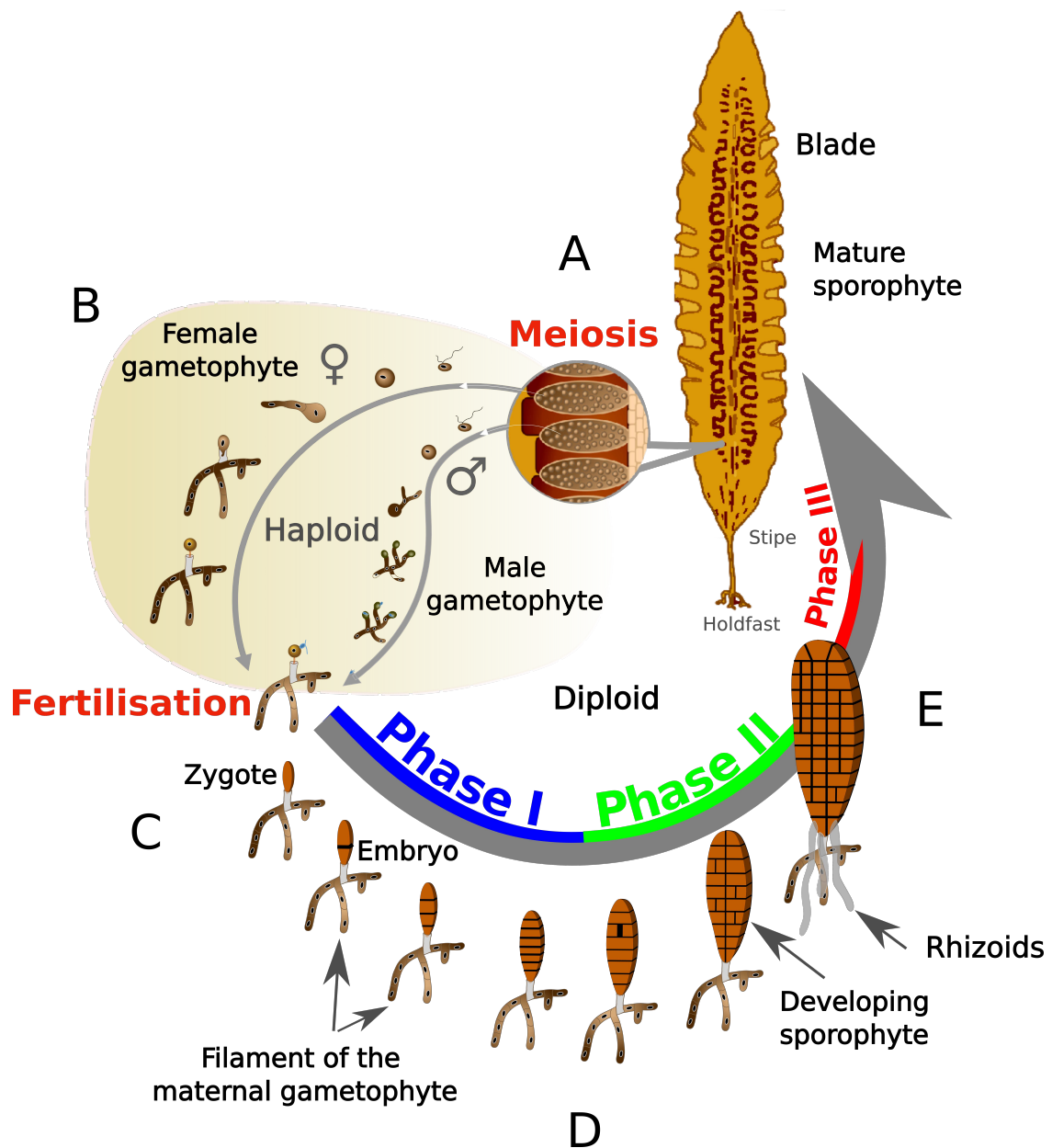


Figure 1: Life cycle of *Saccharina latissima*

A. In mature sporophyte blades, meiosis occurs inside sporangia, and motile meiospores are released in large amounts. The spores fall on the seafloor (or plastic or glassware in the laboratory) and germinate. B. Spores develop into female and male filamentous gametophytes. When the necessary environmental conditions are met, both types of gametophytes mature, and the female gametangium (named oogonium) releases one egg, and the male gametangium (named antheridium) releases one sperm cell. C. After fertilization, the embryo elongates along the X-axis and initially develops attached to the female gametophyte, undergoing a succession of transverse, parallel divisions perpendicular to the zygote axis, up to the formation of a linear stack of 8 cells (Phase I in blue). D. The embryo starts dividing longitudinally and continues growth by alternating longitudinal and transverse cell divisions (Phase II in green). E. About 15 days after fertilization, the embryo initiates the first divisions in the Z-axis and undergoes cell differentiation (Phase III in red). The embryo then continues to develop into a mature sporophyte. Color codes for the three embryogenetic phases are according to Theodorou and Charrier (2023).

Results

To comprehensively investigate the role of maternal tissue in the growth of the embryo, we mechanically detached embryos from the stalk of the female gametophyte at different developmental stages and monitored embryogenesis for up to 14 days in standard culture conditions. Using a micro-needle, we sectioned the embryo from the maternal tissue at the egg (E₀), zygote (E₁), 2-cell (E₂), 4-cell (E₄), 8-cell (E₈) and Phase II (PhII) (embryo) stages. The impact of the separation of the egg/zygote/embryo (hereafter named E/Z/E) was observed in Phase II, when embryos grow along longitudinal and lateral directions.

Detachment from the stalk impairs both growth and development of the embryos

We observed a wide range of resulting morphological alterations. A significant proportion of embryos either immediately ceased developing or perished within five days (less than 20% in E₄ or earlier embryos, not shown). We excluded these embryos from the following analyses.

The remaining living and growing embryos (i.e., at least 80% of the samples) displayed a range of morphogenetic responses illustrated in Fig. 2. Compared with intact embryos (Fig. 2A), those dissected from the stalk before the first cell division (egg E₀, Fig. 2B; zygote E₁, Fig. 2C) displayed the most modified patterns. Although 20% of the growing embryos microdissected from eggs (E₀) experienced only a delay in growth, 80% exhibited morphological alterations (e.g., heart-shaped; Fig. 2B). These percentages were similar for microdissected zygotes (E₁) (Fig. 2C and 2H). In contrast, in E₂ and E₄ microdissected embryos, a significant percentage displayed a developmental pattern comparable to intact embryos (Fig. 2D and 2E, respectively, and Fig. 2H). In the E₈ and PhII embryos, the effect of detachment from the stalk was weak, with nearly 80% of the microdissected embryos exhibiting a typical developmental pattern (Fig. 2F and G, respectively, and Fig. 2H). These data indicate that the connection between the embryo and the stalk before the 8-cell stage is necessary for normal growth and morphogenesis of the embryo.

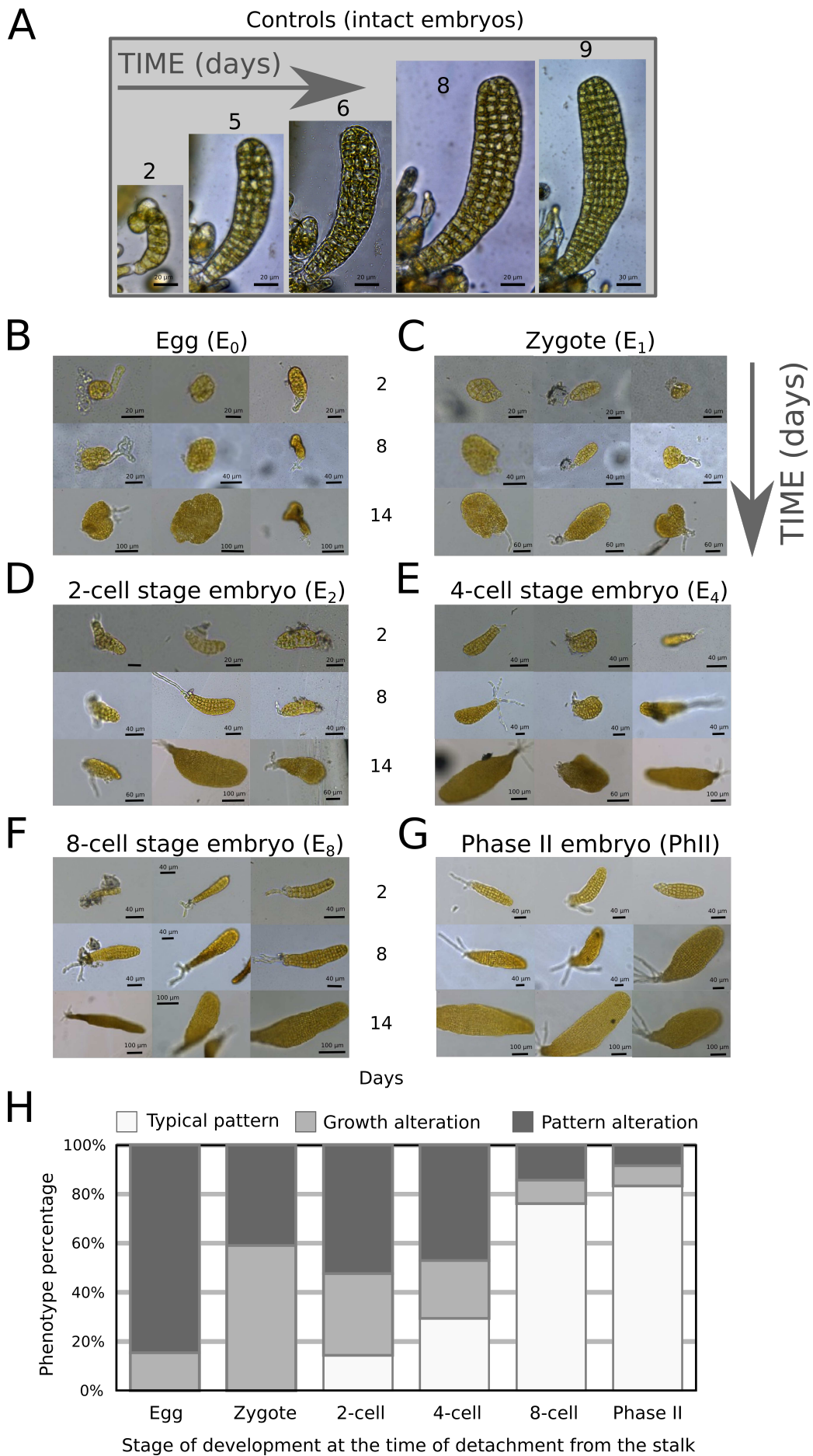


Figure 2 (previous page): Qualitative impact of embryo detachment from the stalk

Comparison of morphologies in control embryos (A) with growing embryos after being detached from the stalk by microdissection at the egg (E₀) (B), zygote (E₁) (C), 2-cell (E₂) (D), 4-cell (E₄) (E), 8-cell (E₈) (F) stage and early Phase II (PhII) (G) and observed 2, 8 and 14 days after microdissection. Three embryos illustrate the representative phenotypes obtained for each microdissection time point. The number of microdissected embryos was n = 4 (A), 100 (B), 100 (C), 80 (D), 80 (E), 40 (F), 40 (G). H) Stacked histogram showing the percentage of each class of phenotype. "Typical pattern" corresponds to morphologies similar to the control; "growth alteration" includes all growth delays, and "pattern alteration" corresponds to morphological differences compared with the developmental pattern in intact embryos as displayed in (A). The percentage of typical phenotypes gradually increases with later stage detachment, up to the E₈ stage after which Phase II embryos generally develop similar to intact embryos.

To quantitatively study the impact of dissection from the maternal stalk on the morphogenesis of embryos, we monitored the development of another series of microdissected embryos for 10 days using bright-field microscopy. First, images were captured every day for 4 days, then every two days, and segmented manually (Suppl. Fig. 1). From the segmentation images, quantitative values of several morphometric parameters were obtained from the analysis of the cell outlines using in-house software (Suppl. Table 1) and then compared with statistical tests (see Methods for details; Suppl Table 2 for the statistical results).

Detachment from the maternal stalk leads to a disruption of the body plan and reduced growth

To observe how the shape of the embryo is affected by separation from the maternal tissue, we measured the length and width of PhII embryos containing between 48 and 103 cells ([48:103]). This developmental interval, expressed in the number of cells and not in the number of days of growth, helped to mitigate the effect of the delay in growth due to the stress of the microdissection experiment. Furthermore, neither egg release nor fertilization are synchronous in *Saccharina*; using embryo age as a reference was therefore impossible with the current protocol of embryo production (Theodorou et al., 2021).

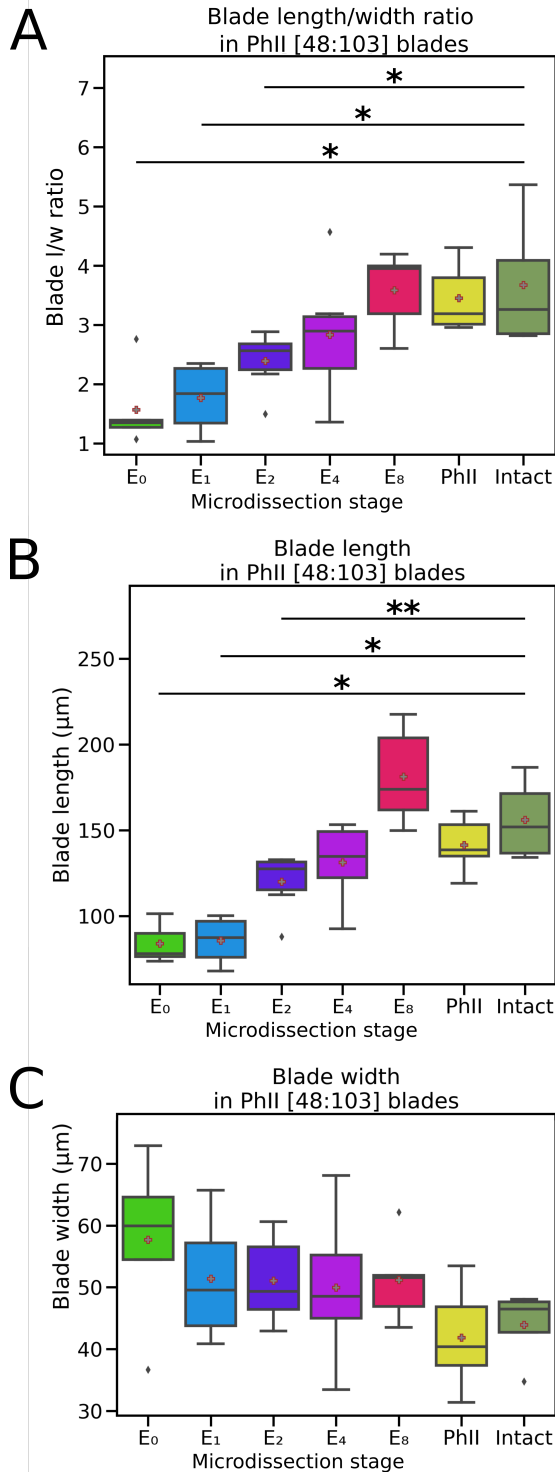


Figure 3: Shape of growing embryos in response to the separation from the maternal tissue

The length and width of Phase II (PhII) embryos made up of 48 to 103 cells [48:103] were measured using in-house bladePainter software and plotted. The middle line represents the median, the box encompasses 25% of the values, and the whiskers represent 75%. The mean is indicated by a plus sign (+). A. Length/width (l/w) ratio of embryo blade (lamina); B. Length of the embryo blade; C. Width of the embryo blade. n=5 for E₀, 4 for E₁, 6 for E₂, 6 for E₄, 5 for E₈, 5 for PhII and 4 for control (Intact). Mann-Whitney test p-value: * <math> < 5.10^{-2}</math>; ** <math> < 1.10^{-2}</math>; *** <math> < 10^{-3}</math>.

We observed that, in contrast to the intact embryos that display a length/width (l/w) ratio of ~ 3.5 reflecting their elongated shape, detaching the egg from the maternal tissue resulted in embryos with a disk-like shape (l/w ratio ~ 1) (Fig. 3A).

Furthermore, detachment at different stages between the egg and PhII embryos revealed a gradient in the response: the earlier the separation, the more disk-like the embryo. Sectioning the stalk resulted in a reduction of growth along the longitudinal axis (Fig. 3B) (1.9 times less in E_0 relative to intact embryos; P value $< 5 \cdot 10^{-2}$) as well as an increase in growth along the medio-lateral axis (Fig. 3C) (1.3 times more in E_0 relative to intact embryos; not statistically supported). Therefore, the stalk controls the balance between the two growth axes.

These changes in the direction of growth were accompanied by a significant reduction in the surface area of the blade, up to 30% less than intact embryos (E_0 and E_1 ; P value $< 5 \cdot 10^{-2}$; Suppl. Table 2).

These changes in l/w ratio (and to a lesser extent in surface area) were not only observed in embryos of 43–103 cells but also in earlier embryos (Suppl. Fig. 2). This suggests that as in intact organisms, the microdissected embryos maintain the ratio that they had at the time of detachment from the maternal tissue, at least in the ‘time’ window between 20 and ~ 100 cells. Beyond that stage, embryos seem to recover from the impact of the detachment from the stalk. For most samples in the cell stage window [104:307], the embryo blades had a similar l/w ratio and surface area to intact embryos (Suppl. Table 2). Thus, the detachment from the stalk appears to be essential in the early stages of embryogenesis. This suggests that a signal related to the maternal stalk controls the development of the embryo. This maternal unknown message (hereafter named “MUM”) operates in real-time from the egg stage to the 8-cell stage, albeit decreasing in importance with time, and its impact on embryo morphology lasts up to the 100-cell stage.

Detachment from the maternal stalk results in altered cell shape and growth

Cell growth

We assessed potential alterations of cell growth by measuring cell area using in-house 'Redraw-blade' software after segmentation (Suppl. Table 3). Cells of embryos separated from their maternal stalk displayed smaller sizes, and the effect was stronger when dissection occurred early on, i.e., between the production of eggs and the formation of PhII blades (Fig. 4A). Although the average cell size in intact embryos is $69.30 \mu\text{m}$, E_0 embryos measured $57.51 \mu\text{m}$. Therefore, MUM controls cell size by up to 17% of the reference cell size. This trait was also

observed in younger (developmental window: [20;47] cells) and older embryos (developmental window: [104;250] cells) (Suppl. Table 3) (Suppl. Fig. 3). A heatmap of cell area showed that cells with reduced size were not located in specific positions within the embryo but were spread throughout the embryo (Fig. 4B).

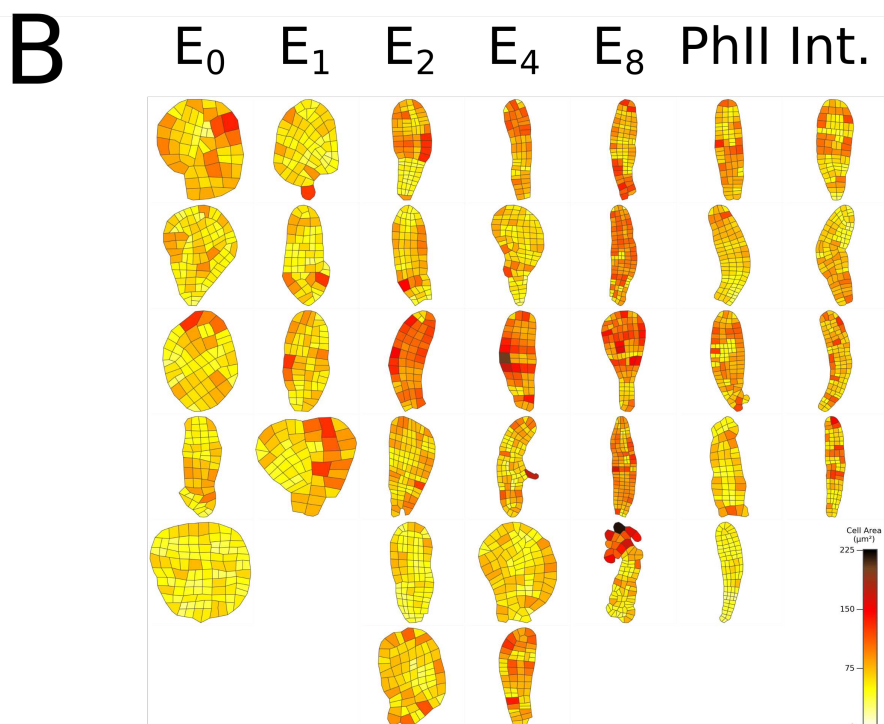
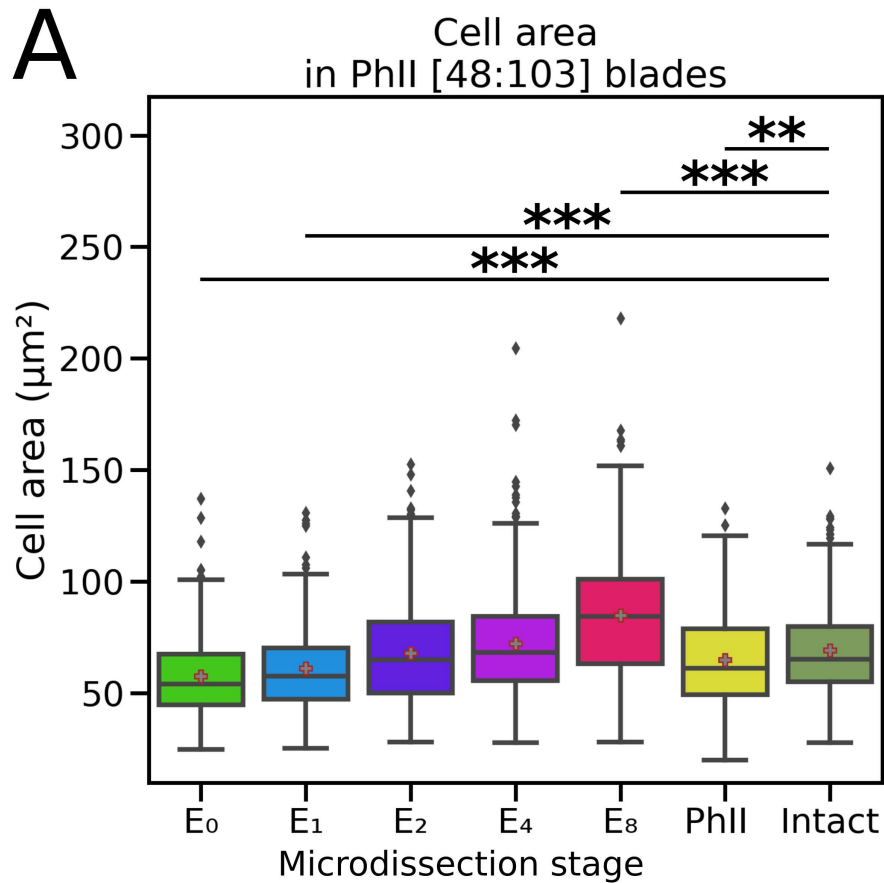


Figure 4 (previous page): Cell size, expressed as cell surface area of growing embryos detached from maternal tissue

The cell surface areas of 48–103 cell embryos ([48;103]) were measured using in-house bladePainter software and plotted. The middle line represents the median, the box encompasses 25% of the values, and the whiskers represent 75%. A. Cell area (μm^2); $n=325$ for E_0 , 220 for E_1 , 423 for E_2 , 415 for E_4 , 430 for E_8 , 462 for PhII and 306 for control embryos (Intact). t -test p -values: * $<5.10^{-2}$; ** $<1.10^{-2}$; *** $<10^{-3}$. B. Heatmap of cell area within each embryo considered in A. The color scale on the right indicates the range of cell areas observed in the intact and microdissected samples. The size of the image was adjusted so that all blade images have the same dimensions (scales are different).

We addressed whether the decrease in cell size was due to a reduction in cell growth or to a faster cell division rate. From another series of microdissected E/Z/E monitored with images taken every 2 h, we measured the cell division rate and compared it with that of intact embryos (Suppl. Fig. 4). In these microdissected E/Z/E, cell division took place at the same pace as in intact ones (Fig. 5). Therefore, in the absence of MUM, we hypothesize that cells are smaller because they expand less while maintaining an unchanged cell division rate. Therefore, MUM appears to promote cell growth independently of cell division.

Cell shape and impact on neighboring cells

We defined a rectangularity factor to quantify cell shapes in microdissected and intact embryos. The rectangularity factor was calculated based on a minimum bounding rectangle fitted around the polygonal contour of each cell. The factor equals one when the cell shape, taken in 2D, is a perfect rectangle (all angles joining two sides are 90°), and tends to zero as the angles deviate from this value, corresponding to a “flatter” quadrilateral or a more irregular polygon.

At the 48–103 cell stage (Suppl. Table 3), we noted that cells from microdissected embryos were less rectangular than those of intact embryos (Fig. 6A). Similar results were obtained in early and late PhII embryos (Suppl. Fig. 5). In intact embryos, cells with a shape distinct from a perfect rectangle were mainly located at the apex of the blade, where the shape of the blade is curved. In the microdissected embryos, irregular polygons were observed scattered throughout the disk-like blade, with no specific location (Fig. 6B).

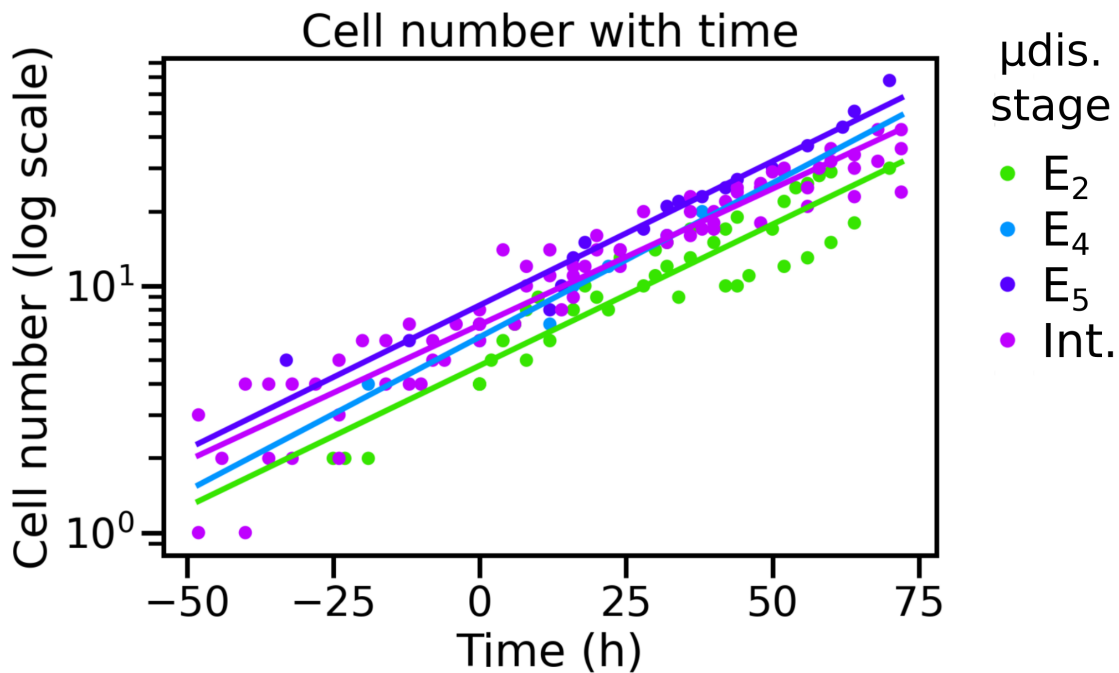


Figure 5: Cell division rate over time in growing embryos detached from maternal tissue

The number of cells of intact (Int.) or microdissected (μ dis.) embryos imaged every two hours was plotted over time (total duration of the time-lapse: 11 days). The slope of the logarithm of this number of cells represents the growth rate. $n=3$ for E₂, 1 for E₄, 1 for E₅, and 5 for the controls.

We studied the impact of this change in cell shapes on the topology of the tissue. Specifically, the number of cell neighbors was calculated for each cell. Intact embryos were excluded from this quantification as controls because they were segmented manually with a different technique that produced more “broken” outlines and resulted in an overestimation of the number of cell neighbors. In Phll embryos, the number of cell neighbors was distributed into two main groups (Fig. 7A): cells at the periphery of the blade that were surrounded by three neighbors (one above, one below, and one side) and cells located inside the blade surrounded by four neighbors (above, below, and both left and right sides) (Fig. 7B). In the Phll embryos, only 8.3% of cells had five neighbors, whereas in E₀ and E₁ microdissected embryos, 15.7% and 21.4% of cells, respectively, were surrounded by five neighbors (Fig. 7A). Similarly, 1.4% of cells of Phll embryos had six cell neighbors, reaching 4.9% and 3.6% in E₀ and E₁, respectively.

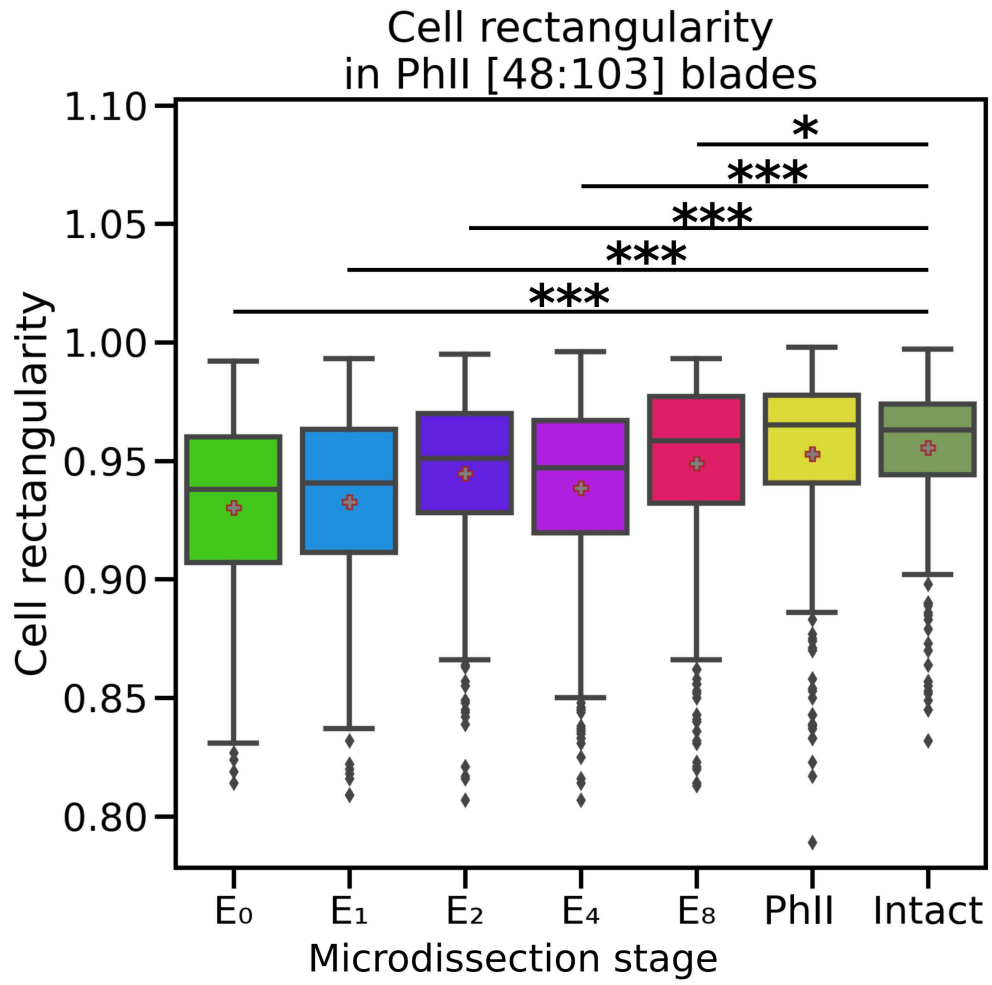
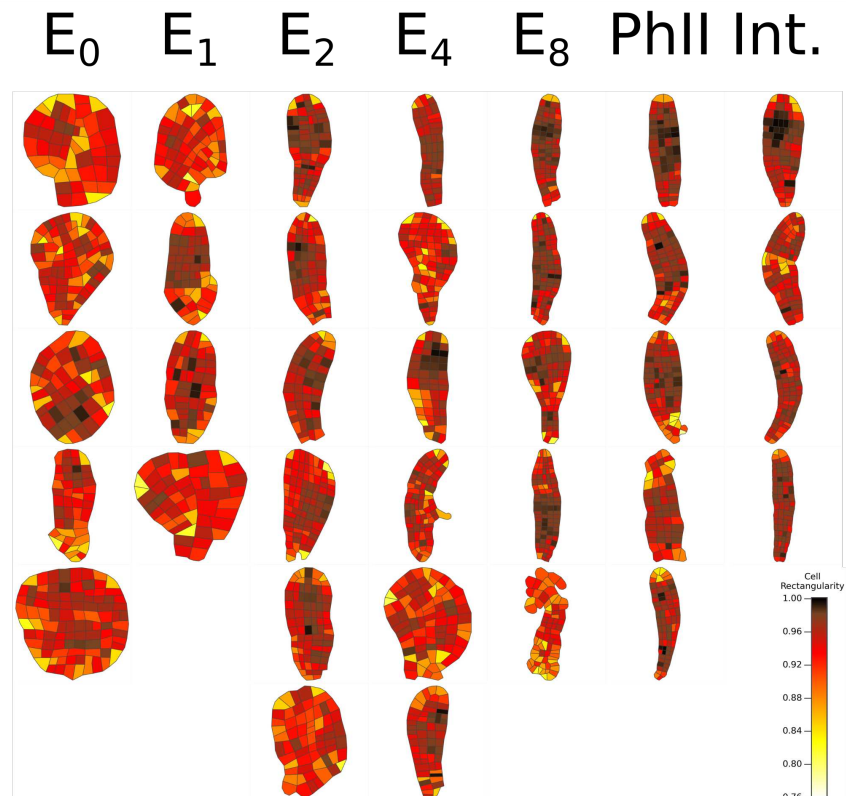
A**B**

Figure 6 (previous page): Cell shape in growing embryos detached from maternal tissue

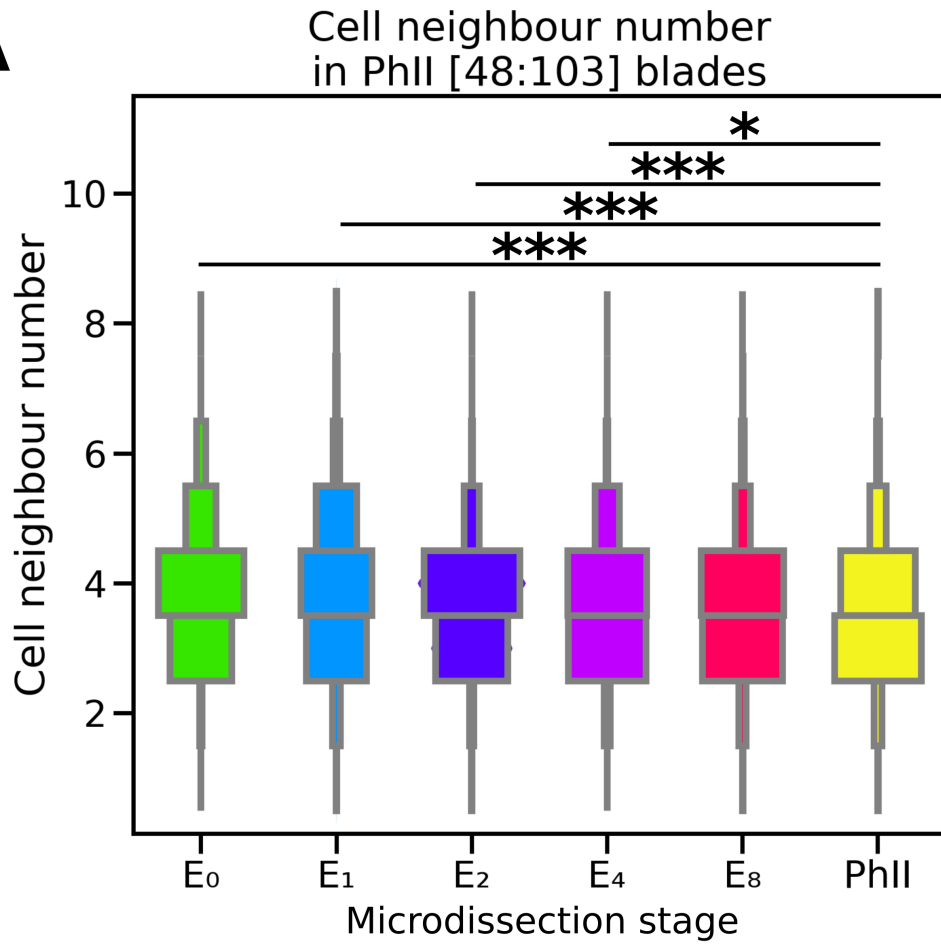
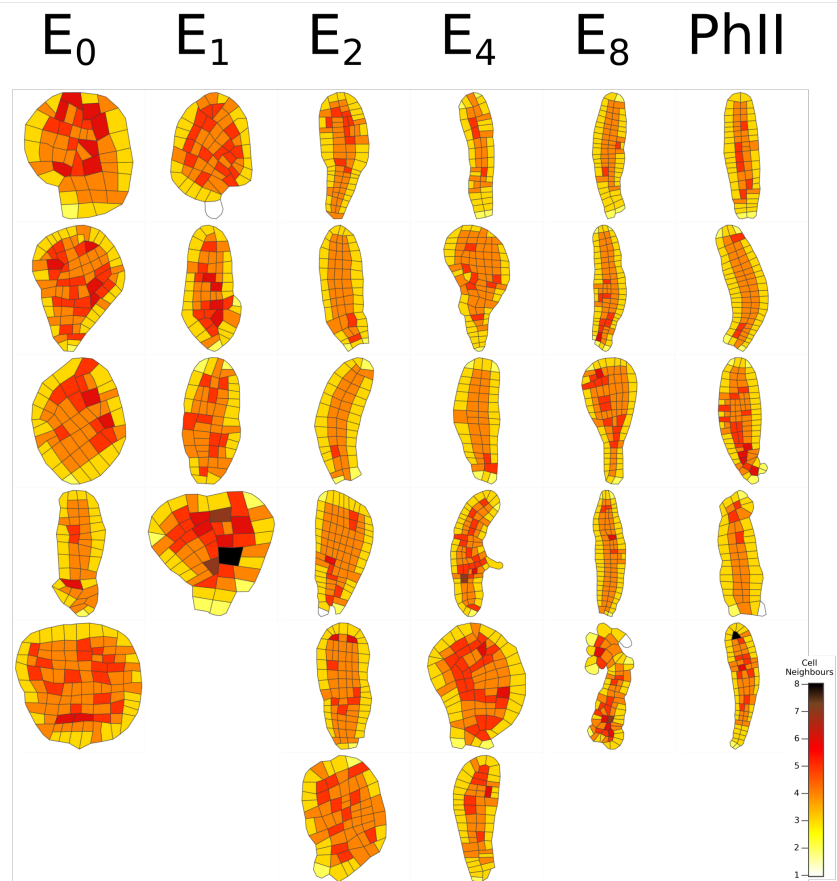
The shape of cells of 48–103 cell embryos ([48;103]) was quantified. A. The shape of the cell, expressed by a rectangularity factor, which assesses the level of rectangularity of a parallelepiped (cuboid cell seen in 2D). The rectangularity factor is 1 for a parallelepiped with perpendicular sides and < 1 for all other cases. This factor is the lowest for parallelepipeds with very acute angles. $n=325$ for E_0 , 220 for E_1 , 423 for E_2 , 415 for E_4 , 430 for E_8 , 462 for PhII and 306 for control embryos. t -test p -values: * $<5.10^{-2}$; ** $<1.10^{-2}$; *** $< 10^{-3}$. B. Heatmap of the rectangularity factor. The color scale on the right indicates the range of values. The size of the image was adjusted so that the image of each blade has the same dimensions as in the figure.

The heatmap shows that these cells were located within the lamina tissue with no specific position related to the apico-basal or medio-lateral axes. Altogether, the general distribution of the number of cell neighbors was significantly different in E_0 , E_1 , E_2 (P value $< 10^{-3}$ for the three embryo stages; Suppl. Table 2) and E_4 (P value $< 5.10^{-2}$; Suppl. Table 2) embryos compared with PhII embryos (Fig. 7A). Similar results were obtained at earlier and later developmental stages (Suppl. Table 3) (Suppl. Fig. 6).

In summary, the blade displayed an altered topology with a higher proportion of cells with more than four neighbors, presumably because these cells were irregularly shaped. In addition, our results showed that cells were smaller than in the intact embryos, which may further contribute to an altered cell arrangement within the blade. Nevertheless, the cells maintain their l/w ratio, at least up to the 100-cell stage (not shown; Suppl. Table 2 for statistical results).

Figure 7 (next page): Topology of the blade in a growing embryos detached from maternal tissue

The topology of the growing embryo was studied by counting the number of cells surrounding each cell of 48–103 cell embryos ([48,103]). A. The number of neighboring cells was plotted. $n=325$ for E_0 , 220 for E_1 , 423 for E_2 , 415 for E_4 , 430 for E_8 , 462 for PhII (used as a control). t -test p -values: * $<5.10^{-2}$; ** $<1.10^{-2}$; *** $< 10^{-3}$. B. Heatmap of the number of neighboring cells for each blade cell. The color scale on the right indicates the range of values. The size of the image was adjusted so that the image of each blade has the same dimensions as in the figure.

A**B**

The disruption of the body plan is due to early longitudinal cell divisions in Phase I

So far, we have shown that the separation of the E/Z/E from the maternal filament resulted in morphological defects in PhII embryos. Namely, the embryos developed as disk-like blades, with smaller, irregularly shaped cells, which are haphazardly arranged within the lamina. To determine whether MUM controls cell shape and size as the main targets, thereby affecting embryo shape, or whether MUM controls embryo shape, which in turn affects cell shape and size, we looked at the earlier steps of embryo development. We observed that the detachment of embryos from the maternal stalk modified the orientation of their initial cell divisions. This effect was stronger when detachment occurred in the E₀ and E₁ stages. Longitudinal cell division parallel to the position of the stalk took place soon after the separation of the egg or zygote from the maternal tissue (Fig. 8A, C), whereas in embryos microdissected at the 8-cell stage or in intact embryos (Fig. 8B), longitudinal cell division rarely took place before the 8-cell stage (transition to Phase II). This difference in the timing of longitudinal cell division suggests that MUM controls the orientation of the cell divisions in the initial stages of embryogenesis.

This result made it possible to identify the cause of the disorganization of the embryo morphology observed in Phase II. In early Phase I, the primary longitudinal, apico-basal axis is not yet fully established, and the occurrence of longitudinal divisions perpendicular to this axis in the absence of MUM results in embryo growth along the medio-lateral axis. This contrasts with intact embryos exposed to MUM, where a linear stack of eight cells is produced before the second body axis is established.

In the absence of MUM, no oblique cell divisions were observed, only divisions either parallel or perpendicular to the stalk prior to dissection (Fig. 8). Therefore, MUM does not control the orientation of cell division *per se*, but only the conditions of when and where longitudinal divisions occur.

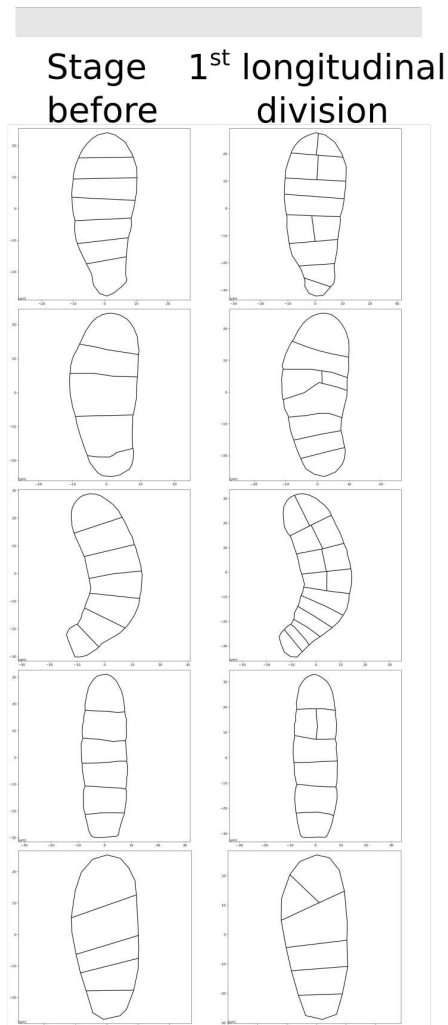
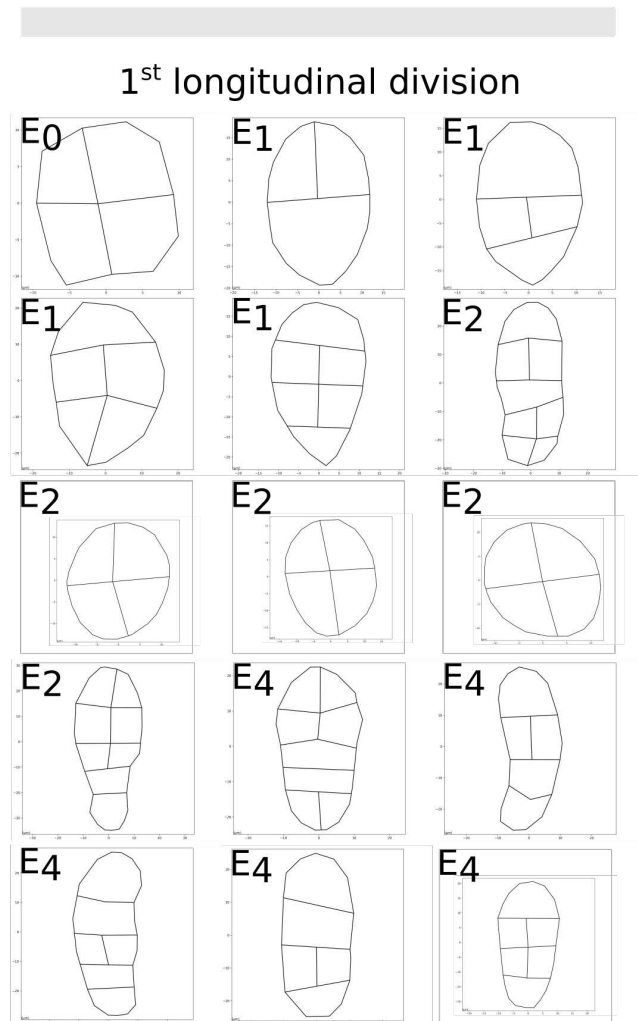
A**Control
(intact stalk)****B****Detachment from the stalk**

Figure 8: Early longitudinal cell division in growing embryos detached from maternal tissue

The pattern of the embryo blade is displayed at the stage of the occurrence of the first longitudinal cell division(s). A. Patterns one time-lapse step before (left) and at the emergence (right) of the first longitudinal cell division are displayed for control organisms for which five time-lapse experiments were monitored. B. Pattern of segmented lamina, which underwent detachment from maternal tissue at the E₀, E₁, E₂ or E₄ stages (stage of microdissection is indicated in the left-hand corner of each picture). Longitudinal cell division takes place much earlier than the 8-cell stage and often just after dissection from the stalk.

MUM is a short-range signal

What is MUM and how does it act ?

MUM is a local signal

Firstly, we tested whether MUM is a diffusible factor by immersing detached E/Z/E into Petri dishes containing intact fertile gametophytes. We did not observe any modification in embryo development compared with experiments in which embryos were isolated from the maternal tissue and transferred into a Petri dish with fresh seawater (not shown). This result suggests that there is no molecular or chemical compound excreted from the maternal gametophyte that diffuses in seawater and controls the development of the embryo. Secondly, we investigated whether maternal tissues distant from the embryo, but belonging to the same gametophyte as the embryo, were necessary for proper embryo development. This experiment aimed to test whether a signaling molecule is transported symplastically or apoplastically through the maternal gametophyte filament up to the embryo. We cut or damaged cells of the gametophyte that were directly adjacent to or separated by a few cells from the stalk, and we monitored the development of the embryos for the following 2 weeks. These zygotes developed similarly to control zygotes (Fig. 9). Most zygotes developed a stack of up to eight cells before their first transverse anticlinal division and continued their growth in 2D, forming long ovoid blades without any bleaching, a sign of stress. Therefore, the proper development of these embryos suggests that maternal cells close to or adjacent to the embryo do not control its early development.

These two experiments support that MUM is neither a signaling factor diffusing in seawater to the E/Z/E, nor a signaling factor transported from cell to cell in the female gametophyte to the stalk. Therefore, MUM is a signaling factor related to the stalk itself.

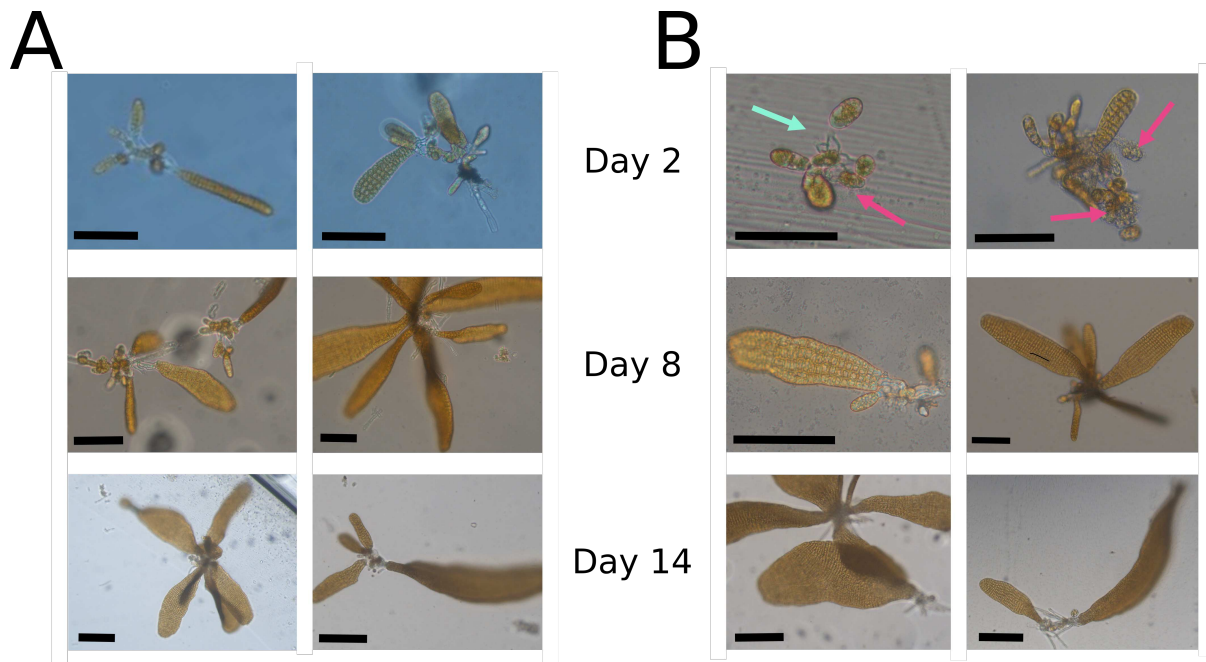


Figure 9: Lack of morphological impact of damaged cells close to the embryo

Because in our experiment, gametophytes are made up of about 10–15 cells, several eggs were produced at different times. Hence, after fertilization, embryos grew within a “bouquet” of several embryos all attached to a single maternal gametophyte. A. Normal conditions of growth. B. Cells of neighboring embryos of the same “bouquet” (pink arrows) or of the maternal gametophyte (light blue arrow) were crushed or pierced with the microdissection pipette. Embryos were monitored 2, 8, and 14 days after damaging the tissues. Two examples of each condition are shown at each time point. Scale bars are 50 μm for 2 days, 100 μm for 8 days, and 200 μm for 14 days post cell damage. $n=4$ gametophytes bearing several embryos at each time point (different embryos are photographed between time points).

The stalk is a dead structure

The literature indicates that, in Laminariales, the oocyte is released from the mature oogonium through the ejection of the cellular content of the oogonium from an opening at its apex, thereby producing a protoplast (the egg) and a remnant cell wall of the oogonium (Lüning, 1981) (Klochkova et al., 2019). We confirmed that the remnant cell wall of the oogonium in *Saccharina latissima* is a dead structure by staining it with Trypan blue (TB), which is a negatively charged dye that living cells with intact membranes do not take up (Farah et al., 2015). TB accumulated in the stalks as well as in dead gametophyte cells, which were used here as controls (Fig. 10). Interestingly, TB staining was stronger at the apex of the stalk near the

connection to the embryo. Previous experiments have shown that the stalk interior is highly viscous, and we have observed this viscous material leaking from the stalk when pierced upon mechanical or laser manipulation (Boscq et al., 2022). Therefore, in addition to confirming that the stalk is a dead structure, TB showed that its interior is dense and heterogeneous.

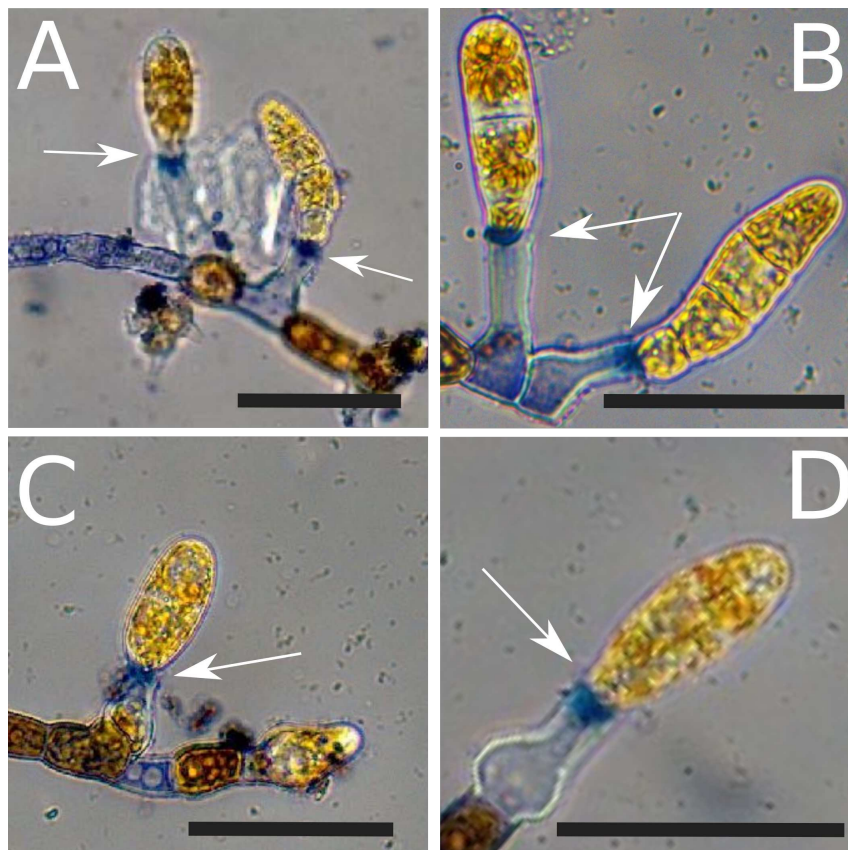


Figure 10: Trypan blue staining of the cell connecting the maternal tissue to the embryo of *Saccharina latissima*

Embryos are fixed to the stalk (white arrows). Tissue exposed to Trypan blue showed blue precipitates in the remaining volume of the gametophyte cell from which the egg emerged. The stalk was more deeply stained at its apex compared with its base. While some empty cells of the maternal gametophyte were also stained, indicating that they are dead (A, C), live cells remain brown (early stage embryos and gametophyte cells). Four examples are shown (A–D). Scale bar, 50 μm .

The stalk is necessary for the control of the formation of the longitudinal axis

It has long been reported that eggs naturally detached from the stalk develop abnormally (Kanda, 1936 ; Sauvageau, 1918 p. 155 on *Laminaria flexicaulis*, former name of *Laminaria digitata*, which also belongs to order Laminariales). Growth is delayed and the distinction of axes is lost (Fig. 11A). Moreover, although uncertainties persist due to the absence of observations of cell division at very early stages of embryogenesis by these authors, it nevertheless seems that this response is different from that observed when the stalk is sectioned. Based on additional observations when the embryo is forcefully pulled apart, instead of delicately cutting the top part of the stalk, we observed that, in addition to the loss of a distinct secondary axis, cells behaved erratically (Fig. 11B, Suppl. Movie 1). Embryos divided in all directions and presented bulging cell shapes. This observation is congruent with previous studies where embryos detached naturally or when flagella were removed (Sauvageau, 1918; Klochkova et al., 2019). These cases are distinct from the induced development in the absence of the stalk (Fig. 8).

Discussion

In this study, we investigated the critical factors that influence the establishment of body axes during embryogenesis in brown algae. Our findings provide insights into the role of maternal tissue, particularly the stalk, in establishing the two primary axes of the body plan.

The first body axis of the embryo is the longitudinal axis (X-axis; (Theodorou and Charrier, 2023), reportedly established upon fertilization of the egg of Laminariales (Kanda, 1936). After fertilization, the egg of *Laminaria angustata*, another member of the Laminariales like *Saccharina latissima*, accumulates vacuoles in the future apical region and chloroplasts in the basal region close to the female flagella (Motomura, 1990). However, in rare cases, we observed the release of elongated eggs (not shown), suggesting that egg elongation can occur before fertilization, also reported in (Lüning, 1981). After fertilization, cells continue to divide transversally. Interestingly, different genera in order Laminariales display different distributions of transverse and longitudinal cell division orientations (Kanda, 1936; Kanda, 1938;

Kanda, 1941; Sauvageau, 1918), resulting in embryos with varied length-to-width ratios. Therefore, control of the Y-axis establishment is a common but plastic trait among individual embryos and among Laminariales species.

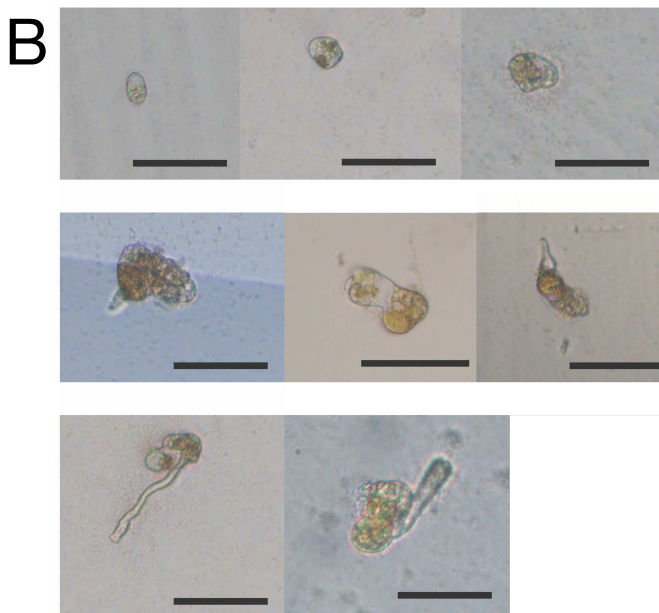


Figure 11: Abnormal embryos growing from eggs naturally detached from the maternal gametophyte

Eggs that were detached from the maternal tissue by sea currents or after shaking the Petri dish developed into embryos with major growth delays (A, embryos circled in red) and loss of the main body axes (B). Scale bar, 100 μm .

The formation of the medio-lateral axis is controlled by a maternal unknown message (MUM)

We showed that detaching the embryo from the maternal tissue in the very early stages of embryogenesis results in embryogenesis defects. The embryo growth axes were disturbed. Intact embryos grew in length, but embryos separated from their parental tissue tended to grow as a disk, thereby losing their anisotropic shape. Looking at the very first steps of embryogenesis, we noticed that longitudinal cell divisions occurred earlier than in intact embryos. Intact embryos first divided only transversally up to the 8–10-cell stage, whereas the microdissected embryos initiated longitudinal cell division as soon as the 2-cell stage. Notably, in the latter case, longitudinal cell division never occurred before the 2-cell stage, suggesting that the egg axis is aligned with the stalk prior to that stage, perhaps before the oocyte is released. Therefore, while the X-axis of the zygote seems to be established at the egg stage at the latest, its maintenance and the establishment of the Y-axis depend on the contact of the sporophyte with the female gametophyte. As well as controlling the formation of body axes, MUM could be a trophic factor, as microdissected embryos have smaller surface areas than intact embryos.

MUM is a local signal emitted from the stalk at the very beginning of embryogenesis

For most morphometric and topological parameters observed in this study, the effect of MUM was stronger at the egg and zygote stages than at the 2-cell, 4-cell, 8-cell, and early Phase II embryos. Furthermore, the embryo response was gradual from the egg-stage to the 8-cell stage. When the embryo has reached Phase II, detachment from the stalk no longer has any effect. Therefore, MUM acts in the very first step of embryogenesis.

Furthermore, sectioned embryos growing together (in the same Petri dish) with the female gametophyte they were sectioned from, or with distinct intact female gametophytes, had similar effects to embryos detached from the maternal tissues and transferred to a distinct Petri dish. Therefore, MUM does not appear to be a signaling factor able to diffuse in seawater from fertile female gametophytes but instead requires direct contact with the E/Z/E. Can MUM diffuse from the filament of

the maternal gametophyte? Very surprisingly, in nature, normal embryos can grow from a maternal gametophyte made up of only one cell (Kanda, 1936). Similarly, in the lab, meiospores collected from a wild fertile sporophyte that were immediately exposed to white light germinate and grow into one cell and immediately produce an oogonium (Lüning, 1981; Theodorou et al., 2021). In both cases, the embryos grow in the same manner as those attached to a multicellular gametophyte. Therefore, MUM cannot be a signal diffusing from the filaments of the maternal gametophyte, which suggests that MUM acts locally at the level of the stalk.

Interestingly, in embryos that have grown up to 1000 cells (end of Phase II), the base of the blade remains the narrowest part of the embryo. Observations show that longitudinal division is less frequent in this region (not shown). However, although the stalk physically remains present up to the end of Phase II when the embryo reaches around 1000 cells, the impact of MUM is reduced to the very early stages of Phase I as shown in this study. Therefore, another factor must relay the inhibitory effect of MUM on the widening of the base after the 8-cell stage.

Is MUM the egg flagella embedded into the stalk?

Female centrioles, through their role in the formation of flagella anchored to the stalk, are thought to be responsible for the formation of the embryo's longitudinal axis (Klochkova et al., 2019). When the egg is devoid of flagella (e.g., manually pulled away from the stalk, or separated by shaking the flask), most eggs stop growing (Klochkova et al., 2019). Furthermore, it is thought that the phenotypes observed by (Kanda, 1936) and (Sauvageau, 1918) on detached embryos (supposedly at the egg stage), which are to some extent reminiscent of those observed in this study, may be due to a loss of flagella at the egg stage. Hence, MUM would be related to — or even be — the flagella. However, several arguments reject this hypothesis. First, the microdissection method that we used, even if not precise, usually left some of the stalk attached to the E/Z/E, and therefore, the flagella were most likely not sectioned and were, at worst, only damaged. Secondly, the female centrioles, which are necessary for flagella, degrade as early as the zygote stage (Motomura, 1990; Motomura, 1991), but the phenotypes that we report were observed when the stalk was detached up to the 4-cell stage, and even the 8-cell stage (cell rectangularity). Some authors have shown that flagella can

remain up to the 2-cell stage (Klochkova et al., 2019). However, it must be a rare case corresponding to the flagella devoid of centrioles trapped in the mucoid component of the stalk. Therefore, the persistence of MUM action throughout most of Phase I embryogenesis excludes that MUM is the flagellar structure itself. Male centrioles replace the female centrioles at the zygote stage (Motomura et al., 2010). In our study, ablation of the stalk was carried out after fertilization (except for E₀ for which we are not sure whether microdissection took place before or after fertilization), and hence the male centrioles were present. Nevertheless, we observed cell division and morphological defects when the stalk was removed up to the 8-cell stage. Therefore, MUM is distinct from the male centrioles as well. Altogether, it appears unlikely that MUM corresponds to either centrioles or flagella.

Is MUM chemical or mechanical?

The stalk is a dead structure composed of an inert cell wall filled with viscous material

The remnant cell wall of the oogonium contains some mucosal compounds (Klochkova et al., 2019) (and our own observations). We never observed any intracellular content, such as autofluorescent chloroplasts, or DAPI-stained nuclei, but some authors have reported the presence of some oogonium cytoplasm leftovers in other families of Laminariales (e.g., *Alaria*: (Klimova and Klochkova, 2017). Interestingly, in other families of Laminariales, the basal cell of the embryo (e.g., in *Eisenia bicyclis*, *Ecklonia* sp.) or the maternal gametophyte itself (in *Undaria* sp.) grows into this empty space once the egg has been released (Kanda, 1941). When the embryo itself grows into the empty stalk, the stalk does not modify its development (Kanda, 1941) (*Eisenia*, plate 37). Therefore, although the stalk appears to be a volume that the embryo can occupy, it is filled with seemingly inert, viscous components. These viscous components are most likely polysaccharides extruded from the stalk cell wall or from the embryo itself. Furthermore, the cell wall of the stalk does not appear to be able to modify cell fate, unlike the cell wall of the rhizoid of the *Fucus* brown alga embryo, as reported by (Berger et al., 1994; Bouget et al., 1998).

Is MUM a constricting collar?

The region of the stalk interacting with the E/Z/E coincides with the presence of a thick cell wall collar (Kanda, 1936; Klimova and Klochkova, 2017), which may clasp the basal region of the zygote and subsequently the early embryo, thereby preventing its growth in the Y-axis. However, how this mechanical constraint could act beyond the very base of the zygote/embryo is difficult to understand.

Is MUM polysaccharides accumulated at the stalk-embryo junction?

Instead, the polysaccharides of the stalk cell wall could serve as a source of signaling glycoconjugates. In the kelps *Saccharina* and *Alaria*, a cocktail of polysaccharides, mainly composed of α -D-glucose, α -D-mannose, and L-fucose, has been shown to accumulate at the junction between the stalk and the egg (Klimova and Klochkova, 2017; Klochkova et al., 2019). This cocktail, which reflects the presence of specific alginates and fucans — being the two main components of the cell wall in brown algae (Charrier et al., 2019) —, can no longer be detected when the egg is free-floating, unattached to the stalk or to another substratum. Therefore, the stalk-zygote junction is a specific site where the composition of the cell wall differs from the rest of the surface of the zygote. Could this cocktail be MUM? The role of sugars as signaling molecules involved in development remains to be demonstrated in brown algae but is well known in other organisms such as plants (Mishra et al., 2022; Wang et al., 2021).

MUM diffuses basipetally through Phase I embryos

In intact embryos, the first longitudinal division usually occurs in the upper half of the embryo, suggesting that the first cells out of MUM control are apical cells. This characteristic is observed in many members of Laminariales (Sauvageau, 1918) and of other orders (e.g., *Sacchoriza*, Tilopteridales (Fritsch, 1945; Norton, 1972). This indicates a ubiquitous and basipetal mode of action of MUM, in which the inhibitory effect is strong in the basal part of the embryo but diminishes towards the apex.

A distance-based inhibitory relationship with a signaling molecule is not a foreign concept in brown algae, especially kelps. For instance, the reproductive structures (sori) are formed away from the growing region that surrounds the transition zone,

due to the action of a sporogenesis inhibitor (Buchholz and Lüning, 1999; Pang and Lüning, 2004), which may be auxin (Kai et al., 2006).

Plasmodesmata, which have been observed in both early (up to the 4-cell stage, not shown) and later stages of *Saccharina* embryogenesis (Theodorou and Charrier, 2023), may contribute to the formation of a symplastically diffusible gradient of molecules originating from the stalk, forcing transverse cell divisions throughout the embryo. This action could be achieved by any type of compound, as long as its size does not exceed 20–40 kDa (10–20 nm) (Nagasato et al., 2017), which is a much larger size compared with land plant plasmodesmata.

Reconsidering all these hypotheses on the nature of MUM, i.e., that of a signal produced directly (MUM is a glycoconjugate) or indirectly (MUM is a degradation product of glycoconjugate) either from the viscous content filling the stalk or from its thick collar, remains the most likely to explain the diffusible nature of MUM, inhibiting longitudinal divisions during the 5-day-long Phase I over a distance of around 100 μm . This hypothesis remains to be confirmed, and the exact chemical nature of MUM characterized.

Evolution of the maternal tissue-embryo connection

The ancestor of the Stramenopiles, the main group comprising brown algae, diverged from their eukaryotic ancestors at least 1 billion years ago (Burki et al., 2020). Among brown algae, at least five orders (Laminariales, Chordales, Sporochnales, Desmarestiales, and to a lesser extent Tilopteridales) display a stalk-mediated, physical connection of the embryo with the maternal tissue that persists over the egg or zygote stages (Fritsch, 1945). Although stalks connecting eggs with maternal tissue are common in Fucales (Burridge et al., 1993), this connection is transient and does not persist after fertilization.

Compared with other multicellular organisms, this type of interaction is rare in the tree of life. In the green alga *Coleochaete* sp. (Chlorophyta), the zygote remains attached to the female gametophyte until it completes a series of divisions and releases up to 32 biflagellate spores. This spore release excludes any gametophyte-dependent development of an embryo. Furthermore, this is a case of matotrophy only (Haig, 2015), unlike the case of *Saccharina*.

In several red algae (Gelidiales, Gracilariales), the (carpo)sporophyte develops on the maternal gametophyte, but in the form of gonimoblasts, diploid filaments that produce carpospores, which disperse before developing into diploid (tetra)sporophytes away from the maternal tissue (van der Meer, 1979). Thus, maternal tissue does not directly control sporophyte morphogenesis, and its relationship with the carposporophyte (filamentous gonimoblast) is trophic (matrotrophy). The trophic link is particularly evident in Gelidiales and Gracilariales, where nutrient cells and nutrient filaments are found, respectively. In the red alga *Palmaria palmata*, however, the situation is similar to that of *Saccharina*: the embryo develops as a macroscopic elongated blade, in physical contact with dwarf haploid maternal tissue (Gall et al., 2004; van der Meer and Todd, 1980). However, it is not known whether the latter has an impact on the development of the embryo's growth axes.

In contrast, in bryophytes (group comprising the mosses, liverworts, and hornworts), the developing embryo is surrounded by a layer of maternal cells, making up the archegonium (Naf, 1962), and subsequently covered by the calyptra, a cell layer of female origin, thereby protecting the embryo from desiccation (Budke et al., 2012). First, the embryo is formed and develops nested within the archegonium cavity, and then emerges out of it. Subsequent evolution of this branch led to increasingly protected embryos surrounded by additional layers of maternal cells, as in the seeds of land plants, where the embryo is embedded in albumen, a triploid tissue resulting from the fertilization of a diploid maternal tissue, and the integuments and fruit differentiating from parental tissues. Although phylogenetically very distant, this latter phanerogam embryo development is reminiscent of the viviparous mode of embryo production in animals, where the embryo remains nested in the maternal body up to its mature stage. In contrast, other organisms, including all other brown algae, grow their embryo outside the parental tissues. In *Fucus* (order Fucales), female and male gametophytes release eggs and sperm cells into the seawater where fertilization takes place (Hatchett et al., 2022), as in fish, amphibians, and many aquatic invertebrates such as tunicates and echinoderms (ovipary). Therefore, *Saccharina* represents an intermediate case, and one can reasonably hypothesize that, in view of the fragile physical connection between its egg and the maternal stalk (eggs detach from the stalk even with gentle

shaking), this mode of interaction will evolve towards either vivipary-like or ovipary-like embryo development. That Laminariales, Tilopteridales, Sporochnales, and especially the Desmarestiales, which diverged early (Bringloe et al., 2020; Silberfeld et al., 2010), are pioneers of a parental-embryo physical connection in brown algae distinct from ovipary is congruent with the fact that they diverged independently during the radiation giving rise to most current brown algal orders. In any case, this particular mode of maternal-embryo interaction has clearly enabled Laminariales to become the largest and most morphologically complex brown algae to thrive in the oceans.

Materials and Methods

Algal culture

The culture and production of embryos of *Saccharina latissima* (Arthrothamnaceae, Laminariales, Phaeophyceae) were carried out according to (Theodorou et al., 2021). Female (F1) and male (M1) gametophytes with a fixed genotype were used to produce the embryos. These genotypes were selected from the offspring of one mature sporophyte collected on the beach at Perharidy (Roscoff, Brittany, France) (48°43'33.5"N 4°00'16.7"W) based on their growth rate and sexual compatibility when cultured in vitro. F1 and M1 gametophytes were amplified by vegetative multiplication as described in (Theodorou et al., 2021). Gametes were obtained from the maturation of gametophytes under 16 $\mu\text{mol photons m}^{-2}\cdot\text{s}^{-1}$ white light intensity and 14:10 light:dark photoperiod at 13 °C. Embryos were observed after transferring the cultures to higher light intensity (50 $\mu\text{mol photons m}^{-2}\cdot\text{s}^{-1}$) for a week.

Excision of the maternal tissue at different developmental stages.

The separation of embryos from their stalk was carried out by using pulled glass micro-needles. First, glass micro-needles were prepared by pulling glass capillaries (GC100F-10) with a pipette puller (SU-P97 Flaming/Brown type micropipette puller) using the following programme: heat, 564°C; pull, 70 U; velocity, 70 ms; time, 250 ms. After pulling, the tip of the needle was sharpened to ensure precision cutting.

Second, developing embryos were selected under a flow hood using an inverted microscope (Olympus CKX41 Inverted with phase contrast). Then, the tip of the stalk was cut using the glass needle in a cutting motion, while holding the embryo down on the bottom of the dish. This action was repeated for embryos of all Phase I and early Phase II developmental stages. For use as controls, i) whole gametophytes, ii) gametophytes with damaged cells distant from the stalk, and iii) embryos attached to the substratum (bottom of the plastic Petri dish), were transferred to another dish using a non-pulled capillary and a manual microinjector (Eppendorf CellTram Air 5176).

Cell staining

Trypan blue. A drop of Trypan blue was added to fertile female gametophytes of *S. latissima* immersed in ~ 0.5 mL of seawater, followed by observation in bright field microscopy (DMI8, Leica Microsystems).

Calcofluor white. Staining of cell walls from embryos separated from the maternal tissue was performed at different times post excision. Embryos were fixed for 1 hour in equal parts of 4% PFA in H₂O and filtered natural seawater (NSW). After fixation, the samples were washed in NSW and twice in PBS to remove any excess fixative. Subsequently, they were incubated with 20 µM Calcofluor white (Sigma-Aldrich) for 3 days at 4°C in the dark. Following incubation, the samples were washed three times with PBS to remove any unbound dye. Finally, the algal samples were mounted using Cityfluor mounting medium (Electron Microscopy Sciences).

Image acquisition

All experiments of time-lapse microscopy of growing embryos were recorded under a bright-field microscope (Leica DMI600 B, Olympus CKX41, or Leica DMI8 inverted phase contrast microscopes) equipped with a DFC450C camera with acquisition intervals of 2 to 24 hours for a duration of at least 10 days after excision. The required temperature and light were set in a carbonate-glass chamber fitted to the microscope and equipped with a thermostatically controlled airflow system (Cube and Box, Life Imaging services) and commercially available LED white light sources. Observations of cell wall staining (see experimental procedure for Calcofluor white staining below) were performed with a Leica TCS SP5 AOBS inverted confocal

microscope (20X objective / N.A. 0.70 and correction 0; Exc/Em band wavelengths: 405/561-596 nm; pinhole, 60.6 μm).

Manual segmentation

Automatic segmentation proved to be challenging due to the constant pigmentation changes of the cells transitioning from high to low coloration. Additionally, daily exposure to UV light required to display Calcofluor white staining proved to be detrimental to the algae. Therefore, we carried out manual segmentation from bright-field images. To minimize image deformation, we selectively segmented predominantly flat-growing embryos. Therefore, Z-stack images of time-lapse acquisition of flat-growing embryos were segmented manually with Fiji (ImageJ2 version 2.9.0) (Schindelin et al., 2012), and the outlines were implemented in Inkscape (version 1.2). Resulting cell wall contours were analyzed using in-house software (see below). The program extracted multiple quantitative parameters for each lamina (blade) and its cells.

Quantitative morphometry

Cell wall vector graphics were processed in dedicated software written in object-oriented Python 3 (Van Rossum and Drake, 2023) that we called `blade_painter`. Reading the SVG file, `blade_painter` extracts various geometric properties for cells and laminae (Rosin, 2005), namely: (a) each cell contour, from which the perimeter length and surface area were directly derived; (b) convex hull, used to compute the minimal bounding rectangle (MBR). The main axis and length/width (l/w) ratio (or elongation) of the cell were assumed to be those of the MBR; (c) rectangularity, computed as the proportion of overlapping surface between the cell and its MBR, rescaled to the same area; (d) neighbor cell count, where two cells were considered neighbors if they shared at least 200 nm of cell wall (this threshold can be modified as a software parameter); (e) blade area; (f) main and secondary axes of orientation and length of the blade, computed according to (Fletcher et al., 2013).

Statistical analysis

Data collected from the segmented cell and blade contours were analyzed using standard Python 3 libraries, namely pandas (The pandas development team, 2020)

(pandas-dev/pandas: Pandas) and scipy (Virtanen et al., 2020). All pairwise comparisons for cell data were conducted using the Student's mean comparison test with Welch's correction, except for neighbor cell numbers and orientation, which were compared using a χ^2 test. Blade data were compared using the nonparametric Mann-Whitney test.

Growth rate

For each observed blade, the date of observation was set to $t=0$ at the transition from Phase I to Phase II (first longitudinal division). Linear regression was performed on the logarithm of cell number as a function of time, for $-48 \leq t \leq 72$. The increase rate was computed as r in the equation $N = N_0 \times r^t$, thus derived from the slope of the regression line $\log(N) = \log(N_0) + \log(r) \times t$. From r , we inferred the doubling time $\tau = 1/\log_2(r)$.

Acknowledgements

S. Boscq was funded by the Bretagne Regional Council ("Primaxis" project, grant number 1749) and Sorbonne University. I. Theodorou was funded by an ARED grant from the Bretagne Regional Council ("PUZZLE" project) and NMBU. We thank Bruno de Revers for fruitful discussion about reproduction of brown algae.

References

- Anlas, K. and Trivedi, V.** (2021). Studying evolution of the primary body axis in vivo and in vitro. *eLife* **10**, e69066.
- Barthélémy, D. and Caraglio, Y.** (2007). Plant Architecture: A Dynamic, Multilevel and Comprehensive Approach to Plant Form, Structure and Ontogeny. *Annals of Botany* **99**, 375–407.
- Berger, F., Taylor, A. and Brownlee, C.** (1994). Cell fate determination by the cell wall in early fucus development. *Science* **263**, 1421–1423.

- Bogaert, K. A., Arun, A., Coelho, S. M. and De Clerck, O.** (2013). Brown Algae as a Model for Plant Organogenesis. In *Plant Organogenesis: Methods and Protocols* (ed. De Smet, I.), pp. 97–125. Totowa, NJ: Humana Press.
- Bogaert, K. A., Beeckman, T. and De Clerck, O.** (2015). Photopolarization of *Fucus* zygotes is determined by time sensitive vectorial addition of environmental cues during axis amplification. *Front. Plant Sci.* **6**, 26.
- Bogaert, K. A., Beeckman, T. and De Clerck, O.** (2017). Two-step cell polarization in algal zygotes. *Nat Plants* **3**, 16221.
- Boscq, S., Dutertre, S., Theodorou, I. and Charrier, B.** (2022). Targeted Laser Ablation in the Embryo of *Saccharina latissima*. *Journal of visualized experiments: JoVE*.
- Bouget, F. Y., Berger, F. and Brownlee, C.** (1998). Position dependent control of cell fate in the *Fucus* embryo: role of intercellular communication. *Development* **125**, 1999–2008.
- Bringloe, T. T., Starko, S., Wade, R. M., Vieira, C., Kawai, H., De Clerck, O., Cock, J. M., Coelho, S. M., Destombe, C., Valero, M., et al. (2020). Phylogeny and Evolution of the Brown Algae. *Crit. Rev. Plant Sci.* **39**, 281–321.
- Buchholz, C. and Lüning, K.** (1999). Isolated, distal blade discs of the brown alga *Laminaria digitata* form sorus, but not discs, near to the meristematic transition zone. *Journal of Applied Phycology* **11**, 579–584.
- Budke, J. M., Goffinet, B. and Jones, C. S.** (2012). The cuticle on the gametophyte calyptra matures before the sporophyte cuticle in the moss *Funaria hygrometrica* (Funariaceae). *American Journal of Botany* **99**, 14–22.
- Burki, F., Roger, A. J., Brown, M. W. and Simpson, A. G. B. (2020). The New Tree of Eukaryotes. *Trends in Ecology & Evolution* **35**, 43–55.
- Burridge, T., Clayton, M. N. and Hallam, N. D.** (1993). Oogenesis and Stalk Mediated Fertilization in *Phyllospora comosa*, (Labillardière) C. Agardh, (Seirococcaceae, Phaeophyta). **36**, 223–232.
- Charrier, B., Le Bail, A. and de Reviers, B.** (2012). Plant Proteus: brown algal morphological plasticity and underlying developmental mechanisms. *Trends in Plant Science* **17**, 468–477.
- Charrier, B., Rabillé, H. and Billoud, B.** (2019). Gazing at Cell Wall Expansion under a Golden Light. *Trends Plant Sci.* **24**, 130–141.
- Cove, D. J.** (2000). The generation and modification of cell polarity. *Journal of Experimental Botany* **51**, 831–838.
- Cribb, A. B.** (1954). *Macrocystis pyrifera* (L.) Ag. in Tasmanian Waters. *Mar. Freshwater Res.* **5**, 1–34.
- Deline, B., Greenwood, J. M., Clark, J. W., Puttick, M. N., Peterson, K. J. and Donoghue, P. C. J. (2018). Evolution of metazoan morphological disparity. *Proceedings of the National Academy of Sciences* **115**, E8909–E8918.

- Farah, M. E., Maia, M., Penha, F. M. and Rodrigues, E. B.** (2015). The Use of Vital Dyes during Vitreoretinal Surgery - Chromovitrectomy.
- Fletcher, A. G., Osborne, J. M., Maini, P. K. and Gavaghan, D. J.** (2013). Implementing vertex dynamics models of cell populations in biology within a consistent computational framework. *Prog Biophys Mol Biol* **113**, 299–326.
- Friml, J., Vieten, A., Sauer, M., Weijers, D., Schwarz, H., Hamann, T., Offringa, R. and Jürgens, G. (2003). Efflux-dependent auxin gradients establish the apical–basal axis of Arabidopsis. *Nature* **426**, 147–153.
- Fritsch, F. E.** (1945). *The Structure And Reproduction Of The Algae*. The University Press. Cambridge: Cambridge University Press.
- Gall, L., Pien, S. and Rusig, A.-M.** (2004). Cultivation of *Palmaria palmata* (Palmariales, Rhodophyta) from isolated spores in semi-controlled conditions. *Aquaculture* **229**, 181–191.
- Goodner, B. and Quatrano, R.** (1993). Fucus Embryogenesis: A Model to Study the Establishment of Polarity. *Plant Cell* **5**, 1471–1481.
- Haig, D.** (2015). Coleochaete and the origin of sporophytes. *American Journal of Botany* **102**, 417–422.
- Hatchett, W. J., Coyer, J. A., Sjøtun, K., Jueterbock, A. and Hoarau, G.** (2022). A review of reproduction in the seaweed genus *Fucus* (Ochrophyta, Fucales): Background for renewed consideration as a model organism. *Front. Mar. Sci.* **9**, 1051838.
- Jaffe, L. F.** (1968). Localization in the Developing FUCUS EGG and the GENERAL ROLE of LOCALIZING CURRENTS. In *Advances in Morphogenesis* (ed. Abercrombie, M.), Brachet, J.), and King, T. J.), pp. 295–328. Elsevier.
- Kai, T., Nimura, K., Yasui, H. and Mizuta, H.** (2006). Regulation of Sorus Formation by Auxin in Laminariales Sporophyte. *J Appl Phycol* **18**, 95–101.
- Kanda, T.** (1936). On the Gametophytes of Some Japanese Species of Laminariales I. Scientific papers of the Institute of Algological Research, Faculty of Science, Hokkaido Imperial University **1**, 221–260.
- Kanda, T.** (1938). On the Gametophytes of Some Japanese Species of Laminariales II. Scientific papers of the Institute of Algological Research, Faculty of Science, Hokkaido Imperial University **2**, 87–111.
- Kanda, T.** (1941). On the Gametophytes of Some Japanese Species of Laminariales III. Scientific papers of the Institute of Algological Research, Faculty of Science, Hokkaido Imperial University **2**, 155–193.
- Kawai, H., Hanyuda, T., Draisma, S. G. A., Wilce, R. T. and Andersen, R. A.** (2015). Molecular phylogeny of two unusual brown algae, *Phaeostrophion irregulare* and *Platysiphon glacialis*, proposal of the Stschapoviales ord. nov. and Platysiphonaceae fam. nov., and a re-examination of divergence times for brown algal orders. *Journal of Phycology* **51**, 918–928.

Klimova, A. V. and Klochkova, T. A. (2017). Peculiarities of development in the marine brown alga *Alaria angusta* Kjellman, 1889 (Alariaceae: Ochrophyta) under laboratory-controlled conditions. *Russ J Mar Biol* **43**, 42–48.

Klochkova, T. A., Motomura, T., Nagasato, C., Klimova, A. V. and Kim, G. H. (2019). The role of egg flagella in the settlement and development of zygotes in two *Saccharina* species. *Phycologia* **58**, 145–153.

Lüning, K. (1981). Egg release in gametophytes of *Laminaria saccharina*: Induction by darkness and inhibition by blue light and u.v. *British Phycological Journal* **16**, 379–393.

Martinez, C. C., Chitwood, D. H., Smith, R. S. and Sinha, N. R. (2016). Left–right leaf asymmetry in decussate and distichous phyllotactic systems. *Philosophical Transactions of the Royal Society B: Biological Sciences* **371**, 20150412.

Mishra, B. S., Sharma, M. and Laxmi, A. (2022). Role of sugar and auxin crosstalk in plant growth and development. *Physiol Plant* **174**, e13546.

Motomura, T. (1990). Ultrastructure of Fertilization in *Laminaria angustata* (Phaeophyta, Laminariales) with Emphasis on the Behavior of Centrioles, Mitochondria and Chloroplasts of the Sperm. *Journal of Phycology* **26**, 80–89.

Motomura, T. (1991). Immunofluorescence Microscopy of Fertilization and Parthenogenesis in *Laminaria angustata*(Phaeophyta). *Journal of Phycology* **27**, 248–257.

Motomura, T., Nagasato, C. and Kimura, K. (2010). Cytoplasmic inheritance of organelles in brown algae. *J Plant Res* **123**, 185–192.

Naf, U. (1962). Developmental Physiology of Lower Archegoniates. *Annual Review of Plant Physiology* **13**, 507–532.

Nagasato, C., Tanaka, A., Ito, T., Katsaros, C. and Motomura, T. (2017). Intercellular translocation of molecules via plasmodesmata in the multiseriate filamentous brown alga, *Halopteris congesta* (Sphacelariales, Phaeophyceae). *Journal of Phycology* **53**, 333–341.

Nagasato, C., Yonamine, R. and Motomura, T. (2022). Ultrastructural Observation of Cytokinesis and Plasmodesmata Formation in Brown Algae. *Methods Mol Biol* **2382**, 253–264.

Norton, T. A. (1972). The development of *Saccorhiza dermatodea* (Phaeophyceae, Laminariales) in culture. *Phycologia* **11**, 81–86.

pandas-dev/pandas: Pandas.

Pang, S. and Lüning, K. (2004). Photoperiodic long-day control of sporophyll and hair formation in the brown alga *Undaria pinnatifida*. *Journal of Applied Phycology* **16**, 83–92.

Rabillé, H., Billoud, B., Tesson, B., Le Panse, S., Rolland, É. and Charrier, B. (2019). The brown algal mode of tip growth: Keeping stress under control. *PLoS Biol.* **17**, e2005258.

Rosin, P. L. (2005). Computing global shape measures. In *Handbook of Pattern Recognition and Computer Vision*, pp. 177–196. WORLD SCIENTIFIC.

Sauvageau, C. (1918). Recherches sur les Laminaires des cotes de France. *Mem. Acad. Sci.* **56**, 1–240.

Schindelin, J., Arganda-Carreras, I., Frise, E., Kaynig, V., Longair, M., Pietzsch, T., Preibisch, S., Rueden, C., Saalfeld, S., Schmid, B., et al. (2012). Fiji - an Open Source platform for biological image analysis. *Nature methods* **9**, 676–682.

Shahbazi, M. N., Siggia, E. D. and Zernicka-Goetz, M. (2019). Self-organization of stem cells into embryos: A window on early mammalian development. *Science* **364**, 948–951.

Silberfeld, T., Leigh, J. W., Verbruggen, H., Cruaud, C., de Reviers, B. and Rousseau, F. (2010). A multi-locus time-calibrated phylogeny of the brown algae (Heterokonta, Ochrophyta, Phaeophyceae): Investigating the evolutionary nature of the “brown algal crown radiation.” *Molecular Phylogenetics and Evolution* **56**, 659–674.

Simsek, M. F. and Özbudak, E. M. (2022). Patterning principles of morphogen gradients. *Open Biology* **12**, 220224.

Terauchi, M., Nagasato, C. and Motomura, T. (2015). Plasmodesmata of brown algae. *J Plant Res* **128**, 7–15.

Theodorou, I. and Charrier, B. (2023). The shift to 3D growth during embryogenesis of kelp species, atlas of cell division and differentiation of *Saccharina latissima*. *Development* **150**, dev201519.

Theodorou, I., Opsahl-Sorteberg, H.-G. and Charrier, B. (2021). Preparation of Zygotes and Embryos of the Kelp *Saccharina latissima* for Cell Biology Approaches. *Bio-protocol* e4132–e4132.

van der Meer, J. P. (1979). Genetics of *Gracilaria* sp. (Rhodophyceae, Gigartinales).V. Isolation and characterization of mutant strains. *Phycologia* **18**, 47–54.

van der Meer, J. P. and Todd, E. R. (1980). The life history of *Palmaria palmata* in culture. A new type for the Rhodophyta. *Can. J. Bot.* **58**, 1250–1256.

Van Rossum, G. and Drake, F. L. (2023). The Python Language Reference, Release 3.11.5, Python Software Foundation.

Virtanen, P., Gommers, R., Oliphant, T. E., Haberland, M., Reddy, T., Cournapeau, D., Burovski, E., Peterson, P., Weckesser, W., Bright, J., et al. (2020). SciPy 1.0: fundamental algorithms for scientific computing in Python. *Nat Methods* **17**, 261–272.

Wang, M., Le Gourrierec, J., Jiao, F., Demotes-Mainard, S., Perez-Garcia, M.-D., Ogé, L., Hamama, L., Crespel, L., Bertheloot, J., Chen, J., et al. (2021). Convergence and Divergence of Sugar and Cytokinin Signaling in Plant Development. *Int J Mol Sci* **22**, 1282.

Wiencke, C. and Clayton, M. N. (1990). Sexual reproduction, life history, and early development in culture of the Antarctic brown alga *Himantothallus grandifolius* (Desmarestiales, Phaeophyceae)*. *Phycologia* **29**, 9–18.

Supplementary material

[Suppl. Table 1: Morphometric parameters of the embryo \(blade\).](#)

[Suppl. Table 2: P-values of statistical tests comparing morphometric parameters characterising *Saccharina* embryos and their cells.](#)

t-test were use to compare the cell features, Wilcoxon tests to compare embryo blades and Chi² for the analyses of the number of cell neighbours.

[Suppl. Table 3: Cell morphometrics in each embryo \(blade\).](#)

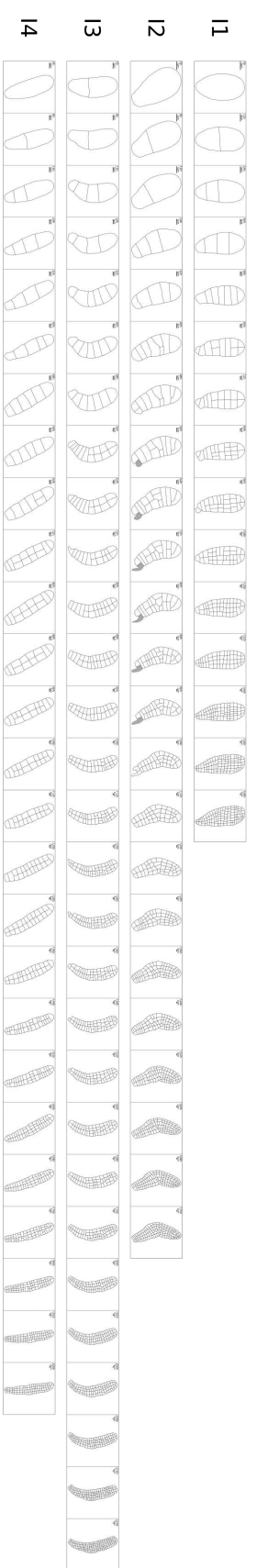
Time point and number of cells are indicated for each embryo. Each cell (one row) was studied for different morphometric parameters. Those relevant for this study are displayed.

[Suppl. Movie 1: Development when egg naturally detached from the stalk](#)

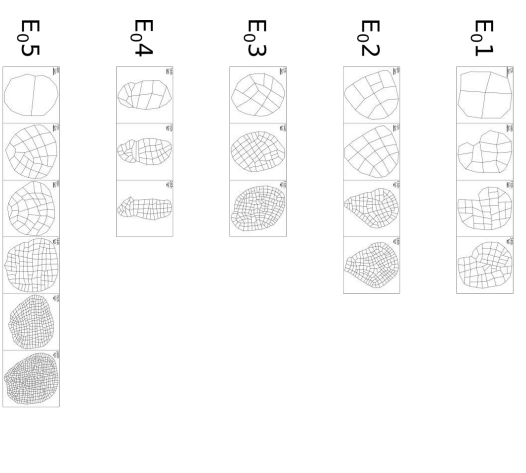
Suppl. Fig. 1 (next page): Results of manual segmentation of the embryos

The cell outlines were drawn manually from a series of bright-field z-stack images (Stack focuser, see Materials and Methods section) and used for quantitative analyses of the morphometry parameters. The stages at which the separation from the stalk took place are indicated with the code used in the article (e.g., E₀ for the separation from the stalk at the egg stage). I is for intact embryos. Replicates are indicated with a number.

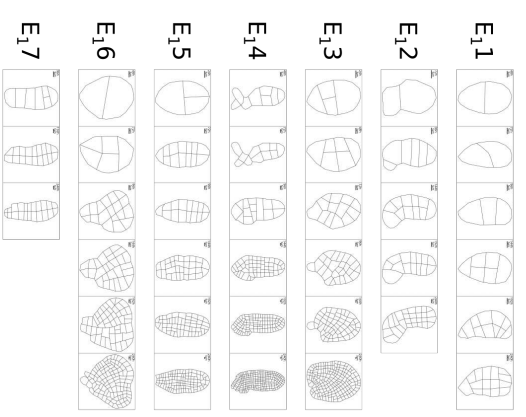
Intact (Control)



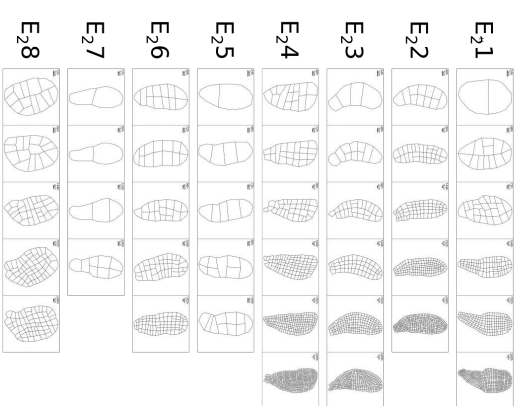
Egg



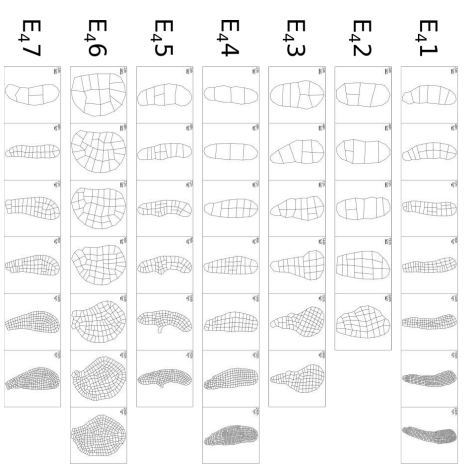
Zygote



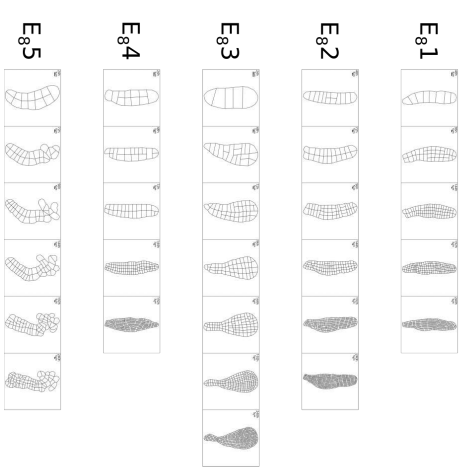
2-cell



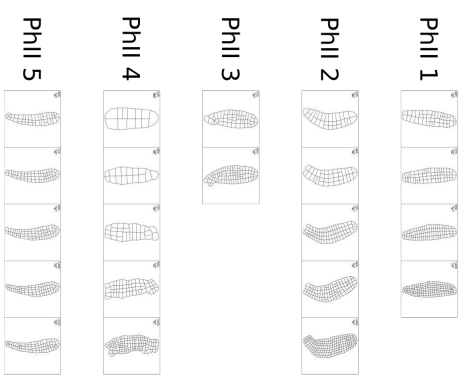
4-cell



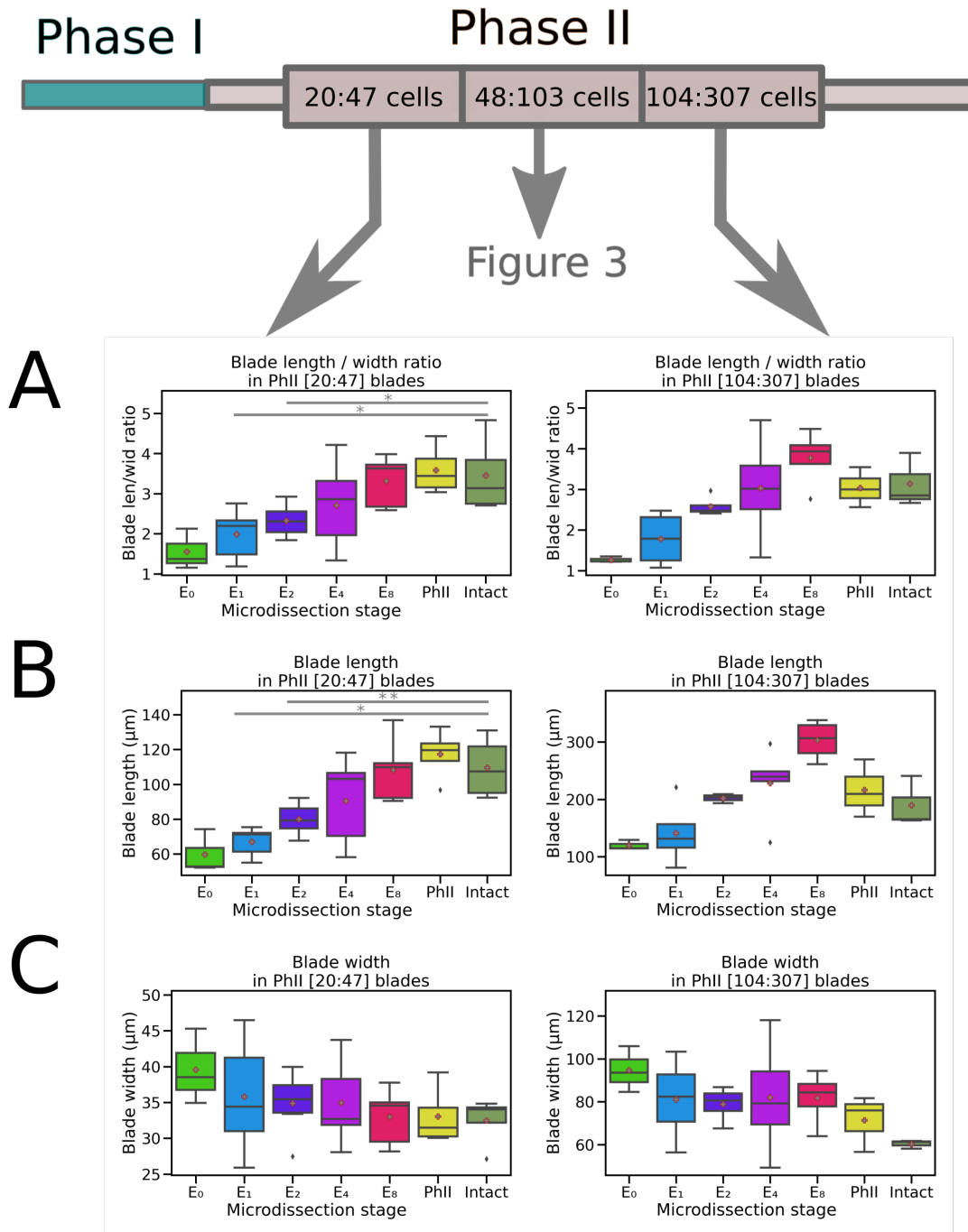
8-cell



Phase II



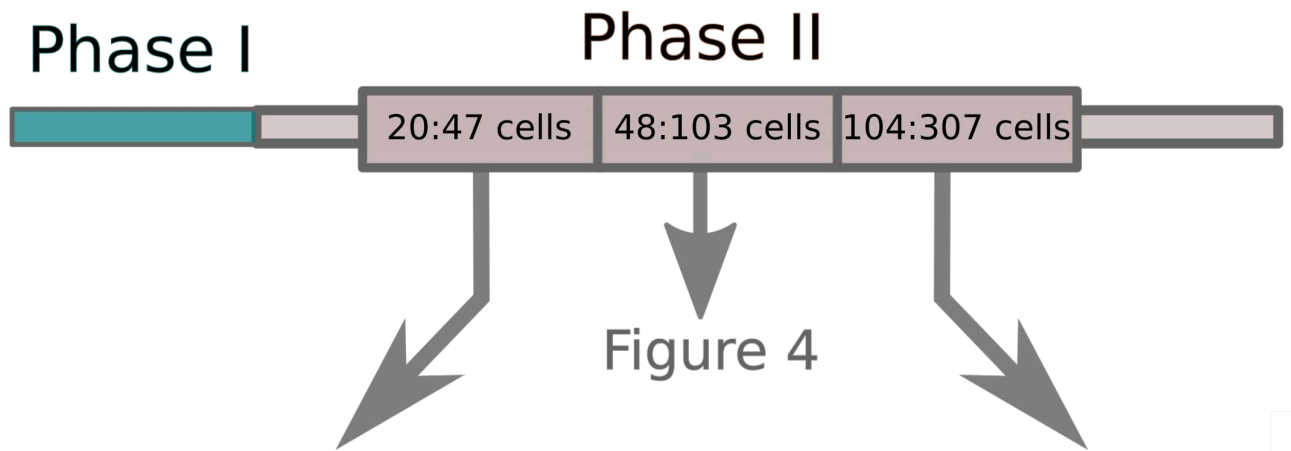
1. Microdissection 2. Observations



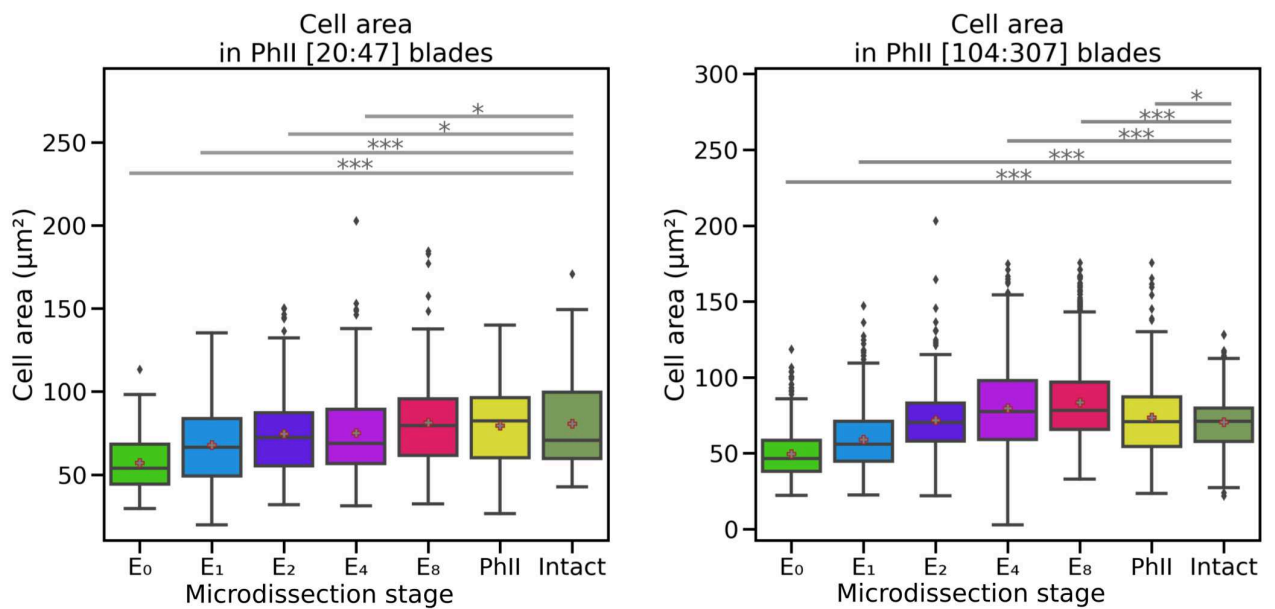
Suppl. Fig. 2: Impact of embryo detachment from the stalk on blade shape at two additional developmental windows

The distribution of the length/width ratios of blade of different stages (20–47-cell, left and 104–307-cell embryos, respectively left and right panels) grown after microdissection of the stalk at the E₀, E₁, E₂, E₄, E₈ and PhII stages was plotted and compared with intact embryos. The line in the box represents the median, the box outlines frame the first quartile and the whiskers indicate the third quartile. Results of the *t*-test are indicated by p-values: * < 5.10⁻²; ** < 1.10⁻²; *** < 10⁻³. This figure supplements Fig. 3.

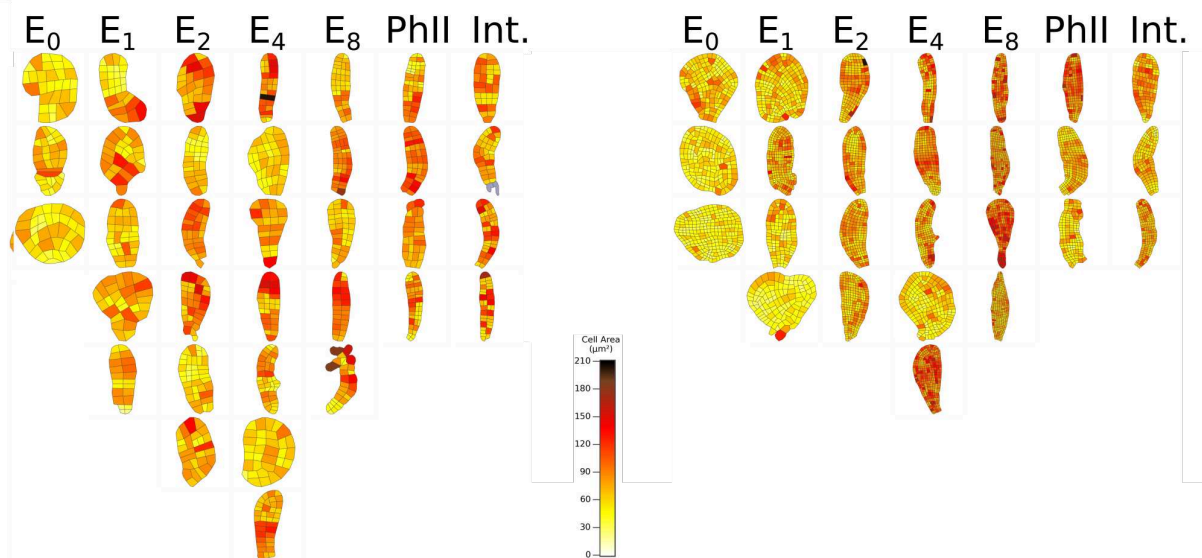
1. Microdissection 2. Observations



A

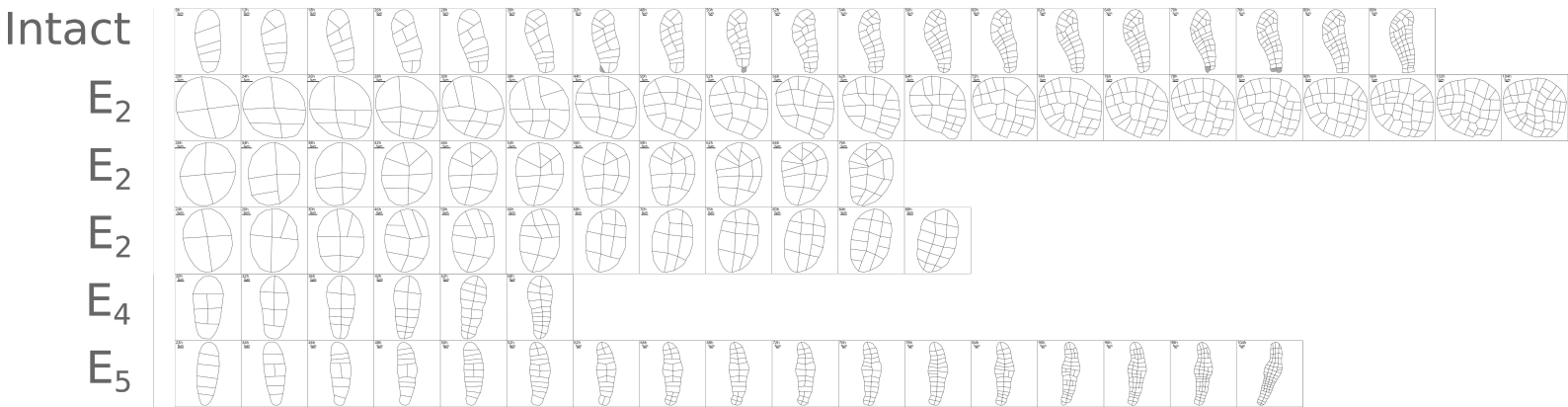


B



Suppl. Fig. 3 (previous page): Impact of detachment from the stalk on cell areas at two additional developmental windows.

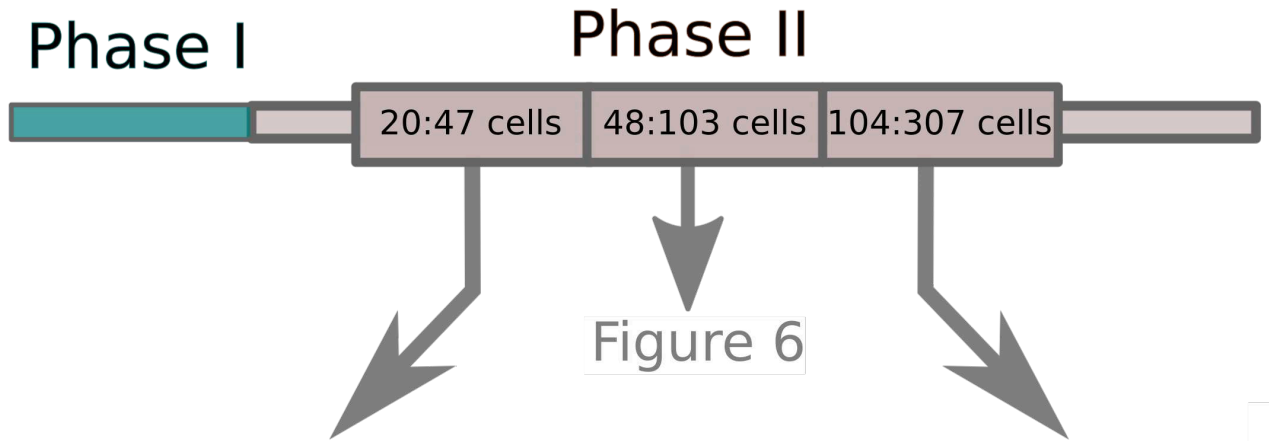
A. The distribution of the cell areas of embryos at different developmental stages (20–47-cell, and 104–307-cell embryos, respectively left and right panels) grown after microdissection of the stalk at E₀, E₁, E₂, E₄, E₈ and PhII stages was plotted and compared with intact embryos. The line in the box shows the median and the box outline frames the first quartile. The asterisk indicates the mean. The whiskers indicate the third quartile. Results of the *t*-test are indicated by p-values: * < 5.10⁻²; ** < 1.10⁻²; *** < 10⁻³. This figure supplements Fig. 4B. Heatmap of cell areas for each embryo considered in A. Color scale indicated on the bottom right-hand side of the figure is specific to the corresponding time window and may be different from that shown in Fig. 4. The scale is adjusted so that the image of each blade has the same dimensions.



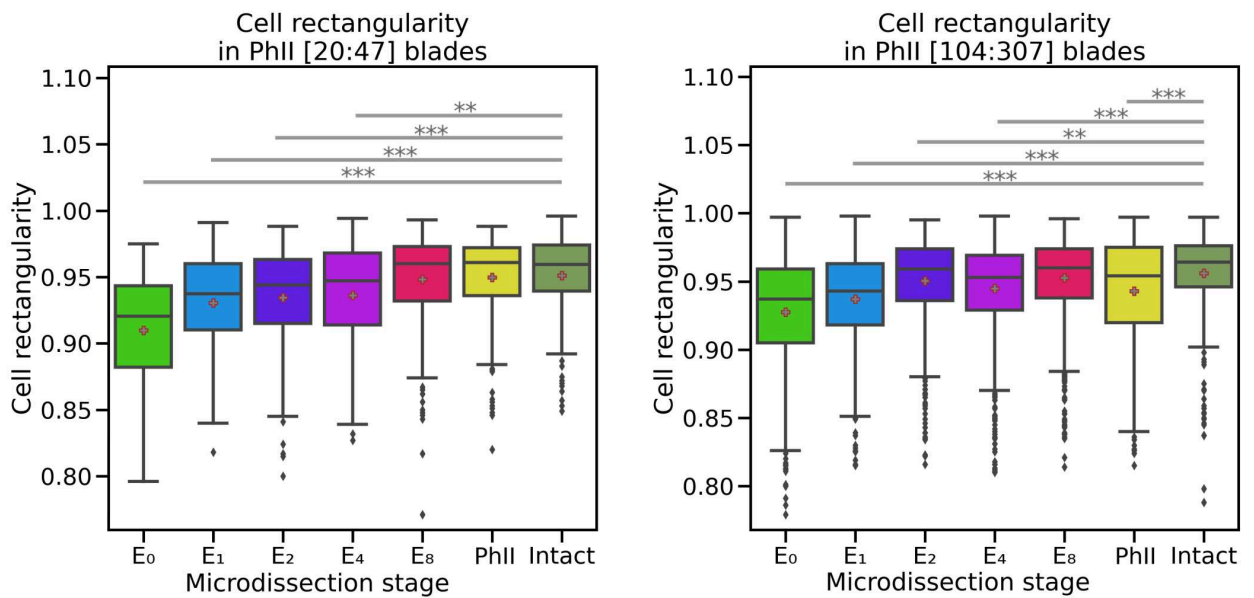
Suppl. Fig. 4: Time series of microdissected embryos.

Photos of embryos imaged every 2 hours were segmented at each additional cell division (the time interval between cell division is about 24 hours, so not all the images were segmented). Each line represents one embryo, the stage at which microdissection took place is indicated on the left. E₅ represents a 5-cell stage embryo.

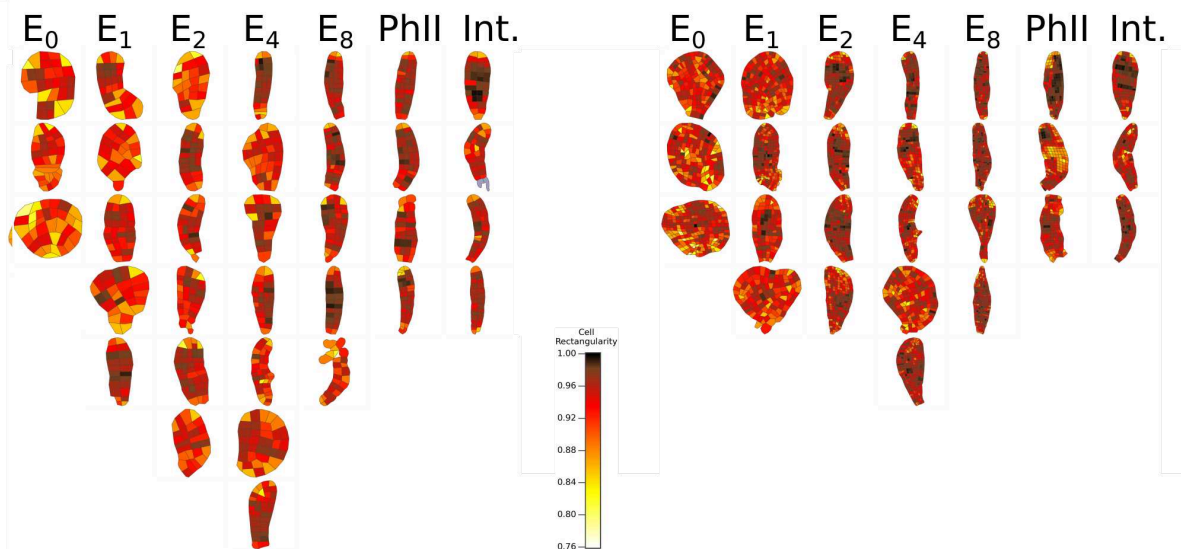
1. Microdissection 2. Observations



A



B



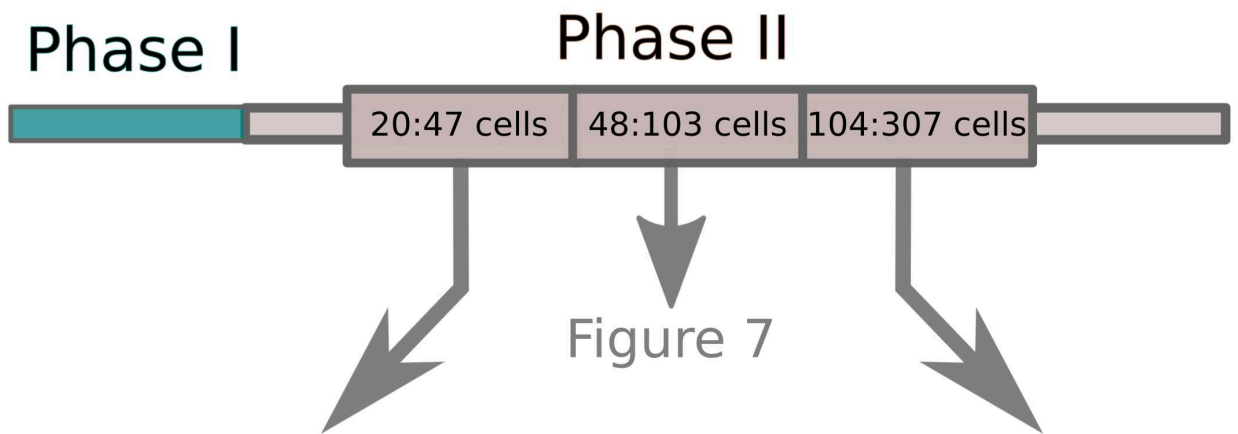
Suppl. Fig. 5 (previous page): Impact of detachment from the stalk on embryo cell shapes at two additional developmental windows.

Cell shape is expressed as a factor of rectangularity. A. The distribution of the cell rectangularity (see Methods for definition) of embryos of different stages (20–47-cell and 104–307-cell embryos, respectively left and right panels) grown after microdissection of the stalk at E₀, E₁, E₂, E₄, E₈ or PhII stages was plotted and compared with intact embryos. The line in the box shows the median, the box outline frames the first quartile and the whiskers indicate the third quartile. Asterisks show the mean. Results of the *t*-test are indicated by *p*-values: * < 5.10⁻²; ** < 1.10⁻²; *** < 10⁻³. This figure supplements Fig. 6. B. Heatmap of cell rectangularity for each embryo considered in A. Color scale indicated on the bottom right-hand side of the figure is specific to the corresponding time window and may be different from that shown in Fig. 6. The scale is adjusted so that the image of each blade has the same dimensions.

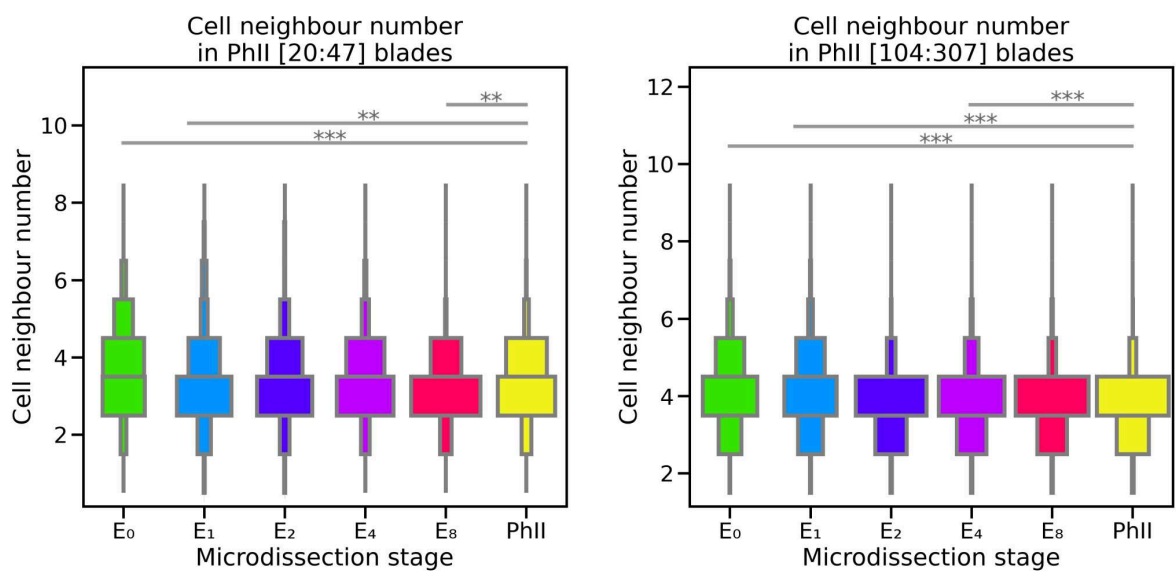
Suppl. Fig. 6 (next page): Impact of dissection from the stalk on the number of cell neighbors in microdissected embryos when observed at two different developmental windows.

A. The distribution of the number of cell neighbors in embryos of different stages (20–47-cell and 104–307-cell embryos, respectively left and right panels) grown after microdissection of the stalk at E₀, E₁, E₂, E₄, E₈ or PhII stage was plotted as violin plots and compared with intact embryos. Results of the Chi²-test are indicated by *p*-values: * < 5.10⁻²; ** < 1.10⁻²; *** < 10⁻³. This figure supplements Fig. 7. B. Heatmap of cell areas for each embryo considered in A. Color scale indicated on the bottom right-hand side of the figure is specific to the corresponding time window and may be different from that shown in Fig. 7. The scale is adjusted so that the image of each blade has the same dimensions.

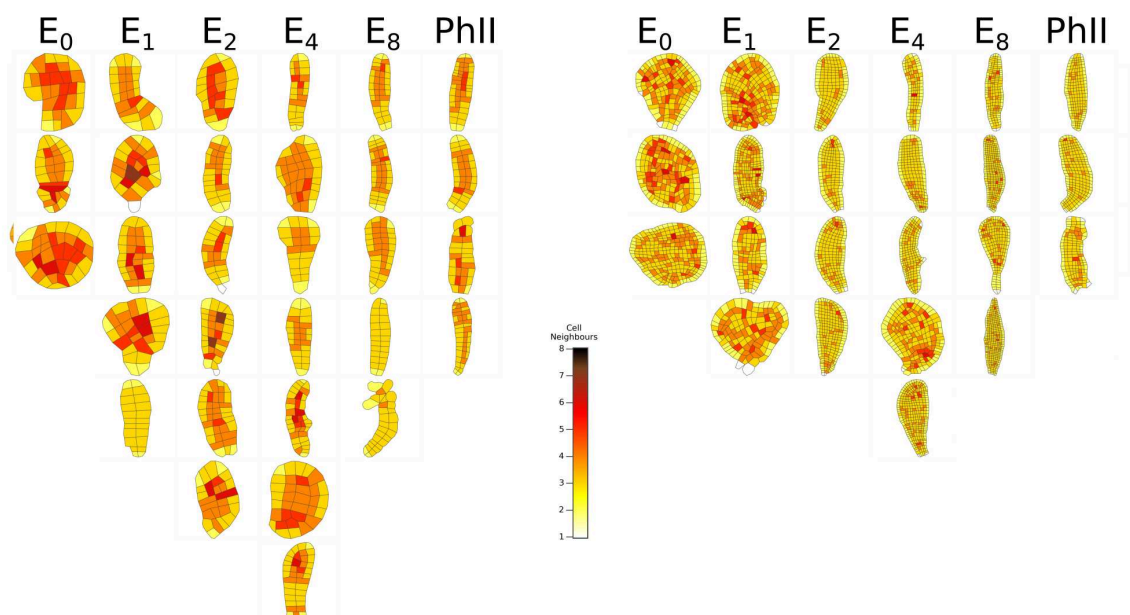
1. Microdissection 2. Observations



A



B



5 - Chapter III

**The cell fate of basal and apical cells
in *Saccharina* embryos is different
and variable over time**

Abstract:

This chapter highlights the role of the embryo's cells in the early development of *Saccharina latissima*. Laser ablation techniques enabled the removal of any cell within the embryo. This revealed that, while embryos up to the 4-cell stage develop with cell-autonomous control of the establishment of their thallus axes, embryos at later stages switch to a non-cell-autonomous mode of embryogenesis where cells act collectively to control the development of the embryo.

Contribution:

I cultivated all embryos used at the platform MRic Core Facility in Rennes. Laser ablation was designed with the help of S. Dutertre, the head of the platform. I performed all laser ablation, monitoring, and segmentation of all embryos. The software to analyze the segments was coded by B. Billoud. I ran software analysis. I contributed significantly to the results, discussion, and writing presented in the corresponding article.

The cell fate of basal and apical cells in *Saccharina* embryos is different and variable over time

Samuel Boscq¹, Bernard Billoud^{1,*}, Stéphanie Dutertre² & Bénédicte Charrier^{1,*}

¹ Morphogenesis of Macro Algae, UMR8227, CNRS - Sorbonne university, Station Biologique de Roscoff, Place Georges Teissier, 29680 Roscoff, France

²MRiC Core Facility, Inserm, Biosit UAR 3480 US_S 018, Rennes University, CNRS, Rennes, France

* Current address:

Institut de Génomique Fonctionnelle de Lyon (IGFL), UMR5242, ENSL, CNRS, INRAE, UCBL, 32-34 avenue Tony Garnier, 69007 Lyon, France

Corresponding authors:

benedicte.charrier@cnrs.fr

samuel.boscq@sb-roscoff.fr

Introduction

Contrary to animals and even land plants, the knowledge of the mechanisms controlling the establishment of growth axes is limited in brown algae. Most brown algae develop from a single cell outside the maternal organism (Fritsch 1934; Fritsch 1945), suggesting an autonomous development devoid of parental influence besides cytoplasmic inheritance (e.g., maternal transcripts; Bogaert et al., 2017; or male centrioles; Motomura 1990; Costa et al., 2014). Different pathways have been shown to participate in the establishment of the first growth axis. In Fucales, the establishment of polarity and axes relies on a wide variety of factors including light perception (Berger and Brownlee., 1994; Bogaert et al., 2015), gravity (Sun et al., 2005), sperm entry-induced Ca²⁺ gradient (Goddard et al., 2000), ROS signaling (Coelho et al., 2002), CDK tyrosine phosphorylation (Brownlee and Wood, 1986), and cell wall determinants (Berger et al., 1994). Similar processes as those in Fucales have been shown to establish the apico-basal axis in Dictyotales, as a response to light direction and cell wall accumulation at the rhizoid pole (Bogaert et

al., 2023). However, differences can also be observed: whereas in response to axis formation, the zygote of Fucales germinates and develops a rhizoid, the whole zygote of *Dictyota* elongates 90 seconds after fertilization, establishing very rapidly the first embryo-proper axis (Bogaert et al., 2017a; Tarakhovskaya et al., 2017). In addition to cell secretion, the F-actin and myosin network are responsible for this rapid change in shape (Bogaert et al., 2017b).

Few groups of brown algae develop their embryos connected to the parent organism. Among them, the Laminariales rely on the connection of the embryo to the parent by a stalk structure for the correct development of the embryo's body plans (previous chapter). As in Dictyotales, the zygote elongates at fertilization (Lüning, 1981). The first cell division is unequal in most cases, making a basal cell slightly smaller than the apical one (Sauvageau 1918; Motomura 1990; Theodorou and Charrier, 2023). Yet, the most important difference between the basal and the apical cell results from the presence of the maternal stalk, which connects the basal cell to the remnant maternal tissue (Bogaert et al., 2023; Theodorou and Charrier, 2023). This connection provides the longitudinal axis along which the zygote elongates, and perpendicularly to which the first unequal cell division takes place. Only once the embryo has reached a stage of around 8 cells stacked on top of each other by a series of transverse cell divisions parallel to the first one, does it establish medio-lateral growth by setting up longitudinal cell divisions perpendicular to the first ones. Therefore, attachment to the stalk is a major process from which the first two growth axes of the thallus are organized. Interestingly, in another species of Laminariales, the egg is polarized prior to and during fertilization, with vacuoles accumulating in the apical region and the chloroplasts near the nucleus in the basal region. After fertilization, the elongating zygote adopts a homogeneous intracellular organization prior to the first cell division. Chloroplasts are then observed around the centered nucleus and vacuoles spread homogeneously at the periphery of the zygote (*Laminaria angustata*, Motomura, 1990). This overall symmetrical intracellular organization is also observed in parthenogenetic zygotes (Motomura, 1991). Therefore, before the first cell division, the intracellular ultrastructural organization is symmetrical along the longitudinal axis of the zygote.

How can we reconcile this homogeneous intracellular organization with the inequality of the first cell division? Apico-basal polarization persists later in

development with embryos displaying a narrower basal part and a wider apical part, giving them the characteristic pear shape in Phase II (monolayered lamina from 10 to 1000 cell-stage, Theodorou & Charrier, 2023). Rhizoids emerge only from the basal part, and when polystromatization is initiated at the beginning of Phase III, apico-basal polarization is reinforced with differentiation only in the basal part of the haptera and the holdfast, which are attachment organs. Therefore, the establishment of the initial longitudinal polarization might be key to the subsequent development of the embryo, even though the *Saccharina* embryo displays a high level of morphological plasticity allowing it to adjust its morphology over time. Here, we study the role of basal cells and apical cells in early embryogenesis of *Saccharina latissima*. More specifically, we investigated the extent to which these cells 1) influence the maintenance of the longitudinal axis and 2) contribute to the establishment of the polarized apico-basal axis.

We used laser ablation to kill basal and apical cells at different embryo developmental stages in the kelp *Saccharina latissima* and monitored the impact on embryogenesis. Laser ablation provides a high degree of spatiotemporal precision within the embryo, enabling multiple developmental events to be studied (Byrn and Hammarlund, 2017). Laser-mediated cell ablation has been successfully used in a wide range of organisms such as metazoans (Johnson et al., 2011; Angelo and Tremblay, 2013; Byrn and Hammarlund, 2017; Fouad A. et al., 2021), plants (Berg et al., 1998; Reinhardt et al., 2004), and brown algae Fucales (Berger et al., 1994; Bouget et al., 1998). We recently developed this technique for the embryo of *Saccharina latissima* (Boscq et al., 2022).

Results

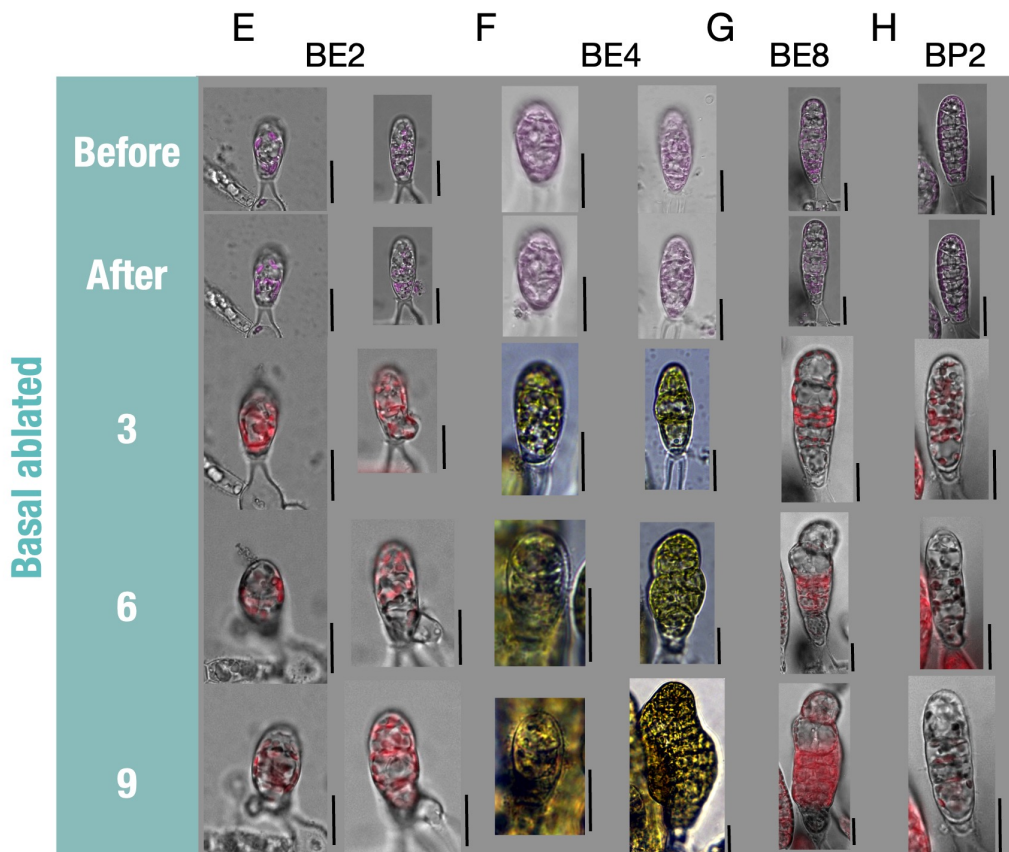
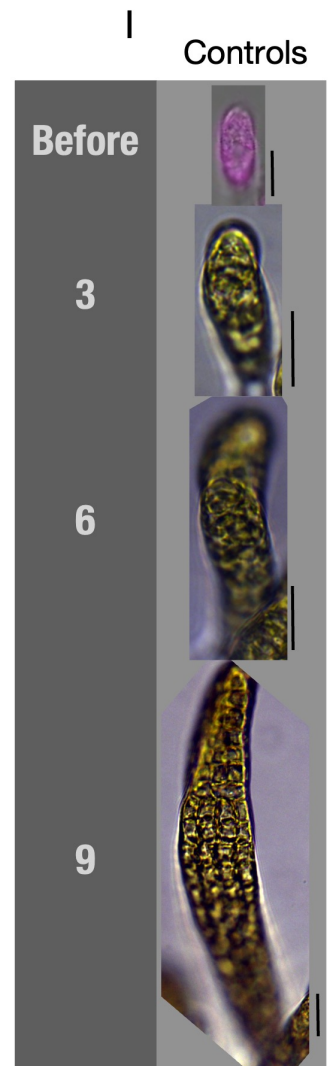
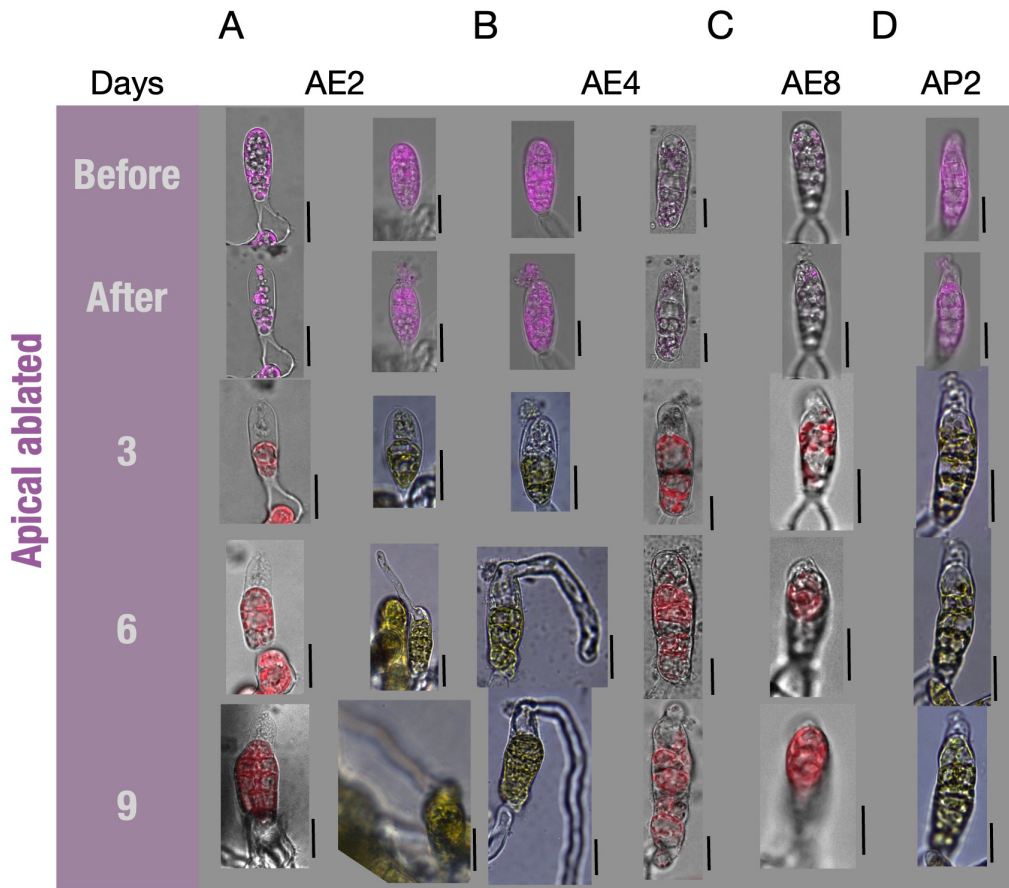
The apical cell and the basal cell are not necessary for the growth of the embryo of *Saccharina*

To study the respective roles of the apical and basal cells of early *Saccharina* embryos in the formation of thallus growth axis and polarized growth, we irradiated these cells using a pulse-UV laser (developed in Boscq et al., 2022). The apical cells

(A) of embryos at the 2-cell stage (AE2), 4-cell stage (AE4), 8-cell stage (AE8), or in early Phase II (AP2) were irradiated. Basal cells (B) were also irradiated at the same stages and consequently named BE2, BE4, BE8, and BP2. Perforation of the cell wall and plasma membrane resulted in the exit of most of the intracellular content in response to the turgor pressure (Suppl. Movie). Monitoring of the growing embryo confirmed that the irradiated cells were dead (Suppl. Figure 1). All embryos were then monitored for up to two weeks, and the morphology was analyzed after segmentation of the images. In response to this treatment, no embryo died, except for AE2 (11.1%), BP2 (5.6%), and BE8 (10%). Among the living embryos, Fig. 1 illustrates representative morphologies of embryos 3, 6, and 9 days post-laser ablation. First, all irradiated embryos presented some level of growth delay as they performed only a few cell divisions compared to control organisms. This is likely attributable to the stress they endured during the micro-surgery procedure (Fig. 1, day 2). This delay ranged from one to eight days following the ablation (Suppl. Fig. 1). After that delay, they started to divide again, and all continued to develop (Fig. 1, day 10). Therefore, neither the apical cell nor the basal cells are necessary for the growth of the embryo, and this occurs as early as the 2-cell stage.

Figure 1 (next page): Embryos keep developing after targeted cell ablation

Morphologies of developing embryos after ablation of the apical cell at the 2-cell stage (A) (AE2), (B) 4-cell stage (AE4), (C) 8-cell stage (AE8), (D) Phase II (AP2), or embryos subjected to basal cell ablation at (E) 2-cell stage (BE2), (F) 4-cell stage (BE4), (G) 8-cell stage (BE8), and (H) Phase II (BP2) were monitored for 3, 6, and 9 days post-ablation. A representative sample of the observed morphology is shown. Embryos not targeted by the laser are displayed as controls (I). The sample size of individuals observed during 3 distinct experiments is $n = 9$ (A), 11 (B), 4 (C), 6 (D), 10 (E), 18 (F), 10 (G), 7 (H), 15 (I). Scale bars represent 20 μ m.



Apical cells controls the growth of *Saccharina* embryo

We evaluated the distribution of observed morphologies 10 days post-laser ablation, accounting for an initial delay. Four distinct morphologies were described: 1) morphology similar to intact embryos (control), 2) growth-altered morphology, where embryos experienced a growth arrest lasting longer than 4 days after the initial delay, 3) shape-altered morphology, characterized by deviations in body axes or disruptions in polarity establishment, and 4) lethal morphology, for organisms that died before the tenth day post-ablation. The percentage of dead embryos remained low overall (Fig. 2). The primary observed morphology was a reduction in growth. Approximately 50% of AE2, AE4, AE8, and AP2 (grouped together as E8+), BE2, and BE4 embryos were significantly smaller 10 days after laser irradiation compared to intact organisms. This morphology includes the delay in resuming growth after laser irradiation described above. While this response increased with the embryo stage at which apical cells were irradiated (60% at the AE8+ stage), it decreased with time for the basal cell (only 20% of embryos for BE8+). This suggests that the apical cell, in contrast to the basal cell, is sustainably involved in growth throughout the whole embryogenetic Phase I.

To enhance the depth of our analysis, we manually segmented several embryos from bright-field images (Suppl. Fig. 1). Utilizing an in-house software, we obtained quantitative data on several morphometric parameters, including the area and shape of the embryo (Suppl. Table 1), as well as the number of cells, cell area, and cell shape (Suppl. Table 2).

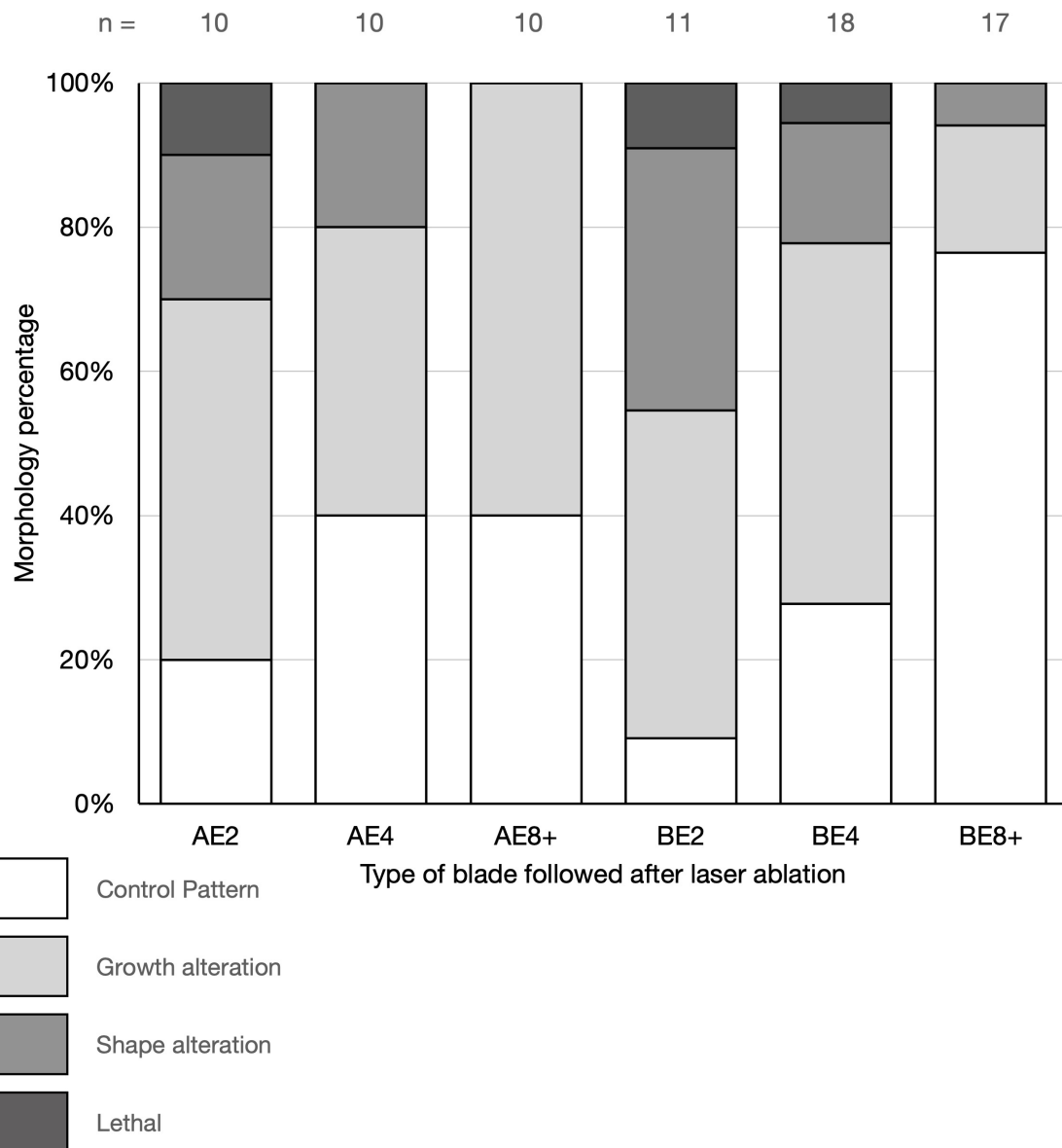


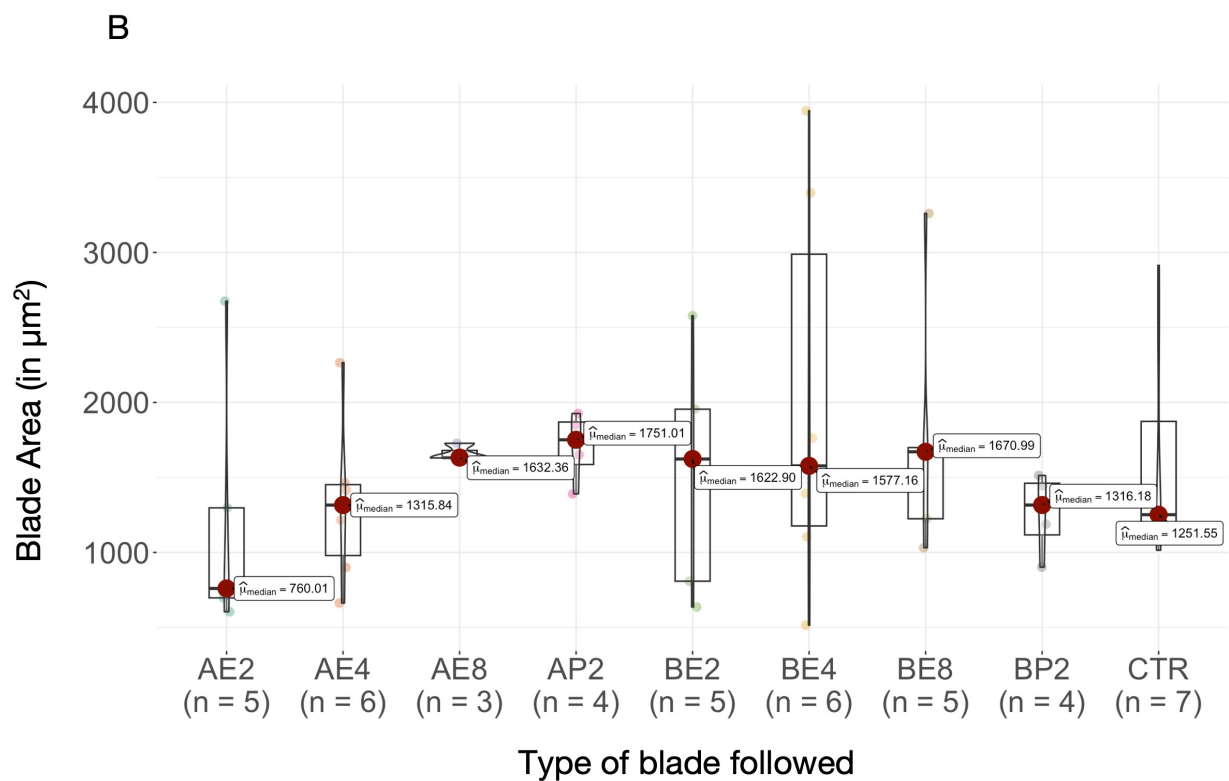
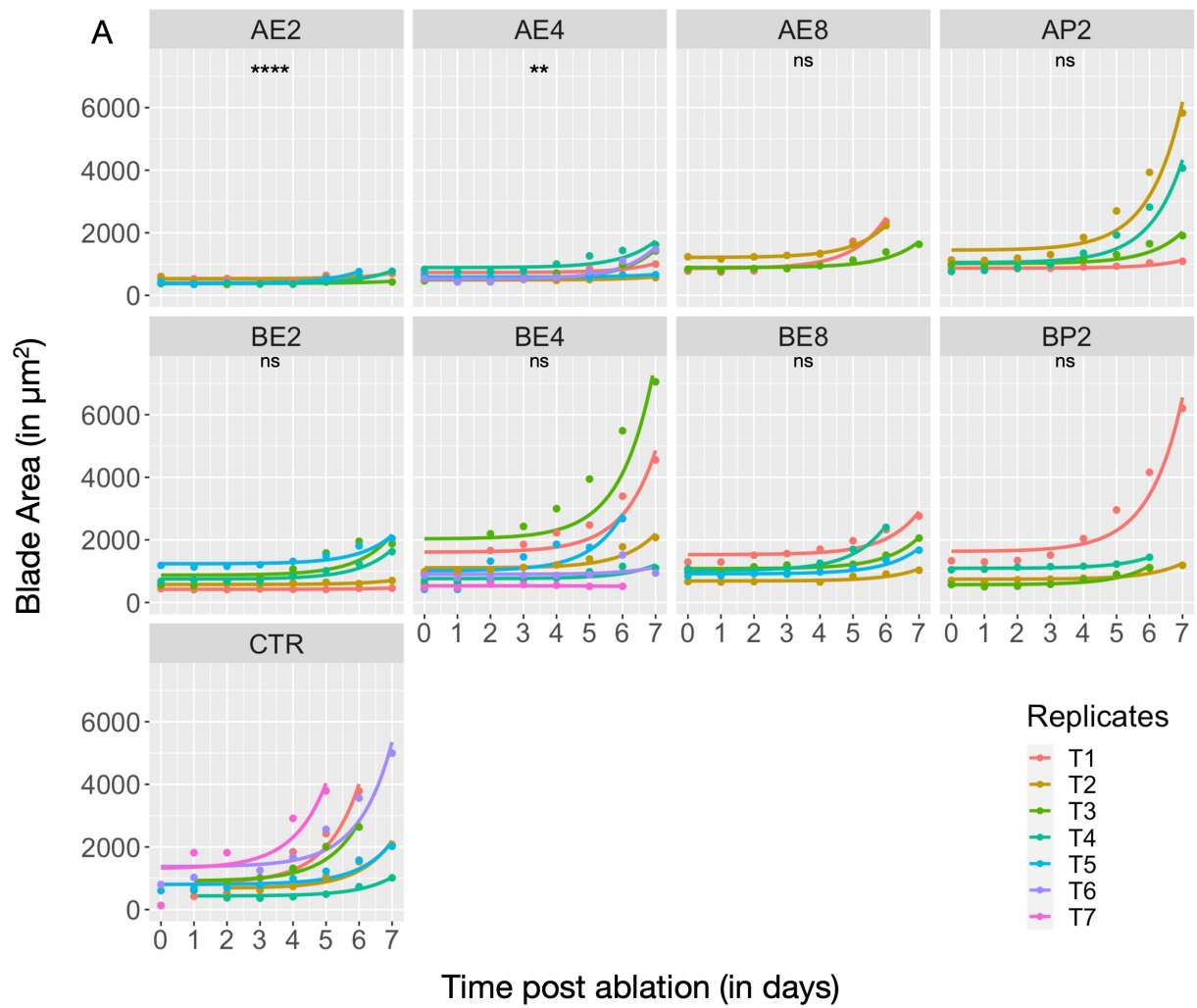
Figure 2: Distribution of morphologies observed after laser ablation

The morphologies of embryos in which either the apical (A series) or the basal (B series) cells were laser irradiated at different stages were grouped into four classes, and the percentage of each class was represented in the stacked histogram. Considering an initial growth delay, the four distinct morphologies were: 1) The "typical" morphology observed in intact embryos; 2) The growth-altered morphology, characterized by embryos encountering developmental delays or exhibiting a growth rate reduction exceeding 4 days beyond the initial delay; 3) The shape-altered morphology, involving embryos displaying variations in body axes or disturbances in the establishment of polarity; 4) The lethal morphology, applicable to organisms that did not survive beyond the tenth day following ablation. Columns represent the distribution of each stage at which laser ablation took place: E2: 2-cell stage; E4: 4-cell stage; E8+: 8-cell stage and early Phase II. The percentage of typical developmental morphologies gradually increases for embryos ablated of the basal cell after the 4-cell stage. The percentage of growth-altered embryos remains constant at all stages of apical cell ablation.

We quantified embryo area for 6 days after laser irradiation of the apical cell or basal cell at the same developmental stages as described above. Statistical comparison of the growth curves between the samples and the intact embryos (control) allowed us to confirm that irradiation of the apical cell at AE2 and AE4 resulted in a significant decrease in the rate of blade growth (expressed as the surface area) compared with the other embryos (Fig. 3A). In contrast, killing the basal cell had no significant impact on blade area at any developmental stage, suggesting that the apical cell in 2-cell stage embryos, or sub-apical cells in later stages, can effectively compensate for the absence of the basal cell. To reduce the developmental window and make the comparison between embryos of similar stages more accurate, we compared embryos of 15 to 25 cells (hereafter referred to as [15;25]). Fig. 3B then shows that AE2 and AE4 irradiated embryos grew 21% and 34% slower than BE2 and BE4 embryos, respectively (although this is not statistically supported).

Figure 3 (next page): Quantitative analysis of the impact of cell irradiation on the growth of the embryos

A) Blade area over time. The area (μm^2) of the embryo blades was measured using the home-made software every day for 7 days after laser irradiation. Time 0 corresponds to the time point before cell irradiation, and time 1 to the day after cell irradiation. The Kruskal-Wallis test showed that the area of AE2 and AE4 embryos was significantly lower compared to the other embryos. B) Blade area in Phase II embryos. Violin plot representation of all measured blade areas of embryos after laser irradiation once they reach an early Phase II. Only embryos with [15,25] cells were considered to allow comparison between blades of similar developmental stages. No significant difference was observed between samples (Kruskal-Wallis statistical test). Horizontal bars in the column display the median value, while the value of the mean is indicated close to the red spot. Above the violin plot is superposed a box plot showing the different quartiles.



To investigate whether a lower cell number or a reduced cell size is the cause of the reduction in the size of the embryos, we quantified the number of cells over time for each embryo (Suppl. Table 2). Plotting the cell areas calculated for each type of embryo did not display any significant difference between embryos in which the apical cell was irradiated and control embryos, and those in which the basal cell was irradiated (Fig. 4A). Therefore, smaller embryos do not have smaller cells. We then plotted the number of cells per embryo over time, and results showed that all irradiated embryos had the same cell number increase rate (Fig. 4B). While the number of cells doubles every 3 days for all the irradiated embryos, it is ~1.5 days for the control. However, as all the embryos have a similar growth rate, the specific impact of laser irradiation at AE2 cannot be explained by a reduction in the activity of cell division. Therefore, neither the cell size nor the cell division rate seems responsible for the observed reduction in the size of the embryo. One hypothesis is that both contribute to it. Alternatively, this could be due to a longer delay in resuming growth, as AE2 and AE4 need 7 and 6 days, respectively, before resuming growth while the other embryos need only 3-4 days (Suppl. Fig. 2).

Basal cells mainly control the shape of *Saccharina* embryo

The second most abundant morphology observed (Fig. 2) was altered embryo shape. While no shape alteration was observed in AE8+ embryos, 20% of AE2 and AE4 embryos displayed altered shapes (Fig. 2). For basal cells, these percentages increased: BE4 and BE8+ embryos showed significant alteration in shape, and this percentage reached 40% for BE2 (Fig. 2). The most common shape anomalies included rounder embryos and the emergence of rhizoids at the apex (Fig. 1). This suggests that the basal cell, more than the apical cell, is involved in controlling the shape of the embryo, and that its role diminishes with time during embryogenic Phase I.

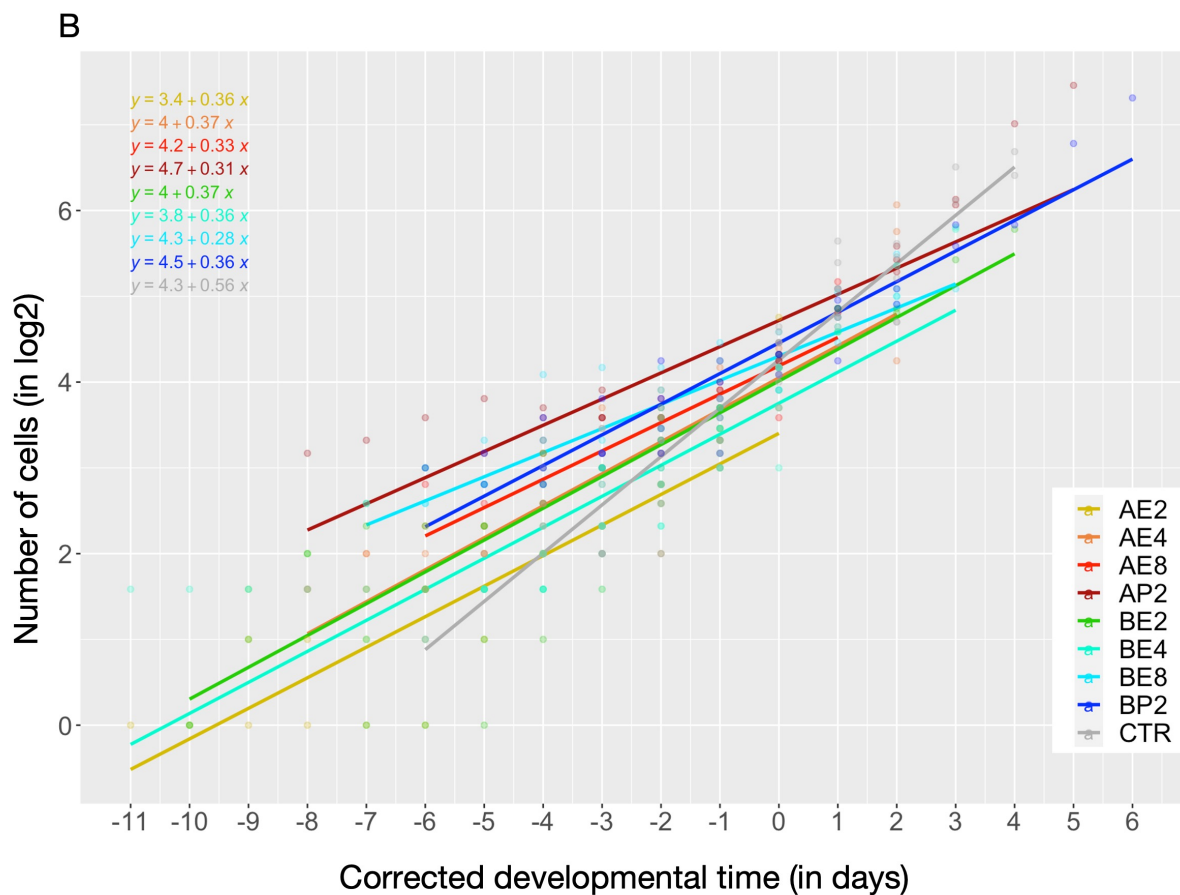
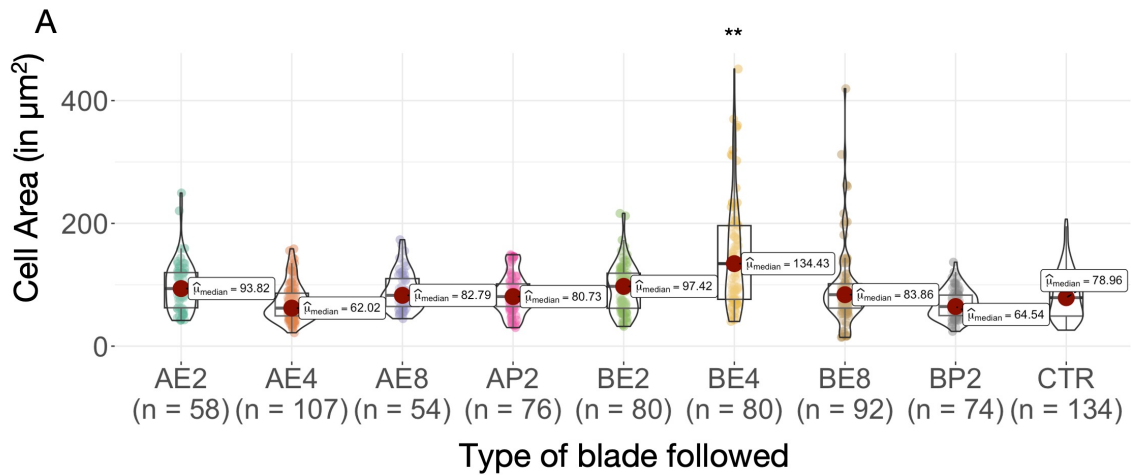


Figure 4: Cell size and cell number in smaller embryos

A) Cell area in Phase II embryos. Violin plots of the cell area (μm^2) for embryos subjected to laser ablation at different developmental stages. Stars indicate the P-value of the Kruskal-Wallis test, with significance determined using the Dunn test statistical test. B) Cell division rate over time. To compare embryos despite different laser irradiation times, embryos between 15 to 25 cells were considered Time 0. The logarithm (base 2) of the number of cells was expressed as a function of time (days).

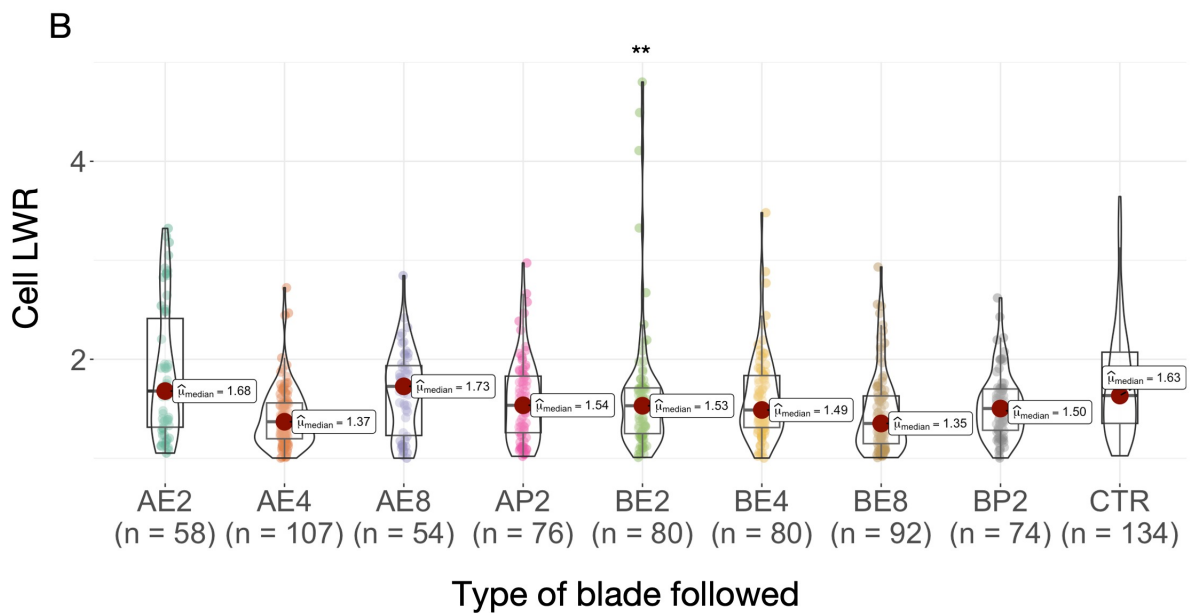
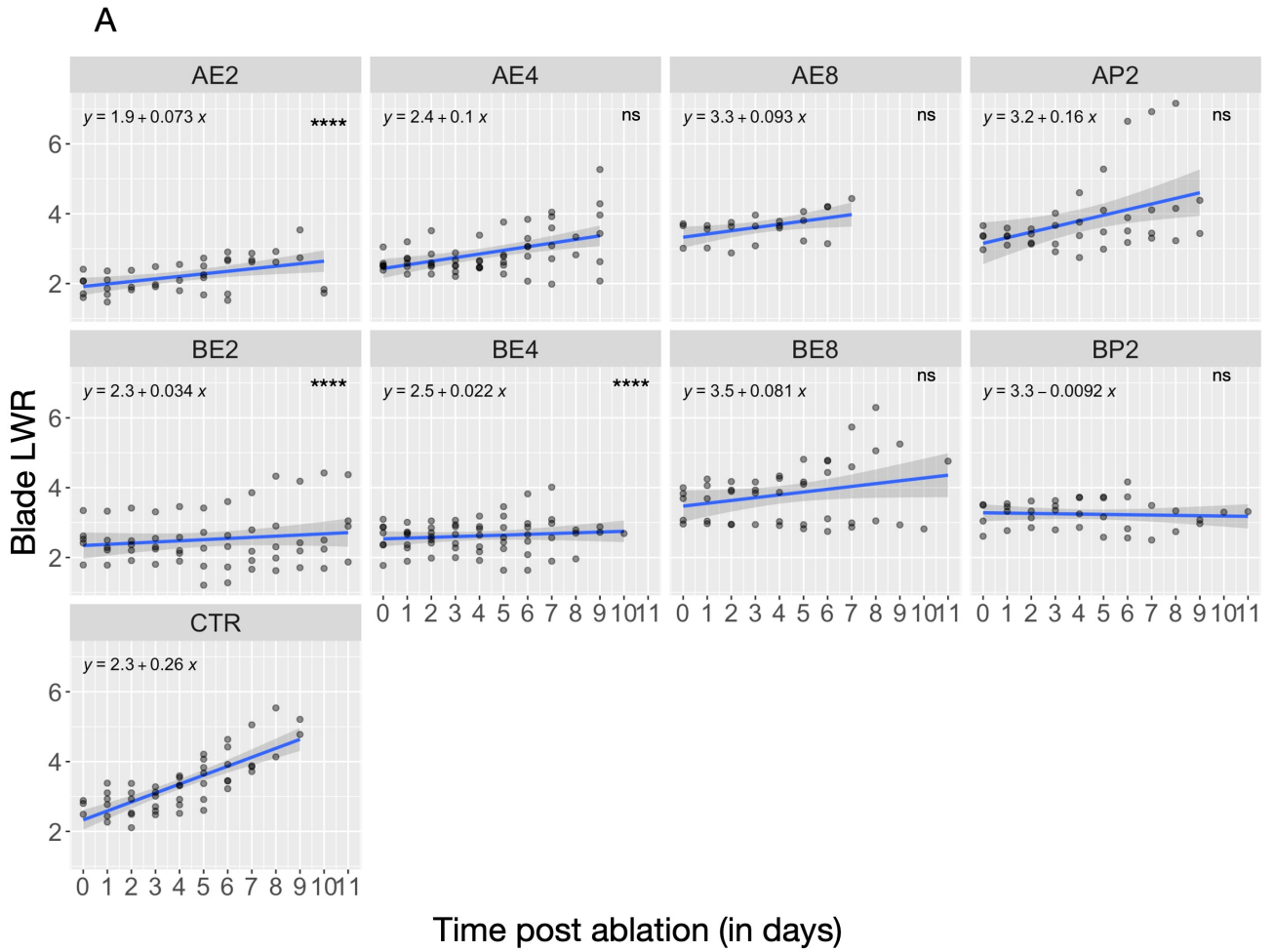
We plotted the ratio of the length to the width (LWR) of each embryo as a function of time up to 10 days after laser irradiation. BE2 and BE4 embryos had an almost stable LWR close to 2, while LWR increased from 2 to more than 4 in intact embryos (Fig. 5A). In embryos irradiated at other stages or cell positions, LWR continued to increase over time as in control embryos, where LWR was stable at a value of about 3.5. This can be explained by the fact that the 8-cell or Phase II embryos were already elongated. The exception was AE2, for which LWR increased slowly from 2 to 2.5 with time, making it significantly different from LWR in intact embryos, as for BE2 and BE4. Therefore, the shape of the embryo was impacted when apical or basal cells were killed at the 2-cell embryo stage. The effect persisted up to the 4-cell stage for the basal cell but not for the apical cell (Fig. 5A).

We then investigated whether a change in cell shape could be related to the change in embryo shape described above. Cell LWRs were calculated from the segmented images and plotted for the different embryo types. Fig. 5B shows that cell LWR was similar to LWR of intact embryos, except for BE2. Cells were more anisotropic because their LWR was higher. This result coincides with rounder embryo shapes. In intact embryos, the main axis of the cell is orthogonal to the main axis of the blade. Consequently, a higher cell LWR results in less elongated blades. Whether the embryo shape impacts cell shape, or the opposite, is still unknown. Overall, our results confirm that the basal cell is primarily involved in the control of embryo shape.

Figure 5 (next page): Cell ablation in 2-cell embryos impacts the establishment of the medio-lateral axis

A) Ratio of the embryo length to embryo width (embryo LWR) measured for 10 days after laser irradiation of either the apical or the basal cells at different developmental stages. The graph shows the mean regression line for each stage post-ablation and presents confidence intervals (grey surface). Embryos in later stages show a lower increase but higher values as the two primary axes are already established.

B) Cell length to width ratio in Phase II embryos. Violin plots of the cell length to width ratio (cell LWR) for embryos subjected to laser irradiation at different developmental stages. Significant differences from intact embryos are indicated by the 2 stars (Kruskal-Wallis statistical test; P value $< 10^{-2}$).



Basal cells negatively control the formation of longitudinal cell divisions

Upon closer examination of the cell division pattern of irradiated embryos, it was observed that the emergence of the first longitudinal division occurs earlier in embryos in which the basal cell was killed than in intact embryos (Fig. 1). While it occurs at the 8-cell stage in intact embryos (Fig. 6A, 6B, Theodorou & Charrier, 2023), it occurs as early as the 3-cell stage in embryos with a dead basal cell (Fig. 6B). The earlier the basal cell is killed, the earlier the longitudinal cell division occurs. This contrasts with embryos with dead apical cells in which the emergence of longitudinal cell division occurs similarly to the intact embryo, i.e., after the 6-cell stage (Fig. 6A,B). This implies that the apical cell behaves non-cell autonomously and requires the basal cell to maintain transverse cell divisions during embryogenic Phase I. This effect diminishes gradually during Phase I until the 8-cell stage.

Discussion

We have demonstrated that in the embryo of *Saccharina latissima*, ablation of the apical or basal cells has an impact only at the very beginning of the embryogenetic stage, i.e., when the embryo reaches up to 4 cells. After that stage, the removal of basal or apical cells no longer affects the embryogenetic developmental pattern or growth. This suggests that while the apical and the basal cells act cell-autonomously just after fertilization, they are then subject to a regulative mode of development in which their behavior is integrated into the rest of the embryo and depends on the behavior of their neighboring cells. Such regulative development at later embryogenetic stages has already been observed in the brown alga *Fucus* (Berger 1994; Bouget 1998), in plants (Gaillochet et al., 2015), and animals (Arias et al., 2013). Furthermore, we have shown that in the early stages, apical and basal cells have different functions. While the basal cell mainly controls the shape of the embryo, the apical cell is only involved in controlling the growth of the embryo. Therefore, at that stage, each cell seems to have its own identity, which argues in favor of a deterministic development where each cell acts autonomously.

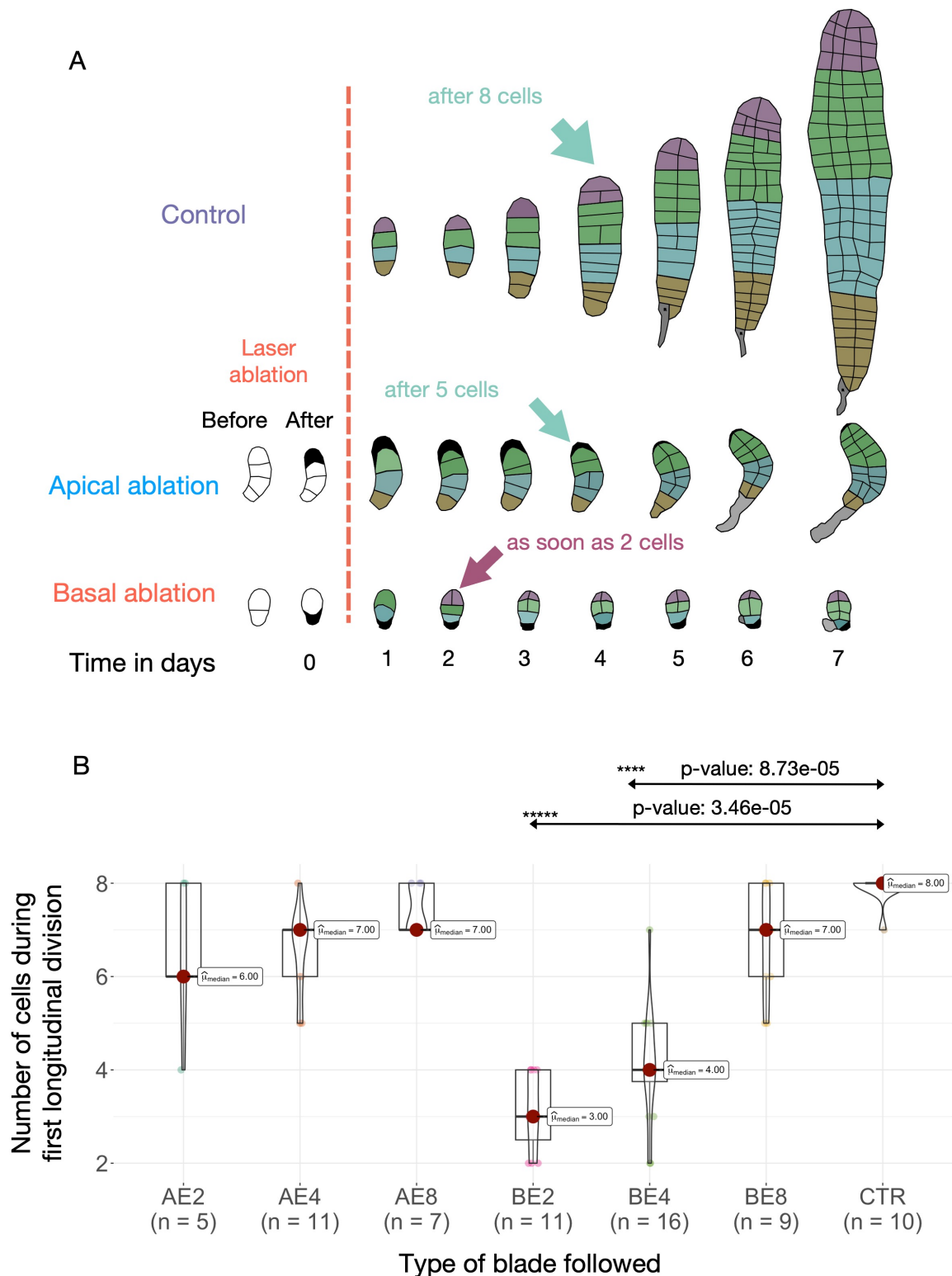


Figure 6: Ablation of the basal cell causes premature longitudinal cell division

A) Schematic representation of the effect of cell killing on the axis establishment of embryos. Embryos devoid of apical cell in Phase II after developing 5 to 8 cells. This time of transition corresponds to the developmental time of controls but suggests that the embryo is likely under tissue organization mechanisms. On the contrary, the embryo ablated of their basal cell presents an almost immediate transition to Phase II, resulting in rounder organisms with less defined axis differentiation. B) Violin plot of the recorded cell number at the time of longitudinal cell division emergence for all embryos. Significance is shown using a Kruskal-Wallis test and Dunn test. BE2 and BE4 presented their first longitudinal cell division almost immediately after ablation, promoting the establishment of the medio-lateral axis.

The first question arises: What is the cue that gives the cells their specific identity at the 2 and 4-cell stages? The basal cell is in contact with the maternal stalk, which is the remnant of the oogonium. It is made of a volume filled with viscous polysaccharides and surrounded by the oogonium cell wall, which persists late during embryogenetic Phase II. Therefore, the maternal tissue might have provided the egg or zygote with determinants involved in the formation of an apico-basal axis. Interestingly, while the ultrastructure of the egg before and after fertilization reveals a polarized distribution of organelles (Motomura, 1990; Motomura, 1991), the zygote before cell division is organized symmetrically. The unequal first cell division might then lead to an unequal distribution of the intracellular content of the zygote in the smaller basal cell and the larger apical cell. Knowledge in plants indicates that size differences between the daughter cells of a first zygotic cell division do not necessarily result in different cell fate though (Lau et al., 2012). Nevertheless, in *Saccharina*, cell lineage up to the 100 cell-stage displayed asymmetrical growth rates consistent with the unequal size of the two daughter cells (Theodorou, 2023). The basal area of the embryo lamina that developed from the initial basal cell contains fewer cells than the apical counterpart (not shown). This supports our current results where the removal of the apical cells up to the 4-cell stage results in smaller embryos compared to control and basally ablated embryos. It is therefore interesting to note that even after this stage, when the embryo contains around 50-100 cells, the impact of the early laser ablation is still visible, meaning that although development is regulative at this stage, the cells cannot catch up with the impact of the event that occurred earlier.

The second question arises: Why do cells lose their identity after the 4-cell stage? Killing the apical cell or the basal cell after the 4-cell stage had no impact on the size and shape of the embryo at later stages. The 8-cell stage corresponds to the end of Phase I (Theodorou and Charrier, 2023) during which growth is longitudinal by means of transverse cell divisions only. After that step, the first longitudinal cell division takes place, initiating medio-lateral growth (Phase II). A flat lamina continued to grow in two dimensions for more than 10 days, through alternating transverse and longitudinal cell divisions, with no apparent cell differentiation. Therefore, the 8-cell stage is a major transition in the embryogenetic pattern of

Saccharina, which could coincide with a change in the allocation of cell function. Whereas the apical and basal cells of the 2-cell embryos would have a specific role in the control of the embryo shape and growth, cells in Phase II would all behave the same way in terms of orientation of cell division, growth rate, and lack of cell differentiation. Thus, the destruction of apical or basal cells in 8-cell and early Phase II embryos has no more impact than the destruction of any other cell of these embryos. Unfortunately, we did not test this hypothesis by irradiating cells located between the apical and basal cells.

Interestingly, the shift to Phase II by initiation of the first longitudinal cell division occurs at the same embryogenetic stage when the apical cell has been killed at the 2-cell stage, as in intact embryos. However, at that stage, the embryo is depleted of half of its cells, and if the basal cell acted autonomously, one would expect the initiation of longitudinal cell division to take place at the 4-cell stage, independently of the absence of the apical part. This observation suggests that the control of longitudinal cell division is dependent on the number of cells in Phase I embryo when the basal cell is present, and not when the basal cell is absent. If the basal cell were to be used as a positional landmark, it could be assumed that it emits an acropetal signal involved in a distance-dependent negative control of longitudinal cell division. Interestingly in *Arabidopsis*, an acropetal transport of auxin from maternal tissue controls the formation of the apico-basal axis of the embryo (Robert et al., 2018). The tissue context is reminiscent of that of the *Saccharina* embryo, which remains physically connected to the maternal tissue via the persistent stalk. However, while auxin appears to be synthesized and to affect development in brown algae (Le Bail et al., 2011; Bogaert et al., 2019; Uji and Mizuta, 2022) its effect remains to be determined in Laminariales, especially during embryogenesis. If auxin or another signaling molecule were transported acropetally to the apical part of the embryo, this could be via plasmodesmata. These cytoplasmic channels facilitating symplastic exchanges of elements up to 20 kDa in brown algae (Nagasato, 2015) have been observed in *Saccharina* sporophytes and gametophytes (Terauchi et al., 2014), and in late embryos (Theodorou & Charrier, 2023). We were even able to observe plasmodesmata in embryos as early as the 6-cell stage (not shown). In

addition, plasmodesmata could underlie the regulative development that takes place after the 4-cell stage.

Laser ablation experiments performed on embryos of the brown alga *Fucus* yielded different results. In *Fucus*, unlike *Saccharina*, eggs and sperm cells are released into the seawater, and fertilization takes place far from the parental organisms. The first cell division of the zygote is unequal and asymmetrical. The large apical cell gives rise to the thallus, while the small basal cell gives rise to the rhizoid (Rusig et al., 2001). Ablation of either rhizoid or thallus cells has shown that the cell wall dictates the fate of the newly growing cell. This cell differentiates into a rhizoid when it grows in contact with the cell wall of the previously irradiated rhizoid cell. Reciprocal observations have been made for new cells growing in contact with the thallus cell wall (Berger et al., 1994). However, because the protoplasts of *Fucus* zygotes differentiate into one thallus and one rhizoid cell in the same way as a native zygote surrounded by its cell wall, the primary role of the cell wall is unclear, and it is possible that other cues control cell differentiation in the early embryo in this species.

The formation of rhizoids observed in irradiated *Saccharina* embryos also suggests different mechanisms of embryogenic cell fate between *Saccharina* and *Fucus*. In Phase II *Saccharina* embryos, rhizoids differentiate at the base of the blade (Yendo, 1911; Kanda, 1936; Sauvageau, 1918). In this study, we observed that they also differentiate from incompletely emptied cells of irradiated embryos or injured embryos. Therefore, while in *Fucus* the differentiation of rhizoid cells from thallus cells requires the presence of a rhizoid cell wall (Berger et al., 1994), in *Saccharina*, rhizoids develop from any cells of the irradiated embryo. The difference may be due to the fact that intact *Saccharina* embryos do not develop rhizoids before Phase II, whereas *Fucus* develops a rhizoid at the zygote stage. Therefore, the cell wall cues responsible for rhizoid differentiation hypothesized in *Fucus* cannot be present in *Saccharina*, and it is more likely that rhizoid differentiation is a response to wounding or mechanical stress (Shirae-Kurabayashi et al., 2022). This is consistent with what has been observed at a later stage of *Fucus* embryogenesis, where rhizoids differentiate from any cells of damaged embryos (Bouget et al., 1998).

Conclusion

Brown algae, like animals, have different ways of regulating the establishment of their body axes. Embryogenetic mechanisms were classically termed deterministic (formerly "mosaic") or non-deterministic (formerly "regulative") based on the inheritance by the egg of maternal polarity cues versus the perception by the cells of the embryo of position-dependent cues from the environment (including neighboring cells) (Stern, 2006; Lawrence and Levine, 2006). Here, we show that while embryos up to the 4-cell stage develop with cell-autonomous control of the establishment of their thallus axes, embryos at later stages switch to a non-cell-autonomous mode of embryogenesis where cells act collectively to control the development of the embryo. Therefore, *Saccharina* embryogenesis seems to rely on both processes, as in animals and plants (Lawrence and Levine, 2006; Robert et al., 2013; Wang et al., 2021). Ongoing RNAseq experiments on apical and basal cells isolated from embryos at 2-cell, 4-cell, 8-cell, and beyond stages will elucidate potential cellular differences at the molecular level, as is the case in plant embryos (Lau et al., 2012).

Material and Methods

Algal culture

The culture and production of *Saccharina latissima* (Arthrothamnaceae, Laminariales, Phaeophyceae) embryos were conducted following the protocol outlined in (Theodorou and Charrier, 2021; Theodorou et al., 2021). Fixed female and male genotypes were utilized by selecting one female gametophyte (F1) and one male gametophyte (M1) from the same sporophyte collected from the beach of Perharidy in Roscoff (48°43'33.5"N 4°00'16.7"W). Upon crossing, F1 and M1 exhibited stable and effective embryo growth. Both embryos and gametophytes were cultivated in Provasoli-enriched natural seawater. Gametophytes (F1&M1) were cultivated together through vegetative multiplication as described in Theodorou et al., 2021. Gametes were obtained through the maturation of gametophytes under 16 $\mu\text{mol photons m}^{-2}\text{s}^{-1}$ white light intensity and a 14:10 light:dark photoperiod at 13

°C. If necessary, they were maintained under such conditions to reach the required stage.

Laser irradiation of embryo cells at different developmental stage

Developing embryos from glass-bottom Petri dishes were selected under a flow hood using an inverted microscope (LSM 880 Zeiss confocal microscope). Laser ablation of either the apical or the basal cell was conducted on embryos following the procedure outlined in Boscq et al., 2022. Embryos within the same dish that were not subjected to laser ablation served as control organisms. Laser irradiation was carried out on embryos at the 2-cell (E2), 4-cell (E4), 8-cell (E8) stage, and in Phase II (P2). To minimize stress during transportation to the cytology platform (Rennes, France), embryos were transported in a cooler set to 13°C. Their growth and development under standard growth conditions were monitored for 10 days using time-lapse microscopy.

Image acquisition

All experiments involving time-lapse microscopy of growing embryos were recorded using a bright-field microscope (Leica DMI600B, Leica Inverted phase contrast, or Leica DMI8) equipped with a DFC450C camera. Acquisition intervals of 24 hours were set for a duration of at least 10 days after irradiation. The required temperature and lighting conditions were maintained within a carbonate-glass chamber attached to the microscope, which was equipped with a thermostatically controlled air flow system (Cube and Box, Life Imaging services), and LED white light sources commercially available.

Manual segmentation

Automatic segmentation was found to be challenging due to the constant pigmentation changes of the cells, which transitioned from high to low coloration. Additionally, daily exposure to UV light to reveal cell wall staining with the chemical Calcofluor White proved detrimental to the algae's survival, making it unsuitable for precise acquisition of cell wall outlines. Therefore, we opted to perform manual segmentation. Images from the time-lapse recordings with intervals of 24 hours were segmented using Fiji (ImageJ2 version 2.9.0). Due to slight inclinations of

individual embryos, segmentation was conducted directly on the z-stacks to improve accuracy. Subsequently, the outlines were implemented in Inkscape (version 1.2). To minimize light deformation, we selectively segmented predominantly flat-growing embryos. To assist in drawing the cell contours, all z-stacks from a time series were compared. The resulting cell wall contours were analyzed using in-house software, which extracted multiple quantitative parameters for each lamina (blade) and its cells.

Quantitative morphometry

Cell walls were manually delineated on bright-field images as segmented lines using the vector graphics editor Inkscape (v1.2.2, <https://inkscape.org>). The resulting drawings were saved as scalable vector graphics (SVG) files. These SVG files were then processed using a dedicated software developed by us, called "blade_painter," written in object-oriented Python 3 (Van Rossum and Drake, 2023). The "blade_painter" software reads the SVG files and extracts various geometric properties for cells and blades, utilizing algorithms based on prior research (Rosin, 2005; Fletcher et al., 2013). Specifically, the software extracts: (a) Each cell contour, from which the perimeter length and surface area are directly derived; (b) Convex hull, which is used to compute the minimal bounding rectangle (MBR). The main axis, length, and width ratio (or elongation) of the cell are assumed to be those of the MBR; (c) Rectangularity, computed as the proportion of overlapping surface between the cell and its MBR, rescaled to the same area; (d) Neighbor cell count, where two cells are considered neighbors if they share at least 200 nm of cell wall (this threshold can be adjusted as a software parameter); (e) Blade area; (f) Blade main and secondary axes orientation and length, computed according to the method described by Fletcher et al. (2013).

Statistical tests

This experiment was repeated two individual times with similar results. All quantitative data were analyzed statistically using Kruskal-Wallis test, except for parameters distributed in multiple major values such as the number of neighbors, which were analyzed using Chi-squared test. Significant Kruskal-Wallis tests were followed by a Dunn test and a Bonferroni adjustment to find the pairs significantly

different. All tests were done under R environment (v4.2.3, R Core Team 2023) using the R Core stats package and the "rstatix" package (v0.7.2, Kassambara 2023).

References

- Angelo, J. R. and Tremblay, K. D.** (2013). Laser-mediated cell ablation during post-implantation mouse development. *Dev. Dyn.* **242**, 1202–1209.
- Arias, A. M., Nichols, J. and Schröter, C.** (2013). A molecular basis for developmental plasticity in early mammalian embryos. *Development* **140**, 3499–3510.
- Berger, F. and Brownlee, C.** (1994). Photopolarization of the *Fucus* sp. Zygote by Blue Light Involves a Plasma Membrane Redox Chain. *Plant Physiol.* **105**, 519–527.
- Berger, F., Taylor, A. and Brownlee, C.** (1994). Cell fate determination by the cell wall in early *Fucus* development. *Science* (80-.). **263**, 1421–1423.
- Bogaert, K. A., Beeckman, T. and de Clerck, O.** (2015). Photopolarization of *Fucus* zygotes is determined by time sensitive vectorial addition of environmental cues during axis amplification. *Front. Plant Sci.* **6**, 126622.
- Bogaert, K. A., Beeckman, T. and De Clerck, O.** (2017a). Two-step cell polarization in algal zygotes. *Nat. Plants* **3**, 1–7.
- Bogaert, K. A., Beeckman, T. and De Clerck, O.** (2017b). Egg activation-triggered shape change in the *Dictyota dichotoma* (Phaeophyceae) zygote is actin-myosin and secretion dependent. *Ann. Bot.* **120**, 529–538.
- Bogaert, K. A., Blommaert, L., Ljung, K., Beeckman, T. and De Clerck, O.** (2019). Auxin Function in the Brown Alga *Dictyota dichotoma*. *Plant Physiol.* **179**, 280–299.
- Bogaert, K. A., Zakka, E. E., Coelho, S. M. and De Clerck, O.** (2023). Polarization of brown algal zygotes. *Semin. Cell Dev. Biol.* **134**, 90–102.
- Bouget, F. Y., Berger, F. and Brownlee, C.** (1998). Position dependent control of cell fate in the *Fucus* embryo: Role of intercellular communication. *Development* **125**, 1999–2008.
- Brownlee, C. and Wood, J. W.** (1986). A gradient of cytoplasmic free calcium in growing rhizoid cells of *Fucus serratus*. *Nat.* 1986 3206063 **320**, 624–626.
- Byrne, A. B. and Hammarlund, M.** (2017). Axon regeneration in *C. elegans*: Worming our way to mechanisms of axon regeneration. *Exp. Neurol.* **287**, 300–309.
- Coelho, S. M., Taylor, A. R., Ryan, K. P., Sousa-Pinto, I., Brown, M. T. and Brownlee, C.** (2002). Spatiotemporal patterning of reactive oxygen production and Ca²⁺ wave propagation in *fucus* rhizoid cells. *Plant Cell* **14**, 2369–2381.
- Costa, L. M., Marshall, E., Tesfaye, M., Silverstein, K. A. T., Mori, M., Umetsu, Y., Otterbach, S. L., Papareddy, R., Dickinson, H. G., Boutiller, K., et al.** (2014). Central cell-derived peptides regulate early embryo patterning in flowering plants. *Science* (80-.). **344**, 168–172.
- Fouad, A. D., Liu, A., Du, A., Bhirgoo, P. D. and Fang-Yen, C.** (2021). Thermal laser ablation with tunable lesion size reveals multiple origins of seizure-like convulsions in *Caenorhabditis elegans*. *Sci. Reports* 2021 111 **11**, 1–9.
- Fritsch, F.E.** (1935). *The structure and reproduction of the algae*. Volume 1 (Cambridge University Press).

- Fritsch, F.E.** (1945) The structure and reproduction of the algae. Volume 2. (Cambridge University Press).
- Gaillochot, C. and Lohmann, J. U.** (2015). The never-ending story: from pluripotency to plant developmental plasticity. *Development* **142**, 2237–2249.
- Goddard, H., Manison, N. F. H., Tomos, D. and Brownlee, C.** (2000). Elemental propagation of calcium signals in response-specific patterns determined by environmental stimulus strength. *Proc. Natl. Acad. Sci. U. S. A.* **97**, 1932–1937.
- Johnson, C. S., Holzemer, N. F. and Wingert, R. A.** (2011). Laser ablation of the zebrafish pronephros to study renal epithelial regeneration. *J. Vis. Exp.* **e2845**.
- Kassambara A.** (2023). *rstatix*: Pipe-Friendly Framework for Basic Statistical Tests. R. package version 0.7.2, <https://CRAN.R-project.org/package=rstatix>
- Lau, S., Slane, D., Herud, O., Kong, J. and Jürgens, G.** (2012). Early embryogenesis in flowering plants: Setting up the basic body pattern. *Annu. Rev. Plant Biol.* **63**, 483–506.
- Lawrence, P. A. and Levine, M.** (2006). Mosaic and regulative development: two faces of one coin. *Curr. Biol.* **16**,.
- Le Bail, A., Billoud, B., le Panse, S., Chenivresse, S. and Charrier, B.** (2011). ETOILE Regulates Developmental Patterning in the Filamentous Brown Alga *Ectocarpus siliculosus*. *Plant Cell* **23**, 1666–1678.
- Lüning, K.** (1981). Egg release in gametophytes of *Laminaria saccharina*: Induction by darkness and inhibition by blue light and u.v. *Br. Phycol. J.* **16**, 379–393.
- Motomura, T.** (1990). Ultrastructure of Fertilization in *Laminaria angustata* (Phaeophyta, Laminariales) with Emphasis on the Behavior of Centrioles, Mitochondria, and Chloroplasts of the Sperm. *J. Phycol.* **26**, 80–89.
- Motomura, T.** (1991). Immunofluorescence Microscopy of Fertilization and Parthenogenesis in *Laminaria angustata* (Phaeophyta). *J. Phycol.* **27**, 248–257.
- Nagasato, C., Terauchi, M., Tanaka, A. and Motomura, T.** (2015). Development and function of plasmodesmata in zygotes of *Fucus distichus*. *Bot. Mar.* **58**, 229–238.
- Reinhardt, D., Frenz, M., Mandel, T. and Kuhlemeier, C.** (2005). Microsurgical and laser ablation analysis of leaf positioning and dorsoventral patterning in tomato. *Development* **132**, 15–26.
- Robert, H. S., Grones, P., Stepanova, A. N., Robles, L. M., Lokerse, A. S., Alonso, J. M., Weijers, D. and Friml, J.** (2013). Local auxin sources orient the apical-basal axis in arabidopsis embryos. *Curr. Biol.* **23**, 2506–2512.
- Robert, H. S., Park, C., Gutiérrez, C. L., Wójcikowska, B., Pěňčík, A., Novák, O., Chen, J., Grunewald, W., Dresselhaus, T., Friml, J., et al.** (2018). Maternal auxin supply contributes to early embryo patterning in Arabidopsis. *Nat. Plants* **2018** **4**, 548–553.
- Rosin, P. L.** (2005). Computing global shape measures. *Handb. Pattern Recognit. Comput. Vision*, **3rd Ed.** 177–196.
- Rusig, A. M., Ouichou, A., Le Guyader, H. and Ducreux, G.** (2001). Ontogenesis in the Fucoiphyceae: case studies and comparison of fucoid zygotes and *Sphacelaria* apical cells. *Cryptogam. Algol.* **22**, 227–248.
- Sauvageau, C.** (1918). Recherches sur les laminaires des côtes de France. *Mem. Acad. Sci. Inst. Fr.* **56**, 1–240.
- Shirae-Kurabayashi, M., Edzuka, T., Suzuki, M. and Goshima, G.** (2022). Cell tip growth underlies injury response of marine macroalgae. *PLoS One* **17**,.
- Stern, C. D.** (2006). Evolution of the mechanisms that establish the embryonic axes. *Curr. Opin. Genet. Dev.* **16**, 413–418.

Sun, H., Basu, S., Brady, S. R., Luciano, R. L. and Muday, G. K. (2004). Interactions between Auxin Transport and the Actin Cytoskeleton in Developmental Polarity of *Fucus distichus* Embryos in Response to Light and Gravity. *Plant Physiol.* **135**, 266–278.

Tarakhovskaya, E., Lemesheva, V., Bilova, T. and Birkemeyer, C. (2017). Early embryogenesis of brown alga *fucus vesiculosus* L. is characterized by significant changes in carbon and energy metabolism. *Molecules* **22**, 1509.

Terauchi, M., Nagasato, C. and Motomura, T. (2015). Plasmodesmata of brown algae. *J. Plant Res.* **128**, 7–15.

Theodorou, I. and Charrier, B. (2021). Brown Algae: *Ectocarpus* and *Saccharina* as experimental models for developmental biology. In *Handbook of Marine Model Organisms in Experimental Biology: Established and Emerging*, pp. 27–47.

Theodorou, I. and Charrier, B. (2023). The shift to 3D growth during embryogenesis of kelp species, atlas of cell division and differentiation of *Saccharina latissima*. *Development* **150**,.

Theodorou, I., Opsahl-Sorteberg, H.-G. and Charrier, B. (2021). Preparation of Zygotes and Embryos of the Kelp *Saccharina latissima* for Cell Biology Approaches. *BIO-PROTOCOL* **11**,.

Uji, T. and Mizuta, H. (2022). The role of plant hormones on the reproductive success of red and brown algae. *Front. Plant Sci.* **13**, 1019334.

van den Berg, C., Hage, W., Weisbeek, P. and Scheres, B. (1998). Laser Ablation In *Arabidopsis* Roots: A Tool To Study Cell-To-Cell Communication. In *Cellular Integration of Signalling Pathways in Plant Development*, pp. 237–250. Springer, Berlin, Heidelberg.

Wang, K., Chen, H., Ortega-Perez, M., Miao, Y., Ma, Y., Henschen, A., Lohmann, J. U., Laubinger, S. and Bayer, M. (2021). Independent parental contributions initiate zygote polarization in *Arabidopsis thaliana*. *Curr. Biol.* **31**, 4810-4816.e5.

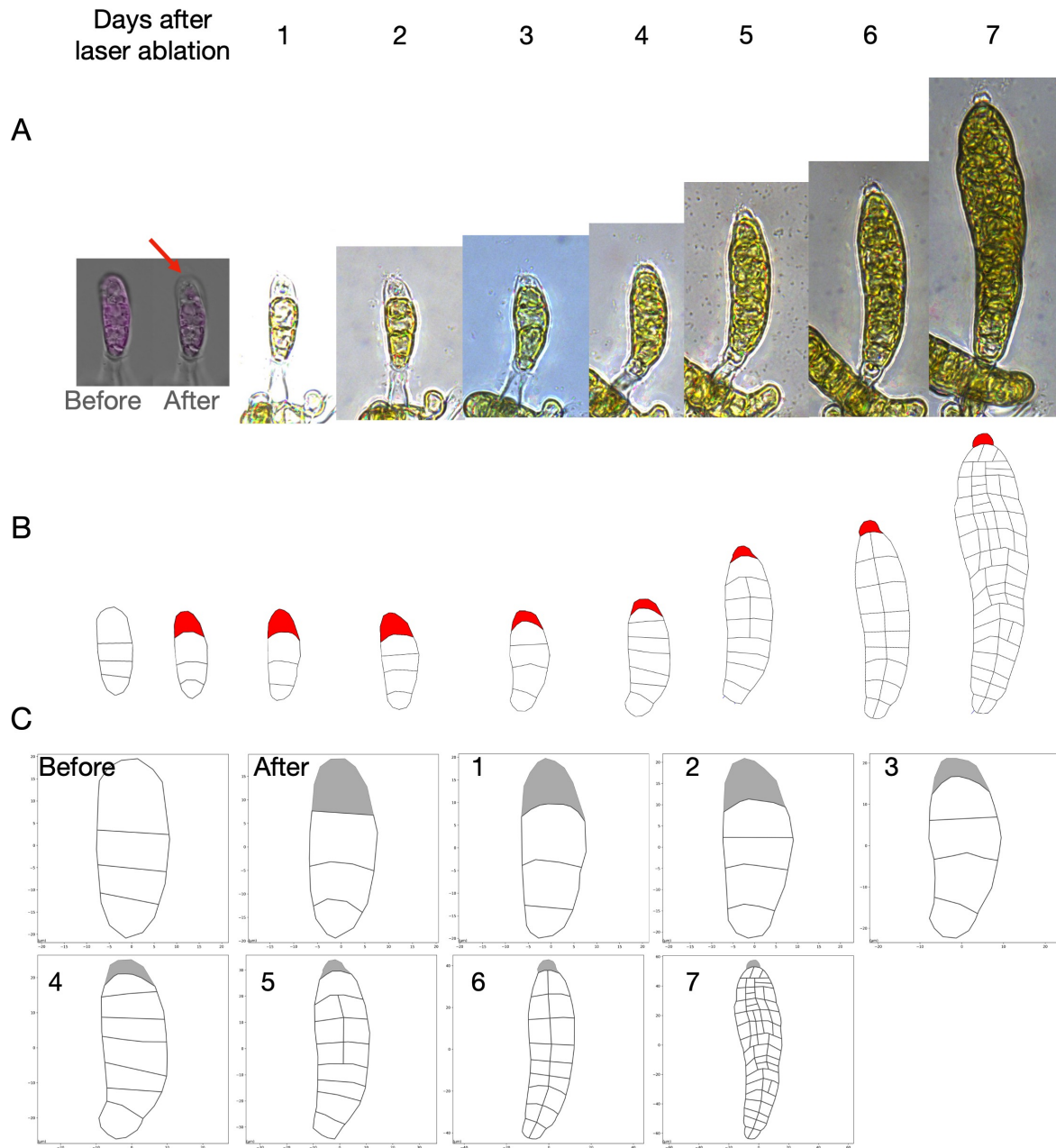
Yendo, K. (1911). The development of *costaria*, *undaria*, and *laminaria* with plates lih-lv. *Ann. Bot. os*-**25**, 691–716.

Supplementary material

[Suppl. Table 1: Morphometric parameters of the embryo \(blade\).](#)

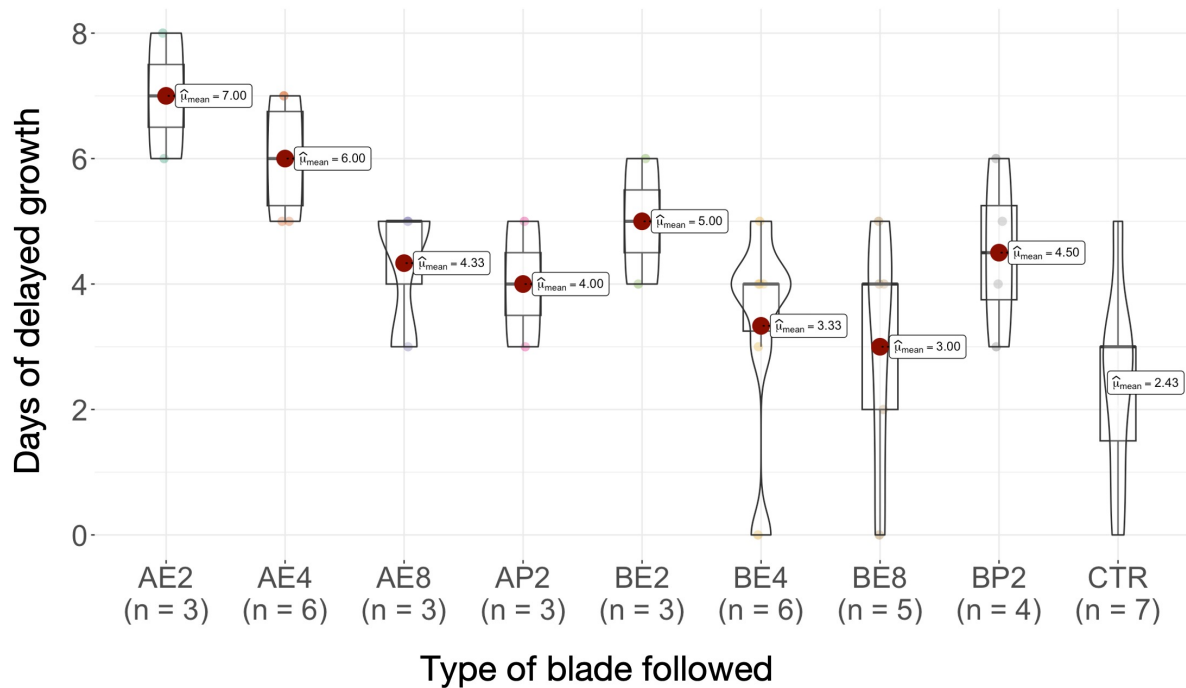
[Suppl. Table 2: Cell morphometrics in each embryo.](#)

[Suppl. Movie: Ablation of apical cell \(left\) or basal cell \(right\) in a 4-cell stage embryo](#)



Suppl. Figure 1: Manual segmentation workflow

A) Brightfield images of *Saccharina latissima*. The red arrow displays the irradiated cell. B) Manually segmented embryos corresponding to the time-lapse images of the above embryo. Segmented embryos were drawn as vectors with the Inkscape software (v1.2.2) to display the cell contours. The region in red represents the outer cell wall of the irradiated cells that are still visible. C) Visual output using the home-made software. Embryos manually segmented in B) were treated by the software to display the cell outlines, the center of gravity, and an ID number for each cell. Additional quantitative data for each cell and the whole blade were computed (Suppl Tables 1 and 2).



Suppl. Figure 2: Delay of growth

Violin plot graph representing the number of days before growth resumes after laser shooting. The end of delay was evaluated based on the start of exponential growth on a graph of number of cells over time. Irradiation of the apical cell caused a stronger delay compared to a similar basal-irradiated stage embryo, especially in 2-cell (AE2) and 4-cell (AE4) embryos.

6 - General Discussion

During this PhD, I explored the embryogenesis of the brown alga *Saccharina latissima*. The results provide insights into the regulation of the establishment of the body plans of this kelp model species. Altogether, the information in the above chapters allows me to present a **comprehensive model**. I also present additional observations, ongoing work, and further questions that will need to be addressed in the future.

Establishment of the first axes involves the cytoskeleton and the cell wall

Similarly to gametes in other brown algae, *Saccharina* gametes lack a cell wall upon release (Kropf et al., 1988; Motomura 1990; Bothwell et al., 2008). During the elongation of the zygote, a diffuse layer of alginates and fucans polysaccharides was observed to envelop the embryo (**Chapter I**). As such, upon elongation, the zygote of *Saccharina latissima* becomes encapsulated in a mucus mostly not present during the egg stage. Based on images of embryos at different points in their elongation, a volume loss was calculated to occur before the first division (not shown). Building upon earlier hypotheses proposed in *Dictyota* (Bogaert et al., 2017a), it is plausible that the secretion of mucosal wall material during embryo elongation serves to prevent the zygote membrane from rupturing as it elongates. Moreover, this layer was observed to possess adhesive properties, potentially aiding zygote attachment to the substrate or stalk structure (**Chapter II**). Additionally, localized occurrences of a denser cell wall spot were observed primarily on the upper half of the embryo (not shown). While precise confirmation would necessitate strict monitoring during a fertilization event, it remains probable that sperm in kelps triggers localized and/or uniform wall synthesis, akin to Fucoiales and Dictyotales embryos (Bogaert et al., 2023). However, observations of *Saccharina latissima* parthenosporophytic embryos show that cell wall synthesis and zygote elongation do not rely solely on sperm entry (Fig. 1). This presents an elongation mechanism similar to Dictyotales but different from Fucales where sperm entry can dictate the orientation of the polarization (Bogaert et al., 2017b). In kelp embryos, the anchoring flagella de facto polarizes the zygote and the resulting elongation follows this predetermined axis (Figure 1; Klochkova et al., 2019; Bogaert et al., 2023). As such, embryos have already undergone the process of "axis formation" and are freed of the "axis selection" step described in *Fucus* and *Dictyota* (Kropf, 1987; Bogaert et

al., 2017b). Yet, *Saccharina* embryos are still required to go through "axis amplification" and "axis fixation". Because an early transition to Phase II results in the loss of the primary axis. The "axis amplification" step occurs through Phase I and "axis fixation" on transition to Phase II (**Chapter II and Chapter III**).

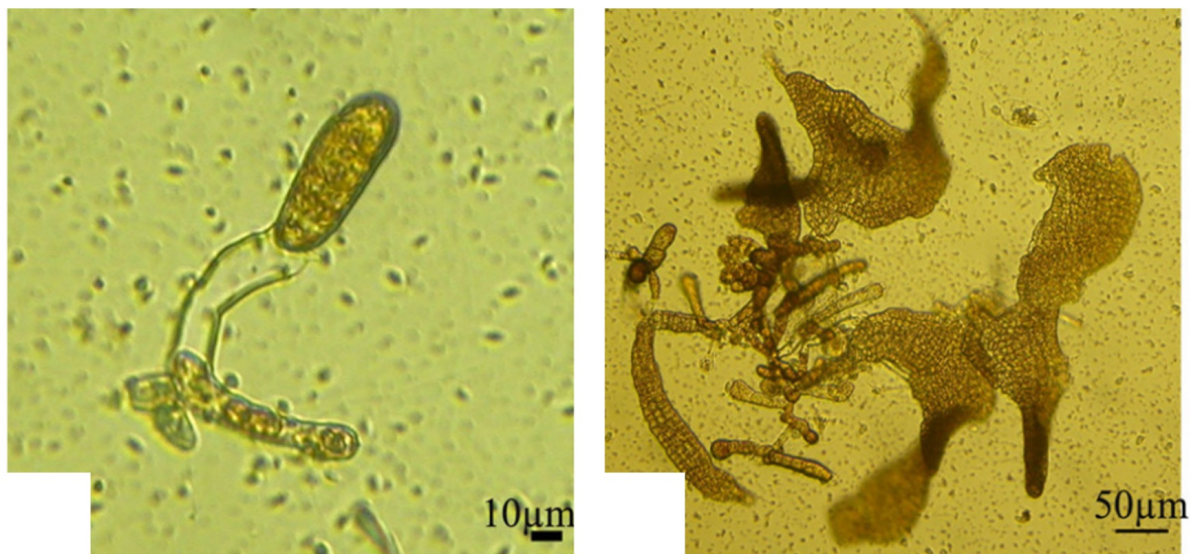


Figure 1: Observation of parthenosporophytic embryos of *S. latissima*.

Under dim white light, the female gametophyte (F1) releases eggs. Among all gamete releases and in the absence of a fertilization event, most parthenosporophytic embryos detach and degenerate. However, a low percentage (~1%) of parthenosporophytic embryos remain attached to their stalk and are observed to develop according to the developmental pattern described in *Saccharina latissima* (Theodorou and Charrier, 2023). However, at some point in late Phase II but before Phase III, they degenerate and are not able to proceed further in their development. Photos are from experiments done by I. Theodorou.

In addition, we also observed structured layers of the cell wall (cellulose, alginates, and fucans). Using calcofluor white, cellulose was observed to be faint before the first division but gradually increased afterward. It is homogeneous during the whole Phase I. For alginates and fucans, monoclonal antibodies commercially available allowed us to describe precisely the organization of the cell wall (Torode et al., 2015, Torode et al., 2016). Contrastingly to cellulose, a precise organization in space and time can be observed during the first two phases of *Saccharina latissima* development. Sulfated fucans were structured homogeneously in the embryo outer wall at the exception of the basal-most region. While also present in the inner cell walls at all stages, alginates rich in G-G blocks were strongly labeled in the outer cell wall with a stronger signal in the apical half of the embryo. Contrarily, M-G mixed alginates were observed initially in the outer cell wall of the elongated zygote but beyond the first division, they are almost uniquely found within the inner cell walls of the embryo and at different intensities between different cell walls. Finally, before Phase II of development, M-M rich alginates were mainly found on the outer cell wall apart from the apices. They appear to form a corset of cell wall around the body of the embryo. However, hereafter Phase II of development, they are uniquely located in the inner cell wall. It has been described that flexibility in alginates was in order $G-G > M-M > M-G$ with M-G mixed alginates being the most flexible (Smidsrød et al., 1973). The fact that M-M and G-G rich alginates are being specifically found on the external layer of the cell wall after the first division while M-G were found on the internal cell wall suggests that the external cell wall is more rigid. Indeed, this is concomitant with the observation from laser ablation where, following the bursting of a cell, the nearest cell yields in elastic movement of the inner cell walls while the outer cell wall of even the burst cell is barely affected (**Chapter III: Suppl. Movie**). In addition, observations with transmission electron microscopes presented that the external cell wall was thicker than the inner cell wall (not shown, Theodorou 2023), similar to what is observed in other Laminariales (Motomura 1990; Klochkova et al., 2019) but also other brown algae (Yonamine et al., 2021, Rabillé et al., 2019, Nagasato et al., 2015). This increase in rigidity in the outer layer, specifically apart from the apices, might be required for the elongation of the embryo and completion of Phase I. Furthermore, vertex models presented that after the initiation of Phase II, the different properties between the outer cell wall and

the inner cell wall were sufficient to explain the robustness of the blade shape (Theodorou, 2023). Additionally, the change in the localization of M-G mixed alginates presents that a fine control of the mannuronan-C5-epimerases (MC5Es) is operated in the embryo, likely in order to maintain the maximum rigidity exclusively on the outer cell wall.

In land plants, the reorganization of cytoskeleton structuration was presented to support the elongation process and formation of the primary axis (Bassel et al., 2014; Shellard and Mayor, 2023). Previous studies hypothesized a similar correspondence between cell wall composition and cytoskeleton in brown algae (Kropf et al., 1982; Karyophyllis et al., 2000; Rabillé et al., 2019). Latrunculin B is a drug stopping the polymerization of actin monomers, thus promoting the depolymerization of actin filaments (Wakatsuki et al., 2001). Interestingly, the switch in the localization of the M-M rich alginate from the outer cell wall in phase I to inner during the transition to Phase II and hereafter, does not fully happen in the presence of Latrunculin B (**Chapter I**). Furthermore, elongation of *Saccharina*'s zygote is hindered by Latrunculin B (**Chapter I**). Embryos of up to two cells affected by the drug are bulging at the apical end, reaching sizes over 100 μm . Altogether, my results support that the cell wall, in coordination with the cytoskeleton, is necessary for the elongation of the zygote, and possibly for the completion of phase I.

Connection to maternal tissue is required for establishment of the embryo body plans

In addition to the cell wall composition described previously, a **ring-like** structure was found between the embryo and the stalk during Phase I and early Phase II when both were in contact (Fig. 2). This could be related to the local thickening of the ECM post connection to the stalk also observed previously in other Laminariales using electron microscopy (Klochkova et al., 2019). Noteworthy, BAM 4, 6, 7, and 10 used during this work did not label efficiently the gametophyte. Furthermore, this ECM structure is absent prior to zygote attachment. Additionally, the stalk constitutes a dead emptied oogonium (**Chapter II**, Fig. 10). Altogether, these arguments imply that this cell wall deposition is linked to zygote secretion and ECM synthesis. This polysaccharide structure is likely to help the embryo bind to its stalk during Phase I and early Phase II. In fact, studies dating from as early as the 1930s

reported that disconnection of the embryo from its maternal tissues resulted in abnormal development of *Saccharina* (Kanda, 1936; Klochkova et al., 2019). The work here reports for the first time in detail the role of the attachment to the maternal tissue in the development of the embryo.

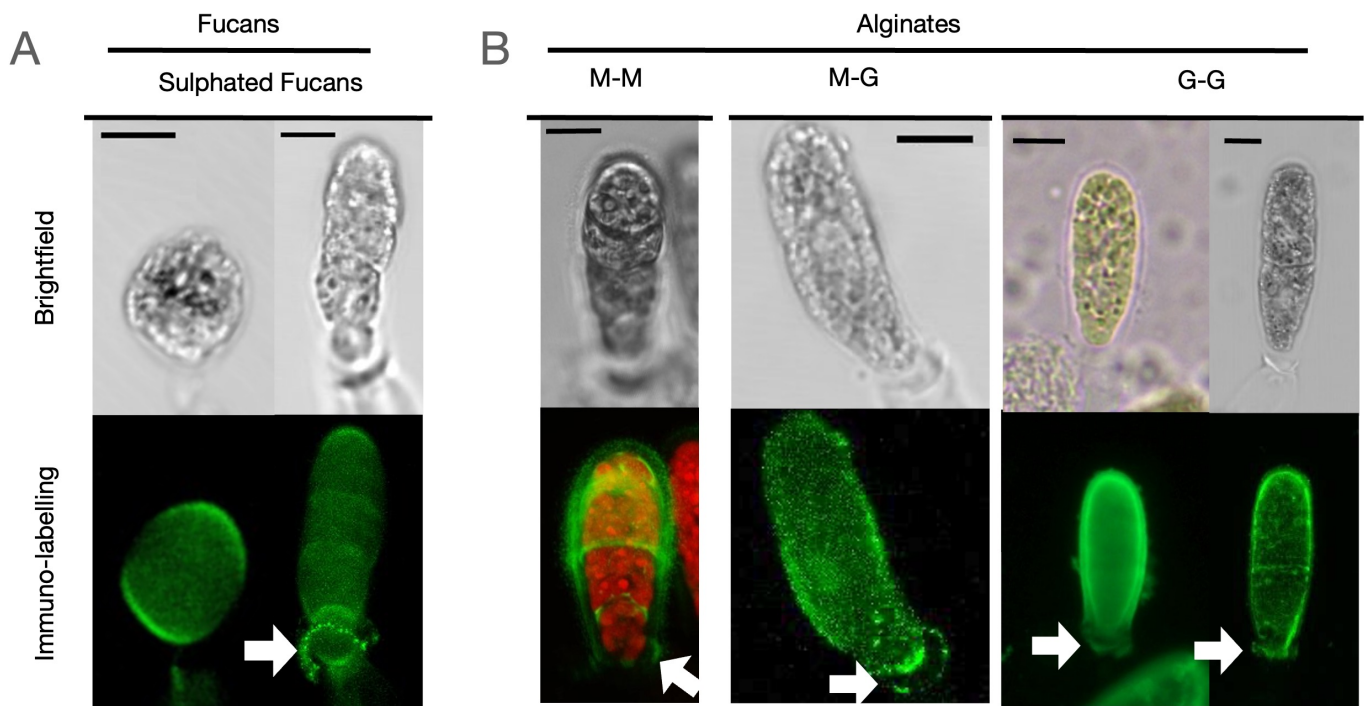


Figure 2: Cell wall material is deposited at the junction between embryo and maternal tissue.

Images are presented for brightfield (top) and maximum projection intensity of BAM immuno-fluorescence (bottom). The ring-like structure of the cell wall at the junction between the embryo and maternal tissue is designated by a white arrow. Scale bars represent 10 μm . (A) Sulfated fucans distribution in the cell wall using the monoclonal antibody BAM4. (B) Alginates distribution in the cell wall. Representative pattern of alginates immunolabeling using the monoclonal antibody BAM6 (left), BAM7 (middle), and BAM10 (right).

Removal of the basal cell or of the stalk causes early transition to Phase II (defined as the transition to longitudinal cell division) and the loss of the anisotropic growth of the embryo (**Chapter II**, Fig. 8; **Chapter III**, Fig. 6). The effect gradually fades up at the 8-cell stage, when removal of the basal cell no longer has any effect on embryo development. Shortening Phase I by impairing the connection of the embryo to the maternal tissue reduces the length-to-width ratio (LWR) of the embryo, which is then maintained during Phase II (**Chapter II**, Suppl. Fig. 2; **Chapter III**, Fig. 5). This shows that during Phase I, the inhibition of longitudinally oriented divisions is necessary for the future embryo to complete its body shape. It underlines the importance of completing Phase I involved in the formation of an anisotropic shape. Additionally, this confirms previous observations on intact embryos showing that Phase II maintains the initial shape established during Phase I (Theodorou, 2023). As such, connection to maternal tissue allows the embryo to acquire an apico-basal axis first during Phase I, and to prevent the establishment of the medio-lateral axis, which takes place only after the 8-cell stage in Phase II. Secondly, the loss of the embryo connection in Phase I causes abnormal cellular shapes in Phase II, such as less rectangular and smaller cells (**Chapter II**, Fig. 4; Fig. 6; **Chapter III**, Fig. 4). This effect becomes more evident through Phase II, showing that this is a consequence of the loss of the anisotropic shape of the embryo rather than a cause.

Altogether, these results present the necessity for embryo connection to the maternal tissue. The alteration of the developmental pattern in embryos disconnected from the maternal tissue suggests that a **signal** inhibits transition to Phase II during Phase I. This signal requires that the maternal tissue and the basal cell are physically connected. As such, the signal was named **MUM** (**M**aternal **U**nknown **M**essage). This naturally brings the following questions: How does MUM act? What is MUM?

How MUM signal delays transition from Phase I to Phase II

The presented findings offer insights into how MUM orchestrates embryo development. First, MUM maintains Phase I (1D growth) and inhibits the transition to Phase II. As such, MUM is able to control the division orientation in Phase I, promoting the "axis amplification" step. It likely signals or directly regulates how to

orientate the spindle of the cell during mitosis to be only in a selected direction. Secondly, the MUM signal is effective in all cells during Phase I. Because this signal originates from the basal cell connection with the stalk, MUM must act acropetally as the signal spreads to the top cells of the embryo. While its inhibitory effect is strong in the basal part of the embryo, it diminishes towards the apex during the transition to Phase II. This way, the MUM effect would be able to affect the embryo for a distance of over 100 μm (length of the 8-cell stage). This suggests an effect based on limited distance diffusion, similar to what is suspected for the inhibition of new branch formation in diverse filamentous organisms (Coudert et al., 2019). This signal diffuses symplastically, as neither neighboring gametophyte cells (adjacent or from another individual), nor the close proximity to the stalk after basal ablation were able to recover embryo development (**Chapter II, Chapter III**). The plasmodesmata found in brown algae (Nagasato et al., 2017), and particularly in *Saccharina* (Fig. 3; Theodorou, 2023), are plausibly involved in the transmission of MUM from one cell to another. Thirdly, most embryos ablated of the apical cell still underwent formation of the 8-cell stack (Chapter III, Fig. 6). This suggests that the MUM effect is not connected to a cellular clock but is somehow informed of the relative size of the embryo.

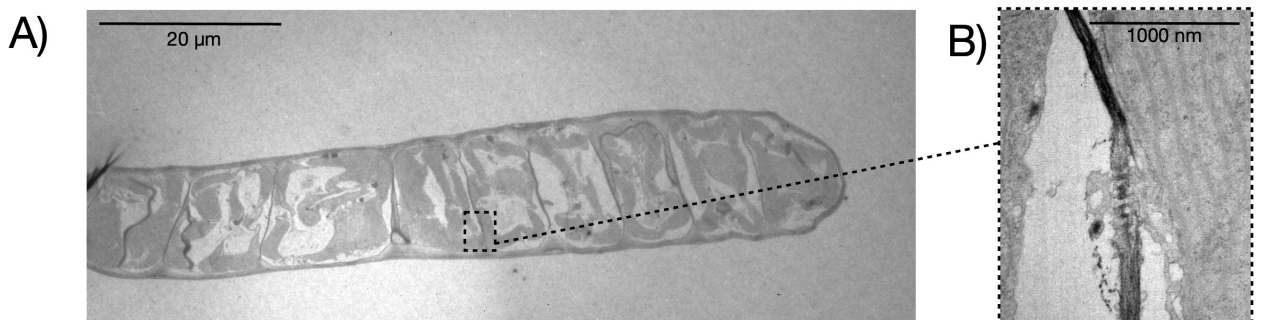


Figure 3: Plasmodesmata observed in the embryos of *S. latissima* from the 8-cell stage and beyond

Plasmodesmata are observable in the embryos of *S. latissima* from the 6-cell stage. Photos of embryos of *S. latissima* are observed with a transmission electron microscope. (A) Whole embryo. Plasmodesmata organized in pit fields were observed in a Phase II embryo from a lateral view (B) or a front view (C).



Nature of MUM

While further investigation is needed to define MUM conclusively, the presented results offer an idea of the nature of MUM. Our findings indicate that MUM is not the maternal or paternal centrioles, neither the anchor flagella, nor a diffusing effector from another gametophyte (**Chapter II**). Although a mechanical effect via the ECM might influence growth orientation in Phase I, it remains unlikely to be the sole effector. This is evidenced by the initial longitudinal anticlinal division occurring immediately after separation of the embryo from the maternal tissue, despite the presence of embryo cell wall structures (**Chapter II**). Hence, the cell wall is not MUM itself. MUM is a signal that originates from the basal cell and that diffuses symplastically within the embryo (**Chapter III**). MUM could be related to a gradient of molecules or ions.

The concept of a distance-inhibitory relation with a signal molecule has already been presented in mature kelps. The generation of reproductive structures (sori) was shown to be under the influence of a sporogenesis inhibitor originating from the growing region surrounding the transition zone (Buchholz and Lüning, 1999; Pang and Lüning, 2004), potentially identified as auxin (Kai et al., 2006). Auxin has been shown to be present in brown algae, and PILS (PIN-like transporter) genes have been found in its genome (Bogaert et al., 2019). Interestingly, preliminary observations on *Saccharina latissima* development reveal that the application of supplemental auxin (IAA) induces the rounding of some attached blades (Fig. 4). However, this would suggest that MUM actually has an opposite influence or inhibits the effect of auxin. The concept of opposite effects of hormones is well-described in plants where, for example, cytokinin and auxin have antagonistic effects on development (Schaller et al., 2015). The application of cytokinin did not exhibit any visible effect on blade development (not shown). However, it would be interesting to explore the impact of cytokinin application on stalk-disconnected blades to determine if it can recover normal blade development.

As a final hypothesis, MUM could be linked to polysaccharides. Using Lectin-FITC as a probe, demonstrated the homogeneous distribution of polysaccharides like N-acetyl-glucosamine, β -D-galactose, and D-galactose- β -galactosamine upon egg release (Klochkova et al., 2019; Klimova et al., 2021). Additionally, when the embryo is in contact with the maternal stalk, these polysaccharides are polarized towards

this junction. The function of sugars as signaling molecules in developmental processes is well-established in various organisms, such as plants (Mishra et al., 2019; Wang et al., 2021) and animals (Radhakrishnan et al., 2023). Moreover, lectins are also identified in brown algae (Boyd et al., 1966; Fajarningsih et al., 2019). Although characterization and functional validation in brown algae are necessary to fully support this hypothesis, the perception of polysaccharides in brown algae could potentially influence their developmental architecture.

Altogether, upon reassessing various hypotheses surrounding the nature of MUM, two compelling explanations surface. The first supposes a gradient of diffusible molecules extending from the stalk through the embryo. The second suggests a signal originating from the cell wall junction between the stalk and the embryo. To solidify these hypotheses and uncover the precise mechanisms underlying the control of MUM in the development of *Saccharina*, additional studies are essential.

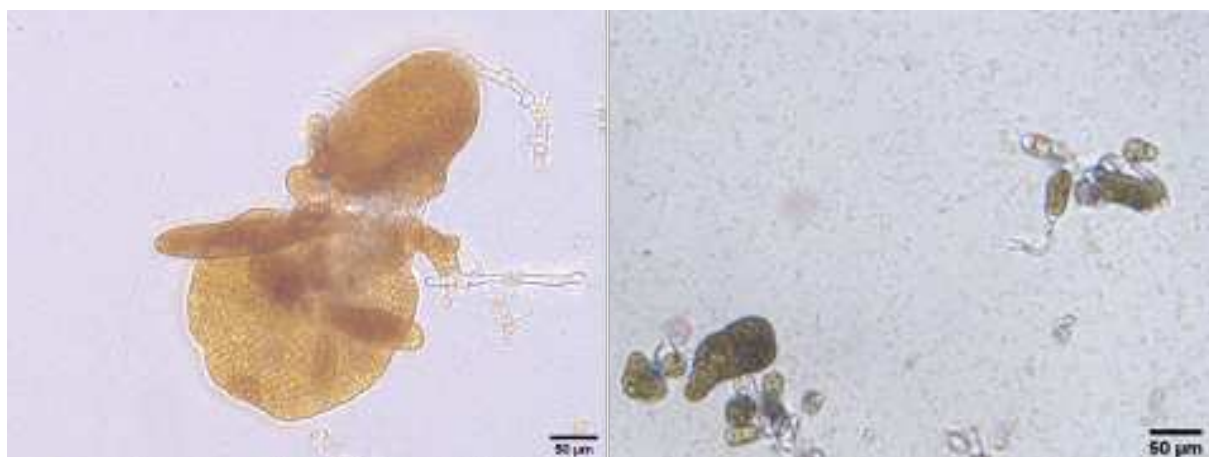
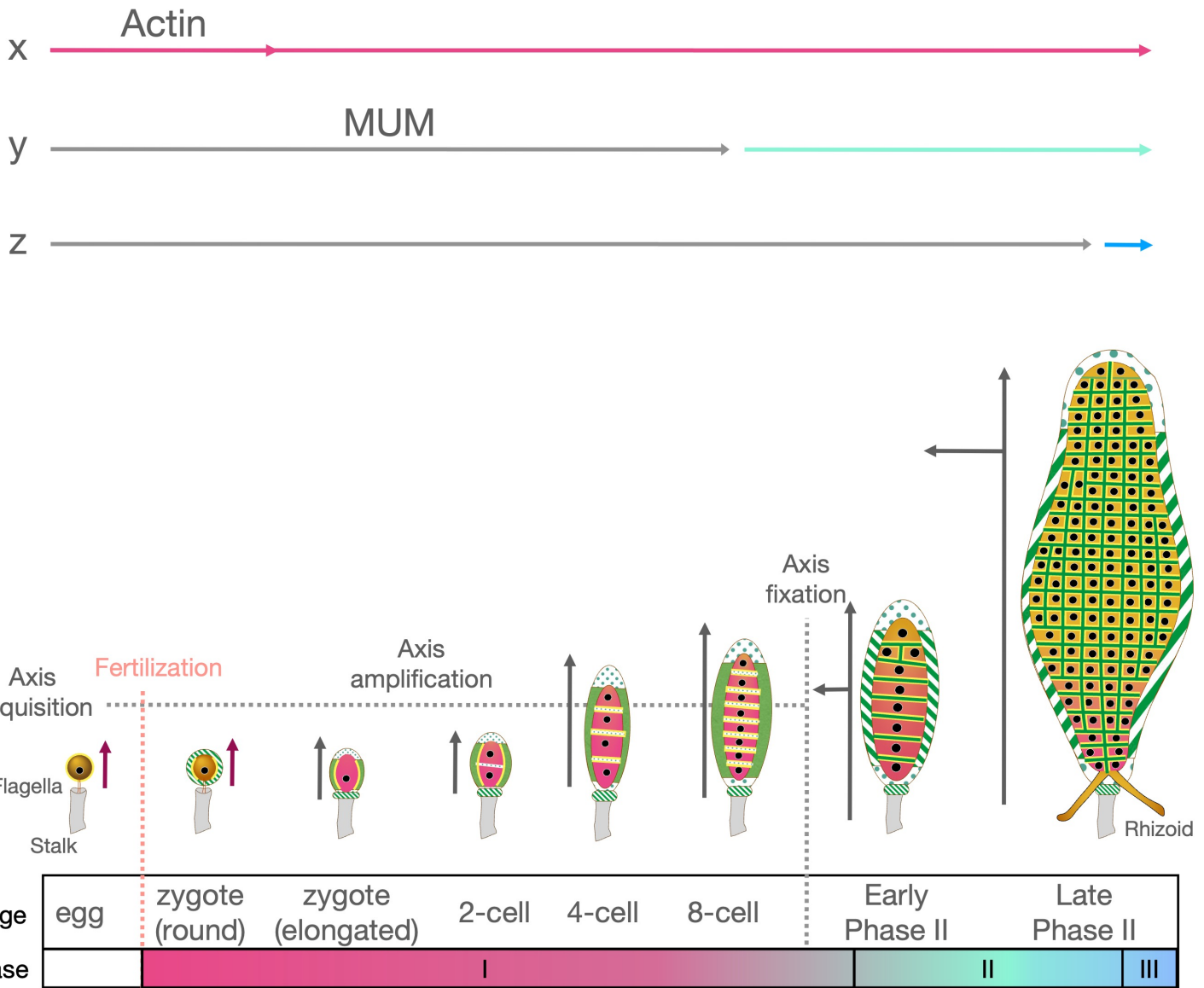


Figure 4: Effect of auxin in the establishment of body axes.

Phenotypes of growing embryos after the post-egg release application of auxin (IAA) at concentrations of 10^{-7} M (left) or 10^{-4} (right) in DMSO 0.1%. As a result, the lamina of the embryo thallus grew more isotropically, making a rounder lamina. Photos were taken as described in **Chapter II** and treated in Fiji using the plugin stack fuser.

An evo-devo approach: Shared developmental process in brown algae

Laminariales exhibit maternal orientation due to the presence of anchor flagella that maintain proximity with the mother gametophyte and the subsequent connection between the mother and embryo (Bogaert et al., 2023; **Chapter II**; **Chapter III**). This attribute might elucidate why they appear unresponsive to environmental cues like light and gravity in establishing the first axis, unlike Fucales and Dictyotales. Among brown algae, at least four orders (Laminariales, Chordales, Sporochnales, and Desmarestiales) display a stalk-mediated physical connection of the embryo with the maternal tissue that persists throughout embryo development (Sauvageau, 1918; Kanda, 1938; Fritsch, 1945). Comparisons of *Saccharina latissima* with visual descriptions and available images of other Laminariales and Chordales show striking similarities in embryo shape with dissimilarities occurring mostly after corresponding Phase II. (Sauvageau 1918; Kanda 1936; Kanda 1938; Fritsch 1945). This suggests that the same maternal regulation could be shared between Chordales and Laminariales. However, Desmarestiales and Sporochnales exhibit limited morphological similarities, suggesting developmental pathways are at least partially distinct. (Sauvageau 1926; Stolpe et al., 2007). Moreover, while stalks connecting eggs and the rest of the maternal tissue are also common in brown algae of the Fucales order (Burridge et al., 1993), this connection is transient and does not persist long after fertilization. A better comprehension of these processes could improve our understanding of the BACR lineage in brown algae and their past evolution, but also possible future evolution of extra- or intra-tissular development (**Chapter II**). Further analyses are necessary to ascertain whether maternal-regulated development extends to these other orders.



Cell Wall

- More rigid cell wall
- Intermediate rigidity
- Less rigid cell wall

Axis Development

- Polarity axis in isotropic egg
- Axis development
- Axis inhibited

MUM Gradient

- MUM inhibition
- Out of MUM effect

Other Symbols

- Denser region of AFs
- Nucleus

Figure 5 (previous page): Concluding model

The egg, polarized upon emergence from the oogonium undergoes changes triggered by sperm entry. This includes cell wall secretion and synthesis, facilitating egg elongation (x-axis). The transition from egg to embryo involves three steps: Axis acquisition (maternally inherited), Axis elongation, and Axis Perpetuation. Axis perpetuation completes during the first cytokinesis. During elongation, the basal region of the embryo firmly attaches to the maternal stalk. Fixation is concomitant with the deposition of cell wall between the embryo and the stalk in a ring-like structure that could help strengthen the bond between embryo and maternal tissue. The filamentous cortical actin network regulates cell wall synthesis, influencing cell wall properties differently on the embryo body. Simultaneously, The MUM signal inhibits division on the y-axis plane, thereby strengthening the anisotropic shape of the embryo during its elongation in Phase I. The MUM signal diffuses from the basal region connected to the stalk, inhibiting longitudinal (x-axis) anticlinal divisions (y-axis) over 100 μm . The specific nature and mechanism of action of the MUM signal remain to be determined.

Conclusion and Perspectives

Multiple parameters orchestrate the embryogenesis of *Saccharina latissima* during which it sequentially establishes body plans in the three main axes. The cell wall properties are fine-tuned by the cytoskeleton network. Arrangement of the cell wall properties promotes elongation of the embryo (x-axis) in Phase I and supports its 2D growth in Phase II (x-y-axes) (**Chapter I**). In parallel, connection of the maternal gametophyte to the embryo basal cell generates a signal named MUM (Maternal Unknown Message). This signal delays transition to Phase II by inhibiting longitudinal cell divisions, and thus promotes elongation of the embryo (x-axis) (**Chapter II, Chapter III**). This process is required for developing the body plan of *Saccharina*. Altogether, the results presented in this work enable improvement of the model of *Saccharina latissima*'s development, depicting the sequential establishment of body axes and how it is regulated (Figure 5).

Several open questions remain and need to be addressed to better understand the development in *Saccharina* and complete the model described above. The nature of the MUM signal and the exact mechanisms it uses to regulate the establishment of the body axes require investigation. Directly or indirectly, MUM regulates the cytoskeleton as it orients cell divisions. The filamentous actin network is partly responsible for the regulation of cell wall properties; hence, MUM could affect the

mechanical properties of the cell wall to promote amplification of the primary axis. This hypothesis could be tested by immunolocalization of cell wall epitopes using BAM antibodies in embryos disconnected from their stalks and by using mutants lacking alginates, fucans, or ManC5Es (single or multiple epimerases). Exploring the hypotheses provided on MUM's nature would provide additional insights into polysaccharide sensing or response to phytohormone involvement in the development of kelps and other brown algae.

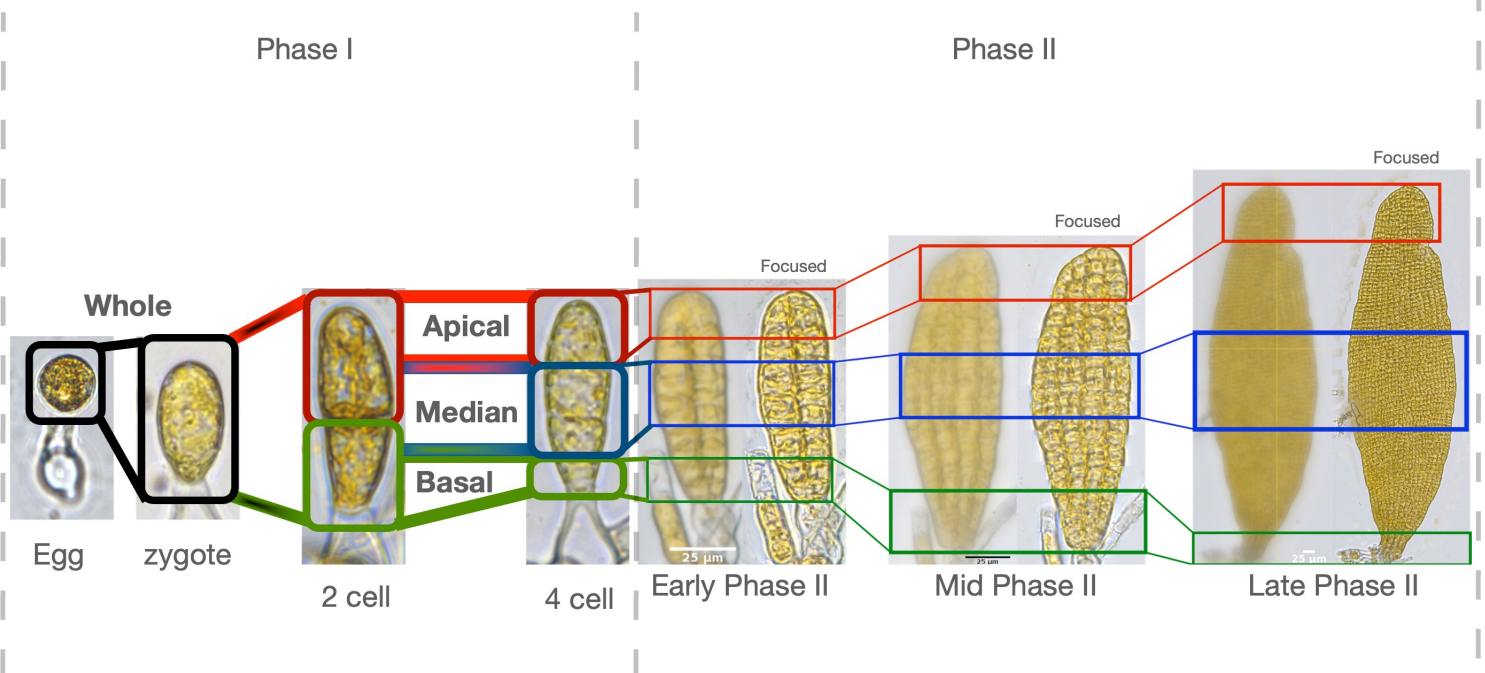


Figure 6: Schematic representation of section of tissue used in LCM transcriptomic experiment.

Embryos of *Saccharina latissima* were grown on glass slides coated with Nuclease-free 1.0 polyethylene naphthalate (PEN) membrane (Zeiss Microscopy, #415190-9081-000). They were fixed in acetone for 30 minutes. Using Laser Capture Microdissection (LCM), individual cells were isolated from embryos at the 1-, 2-, and 4-cell stage (Phase I). Alternatively, apical, median, or basal sections were isolated from embryos in early, mid, or late Phase II. Laser capture was performed using a Carl Zeiss PALM MicroBeam unit equipped with an AxioVert 200 microscope and a CryLas UV laser, and assisted by the PalmRobo 4.5 software. Extraction of cDNA from all collected samples was performed using the PicoPure RNA extraction kit from Life Technologies (#KIT0204) and NEBNext Single Cell cDNA Synthesis & Amplification module kit from New England Biolabs (#E6421L).

Finally, studying the transcriptomic changes during the development of brown algae with cellular precision could allow us to better understand the processes of symmetry breaking, genomic activation of the embryo, and the parental determinants inherited by the embryo. Exploration in space and time of the transcriptomic changes is necessary to locate and identify the nucleic determinants of importance. Laser capture microdissection (LCM) allows transcriptomic analysis of individual cells isolated from tissue sections (Espina et al., 2006). This technique has been optimized in brown algal species (Saint-Marcoux et al., 2015). Expansive ongoing work has been undertaken by the team to unravel these mechanisms during the development of the embryo of *Saccharina latissima* (Figure 6). The transcriptome was sequenced from each individual cell isolated from embryos at the 1-, 2-, or 4-cell stages in Phase I, or from distinct sections (apical, median, basal) of the embryo in early, mid, or late Phase II. Sequences are currently being analyzed and should provide information on the transcriptomic landscape, parental regulation, and zygotic genome activation timing during the development of the embryo of *Saccharina latissima*.

The work conducted during this thesis has led to several technical improvements for studying brown algae. Most of these advancements stem from the need to address technical difficulties in studying the development of brown algae. Firstly, a single female (F1) and male (M1) gametophyte were selected and grown vegetatively. This allowed all experiments to use embryos with an identical genome. The use of fixed genotypes helped reduce variability in the embryo development process studied. Additionally, by inducing a cold shock (4°C for 8 hours in blades of 30cm and more), we were able to complete the life cycle of *Saccharina* in lab conditions in under 4 months. Secondly, the adaptation of laser dissection microscopy allowed manipulation of brown algal embryos with temporal accuracy and sub-cellular spatial precision (Boscq et al., 2022; Annex 1). Thirdly, the use of continuous time-lapse imaging allows observation of the dynamic development and access to parameters such as division timing, cell lineage, or cellular quantitative morphological parameters over time. A key challenge in such imaging experiments is maintaining physiological conditions for the chosen model organism (e.g., medium, light, temperature) (Kirchhelle and Moore, 2017). A particular difficulty in

time-lapse imaging of brown algae embryos arises from their vertical growth in various orientations. To address this problem, we devised microfluidic devices that confine embryo growth to a focal plane. Initially designed for constraining 1D filamentous growth in *Ectocarpus* (Charrier et al., 2021; Annex 2), we subsequently developed microfluidic channels for *Saccharina* to restrict parenchymatous growth in 2D parallel to the focal plane (Clerc et al., 2022; Annex 3). These microfluidic devices offer an additional advantage: their geometrical design can be tailored to suit various experiments, facilitating controlled flow of chemical compounds, among other applications. Looking ahead, advancements in microscopy technologies (e.g., light sheet and bi-photon microscopy) will broaden our ability to precisely observe development and cell growth in space and time. These innovations will enable us to pose more complex questions concerning morphogenesis and cellular dynamics.

7 - References

- Aaziz, R., Dinant, S., Epel, B. L.** (2001). Plasmodesmata and plant cytoskeleton. *Trends Plant Sci.* 6, 326–330.
- Ahmed, S., Cock, J. M., Pessia, E., Luthringer, R., Cormier, A., Robuchon, M., Sterck, L., Peters, A. F., Dittami, S. M., Corre, E., et al.** (2014). A haploid system of sex determination in the brown alga *Ectocarpus sp.* *Curr. Biol.* 24, 1945–1957.
- Anderson, J. M. and Barrett, J.** (1978). Chlorophyll-protein complexes of brown algae: P700 reaction centre and light-harvesting complexes. *Ciba Found. Symp.* 81–104.
- Anderson, S. N., Johnson, C. S., Chesnut, J., Jones, D. S., Khanday, I., Woodhouse, M., Li, C., Conrad, L. J., Russell, S. D., Sundaresan, V.** (2017). The Zygotic Transition Is Initiated in Unicellular Plant Zygotes with Asymmetric Activation of Parental Genomes. *Dev. Cell* 43, 349–358.e4.
- Angelo, J. R. and Tremblay, K. D.** (2013). Laser-mediated cell ablation during post-implantation mouse development. *Dev. Dyn.* 242, 1202–1209.
- Anlas, K. and Trivedi, V.** (2021). Studying evolution of the primary body axis in vivo and in vitro. *Elife* 10, e69066.
- Arias, A. M., Nichols, J., Schröter, C.** (2013). A molecular basis for developmental plasticity in early mammalian embryos. *Development* 140, 3499–3510.
- Arnold, S. J., Stappert, J., Bauer, A., Kispert, A., Herrmann, B. G., Kemler, R.** (2000). Brachyury is a target gene of the Wnt/beta-catenin signaling pathway. *Mech. Dev.* 91, 249–258.
- Assis, J., Fragkopoulou, E., Frade, D., Neiva, J., Oliveira, A., Abecasis, D., Faugeron, S., Serrão, E. A.** (2020). A fine-tuned global distribution dataset of marine forests. *Sci. data* 7, 119.
- Augyte, S., Yarish, C., Neefus, C. D., Augyte, S., Yarish, C., Neefus, C. D.** (2019). Thermal and light impacts on the early growth stages of the kelp *Saccharina angustissima* (Laminariales, Phaeophyceae). *Algae* 34, 153–162.
- Avia, K., Coelho, S. M., Montecinos, G. J., Cormier, A., Lerck, F., Mauger, S., Faugeron, S., Valero, M., Cock, J. M., Boudry, P.** (2017). High-density genetic map and identification of QTLs for responses to temperature and salinity stresses in the model brown alga *Ectocarpus*. *Sci. Rep.* 7, 43241.
- Badis, Y., Scornet, D., Harada, M., Caillard, C., Godfroy, O., Raphalen, M., Gachon, C. M. M., Coelho, S. M., Motomura, T., Nagasato, C., et al.** (2021). Targeted CRISPR-Cas9-based gene knockouts in the model brown alga *Ectocarpus*. *New Phytol.* 231, 2077–2091.
- Bagaeva, T., Aman, A. J., Graf, T., Niedermoser, I., Zimmermann, B., Kraus, Y., Schatka, M., Demilly, A., Technau, U., Genikhovich, G.** (2020). β -catenin dependent axial patterning in Cnidaria and Bilateria uses similar regulatory logic. *bioRxiv* 2020.09.08.287821.
- Baldauf, S., Romeralo, M., Carr, M.** (2013). The Evolutionary Origin of Animals and Fungi. In *Evolution from the Galapagos: Two Centuries after Darwin* (ed. Trueba, G.) and Montúfar, C.), pp. 73–106. New York, NY: Springer New York.
- Barbier, M., Charrier, B., Araujo, R., Holdt, S., Jacquemin, B., Rebours, C., Chopin, T.** (2019). Pegasus - Phycomorph European Guideline for a Sustainable Aquaculture of Seaweeds.
- Baroux, C. and Grossniklaus, U.** (2015). The Maternal-to-Zygotic Transition in Flowering Plants: Evidence, Mechanisms, and Plasticity. *Curr. Top. Dev. Biol.* 113, 351–371.
- Barthélémy, D. and Caraglio, Y.** (2007). Plant Architecture: A Dynamic, Multilevel and Comprehensive Approach to Plant Form, Structure and Ontogeny. *Ann. Bot.* 99, 375–407.
- Baskin, T. I., Beemster, G. T. S., Judy-March, J. E., Marga, F.** (2004). Disorganization of cortical microtubules stimulates tangential expansion and reduces the uniformity of cellulose microfibril alignment among cells in the root of *Arabidopsis*. *Plant Physiol.* 135, 2279–2290.
- Bayer, M., Nawy, T., Giglione, C., Galli, M., Meinel, T., Lukowitz, W.** (2009). Paternal control of embryonic patterning in *Arabidopsis thaliana*. *Science* 323, 1485–1488.
- Bellande, K., Bono, J.-J., Savelli, B., Jamet, E., Canut, H.** (2017). Plant Lectins and Lectin Receptor-Like Kinases: How Do They Sense the Outside? *Int. J. Mol. Sci.* 18, .

- Berger, F. and Brownlee, C.** (1994). Photopolarization of the *Fucus* sp. Zygote by Blue Light Involves a Plasma Membrane Redox Chain. *Plant Physiol.* 105, 519–527.
- Berger, F., Taylor, A., Brownlee, C.** (1994). Cell fate determination by the cell wall in early *Fucus* development. *Science* (80-.). 263, 1421–1423.
- Besson, S. and Dumais, J.** (2011). Universal rule for the symmetric division of plant cells. *Proc. Natl. Acad. Sci. U. S. A.* 108, 6294–6299.
- Bi, E. and Park, H.-O.** (2012). Cell polarization and cytokinesis in budding yeast. *Genetics* 191, 347–387.
- Birkemeyer, C., Lemesheva, V., Billig, S., Tarakhovskaya, E.** (2020). Composition of Intracellular and Cell Wall-Bound Phlorotannin Fractions in Furoid Algae Indicates Specific Functions of These Metabolites Dependent on the Chemical Structure. *Metabolites* 10,.
- Bisgrove, S. R. and Kropf, D. L.** (2008). Asymmetric cell divisions: zygotes of furoid algae as a model system. In *Cell Division Control in Plants* (ed. Verma, D. P. S.) and Hong, Z.), pp. 323–341. Berlin, Heidelberg: Springer Berlin Heidelberg.
- Bisgrove, S. R. and Kropf, D. L.** (2001). Cell wall deposition during morphogenesis in furoid algae. *Planta* 212, 648–658.
- Bogaert, K. A., Beeckman, T., De Clerck, O.** (2017a). Two-step cell polarization in algal zygotes. *Nat. Plants* 3, 16221.
- Bogaert, K. A., Beeckman, T., De Clerck, O.** (2017b). Egg activation-triggered shape change in the *Dictyota dichotoma* (Phaeophyceae) zygote is actin-myosin and secretion dependent. *Ann. Bot.* 120, 529–538.
- Bogaert, K. A., Zakka, E. E., Coelho, S. M., De Clerck, O.** (2023). Polarization of brown algal zygotes. *Semin. Cell Dev. Biol.* 134, 90–102.
- Bogaert, K. A., Beeckman, T., de Clerck, O.** (2015). Photopolarization of *Fucus* zygotes is determined by time sensitive vectorial addition of environmental cues during axis amplification. *Front. Plant Sci.* 6, 126622.
- Bogaert, K. A., Blommaert, L., Ljung, K., Beeckman, T., De Clerck, O.** (2019). Auxin Function in the Brown Alga *Dictyota dichotoma*. *Plant Physiol.* 179, 280–299.
- Bogaert, K. A., Zakka, E. E., Coelho, S. M., De Clerck, O.** (2023). Polarization of brown algal zygotes. *Semin. Cell Dev. Biol.* 134, 90–102.
- Bogaert, K. A., Blomme, J., Beeckman, T., De Clerck, O.** (2022). Auxin's origin: do PILS hold the key? *Trends Plant Sci.* 27, 227–236.
- Bogaert, K., Arun, A., Coelho, S., Clerck, O.** (2013). Brown Algae as a Model for Plant Organogenesis. *Methods Mol. Biol.* 959, 97–125.
- Bogaert, K., Beeckman, T., De Clerck, O.** (2016). Abiotic regulation of growth and fertility in the sporophyte of *Dictyota dichotoma* (Hudson) J.V. Lamouroux (Dictyotales, Phaeophyceae). *J. Appl. Phycol.* 28, 2915–2924.
- Boscq, S., Dutertre, S., Theodorou, I. and Charrier, B.** (2022). Targeted Laser Ablation in the Embryo of *Saccharina latissima*. *Journal of visualized experiments: JoVE*.
- Bouget, F. Y., Berger, F., Brownlee, C.** (1998). Position dependent control of cell fate in the *Fucus* embryo: role of intercellular communication. *Development* 125, 1999–2008.
- Bowerman, B., Ingram, M. K., Hunter, C. P.** (1997). The maternal par genes and the segregation of cell fate specification activities in early *Caenorhabditis elegans* embryos. *Development* 124, 3815–3826.
- Breton, S. and Stewart, D. T.** (2015). Atypical mitochondrial inheritance patterns in eukaryotes. *Genome* 58, 423–431.
- Bringloe, T., Starko, S., Wade, R., Vieira, C., Kawai, H., Clerck, O., Cock, J., Coelho, S., Destombe, C., Valero, M., et al.** (2020). Phylogeny and Evolution of the Brown Algae. *CRC. Crit. Rev. Plant Sci.*
- Brownlee, C. and Wood, J. W.** (1986). A gradient of cytoplasmic free calcium in growing rhizoid cells of *Fucus serratus*. *Nat.* 1986 3206063 320, 624–626.
- Büchel, C.** (2020). Light harvesting complexes in chlorophyll c-containing algae. *Biochim. Biophys. acta. Bioenerg.* 1861, 148027.

- Buchholz, C. and Lüning, K.** (1999). Isolated, distal blade discs of the brown alga *Laminaria digitata* form sorus, but not discs, near to the meristematic transition zone. *Journal of Applied Phycology* **11**, 579–584.
- Budke, J. M., Goffinet, B. and Jones, C. S.** (2012). The cuticle on the gametophyte calyptra matures before the sporophyte cuticle in the moss *Funaria hygrometrica* (Funariaceae). *American Journal of Botany* **99**, 14–22.
- Burki, F., Roger, A. J., Brown, M. W., Simpson, A. G. B.** (2020). The New Tree of Eukaryotes. *Trends Ecol. Evol.* **35**, 43–55.
- Burki, F., Shalchian-Tabrizi, K., Minge, M., Skjaeveland, A., Nikolaev, S. I., Jakobsen, K. S., Pawlowski, J.** (2007). Phylogenomics reshuffles the eukaryotic supergroups. *PLoS One* **2**, e790.
- Burridge, T., Clayton, M. N. and Hallam, N. D.** (1993). Oogenesis and Stalk Mediated Fertilization in *Phyllospora comosa*, (Labillardière) C. Agardh, (Seirococcaceae, Phaeophyta). **36**, 223–232.
- Byrne, A. B. and Hammarlund, M.** (2017). Axon regeneration in *C. elegans*: Worming our way to mechanisms of axon regeneration. *Exp. Neurol.* **287**, 300–309.
- Charrier, B., Coelho, S. M., Le Bail, A., Tonon, T., Michel, G., Potin, P., Kloareg, B., Boyen, C., Peters, A. F., Cock, J. M.** (2008). Development and physiology of the brown alga *Ectocarpus siliculosus*: two centuries of research. *New Phytol.* **177**, 319–332.
- Charrier, B., Le Bail, A., de Reviere, B.** (2012). Plant Proteus: brown algal morphological plasticity and underlying developmental mechanisms. *Trends Plant Sci.* **17**, 468–477.
- Charrier, B., Rabillé, H., Billoud, B.** (2019). Gazing at Cell Wall Expansion under a Golden Light. *Trends Plant Sci.* **24**, 130–141.
- Chen, J., Strieder, N., Krohn, N. G., Cyprys, P., Sprunck, S., Engelmann, J. C., Dresselhaus, T.** (2017). Zygotic Genome Activation Occurs Shortly after Fertilization in Maize. *Plant Cell* **29**, 2106–2125.
- Cheverud, J. M.** (1984). Evolution by Kin Selection: A Quantitative Genetic Model Illustrated by Maternal Performance in Mice. *Evolution (N. Y.)*. **38**, 766–777.
- Chia, W., Somers, W. G., Wang, H.** (2008). *Drosophila* neuroblast asymmetric divisions: cell cycle regulators, asymmetric protein localization, and tumorigenesis. *J. Cell Biol.* **180**, 267–272.
- Chiou, J.-G., Balasubramanian, M. K., Lew, D. J.** (2017). Cell Polarity in Yeast. *Annu. Rev. Cell Dev. Biol.* **33**, 77–101.
- Chipman, A. D.** (2015). Hexapoda: Comparative aspects of early development. *Evol. Dev. Biol. Invertebr.* **5** Ecdysozoa III Hexapoda 93–110.
- Christodoulou, N., Weberling, A., Strathdee, D., Anderson, K. I., Timpson, P., Zernicka-Goetz, M.** (2019). Morphogenesis of extra-embryonic tissues directs the remodelling of the mouse embryo at implantation. *Nat. Commun.* **10**, 3557.
- Chugh, P. and Paluch, E. K.** (2018). The actin cortex at a glance. *J. Cell Sci.* **131**,.
- Cock, J. M., Sterck, L., Rouzé, P., Scornet, D., Allen, A. E., Amoutzias, G., Anthouard, V., Artiguenave, F., Aury, J.-M., Badger, J. H., et al.** (2010). The *Ectocarpus* genome and the independent evolution of multicellularity in brown algae. *Nature* **465**, 617–621.
- Coelho, S. M. and Cock, J. M.** (2020). Brown Algal Model Organisms. *Annu. Rev. Genet.* **54**, 71–92.
- Coelho, S. M., Godfroy, O., Arun, A., Le Corguillé, G., Peters, A. F., Cock, J. M.** (2011). Genetic regulation of life cycle transitions in the brown alga *Ectocarpus*. *Plant Signal. Behav.* **6**, 1858–1860.
- Coelho, S. M., Peters, A. F., Müller, D., Cock, J. M.** (2020). *Ectocarpus*: an evo-devo model for the brown algae. *Evodevo* **11**, 19.
- Coelho, S. M., Taylor, A. R., Ryan, K. P., Sousa-Pinto, I., Brown, M. T., Brownlee, C.** (2002). Spatiotemporal patterning of reactive oxygen production and Ca²⁺ wave propagation in fucus rhizoid cells. *Plant Cell* **14**, 2369–2381.

- Cormier, A., Avia, K., Sterck, L., Derrien, T., Wucher, V., Andres, G., Monsoor, M., Godfroy, O., Lipinska, A., Perrineau, M.-M., et al.** (2017). Re-annotation, improved large-scale assembly and establishment of a catalogue of noncoding loci for the genome of the model brown alga *Ectocarpus*. *New Phytol.* 214, 219–232.
- Cosgrove, D. J.** (2016). Plant cell wall extensibility: connecting plant cell growth with cell wall structure, mechanics, and the action of wall-modifying enzymes. *J. Exp. Bot.* 67, 463–476.
- Cosgrove, D. J.** (2005). Growth of the plant cell wall. *Nat. Rev. Mol. Cell Biol.* 6, 850–861.
- Cosgrove, D. J. and Jarvis, M. C.** (2012). Comparative structure and biomechanics of plant primary and secondary cell walls. *Front. Plant Sci.* 3, 204.
- Cosson, J., Gayral, P., Jacques, R.** (1976). Action de la composition spectrale de la lumière sur la croissance et la reproduction des gamétophytes de la *Laminaria digitata* (Phéophycée, Laminarale). *hebd. Séanc. Acad. Sci. Paris* 283, 1293–1296.
- Costa, L. M., Marshall, E., Tesfaye, M., Silverstein, K. A. T., Mori, M., Umetsu, Y., Otterbach, S. L., Papareddy, R., Dickinson, H. G., Boutiller, K., et al.** (2014). Central cell-derived peptides regulate early embryo patterning in flowering plants. *Science* (80-). 344, 168–172.
- Cove, D. J.** (2000). The generation and modification of cell polarity. *J. Exp. Bot.* 51, 831–838.
- Crean, A. J. and Bonduriansky, R.** (2014). What is a paternal effect? *Trends Ecol. Evol.* 29, 554–559.
- Cribb, A. B.** (1954). *Macrocystis pyrifera* (L.) Ag. in Tasmanian Waters. *Mar. Freshw. Res.* 5, 1–34.
- De Coninck, T. and Van Damme, E. J. M.** (2021). Review: The multiple roles of plant lectins. *Plant Sci.* 313, 111096.
- Deline, B., Greenwood, J. M., Clark, J. W., Puttick, M. N., Peterson, K. J., Donoghue, P. C. J.** (2018). Evolution of metazoan morphological disparity. *Proc. Natl. Acad. Sci.* 115, E8909–E8918.
- Deniaud-Bouët, E., Hardouin, K., Potin, P., Kloareg, B., Hervé, C.** (2017). A review about brown algal cell walls and fucose-containing sulfated polysaccharides: Cell wall context, biomedical properties and key research challenges. *Carbohydr. Polym.* 175, 395–408.
- Deniaud-Bouët, E., Kervarec, N., Michel, G., Tonon, T., Kloareg, B., Hervé, C.** (2014). Chemical and enzymatic fractionation of cell walls from Fucales: insights into the structure of the extracellular matrix of brown algae. *Ann. Bot.* 114, 1203–1216.
- Dickerson, G. E.** (1947). Composition of hog carcasses as influenced by heritable differences in rate and economy of gain. *Res. Bull. Iowa Agric.* 489–524.
- Eger, A. M., Marzinelli, E. M., Beas-Luna, R., Blain, C. O., Blamey, L. K., Byrnes, J. E. K., Carnell, P. E., Choi, C. G., Hessing-Lewis, M., Kim, K. Y., et al.** (2023). The value of ecosystem services in global marine kelp forests. *Nat. Commun.* 14, 1894.
- Espina, V., Wulfschlegel, J. D., Calvert, V. S., VanMeter, A., Zhou, W., Coukos, G., Geho, D. H., Petricoin, E. F., Liotta, L. A.** (2006). Laser-capture microdissection. *Nat. Protoc.* 1, 586–603.
- Evans, L. V and Callow, M. E.** (1974). Polysaccharide sulphation in *Laminaria*. *Planta* 117, 93–95.
- Evans, L. V and Holligan, M. S.** (1972). Correlated Light and Electron Microscope Studies on Brown Algae I: Localization of Alginic Acid and Sulphated Polysaccharides in Dictyota. *New Phytol.* 71, 1161–1172.
- Farah, M. E., Maia, M., Penha, F. M., Rodrigues, E. B.** (2010). CHAPTER 48 - The use of vital dyes during vitreoretinal surgery – chromovitrectomy. In *Retinal Pharmacotherapy* (ed. Nguyen, Q. D.), Rodrigues, E. B.), Farah, M. E.), and Mieler, W. F.), pp. 331–335. Edinburgh: W.B. Saunders.
- Fischl, R., Bertelsen, K., Gaillard, F., Coelho, S., Michel, G., Klinger, M., Boyen, C., Czjzek, M., Hervé, C.** (2016). The cell-wall active mannuronan C5-epimerases in the model brown alga *Ectocarpus*: From gene context to recombinant protein. *Glycobiology* 26, 973–983.

- Fletcher, D. A. and Mullins, R. D.** (2010). Cell mechanics and the cytoskeleton. *Nature* 463, 485–492.
- Fletcher, A. G., Osborne, J. M., Maini, P. K. and Gavaghan, D. J.** (2013). Implementing vertex dynamics models of cell populations in biology within a consistent computational framework. *Prog Biophys Mol Biol* 113, 299–326.
- Fouad, A. D., Liu, A., Du, A., Bhirgoo, P. D., Fang-Yen, C.** (2021). Thermal laser ablation with tunable lesion size reveals multiple origins of seizure-like convulsions in *Caenorhabditis elegans*. *Sci. Reports* 2021 111 11, 1–9.
- Franceschi, V. R., Ding, B., Lucas, W. J.** (1994). Mechanism of plasmodesmata formation in characean algae in relation to evolution of intercellular communication in higher plants. *Planta* 192, 347–358.
- Friml, J., Vieten, A., Sauer, M., Weijers, D., Schwarz, H., Hamann, T., Offringa, R., Jürgens, G.** (2003). Efflux-dependent auxin gradients establish the apical–basal axis of *Arabidopsis*. *Nature* 426, 147–153.
- Fritsch, F.E.** (1935). The structure and reproduction of the algae. Volume 1 (Cambridge University Press).
- Fritsch, F.E.** (1945) The structure and reproduction of the algae. Volume 2. (Cambridge University Press).
- Fuchs, M. and Lohmann, J. U.** (2020). Aiming for the top: non-cell autonomous control of shoot stem cells in *Arabidopsis*. *J. Plant Res.* 133, 297–309.
- Gaillochet, C. and Lohmann, J. U.** (2015). The never-ending story: from pluripotency to plant developmental plasticity. *Development* 142, 2237–2249.
- Gall, L., Pien, S. and Rusig, A.-M.** (2004). Cultivation of *Palmaria palmata* (Palmariales, Rhodophyta) from isolated spores in semi-controlled conditions. *Aquaculture* 229, 181–191.
- GeBele, R., Halatek, J., Würthner, L., Frey, E.** (2020). Geometric cues stabilise long-axis polarisation of PAR protein patterns in *C. elegans*. *Nat. Commun.* 2020 111 11, 1–12.
- Goddard, H., Manison, N. F. H., Tomos, D., Brownlee, C.** (2000). Elemental propagation of calcium signals in response-specific patterns determined by environmental stimulus strength. *Proc. Natl. Acad. Sci. U. S. A.* 97, 1932–1937.
- Goldstein, B. and Freeman, G.** (1997). Axis specification in animal development. *BioEssays* 19, 105–116.
- Goode, B. L., Drubin, D. G., Barnes, G.** (2000). Functional cooperation between the microtubule and actin cytoskeletons. *Curr. Opin. Cell Biol.* 12, 63–71.
- Goodner, B. and Quatrano, R. S.** (1993). *Fucus* Embryogenesis: A Model to Study the Establishment of Polarity. *Plant Cell* 5, 1471–1481.
- Gorfinkiel, N. and Martinez Arias, A.** (2021). The cell in the age of the genomic revolution: Cell Regulatory Networks. *Cells Dev.* 168, 203720.
- Guiry, M.D. and Guiry, G.M.** (2023). AlgaeBase. World-wide electronic publication, National University of Ireland, Galway. (<https://www.algaebase.org>; searched on Oct 25, 2023).
- Gundersen, G. G.** (2002). Evolutionary conservation of microtubule-capture mechanisms. *Nat. Rev. Mol. Cell Biol.* 3, 296–304.
- Hable, W. E.** (2014). Rac1 signaling in the establishment of the fucoid algal body plan. *Front. Plant Sci.* 5, 690.
- Hable, W. E. and Kropf, D. L.** (2005). The Arp2/3 complex nucleates actin arrays during zygote polarity establishment and growth. *Cell Motility* 61, 9–20.
- Hable, W. E., Miller, N. R. and Kropf, D. L.** (2003). Polarity establishment requires dynamic actin in fucoid zygotes. *Protoplasma* 221, 193–204.
- Hable, W. E., Reddy, S. and Julien, L.** (2008). The Rac1 inhibitor, NSC23766, depolarizes adhesive secretion, endomembrane cycling, and tip growth in the fucoid alga, *Silvetia compressa*. *Planta* 227, 991–1000.
- Haig, D.** (2015). Coleochaete and the origin of sporophytes. *American Journal of Botany* 102, 417–422.

- Hamant, O., Inoue, D., Bouchez, D., Dumais, J., Mjolsness, E.** (2019). Are microtubules tension sensors? *Nat. Commun.* 2019 101 10, 1–12.
- Harnvanichvech, Y., Borassi, C., Daghma, D. E. S., van der Kooij, H. M., Sprakel, J. and Weijers, D.** (2023). An elastic proteinaceous envelope encapsulates the early Arabidopsis embryo. *Development* dev.201943.
- Hatchett, W. J., Coyer, J. A., Sjøtun, K., Jueterbock, A. and Hoarau, G.** (2022). A review of reproduction in the seaweed genus *Fucus* (Ochrophyta, Fucales): Background for renewed consideration as a model organism. *Front. Mar. Sci.* **9**, 1051838.
- Hawes, D., Shi, S.-R., Dabbs, D. J., Taylor, C. R. and Cote, R. J.** (2009). Immunohistochemistry. *Modern Surgical Pathology* 48–70.
- He, F., Chen, H. and Han, R.** (2020). The Plant Cytoskeleton and Crosslinking Factors. *CellBio* 09, 85–99.
- Heesch, S., Serrano-Serrano, M., Barrera-Redondo, J., Luthringer, R., Peters, A. F., Destombe, C., Cock, J. M., Valero, M., Roze, D., Salamin, N., et al.** (2021). Evolution of life cycles and reproductive traits: Insights from the brown algae. *J. Evol. Biol.* **34**, 992–1009.
- Hervé, C., Siméon, A., Jam, M., Cassin, A., Johnson, K. L., Salmeán, A. A., Willats, W. G. T., Doblin, M. S., Bacic, A., Kloareg, B.** (2016). Arabinogalactan proteins have deep roots in eukaryotes: identification of genes and epitopes in brown algae and their role in *Fucus serratus* embryo development. *New Phytol.* **209**, 1428–1441.
- Henry, C. A., Jordan, J. R. and Kropf, D. L.** (1996). Localized membrane-wall adhesions in *Pelvetia* zygotes. *Protoplasma* **190**, 39–52.
- Inoue, A. and Ojima, T.** (2019). Functional identification of alginate lyase from the brown alga *Saccharina japonica*. *Sci Rep* **9**, 4937.
- Hisanaga, T., Fujimoto, S., Cui, Y., Sato, K., Sano, R., Yamaoka, S., Kohchi, T., Berger, F. and Nakajima, K.** (2021). Correction: Deep evolutionary origin of gamete-directed zygote activation by KNOX/BELL transcription factors in green plants. *Elife* **10**,.
- Ho-Plágaro, T., Tamayo-Navarrete, M. I., García Garrido, J. M.** (2022). Microtubule cytoskeleton and mycorrhizal roots. *Plant Signal. Behav.* **17**, 2031504.
- Hoffmann, N., King, S., Samuels, A. L., McFarlane, H. E.** (2021). Subcellular coordination of plant cell wall synthesis. *Dev. Cell* **56**, 933–948.
- Hohmann, T. and Dehghani, F.** (2019). The Cytoskeleton-A Complex Interacting Meshwork. *Cells* **8**,.
- Horio, T. and Oakley, B. R.** (2005). The role of microtubules in rapid hyphal tip growth of *Aspergillus nidulans*. *Mol. Biol. Cell* **16**, 918–926.
- Hurd, A. M.** (1920). Effect of Unilateral Monochromatic Light and Group Orientation on the Polarity of Germinating *Fucus* Spores. *Bot. Gaz.* **70**, 25–50.
- Immler, S.** (2018). The sperm factor: paternal impact beyond genes. *Hered.* 2018 1213 121, 239–247.
- Inoue, A. and Ojima, T.** (2019). Functional identification of alginate lyase from the brown alga *Saccharina japonica*. *Sci. Rep.* **9**, 4937.
- Inoue, A., Satoh, A., Morishita, M., Tokunaga, Y., Miyakawa, T., Tanokura, M., Ojima, T.** (2016). Functional heterologous expression and characterization of mannuronan C5-epimerase from the brown alga *Saccharina japonica*. *Algal Res.* **16**, 282–291.
- J. Marshall, D. and Uller, T.** (2007). When is a maternal effect adaptive? *Oikos* **116**, 1957–1963.
- Jaffe, L. F.** (1968). Localization in the Developing FUCUS EGG and the GENERAL ROLE of LOCALIZING CURRENTS. In *Advances in Morphogenesis* (ed. Abercrombie, M.), Brachet, J.), and King, T. J.), pp. 295–328. Elsevier.
- Jan, Y. N. and Jan, L. Y.** (1998). Asymmetric cell division. *Nature* **392**, 775–778.
- Jeong, S., Eilbert, E., Bolbol, A., Lukowitz, W.** (2016). Going mainstream: How is the body axis of plants first initiated in the embryo? *Dev. Biol.* **419**, 78–84.

- Johnson, C. S., Holzemer, N. F., Wingert, R. A.** (2011). Laser ablation of the zebrafish pronephros to study renal epithelial regeneration. *J. Vis. Exp.* e2845.
- Jürgens, G.** (2001). Apical-basal pattern formation in Arabidopsis embryogenesis. *EMBO J.* 20, 3609–3616.
- Kai, T., Nimura, K., Yasui, H. and Mizuta, H.** (2006). Regulation of Sorus Formation by Auxin in Laminariales Sporophyte. *J Appl Phycol* **18**, 95–101.
- Kalinka, A. T. and Tomancak, P.** (2012). The evolution of early animal embryos: conservation or divergence? *Trends Ecol. Evol.* 27, 385–393.
- Kanda, T.** (1936). On the Gametophytes of Some Japanese Species of Laminariales I. Scientific papers of the Institute of Algological Research, Faculty of Science, Hokkaido Imperial University **1**, 221–260.
- Kanda, T.** (1938). On the Gametophytes of Some Japanese Species of Laminariales II. Scientific papers of the Institute of Algological Research, Faculty of Science, Hokkaido Imperial University **2**, 87–111.
- Kanda, T.** (1941). On the Gametophytes of Some Japanese Species of Laminariales III. Scientific papers of the Institute of Algological Research, Faculty of Science, Hokkaido Imperial University **2**, 155–193.
- Karami, O., Philippsen, C., Rahimi, A., Nurillah, A. R., Boutilier, K., Offringa, R.** (2023). Endogenous auxin maintains embryonic cell identity and promotes somatic embryo development in Arabidopsis. *Plant J.* 113, 7–22.
- Karyophyllis, D., Katsaros, C., Galatis, B.** (2000). F-actin involvement in apical cell morphogenesis of *Sphacelaria rigidula* (Phaeophyceae): mutual alignment between cortical actin filaments and cellulose microfibrils. *Eur. J. Phycol.* 35, 195–203.
- Kassambara A.** (2023). *rstatix: Pipe-Friendly Framework for Basic Statistical Tests*. R. package version 0.7.2, <https://CRAN.R-project.org/package=rstatix>
- Katsaros, C. and Galatis, B.** (1992). Immunofluorescence and electron microscopic studies of microtubule organization during the cell cycle of *Dictyota dichotoma* (Phaeophyta, Dictyotales). *Protoplasma* 169, 75–84.
- Katsaros, C., Galatis, B., Mitrakos, K.** (1983). Fine Structural Studies on the Interphase and Dividing Apical Cells of *Sphacelaria tribuloides* (Phaeophyta). *J. Phycol.* 19, 16–30.
- Katsaros, C., Karyophyllis, D., Galatis, B.** (2006). Cytoskeleton and morphogenesis in brown algae. *Ann. Bot.* 97, 679–693.
- Katsaros, C. I., Karyophyllis, D. A. and Galatis, B. D.** (2002). Cortical F-actin underlies cellulose microfibril patterning in brown algal cells. *Phycologia* **41**, 178–183.
- Katsaros, C., Karyophyllis, D. and Galatis, B.** (2003). F-actin cytoskeleton and cell wall morphogenesis in brown algae. *Cell Biology International* **27**, 209–210.
- Katsaros, C., Nagasato, C., Terauchi, M. and Motomura, T.** (2013). Cytokinesis in brown algae. In *Advances in Algal Cell Biology*, p. 224. Berlin, Boston: De Gruyter.
- Kawai, H., Hanyuda, T., Draisma, S. G. A., Wilce, R. T., Andersen, R. A.** (2015). Molecular phylogeny of two unusual brown algae, *Phaeostrophion irregulare* and *Platysiphon glacialis*, proposal of the Stschapoviales ord. nov. and Platysiphonaceae fam. nov., and a re-examination of divergence times for brown algal orders. *J. Phycol.* 51, 918–928.
- Kawashima, T. and Berger, F.** (2014). Epigenetic reprogramming in plant sexual reproduction. *Nat. Rev. Genet.* 15, 613–624.
- Kim, G. H., Nagasato, C., Kwak, M., Lee, J. W., Hong, C. Y., Klochkova, T. A., Motomura, T.** (2022). Intercellular transport across pit-connections in the filamentous red alga *Griffithsia monilis*. *Algae* 37, 75–84.
- King, N., Westbrook, M. J., Young, S. L., Kuo, A., Abedin, M., Chapman, J., Fairclough, S., Hellsten, U., Isogai, Y., Letunic, I., et al.** (2008). The genome of the choanoflagellate *Monosiga brevicollis* and the origin of metazoans. *Nature* 451, 783–788.
- Kirchhelle, C. and Moore, I.** (2017). A Simple Chamber for Long-term Confocal Imaging of Root and Hypocotyl Development. *J. Vis. Exp.* 2017, 55331.

Klimova, A. and Klochkova, T. (2021). Cytological and Chromosomal Features of *Alaria* Species (Laminariales, Phaeophyceae) from Kamchatka. *Bull. of Kamchatka State Tech. Univ.* 58, 86.

Klimova, A. V. and Klochkova, T. A. (2017). Peculiarities of development in the marine brown alga *Alaria angusta* Kjellman, 1889 (Alariaceae: Ochrophyta) under laboratory-controlled conditions. *Russ J Mar Biol* 43, 42–48. **Kloareg, B., Badis, Y., Cock, J. M., Michel, G.** (2021). Role and Evolution of the Extracellular Matrix in the Acquisition of Complex Multicellularity in Eukaryotes: A Macroalgal Perspective. *Genes* (Basel). 12,.

Klochkova, T. A., Motomura, T., Nagasato, C., Klimova, A. V, Kim, G. H. (2019). The role of egg flagella in the settlement and development of zygotes in two *Saccharina* species. *Phycologia* 58, 145–153.

Kraus, Y., Aman, A., Technau, U., Genikhovich, G. (2016). Pre-bilaterian origin of the blastoporal axial organizer. *Nat. Commun.* 7, 11694.

Kropf, D. L., Bisgrove, S. R., Hable, W. E. (1999). Establishing a growth axis in fucoid algae. *Trends Plant Sci.* 4, 490–494.

Kropf, D. L., Kloareg, B., Quatrano, R. S. (1988). Cell wall is required for fixation of the embryonic axis in *Fucus* zygotes. *Science* 239, 187–190.

Lähteenmäki-Uutela, A., Rahikainen, M., Camarena-Gómez, M. T., Piiparinen, J., Spilling, K., Yang, B. (2021). European Union legislation on macroalgae products. *Aquac. Int.* 29, 487–509.

Landrein, B. and Hamant, O. (2013). How mechanical stress controls microtubule behavior and morphogenesis in plants: history, experiments and revisited theories. *Plant J.* 75, 324–338.

Latinkić, B. V, Umbhauer, M., Neal, K. A., Lerchner, W., Smith, J. C., Cunliffe, V. (1997). The *Xenopus* Brachyury promoter is activated by FGF and low concentrations of activin and suppressed by high concentrations of activin and by paired-type homeodomain proteins. *Genes Dev.* 11, 3265–3276.

Lau, S., Slane, D., Herud, O., Kong, J., Jürgens, G. (2012). Early embryogenesis in flowering plants: Setting up the basic body pattern. *Annu. Rev. Plant Biol.* 63, 483–506.

Lawrence, P. A. and Levine, M. (2006). Mosaic and regulative development: two faces of one coin. *Curr. Biol.* 16,.

Le Bail, A., Billoud, B., Kowalczyk, N., Kowalczyk, M., Gicquel, M., Le Panse, S., Stewart, S., Scornet, D., Cock, J. M., Ljung, K., et al. (2010). Auxin metabolism and function in the multicellular brown alga *Ectocarpus siliculosus*. *Plant Physiol.* 153, 128–144.

le Bail, A., Billoud, B., le Panse, S., Chenivresse, S., Charrier, B. (2011). ETOILE Regulates Developmental Patterning in the Filamentous Brown Alga *Ectocarpus siliculosus*. *Plant Cell* 23, 1666–1678.

Le Bail, A., Billoud, B., Maisonneuve, C., Peters, A. F., Mark Cock, J., Charrier, B. (2008). Early Development Pattern of the Brown Alga *Ectocarpus siliculosus* (Ectocarpales, Phaeophyceae) Sporophyte. *J. Phycol.* 44, 1269–1281.

Le Bail, A. and Charrier, B. (2013). Culture Methods and Mutant Generation in the Filamentous Brown Algae *Ectocarpus siliculosus*. In *Plant Organogenesis* (ed. De Smet, I.), pp. 323–332. Humana Press.

Lee, M. T., Bonneau, A. R., Giraldez, A. J. (2014). Zygotic genome activation during the maternal-to-zygotic transition. *Annu. Rev. Cell Dev. Biol.* 30, 581–613.

Li, R. and Bowerman, B. (2010). Symmetry breaking in biology. *Cold Spring Harb. Perspect. Biol.* 2,.

Li, X., Diao, M., Zhang, Y., Chen, G., Huang, S., Chen, N. (2019). Guard Cell Microfilament Analyzer Facilitates the Analysis of the Organization and Dynamics of Actin Filaments in Arabidopsis Guard Cells. *Int. J. Mol. Sci.* 2019, Vol. 20, Page 2753 20, 2753.

Li, Y. J., Yu, Y., Liu, X., Zhang, X. S., Su, Y. H. (2021). The Arabidopsis MATERNAL EFFECT EMBRYO ARREST45 protein modulates maternal auxin biosynthesis and controls seed size by inducing AINTEGUMENTA. *Plant Cell* 33, 1907–1926.

- Li, Y., Zheng, L., Corke, F., Smith, C., Bevan, M. W.** (2008). Control of final seed and organ size by the DA1 gene family in *Arabidopsis thaliana*. *Genes Dev.* 22, 1331–1336.
- Lin, X., Alspaugh, J. A., Liu, H., Harris, S.** (2014). Fungal morphogenesis. *Cold Spring Harb. Perspect. Med.* 5, a019679.
- Linardić, M.** (2018). The role of brown algal cell walls in morphogenesis and development.
- Lipinska, A. P., Serrano-Serrano, M. L., Cormier, A., Peters, A. F., Kogame, K., Cock, J. M., Coelho, S. M.** (2019). Rapid turnover of life-cycle-related genes in the brown algae. *Genome Biol.* 20, 35.
- Livanos, P. and Müller, S.** (2019). Division Plane Establishment and Cytokinesis. *Annu. Rev. Plant Biol.* 70, 239–267.
- Lockhart, J. A.** (1965). An analysis of irreversible plant cell elongation. *J. Theor. Biol.* 8, 264–275.
- Loh, K. M., van Amerongen, R., Nusse, R.** (2016). Generating Cellular Diversity and Spatial Form: Wnt Signaling and the Evolution of Multicellular Animals. *Dev. Cell* 38, 643–655.
- Lüning, K.** (1981). Egg release in gametophytes of *Laminaria saccharina*: Induction by darkness and inhibition by blue light and u.v. *Br. Phycol. J.* 16, 379–393.
- Lüning, K. and Dring, M. J.** (1972). Reproduction induced by blue light in female gametophytes of *Laminaria saccharina*. *Planta* 104, 252–256.
- Lüning, K. and Dring, M.** (1975). Reproduction, growth and photosynthesis of gametophytes of *Laminaria saccharina* grown in blue and red light. *Mar. Biol.* 29, 195–200.
- Lüning, K. and Müller, D.** (1978). Chemical interaction in sexual reproduction of several Laminariales (Phaeophyceae): Release and attraction of spermatozoids. *Zeitschrift für Pflanzenphysiologie* 89, 333–341.
- Macaisne, N., Liu, F., Scornet, D., Peters, A. F., Lipinska, A., Perrineau, M.-M., Henry, A., Strittmatter, M., Coelho, S. M., Cock, J. M.** (2017). The *Ectocarpus* IMMEDIATE UPRIGHT gene encodes a member of a novel family of cysteine-rich proteins with an unusual distribution across the eukaryotes. *Development* 144, 409–418.
- Maier, I., Hertweck, C. and Boland, W.** (2001). Stereochemical specificity of lamoxirene, the sperm-releasing pheromone in kelp (Laminariales, Phaeophyceae). *Biol. Bull.* 201, 121–125.
- Maier, I. and Müller, D. G.** (1982). Antheridium fine structure and spermatozoid release in *Laminaria digitata* (Phaeophyceae). *Phycologia* 21, 1–8.
- Mansfield, S. G. and Briarty, L. G.** (1991). Early embryogenesis in *Arabidopsis thaliana*. II. The developing embryo. *Can. J. Bot.* 69, 461–476.
- Mariani, P., Tolomio, C. and Braghetta, P.** (1985). An ultrastructural approach to the adaptive role of the cell wall in the intertidal alga *Fucus virsoides*. *Protoplasma* 128, 208–217.
- Marlow FL. (2010)** Maternal Control of Development in Vertebrates: My Mother Made Me Do It! San Rafael (CA): Morgan & Claypool Life Sciences; Introduction.
- Martindale, M. Q. and Hejnal, A.** (2009). A developmental perspective: changes in the position of the blastopore during bilaterian evolution. *Dev. Cell* 17, 162–174.
- Martinez, C. C., Chitwood, D. H., Smith, R. S., Sinha, N. R.** (2016). Left–right leaf asymmetry in decussate and distichous phyllotactic systems. *Philos. Trans. R. Soc. B Biol. Sci.* 371, 20150412.
- Mazéas, L., Yonamine, R., Barbeyron, T., Henrissat, B., Drula, E., Terrapon, N., Nagasato, C., Hervé, C.** (2023). Assembly and synthesis of the extracellular matrix in brown algae. *Semin. Cell Dev. Biol.* 134, 112–124.
- McCully, M. E.** (1965). A note on the structure of the cell walls of the brown alga *fucus*. *Can. J. Bot.* 43, 1001–1004.
- Michel, G., Tonon, T., Scornet, D., Cock, J. M., Kloareg, B.** (2010). The cell wall polysaccharide metabolism of the brown alga *Ectocarpus siliculosus*. Insights into the evolution of extracellular matrix polysaccharides in Eukaryotes. *New Phytol.* 188, 82–97.

- Mishra, B. S., Sharma, M. and Laxmi, A.** (2022). Role of sugar and auxin crosstalk in plant growth and development. *Physiol Plant* **174**, e13546.
- Miyazaki, S., Murata, T., Sakurai-Ozato, N., Kubo, M., Demura, T., Fukuda, H., Hasebe, M.** (2009). ANXUR1 and 2, Sister Genes to FERONIA/SIRENE, Are Male Factors for Coordinated Fertilization. *Curr. Biol.* **19**, 1327–1331.
- Mørch, Y. A., Holtan, S., Donati, I., Strand, B. L., Skjåk-Braek, G.** (2008). Mechanical properties of C-5 epimerized alginates. *Biomacromolecules* **9**, 2360–2368.
- Motomura, T.** (1994). Electron and immunofluorescence microscopy on the fertilization of *Fucus distichus* (Fucales, Phaeophyceae). *Protoplasma* **178**, 97–110.
- Motomura, T.** (1991). Immunofluorescence Microscopy of Fertilization and Parthenogenesis in *Laminaria angustata* (Phaeophyta). *J. Phycol.* **27**, 248–257.
- Motomura, T.** (1990). Ultrastructure of Fertilization in *Laminaria angustata* (Phaeophyta, Laminariales) with Emphasis on the Behavior of Centrioles, Mitochondria, and Chloroplasts of the Sperm. *J. Phycol.* **26**, 80–89.
- Motomura, T., Nagasato, C. and Kimura, K.** (2010). Cytoplasmic inheritance of organelles in brown algae. *J Plant Res* **123**, 185–192.
- Münster, S., Jain, A., Mietke, A., Pavlopoulos, A., Grill, S. W., Tomancak, P.** (2019). Attachment of the blastoderm to the vitelline envelope affects gastrulation of insects. *Nature* **568**, 395–399.
- Muth, A. F., Graham, M. H., Lane, C. E., Harley, C. D. G.** (2019). Recruitment tolerance to increased temperature present across multiple kelp clades. *Ecology* **100**, e02594.
- Muzzy, R. and Hable, W.** (2013). RAC1 regulates actin arrays during polarity establishment in the brown alga, *Silvetia compressa*. *Developmental Biology* **383**, 28–38.
- Myklestad, S. and Granum, E.** (2009). Biology of (1,3)- β -Glucans and Related Glucans in Protozoans and Chromistans. In *Chemistry, Biochemistry, and Biology of 1-3 Beta Glucans and Related Polysaccharides*, pp. 353–385.
- Naf, U.** (1962). Developmental Physiology of Lower Archegoniates. *Annual Review of Plant Physiology* **13**, 507–532.
- Nagasato, C., Inoue, A., Mizuno, M., Kanazawa, K., Ojima, T., Okuda, K., Motomura, T.** (2010). Membrane fusion process and assembly of cell wall during cytokinesis in the brown alga, *Silvetia babingtonii* (Fucales, Phaeophyceae). *Planta* **232**, 287–298.
- Nagasato, C. and Motomura, T.** (2009). Effect of Latrunculin B and Brefeldin a on Cytokinesis in the Brown Alga *Scytosiphon lomentaria* (scytosiphonales, Phaeophyceae)1. *Journal of Phycology* **45**, 404–412.
- Nagasato, C. and Motomura, T.** (2002). Influence of the centrosome in cytokinesis of brown algae: polyspermic zygotes of *Scytosiphon lomentaria* (Scytosiphonales, Phaeophyceae). *J. Cell Sci.* **115**, 2541–2548.
- Nagasato, C., Terauchi, M., Tanaka, A., Motomura, T.** (2015). Development and function of plasmodesmata in zygotes of *Fucus distichus*. *Bot. Mar.* **58**, 229–238.
- Nagasato, C., Tanaka, A., Ito, T., Katsaros, C. and Motomura, T.** (2017). Intercellular translocation of molecules via plasmodesmata in the multiserial filamentous brown alga, *Halopteris congesta* (Sphacelariales, Phaeophyceae). *Journal of Phycology* **53**, 333–341.
- Nagasato, C., Yonamine, R. and Motomura, T.** (2022). Ultrastructural Observation of Cytokinesis and Plasmodesmata Formation in Brown Algae. *Methods Mol Biol* **2382**, 253–264.
- Niklas, K. J.** (2000). The Evolution of Plant Body Plans—A Biomechanical Perspective. *Ann. Bot.* **85**, 411–438.
- Niklas, K. J. and Kutschera, U.** (2009). The evolutionary development of plant body plans. *Funct. Plant Biol.* **36**, 682–695.
- Niklas, K. J. and Newman, S. A.** (2020). The many roads to and from multicellularity. *J. Exp. Bot.* **71**, 3247–3253.

- Niklas, K. J. and Tiffney, B. H.** (2022). Viridiplantae Body Plans Viewed Through the Lens of the Fossil Record and Molecular Biology. *Integr. Comp. Biol.* icac150.
- Noatynska, A. and Gotta, M.** (2012). Cell polarity and asymmetric cell division: the *C. elegans* early embryo. *Essays Biochem.* 53, 1–14.
- Norton, T. A.** (1972). The development of Saccorhiza dermatodea (Phaeophyceae, Laminariales) in culture. *Phycologia* 11, 81–86.
- Novotny, A. M. and Forman, M.** (1975). The composition and development of cell walls of *Fucus* embryos. *Planta* 122, 67–78.
- Nyvall, P., Corre, E., Boisset, C., Barbeyron, T., Rousvoal, S., Scornet, D., Kloareg, B., Boyen, C.** (2003). Characterization of mannuronan C-5-epimerase genes from the brown alga *Laminaria digitata*. *Plant Physiol.* 133, 726–735.
- O'Malley, M. A., Leger, M. M., Wideman, J. G., Ruiz-Trillo, I.** (2019). Concepts of the last eukaryotic common ancestor. *Nat. Ecol. & Evol.* 3, 338–344.
- Pang, S. and Lüning, K.** (2004). Photoperiodic long-day control of sporophyll and hair formation in the brown alga *Undaria pinnatifida*. *Journal of Applied Phycology* 16, 83–92.
- Panteris, E. and Pappas, D.** (2023). F-Actin Organization and Epidermal Cell Morphogenesis in the Brown Alga *Sargassum vulgare*. *Int. J. Mol. Sci.* 24,.
- Paredes, A. R., Somerville, C. R. and Ehrhardt, D. W.** (2006). Visualization of cellulose synthase demonstrates functional association with microtubules. *Science* 312, 1491–1495.
- Pauklin, S. and Vallier, L.** (2015). Activin/Nodal signalling in stem cells. *Development* 142, 607–619.
- Pedersen, G. B., Blaschek, L., Frandsen, K. E. H., Noack, L. C. and Persson, S.** (2023). Cellulose synthesis in land plants. *Mol. Plant* 16, 206–231.
- Pelegri, F.** (2003). Maternal factors in zebrafish development. *Dev. Dyn.* an Off. Publ. Am. Assoc. Anat. 228, 535–554.
- Petersen, C. P. and Reddien, P. W.** (2009). Wnt signaling and the polarity of the primary body axis. *Cell* 139, 1056–1068.
- Piñeiro-Corbeira, C., Barrientos, S., Barreiro, R., de la Cruz-Modino, R.** (2022). Assessing the importance of kelp forests for small-scale fisheries under a global change scenario. *Front. Mar. Sci.* 9,.
- Pollock, E. G.** (1970). Fertilization in *Fucus*. *Planta* 92, 85–99.
- Quatrano, R.** (2003). Development of Cell Polarity. *Ann. Rev. Plant Physiol.* 29, 487–510.
- Quatrano, R. S. and Shaw, S. L.** (1997). Role of the cell wall in the determination of cell polarity and the plane of cell division in *Fucus* embryos. *Trends Plant Sci.* 2, 15–21.
- Rabillé, H., Billoud, B., Tesson, B., Le Panse, S., Rolland, É. and Charrier, B.** (2019a). The brown algal mode of tip growth: Keeping stress under control. *PLoS Biol.* 17, e2005258.
- Rabillé, H., Torode, T. A., Tesson, B., Le Bail, A., Billoud, B., Rolland, E., Le Panse, S., Jam, M. and Charrier, B.** (2019b). Alginates along the filament of the brown alga *Ectocarpus* help cells cope with stress. *Sci. Rep.* 9, 12956.
- Rabillé, H., Koutalianou, M., Charrier, B. and Katsaros, C.** (2018). Actin fluorescent staining in the filamentous brown alga *Ectocarpus siliculosus*. In *Protocols for Macroalgae Research* (ed. Charrier, B.), Wichard, T.), and Reddy, C.), pp. 365–379. Boca Raton: Taylor & Francis group, CRC Press.
- Rando, O. J.** (2012). Daddy issues: paternal effects on phenotype. *Cell* 151, 702–708.
- Reinhardt, D., Frenz, M., Mandel, T. and Kuhlemeier, C.** (2005). Microsurgical and laser ablation analysis of leaf positioning and dorsoventral patterning in tomato. *Development* 132, 15–26.
- Reviere, B. and Rousseau, F.** (1999). Towards a new classification of the brown algae. *Prog. Phycol. Res.* 13, 107–201.
- Reviere, B., Rousseau, F., Draisma, S.** (2007). Classification of the Phaeophyceae from past to present and current challenges. In *Unravelling the algae – the past, present and*

future of algal molecular (ed. Brodie, J.) and Lewis, J.), pp. 267–284. Boca Raton, FL, USA: CRC Press, Taylor & Francis Group.

Reyes-Prieto, A., Weber, A. P. M., Bhattacharya, D. (2007). The origin and establishment of the plastid in algae and plants. *Annu. Rev. Genet.* 41, 147–168.

Rishmawi, L., Pesch, M., Juengst, C., Schauss, A. C., Schrader, A., Hülskamp, M. (2014). Non-cell-autonomous regulation of root hair patterning genes by WRKY75 in *Arabidopsis*. *Plant Physiol.* 165, 186–195.

Robert, H. S., Crhak Khaitova, L., Mroue, S. and Benková, E. (2015). The importance of localized auxin production for morphogenesis of reproductive organs and embryos in *Arabidopsis*. *J. Exp. Bot.* 66, 5029–5042.

Robert, H. S., Park, C., Gutiérrez, C. L., Wójcikowska, B., Pěňčík, A., Novák, O., Chen, J., Grunewald, W., Dresselhaus, T., Friml, J., et al. (2018). Maternal auxin supply contributes to early embryo patterning in *Arabidopsis*. *Nat. plants* 4, 548–553.

Robert, H. S., Grones, P., Stepanova, A. N., Robles, L. M., Lokerse, A. S., Alonso, J. M., Weijers, D., Friml, J. (2013). Local auxin sources orient the apical-basal axis in *Arabidopsis* embryos. *Curr. Biol.* 23, 2506–2512.

Robert, H. S., Park, C., Gutiérrez, C. L., Wójcikowska, B., Pěňčík, A., Novák, O., Chen, J., Grunewald, W., Dresselhaus, T., Friml, J., et al. (2018). Maternal auxin supply contributes to early embryo patterning in *Arabidopsis*. *Nat. Plants* 2018 48 4, 548–553.

Robertson, S. and Lin, R. (2015). The Maternal-to-Zygotic Transition in *C. elegans*. *Curr. Top. Dev. Biol.* 113, 1–42.

Rosin, P. L. (2005). Computing global shape measures. *Handb. Pattern Recognit. Comput. Vision*, 3rd Ed. 177–196.

Rusig, A. M., Ouichou, A., Le Guyader, H., Ducreux, G. (2001). Ontogenesis in the Fucophyceae: case studies and comparison of fucoid zygotes and *Sphacelaria* apical cells. *Cryptogam. Algal.* 22, 227–248.

Sakakibara, K., Reisewitz, P., Aoyama, T., Friedrich, T., Ando, S., Sato, Y., Tamada, Y., Nishiyama, T., Hiwatashi, Y., Kurata, T., et al. (2014). WOX13-like genes are required for reprogramming of leaf and protoplast cells into stem cells in the moss *Physcomitrella patens*. *Development* 141, 1660–1670.

Sampathkumar, A. (2020). Mechanical feedback-loop regulation of morphogenesis in plants. *Dev.* 147,.

Sampathkumar, A., Peaucelle, A., Fujita, M., Schuster, C., Persson, S., Wasteneys, G. O. and Meyerowitz, E. M. (2019). Primary wall cellulose synthase regulates shoot apical meristem mechanics and growth. *Development* 146,.

Sato, A., Toyooka, K., Okamoto, T. (2010). Asymmetric cell division of rice zygotes located in embryo sac and produced by in vitro fertilization. *Sex. Plant Reprod.* 23, 211–217.

Sauvageau, C. (1918). Recherches sur les laminaires des côtes de France. *Mem. Acad. Sci. Inst. Fr.* 56, 1–240.

Schaller, G. E., Bishopp, A., Kieber, J. J. (2015). The Yin-Yang of Hormones: Cytokinin and Auxin Interactions in Plant Development. *Plant Cell* 27, 44.

Schindelin, J., Arganda-Carreras, I., Frise, E., Kaynig, V., Longair, M., Pietzsch, T., Preibisch, S., Rueden, C., Saalfeld, S., Schmid, B., et al. (2012). Fiji - an Open Source platform for biological image analysis. *Nature methods* 9, 676–682.

Schneider, R., Ehrhardt, D. W., Meyerowitz, E. M., Sampathkumar, A. (2022). Tethering of cellulose synthase to microtubules dampens mechano-induced cytoskeletal organization in *Arabidopsis* pavement cells. *Nat. plants* 8, 1064–1073.

Shahbazi, M. N., Siggia, E. D., Zernicka-Goetz, M. (2019). Self-organization of stem cells into embryos: A window on early mammalian development. *Science* 364, 948–951.

Shan, T. F., Pang, S. J., Gao, S. Q. (2013). Novel means for variety breeding and sporeling production in the brown seaweed *Undaria pinnatifida* (Phaeophyceae): Crossing female gametophytes from parthenosporophytes with male gametophyte clones. *Phycol. Res.* 61, 154–161.

- Shaw, S. L. and Quatrano, R. S.** (1996). The role of targeted secretion in the establishment of cell polarity and the orientation of the division plane in *Fucus* zygotes. *Development* 122, 2623–2630.
- Shen, K.-F., Osmani, A. H., Govindaraghavan, M., Osmani, S. A.** (2014). Mitotic regulation of fungal cell-to-cell connectivity through septal pores involves the NIMA kinase. *Mol. Biol. Cell* 25, 763–775.
- Shen, Y., Motomura, T., Ichihara, K., Matsuda, Y., Yoshimura, K., Kosugi, C. and Nagasato, C.** (2023). Application of CRISPR-Cas9 genome editing by microinjection of gametophytes of *Saccharina japonica* (Laminariales, Phaeophyceae). *J. Appl. Phycol.* 35, 1–11.
- Sheng, G. and Foley, A. C.** (2012). Diversification and conservation of the extraembryonic tissues in mediating nutrient uptake during amniote development. *Ann. N. Y. Acad. Sci.* 1271, 97–103.
- Shimamura, M.** (2016). *Marchantia polymorpha*: Taxonomy, Phylogeny and Morphology of a Model System. *Plant Cell Physiol.* 57, 230–256.
- Shimizu, K. and Stopfer, M.** (2013). Gap junctions. *Curr. Biol.* 23, R1026-31.
- Shirae-Kurabayashi, M., Edzuka, T., Suzuki, M., Goshima, G.** (2022). Cell tip growth underlies injury response of marine macroalgae. *PLoS One* 17,.
- Silberfeld, T., Leigh, J. W., Verbruggen, H., Cruaud, C., de Reviers, B., Rousseau, F.** (2010). A multi-locus time-calibrated phylogeny of the brown algae (Heterokonta, Ochrophyta, Phaeophyceae): Investigating the evolutionary nature of the “brown algal crown radiation”. *Mol. Phylogenet. Evol.* 56, 659–674.
- Simsek, M. F. and Özbudak, E. M.** (2022). Patterning principles of morphogen gradients. *Open Biol.* 12, 220224.
- Stern, C. D.** (2006). Evolution of the mechanisms that establish the embryonic axes. *Curr. Opin. Genet. Dev.* 16, 413–418.
- Steventon, B., Busby, L. and Arias, A. M.** (2021). Establishment of the vertebrate body plan: Rethinking gastrulation through stem cell models of early embryogenesis. *Dev. Cell* 56, 2405–2418.
- Strassert, J. F. H., Jamy, M., Mylnikov, A. P., Tikhonenkov, D. V, Burki, F.** (2019). New Phylogenomic Analysis of the Enigmatic Phylum Telonemia Further Resolves the Eukaryote Tree of Life. *Mol. Biol. Evol.* 36, 757–765.
- Sun, H., Basu, S., Brady, S. R., Luciano, R. L., Muday, G. K.** (2004). Interactions between Auxin Transport and the Actin Cytoskeleton in Developmental Polarity of *Fucus distichus* Embryos in Response to Light and Gravity. *Plant Physiol.* 135, 266–278.
- Sunchu, B. and Cabernard, C.** (2020). Principles and mechanisms of asymmetric cell division. *Development* 147,.
- Swalla, B. J.** (2006). Building divergent body plans with similar genetic pathways. *Heredity (Edinb).* 97, 235–243.
- Tadros, W. and Lipshitz, H. D.** (2009). The maternal-to-zygotic transition: a play in two acts. *Development* 136, 3033–3042.
- Takahashi, K., Hirata, S., Kido, N., Katou, K.** (2006). Wall-Yielding Properties of Cell Walls from Elongating Cucumber Hypocotyls in Relation to the Action of Expansin. *Plant Cell Physiol.* 47, 1520–1529.
- Takeuchi, M., Staehelin, L. A., Mineyuki, Y., Takeuchi, M., Staehelin, L. A., Mineyuki, Y.** (2017). Actin-Microtubule Interaction in Plants. *Cytoskelet. - Struct. Dyn. Funct. Dis.*
- Tarakhovskaya, E., Lemesheva, V., Bilova, T., Birkemeyer, C.** (2017). Early embryogenesis of brown alga *Fucus vesiculosus* L. is characterized by significant changes in carbon and energy metabolism.
- Technau, U. and Scholz, C. B.** (2003). Origin and evolution of endoderm and mesoderm. *Int. J. Dev. Biol.* 47, 531–539.
- Terauchi, M., Nagasato, C., Motomura, T.** (2015). Plasmodesmata of brown algae. *J. Plant Res.* 128, 7–15.

- Terauchi, M., Yamagishi, T., Hanyuda, T., Kawai, H.** (2017). Genome-wide computational analysis of the secretome of brown algae (Phaeophyceae). *Mar. Genomics* 32, 49–59.
- Terauchi, M., Nagasato, C., Inoue, A., Ito, T. and Motomura, T.** (2016). Distribution of alginate and cellulose and regulatory role of calcium in the cell wall of the brown alga *Ectocarpus siliculosus* (Ectocarpales, Phaeophyceae). *Planta* 244, 361–377.
- Theodorou, I. and Charrier, B.** (2021). Brown Algae: *Ectocarpus* and *Saccharina* as experimental models for developmental biology. In *Handbook of Marine Model Organisms in Experimental Biology: Established and Emerging*, pp. 27–47.
- Theodorou, I. and Charrier, B.** (2023). The shift to 3D growth during embryogenesis of kelp species, atlas of cell division and differentiation of *Saccharina latissima*. *Development* 150,.
- Theodorou, I. and Charrier, B.** (2023). The shift to 3D growth during embryogenesis of kelp species, atlas of cell division and differentiation of *Saccharina latissima*. *Development* 150,.
- Theodorou, I., Opsahl-Sorteberg, H.-G., Charrier, B.** (2021). Preparation of Zygotes and Embryos of the Kelp *Saccharina latissima* for Cell Biology Approaches. *BIO-PROTOCOL* 101,.
- Torode, T. A., Marcus, S. E., Jam, M., Tonon, T., Blackburn, R. S., Hervé, C., Knox, J. P.** (2015). Monoclonal Antibodies Directed to Fucoidan Preparations from Brown Algae. *PLoS One* 10, 1–19.
- Torode, T. A., Siméon, A., Marcus, S. E., Jam, M., Le Moigne, M.-A., Duffieux, D., Knox, J. P., Hervé, C.** (2016). Dynamics of cell wall assembly during early embryogenesis in the brown alga *Fucus*. *J. Exp. Bot.* 67, 6089–6100.
- Torres-Paz, J. and Rétaux, S.** (2021). Pescoids and Chimeras to Probe Early Evo-Devo in the Fish *Astyanax mexicanus*. *Front. cell Dev. Biol.* 9, 667296.
- Trinh, D.-C., Alonso-Serra, J., Asaoka, M., Colin, L., Cortes, M., Malivert, A., Takatani, S., Zhao, F., Traas, J., Trehin, C., et al.** (2021). How Mechanical Forces Shape Plant Organs. *Curr. Biol.* 31, R143–R159.
- Turner, D. A., Girgin, M., Alonso-Crisostomo, L., Trivedi, V., Baillie-Johnson, P., Glodowski, C. R., Hayward, P. C., Collignon, J., Gustavsen, C., Serup, P., et al.** (2017). Anteroposterior polarity and elongation in the absence of extra-embryonic tissues and of spatially localised signalling in gastruloids: mammalian embryonic organoids. *Development* 144, 3894–3906.
- Turner, D. A., Rué, P., Mackenzie, J. P., Davies, E., Martinez Arias, A.** (2014). Brachyury cooperates with Wnt/ β -catenin signalling to elicit primitive-streak-like behaviour in differentiating mouse embryonic stem cells. *BMC Biol.* 12, 63.
- Ueda, M., Aichinger, E., Gong, W., Groot, E., Verstraeten, I., Vu, L. D., De Smet, I., Higashiyama, T., Umeda, M., Laux, T.** (2017). Transcriptional integration of paternal and maternal factors in the Arabidopsis zygote. *Genes Dev.* 31, 617–627.
- Ueda, M. and Berger, F.** (2019). New cues for body axis formation in plant embryos. *Curr. Opin. Plant Biol.* 47, 16–21.
- Uji, T. and Mizuta, H.** (2022). The role of plant hormones on the reproductive success of red and brown algae. *Front. Plant Sci.* 13, 1019334.
- Valentine, J. W.** (2004). *On the origin of phyla*. University of Chicago Press.
- van den Berg, C., Hage, W., Weisbeek, P., Scheres, B.** (1998). Laser Ablation In Arabidopsis Roots: A Tool To Study Cell-To-Cell Communication. In *Cellular Integration of Signalling Pathways in Plant Development*, pp. 237–250. Springer, Berlin, Heidelberg.
- van der Meer, J. P.** (1979). Genetics of *Gracilaria sp.* (Rhodophyceae, Gigartinales). V. Isolation and characterization of mutant strains. *Phycologia* 18, 47–54.
- van der Meer, J. P. and Todd, E. R.** (1980). The life history of *Palmaria palmata* in culture. A new type for the Rhodophyta. *Can. J. Bot.* 58, 1250–1256.
- Van Rossum, G. and Drake, F. L.** (2023). *The Python Language Reference*, Release 3.11.5, Python Software Foundation.

- Varvarigos, V., Katsaros, C., Galatis, B.** (2004). Radial F-actin configurations are involved in polarization during protoplast germination and thallus branching of *Macrocystis pyrifera* (Phaeophyceae, Laminariales). *Phycologia* 43, 693–702.
- Varvarigos, V., Galatis, B. and Katsaros, C.** (2007). Radial endoplasmic reticulum arrays co-localize with radial F-actin in polarizing cells of brown algae. *European Journal of Phycology* 42, 253–262.
- Vastenhouw, N. L., Cao, W. X., Lipshitz, H. D.** (2019). The maternal-to-zygotic transition revisited. *Development* 146,.
- Vázquez-Gutiérrez, J. L. and Langton, M.** (2015). Current potential and limitations of immunolabeling in cereal grain research. *Trends in Food Science & Technology* 41, 105–117.
- Verbruggen, H., Ashworth, M., LoDuca, S. T., Vlaeminck, C., Cocquyt, E., Sauvage, T., Zechman, F. W., Littler, D. S., Littler, M. M., Leliaert, F., et al.** (2009). A multi-locus time-calibrated phylogeny of the siphonous green algae. *Mol. Phylogenet. Evol.* 50, 642–653.
- Virtanen, P., Gommers, R., Oliphant, T. E., Haberland, M., Reddy, T., Cournapeau, D., Burovski, E., Peterson, P., Weckesser, W., Bright, J., et al.** (2020). SciPy 1.0: fundamental algorithms for scientific computing in Python. *Nat Methods* 17, 261–272.
- Visch, W., Rad-Menéndez, C., Nylund, G. M., Pavia, H., Ryan, M. J., Day, J.** (2019). Underpinning the development of seaweed biotechnology: Cryopreservation of brown algae (*Saccharina latissima*) gametophytes. *Biopreserv. Biobank.* 17, 378–386.
- Vonica, A. and Gumbiner, B. M.** (2002). Zygotic Wnt activity is required for Brachyury expression in the early *Xenopus laevis* embryo. *Dev. Biol.* 250, 112–127.
- Wakatsuki, T., Schwab, B., Thompson, N. C. and Elson, E. L.** (2001). Effects of cytochalasin D and latrunculin B on mechanical properties of cells. *Journal of Cell Science* 114, 1025–1036.
- Wang, K., Chen, H., Miao, Y., Bayer, M.** (2020). Square one: zygote polarity and early embryogenesis in flowering plants. *Curr. Opin. Plant Biol.* 53, 128–133.
- Wang, K., Chen, H., Ortega-Perez, M., Miao, Y., Ma, Y., Henschen, A., Lohmann, J. U., Laubinger, S., Bayer, M.** (2021). Independent parental contributions initiate zygote polarization in *Arabidopsis thaliana*. *Curr. Biol.* 31, 4810–4816.e5.
- Wang, M., Le Gourrierec, J., Jiao, F., Demotes-Mainard, S., Perez-Garcia, M.-D., Ogé, L., Hamama, L., Crespel, L., Bertheloot, J., Chen, J., et al.** (2021). Convergence and Divergence of Sugar and Cytokinin Signaling in Plant Development. *Int J Mol Sci* 22, 1282.
- Wasteneys, G. O. and Yang, Z.** (2004). New views on the plant cytoskeleton. *Plant Physiol.* 136, 3884–3891.
- Weiss, M. C., Sousa, F. L., Mrnjavac, N., Neukirchen, S., Roettger, M., Nelson-Sathi, S., Martin, W. F.** (2016). The physiology and habitat of the last universal common ancestor. *Nat. Microbiol.* 1, 16116.
- West, C. M., Malzl, D., Hykollari, A., Wilson, I. B. H.** (2021). Glycomics, Glycoproteomics, and Glycogenomics: An Inter-Taxa Evolutionary Perspective. *Mol. Cell. Proteomics* 20, 100024.
- Wiencke, C. and Clayton, M. N.** (1990). Sexual reproduction, life history, and early development in culture of the Antarctic brown alga *Himantothallus grandifolius* (Desmarestiales, Phaeophyceae)*. *Phycologia* 29, 9–18.
- Williamson, R. E.** (1990). Alignment of Cortical Microtubules by Anisotropic Wall Stresses. *Funct. Plant Biol.* 17, 601–613.
- Willmore, K. E.** (2012). The Body Plan Concept and Its Centrality in Evo-Devo. *Evol. Educ. Outreach* 5, 219–230.
- Winnier, G., Blessing, M., Labosky, P. A., Hogan, B. L.** (1995). Bone morphogenetic protein-4 is required for mesoderm formation and patterning in the mouse. *Genes Dev.* 9, 2105–2116.
- Wolf, J. B. and Wade, M. J.** (2009). What are maternal effects (and what are they not)? *Philos. Trans. R. Soc. B Biol. Sci.* 364, 1107–1115.

- Woodger, J. H.** (1945). On Biological Transformations. In Essays on Growth and Form, presented to D'Arcy Wentworth Thompson. (ed. Le Gros Clark, W. E.) and Medawar, P.), pp. 95–120. Oxford: Oxford University Press.
- WoRMS Editorial Board** (2023). World Register of Marine Species. Available from <https://www.marinespecies.org> at VLIZ. Accessed 2023-11-04.
- Xu, P.-F., Houssin, N., Ferri-Lagneau, K. F., Thisse, B., Thisse, C.** (2014). Construction of a vertebrate embryo from two opposing morphogen gradients. *Science* 344, 87–89.
- Xu, Y. and Huang, S.** (2020). Control of the Actin Cytoskeleton Within Apical and Subapical Regions of Pollen Tubes. *Front. Cell Dev. Biol.* 8, 614821.
- Yamada, A., Martindale, M. Q., Fukui, A., Tochinal, S.** (2010). Highly conserved functions of the Brachyury gene on morphogenetic movements: insight from the early-diverging phylum Ctenophora. *Dev. Biol.* 339, 212–222.
- Yamamoto, M., Tantikanjana, T., Nishio, T., Nasrallah, M. E., Nasrallah, J. B.** (2014). Site-Specific N-Glycosylation of the S-Locus Receptor Kinase and Its Role in the Self-Incompatibility Response of the Brassicaceae. *Plant Cell* 26, 4749–4762.
- Ye, N., Zhang, X., Miao, M., Fan, X., Zheng, Y., Xu, D., Wang, J., Zhou, L., Wang, D., Gao, Y., et al.** (2015). *Saccharina* genomes provide novel insight into kelp biology. *Nat. Commun.* 6, 6986.
- Yendo, K.** (1911). The development of costaria, undaria, and laminaria with plates lih-lv. *Ann. Bot.* os-25, 691–716.
- Yonamine, R., Ichihara, K., Tsuyuzaki, S., Hervé, C., Motomura, T., Nagasato, C.** (2021). Changes in Cell Wall Structure During Rhizoid Formation of *Silvetia babingtonii* (Fucales, Phaeophyceae) Zygotes. *J. Phycol.* 57, 1356–1367.
- Yoon, H. S., Hackett, J. D., Ciniglia, C., Pinto, G., Bhattacharya, D.** (2004). A molecular timeline for the origin of photosynthetic eukaryotes. *Mol. Biol. Evol.* 21, 809–818.
- Yoshida, S., Barbier de Reuille, P., Lane, B., Bassel, G. W., Prusinkiewicz, P., Smith, R. S., Weijers, D.** (2014). Genetic control of plant development by overriding a geometric division rule. *Dev. Cell* 29, 75–87.
- Zhang, J., Wang, X., Yao, J., Li, Q., Liu, F., Yotsukura, N., Krupnova, T. N., Duan, D.** (2017). Effect of domestication on the genetic diversity and structure of *Saccharina japonica* populations in China. *Sci. Rep.* 7, 42158.
- Zhang, J., Wu, W., Ren, J., Lin, F.** (2016). A model for the growth of mariculture kelp *Saccharina japonica* in Sanggou Bay, China. *Aquac. Environ. Interact.* 8, .
- Zhang, J., Liu, T., Feng, R., Liu, C., Chi, S.** (2015). Genetic Map Construction and Quantitative Trait Locus (QTL) Detection of Six Economic Traits Using an F2 Population of the Hybrid from *Saccharina longissima* and *Saccharina japonica*. *PLoS One* 10, e0128588.
- Zhang, M., Wu, H., Su, J., Wang, H., Zhu, Q., Liu, Y., Xu, J., Lukowitz, W. and Zhang, S.** (2017). Maternal control of embryogenesis by MPK6 and its upstream MKK4/MKK5 in Arabidopsis. *Plant J.* 92, 1005–1019.
- Zhang, X., Wang, K., Hu, J., Zhang, Y., Dai, Y. and Xia, F.** (2020). Role of a high calcium ion content in extending the properties of alginate dual-crosslinked hydrogels. *J. Mater. Chem. A* 8, 25390–25401.
- Zhao, P., Zhou, X., Shen, K., Liu, Z., Cheng, T., Liu, D., Cheng, Y., Peng, X. and Sun, M.-X.** (2019). Two-Step Maternal-to-Zygotic Transition with Two-Phase Parental Genome Contributions. *Dev. Cell* 49, 882–893.e5.

8 - Annexes

Annexe 1: Targeted Laser Ablation in the Embryo of *Saccharina latissima*

[JOVE Movie](#): Targeted Laser Ablation in the Embryo of *Saccharina latissima*.

[Table of Material](#)

Targeted Laser Ablation in the Embryo of *Saccharina latissima*

Samuel Boscq¹, Stéphanie Dutertre², Ioannis Theodorou¹, Bénédicte Charrier¹

¹UMR8227, CNRS / Sorbonne University ²Univ Rennes, CNRS, Inserm, Biosit UAR 3480 US_S 018, MRic Core Facility

Corresponding Authors

Samuel Boscq

samuel.boscq@sb-roscoff.fr

Bénédicte Charrier

benedicte.charrier@sb-roscoff.fr

Citation

Boscq, S., Dutertre, S., Theodorou, I., Charrier, B. Targeted Laser Ablation in the Embryo of *Saccharina latissima*. *J. Vis. Exp.* (181), e63518, doi:10.3791/63518 (2022).

Date Published

March 11, 2022

DOI

10.3791/63518

URL

jove.com/video/63518

Introduction

Laser ablation has been used for decades to study embryo development. Irradiating embryo cells with a laser beam makes it possible to monitor the regenerative potential and the modification of the cell lineage during embryogenesis and investigate the impact of targeted ablation on cell division and cell fate. The model organisms used in laser ablation methods are typically animals, such as insects^{1,2}, nematodes^{3,4}, vertebrates^{5,6}, and occasionally plants^{7,8}. In addition, a laser micro-ablation approach was used on the brown alga

Fucus in 1994 and 1998 to demonstrate the role of the cell wall in the photopolarization of the early embryo^{9,10}.

Brown algae belong to the group Stramenopiles, diverged at the root of the eukaryotic tree 1.6 billion years ago. As a result, they are phylogenetically independent of other multicellular organisms, such as animals and plants¹¹. *Saccharina latissima* belongs to the order Laminariales, more commonly known as kelps, and they are among the largest organisms on earth, reaching sizes of over 30 m. *Saccharina*

Abstract

In *Saccharina latissima*, the embryo develops as a monolayered cell sheet called the lamina or the blade. Each embryo cell is easy to observe, readily distinguishable from its neighbors, and can be individually targeted. For decades, laser ablation has been used to study embryo development. Here, a protocol for cell-specific laser ablation was developed for early embryos of the brown alga *S. latissima*. The presented work includes: (1) the preparation of *Saccharina* embryos, with a description of the critical parameters, including culture conditions, (2) the laser ablation settings, and (3) the monitoring of the subsequent growth of the irradiated embryo using time-lapse microscopy. In addition, details are provided on the optimal conditions for transporting the embryos from the imaging platform back to the lab, which can profoundly affect subsequent embryo development. Algae belonging to the order Laminariales display embryogenesis patterns similar to *Saccharina*; this protocol can thus be easily transferred to other species in this taxon.

sp. is a large seaweed used for many applications such as food and feed, and its polysaccharides are extracted for use in the agricultural, pharmacological and cosmetic industries worldwide^{12,13}. Its cultivation, mainly in Asia and more recently in Europe, requires the preparation of embryos in hatcheries before releasing juveniles in the open sea. Like all kelps, it has a biphasic life cycle composed of a microscopic gametophytic phase, during which a haploid gametophyte grows and produces gametes for fertilization, and a diploid macroscopic sporophytic phase, where a large planar blade develops from its holdfast attached to the seafloor or rocks. The sporophyte releases haploid spores at maturity, thereby completing the life cycle^{14,15,16}.

S. latissima presents some interesting morphological features¹⁷. Its embryo develops as a monolayered planar sheet^{15,18,19} before acquiring a multilayered structure coinciding with the emergence of different tissue types. In addition, Laminariales is one of the only taxa of brown algae whose embryos remain attached to their maternal gametophytic tissue (Desmarestiales and Sporochnales do too¹⁵). This feature offers the opportunity to study the role of maternal tissue in this developmental process and compare maternal control mechanisms in brown algae with those in animals and plants.

This article presents the first complete protocol for laser ablation in an early kelp embryo. This protocol involving UV ns-pulsed technique results in the specific destruction of individual embryo cells to study their respective roles during embryogenesis. The procedure offers a reliable approach for investigating cell interactions and cell fate during embryogenesis in Laminariales.

Protocol

1. Production of *Saccharina latissima* gametophytes

1. Collect mature sporophytes of *S. latissima* from the wild as previously described^{20,21}. Ensure that the selected sporophytes are devoid of epiphytes (small organisms visible on the blade's surface) or internal parasites (found in the bleached areas or spots on the blade).
 2. Using a scalpel, cut the darkest part in the center of the blade (fertile spore-producing tissue²²) into 1-5 square pieces (1 cm²), avoiding any bleached spots, if present.
 3. Remove any remaining epiphytes by gently cleaning the cut pieces with the back of a scalpel and some absorbent paper.
 4. Place the cleaned pieces in a glass dish filled with sterile natural seawater (see **Table of Materials**) for 45 min to release spores following previously published report²².
 5. Remove the blade pieces and filter the seawater through a 40 μm cell strainer to remove debris or unwanted organisms.
 6. Dilute the spores in the filtrate to a 20-40 spores/mL concentration in plastic Petri dishes²².
 7. Place the spore solution in a culture cabinet (see **Table of Materials**) configured with the optimal culture conditions (13 °C, 24 μE.m⁻².s⁻¹, photoperiod 16:8 L:D).
 8. Allow the spores to germinate and develop into gametophytes.
- NOTE:** Spore germination is visible after 2 days in the cabinet, and the first cell division of the gametophytic cells usually occurs within the following 48 h.

- Replace the growth medium after 5 days with micro-filtered natural seawater enriched with a 0.5x Provasoli solution (NSW1/2) (see **Table of Materials**).

NOTE: To avoid repeating these steps, specific male and female gametophytes can be selected and vegetatively propagated for several months. The gametophytes remain vegetative when grown under red light ($4 \mu\text{E}\cdot\text{m}^{-2}\cdot\text{s}^{-1}$ with a wavelength of at least 580 nm)²³ in the same culture conditions described above (step 1.7).

2. Fragmentation and induction of oogenesis

- Harvest gametophytes with a cell scraper.
- Using a small plastic pestle, crush the collected gametophytes in a 1.5 mL tube into 4-5-celled pieces.
- Fill the tube with 1 mL NSW1/2 (step 1.9).
- Add 2.5 μL of the crushed gametophyte solution into 3 mL of natural seawater enriched with 1x Provasoli solution (NSW) and place them in a Petri dish.

NOTE: A 25 mm, glass-bottomed Petri dish is recommended for easier handling.

- Place the prepared dishes in a culture cabinet and induce gametogenesis at 13 °C under white light with an intensity of $24 \mu\text{E}\cdot\text{m}^{-2}\cdot\text{s}^{-1}$ (dim light, photoperiod 16:8 L:D).

NOTE: The first gametangia (female oogonia and male archegonia) can be observed after 5 days. The male is hyper-branched with small cells, and the female is composed of larger cells forming long filaments^{15,22}. The first eggs are observed ~10 days later, and the first division of zygotes usually occurs within the following 2 days.

- Six days after observing the first eggs, transfer the dishes to brighter white light conditions: $50 \mu\text{E}\cdot\text{m}^{-2}\cdot\text{s}^{-1}$, photoperiod 16:8 L:D, still at 13 °C.

3. Image acquisition for selecting embryos for ablation and monitoring subsequent growth

- Image the entire Petri dish to (re)locate the embryos selected during the ablation step (no need to return the dish to the ocular microscope) and monitor the subsequent development of the selected embryos.

NOTE: Use an inverted laser scanning confocal microscope (see **Table of Materials**) for imaging (**Figure 1**), and the laser ablation is described in step 5.

- Place the Petri dish on the stage and orientate it with a visual mark (e.g., draw a line with a permanent marker).
- Use the 10x/0.45 objective to focus on an embryo. Record the position of the four cardinal points of the Petri dish.
- Start the tile scan. Acquire transmitted/fluorescent images of the whole Petri dish at low resolution: 256 x 256 pixels, a pixel dwell time of 1.54 μs with bidirectional scanning, and a digital zoom of 0.6x using a 561 nm laser at 1.2% transmission.

NOTE: The scan time for a whole 2.5 cm Petri dish is ~6 min for 225 tiles (**Figure 2**). Here, the 561 nm laser was used for transmission and fluorescence imaging. The fluorescence signal was collected between 580–720 nm on the confocal photomultipliers (PMT) and the transmitted light was collected on the transmitted PMT. The 561 nm laser can also monitor chlorophyll at this step, but it is unnecessary because it only helps distinguish the signal noise and the organisms correctly.

5. Save the tile scan image and keep it open in the image acquisition software (see **Table of Materials**) window.
6. Change the objective, do not remove the Petri dish.
NOTE: The 40x/1.2 water objective was moved to the side of the stage so that the immersion medium (water) could be added to the objective without moving the Petri dish from its initial position.
7. Navigate through the previously acquired tile scan image to select the appropriate embryo. Once an embryo has been identified on this image, move the stage to the exact position of the embryo and acquire transmitted/fluorescent images of that embryo at high resolution.
NOTE: High-resolution settings: 512 x 512 pixels, 0.130 $\mu\text{m}/\text{pixel}$, 0.208 μs pixel dwell time with mono-directional scanning and 2x digital zoom using a 561 nm laser at 0.9% transmission.
8. Annotate the tile scan image for each embryo candidate for laser ablation (**Figure 2B**) and proceed to the laser ablation step.

4. Laser calibration

1. Calibrate the laser and synchronize the image acquisition software with the laser-driver software in the "Click & Fire mode" and a pulsed 355 nm laser.
NOTE: This step is crucial to ensure perfect synchronization between the mouse cursor's position in the laser-driver software (see **Table of Materials**) with the position in the live image of the acquisition software.
2. Open the laser-driver software package and click on **Live** in the image acquisition software package.
3. Synchronize both software packages by clicking on **Start acquisition** in the laser-driver software package. The

live image is now also recorded in the UV laser-driver software.

4. Define an area of interest (AOI) by clicking on **Choose AOI** button and clicking on the edges of the image (right, left, top and bottom) in the UV laser-driver software package.
NOTE: After this calibration step, the settings for pixel size, image format, and zoom in the acquisition software package must remain constant.
5. Select an empty area on the dish and lower the level of the stage to 20 μm below the sample focal plane to focus on the glass bottom.
6. Set the ablation laser and imaging laser trajectories by clicking on **Start calibration** and choose **Manual calibration**.
7. Select a laser power high enough to see a black dot in the center of the live image corresponding to the hole in the glass coverslip (all the shutters must be open).
8. Click on this central black dot with the mouse cursor and click on **18 additional dots** proposed by the software to complete the alignment procedure.
9. Check the calibration in the "Click & Fire mode" on the same coverslip.
NOTE: Laser calibration depends on the imaging parameters. Once the laser has been calibrated, ensure that the imaging parameters (i.e., 512 x 512 pixels, 0.130 $\mu\text{m}/\text{pixel}$, 0.208 μs pixel dwell time with mono-directional scanning and 2x digital zoom) have not changed.

5. Laser ablation

1. Select an embryo of interest. Start a time-lapse recording in the image-acquisition software.

2. Acquire transmitted/fluorescence images with a 40x/1.2 W objective at high resolution (i.e., 512 x 512 pixels, 0.130 $\mu\text{m}/\text{pixel}$, 1.54 μs pixel dwell time with mono-directional scanning and 2x digital zoom using a 561 nm laser at 0.9% transmission). Acquire the time-lapse recording at maximum speed.
3. Zoom out of the area at the beginning of the time-lapse recording. Zoom in on the AOI.
4. Use the "Click & Fire" function of the laser-driver software to apply the damaging irradiation on the cell of interest in the embryo. Use the following parameters: 45% laser transmission (corresponding to a maximum of 40 μW) and 1 ms pulse time duration (step 4).
NOTE: Video recording during the laser shooting is recommended.
5. Under 688 nm, monitor the ejection of autofluorescent chloroplasts from the cytoplasm.
6. If cell contents remain in the cell, use the "Click & Fire" function once more to increase the size of the breach in the cell. Repeat, keeping the number of shots to a minimum until most of the cell contents have been released.
7. Stop the time-lapse recording after the embryo has stabilized (i.e., no further intracellular movement can be detected (~1-5 min)).
8. Update the annotation on the tile scan image, if necessary.

6. Monitoring the growth of irradiated embryos

NOTE: Monitoring is carried out over several days.

1. Determine the survival rate by monitoring the number of embryos that develop after laser ablation and compare them to those that die.
NOTE: Some embryos die immediately after ablation for various reasons. A high and rapid mortality rate is usually a sign of inappropriate laser parameters or higher/longer exposure to stress during the experiment or subsequent transport.
2. Determine the growth delay by measuring the length of the laser-shot embryos every day and comparing it to intact embryos.
NOTE: The growth rate of laser-shot organisms is generally slower than that of untreated organisms. However, some (inappropriate) laser settings can inhibit growth for more than a week, with growth resuming after that.
3. Find out the adjacent damage by monitoring the reaction of cells adjacent to the ablated cells. In some cases, post-burst depressurization may cause neighboring cells to burst.
4. Check for microbe contaminations. Monitor the growth of microalgae and bacteria in the medium. If an unusual level of microbes are present in the dish, then discard it and repeat the protocol from step 2 or step 3.
NOTE: After laser ablation, damaged *S. latissima* embryos are already highly stressed, and additional external stress can cause increased mortality. Bacterial or viral outbreaks are possible because the treated embryos cannot grow in axenic conditions.
5. Check the global development of the shot organisms by studying the phenotype and understanding the role in the development of the targeted region.

Representative Results

Gametophytes of *S. latissima* were grown, and gametogenesis was induced to produce zygotes and embryos. Twelve days after the induction of gametogenesis, the embryos underwent laser ablation. Here, the experiment aimed to assess the role of specific cells in the overall development of *S. latissima* embryos. The most apical cell, the most basal cell, and the median cells were targeted. After tile scanning, the entire Petri dish (**Figure 2A**), an embryo of interest, was identified as a suitable candidate for laser shooting (**Figure 2B**). A specific cell of this embryo was chosen, targeted, and shot with a pulsed UV laser beam with a maximum of 40 μW of laser power (corresponding to 45% of maximum power for the equipment used here) for 1 ms (**Movie 1**). The cell released its contents (chloroplasts

and cytoplasm). Interestingly, adjacent cells responded to the bursting of the irradiated cell by expanding into the intercellular space. The position of the irradiated embryos was recorded for subsequent monitoring over 10 days (**Figure 3**). Most of the irradiated embryos continued to develop but showed growth alteration (embryo shape). A detailed analysis of the morphological changes needs to be undertaken before a specific function can be attributed to each irradiated cell in controlling the overall developmental mechanism.

In contrast, embryos tested with other laser parameters (e.g., 33 ms for the shooting duration of 60%-80% laser power; **Movie 2**) quickly showed signs of severe stress such as cell bleaching, fading, or shape changes (rounding). Almost all embryos shot in this way died within five days after the experiment (**Figure 4**).

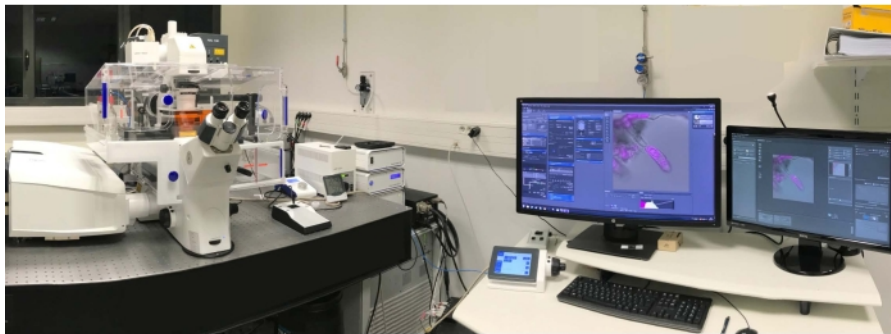


Figure 1: Photograph of the laser ablation microscope set-up. [Please click here to view a larger version of this figure.](#)

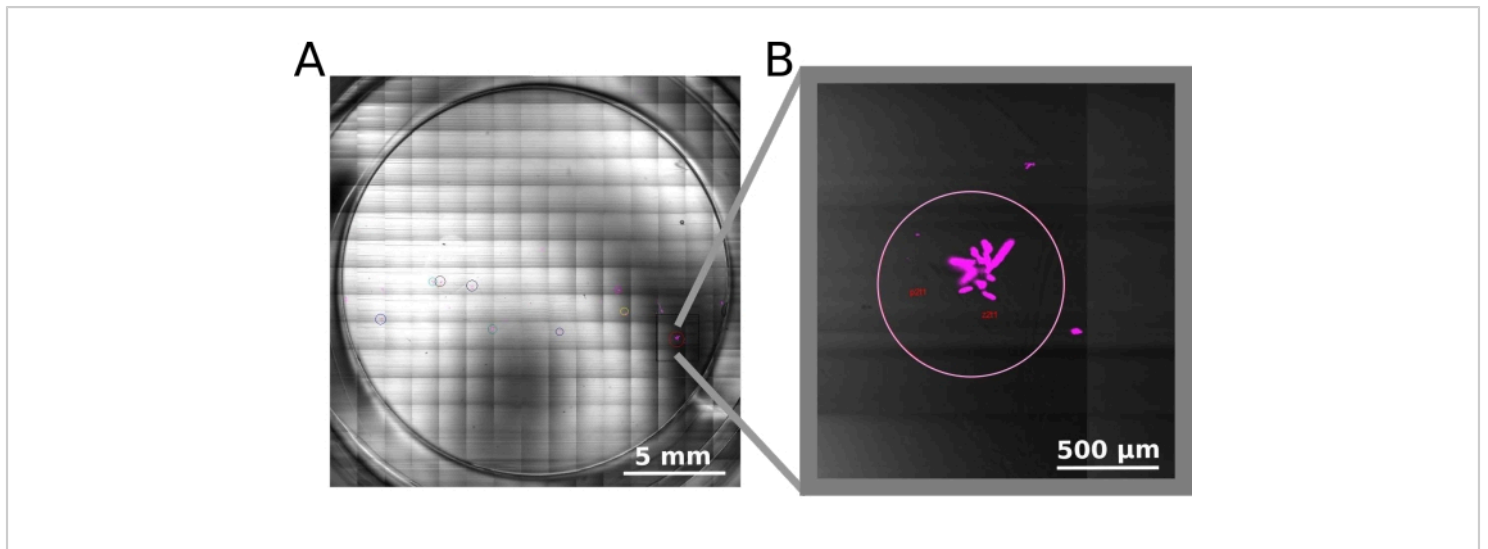


Figure 2: Annotated tile scan of a whole Petri dish. (A) Tile scan of the entire Petri dish used for laser ablation. The transmission PMT was used to obtain a brightfield scan. Once an embryo of interest has been located, the user clicks on the embryo's position in the tile scan, and the software positions the stage directly over the embryo. **(B)** The tile scan can then be annotated specifically to locate the embryo in the subsequent steps, to track and monitor the embryo. Here, the image shows an embryo attached to the bottom of the Petri dish, which can be easily located using the 561 nm laser. [Please click here to view a larger version of this figure.](#)

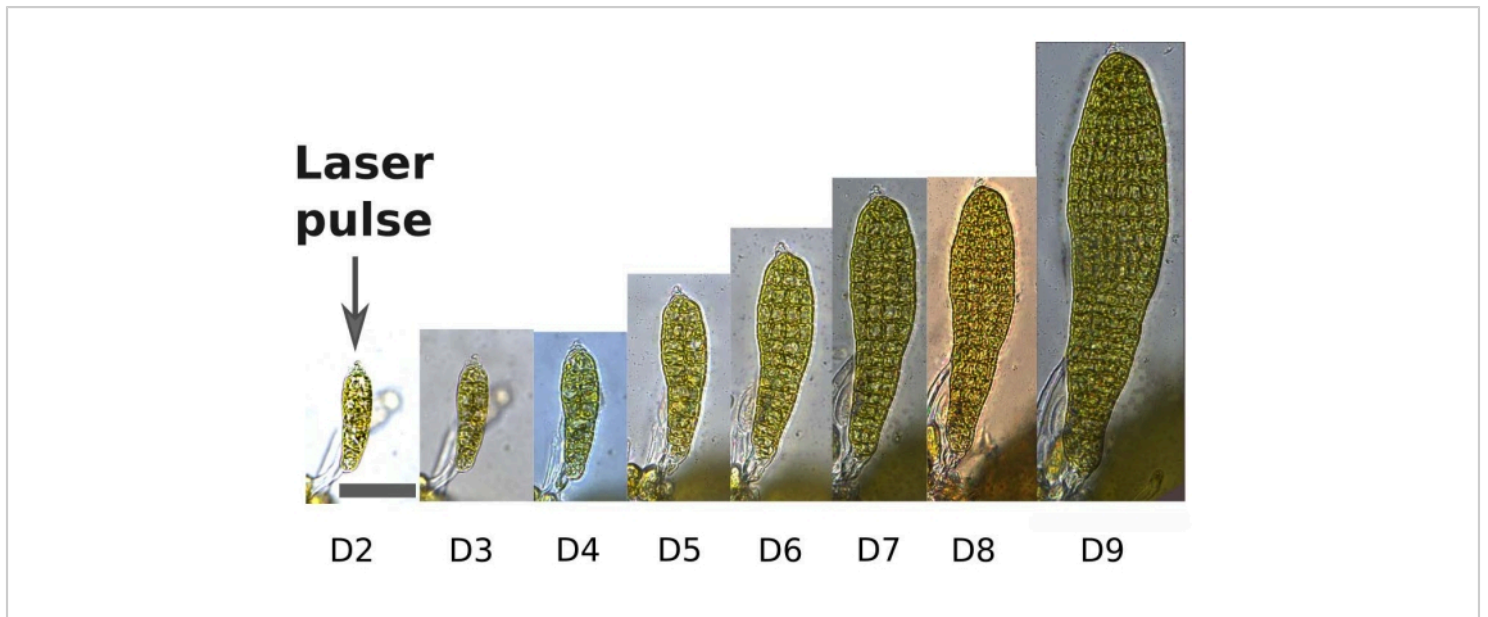


Figure 3: Time series of the growing *S. latissima* embryo after irradiation. This is shown in Movie 1. Laser ablation of the most apical cell of the embryo did not bleach the adjacent cells of the embryo. They continued to grow and divide, forming a normal embryo after a few days. Images were taken every 24 h, 2-9 days after ablation. The scale bar is 50 μm and is the same for all photos. D2-D9 corresponds to day-2 to day-9. [Please click here to view a larger version of this figure.](#)

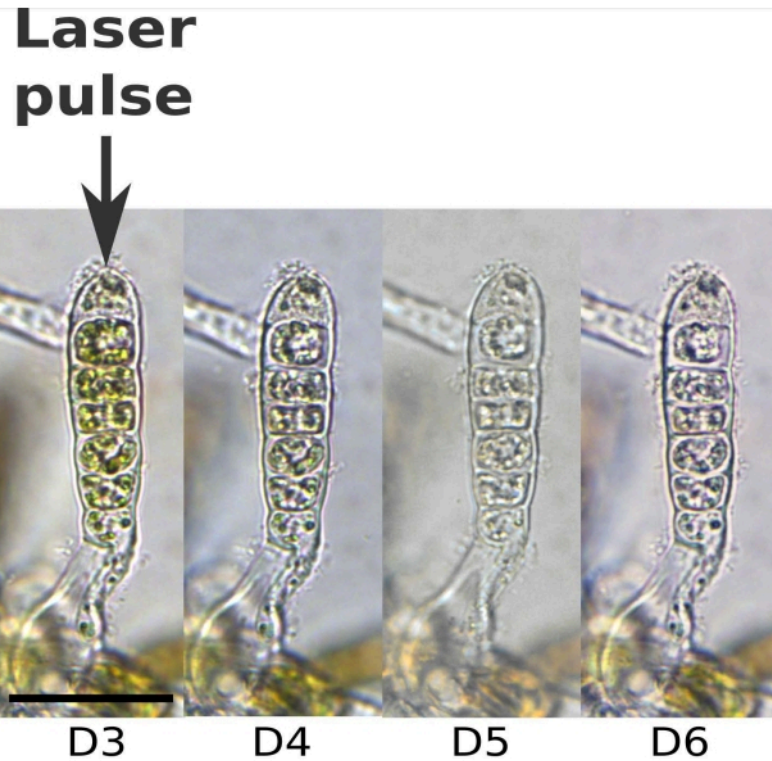


Figure 4: Time series of *S. latissima* embryo death after laser ablation using suboptimal parameters. Overexposure to laser irradiation can easily lead to higher death rates of the target embryo and also the neighboring ones. A time series of the embryo shot in Movie 2 is shown, with the time after ablation indicated above each photo (3-6 days after ablation). Scale bar is 30 μm and applies to each photo. [Please click here to view a larger version of this figure.](#)

Movie 1: Laser ablation of the most apical cell of an 8-celled embryo of *S. latissima*. The focus was first adjusted on the embryo selected among a bouquet of *Saccharina* sporophytes (at different fields, first wide, then narrow). The most apical cell of the embryo was then shot using 45% laser power for 1 ms. The apical cell rapidly burst and released its contents. The adjacent cells, freed from the turgor of the burst cell, filled the empty space. After 5 min, the cell and its contents have stopped moving and have reached a state of equilibrium. The movie has been accelerated 4 times (from 1 image per 632 ms to 6 fps). The follow-up of

embryo development is shown in **Figure 3**. [Please click here to download this Movie.](#)

Movie 2: Significant bleaching of cells adjacent to a burst cell caused by suboptimal laser settings. Using a laser power of 60%-80% for 1 ms or a laser power of 45% for 10 ms resulted in significant bleaching of adjacent cells and a much lower survival rate. The settings used for the laser should not cause bleaching or partial damage to adjacent cells. Best results were obtained by reducing the power and/or duration of the laser pulse, and targeting the point furthest from the adjacent cells. Here, the most apical cell of a 4-celled embryo

of *S. latissima* isshot (80% laser power, 1 ms) (lateral/top view). Overbleaching of the lower and lateral cells is readily observable. The subsequent development of the embryo is shown in **Figure 4**. [Please click here to download this Movie.](#)

Supplementary Figure 1: Schematic flowchart of the entire protocol. [Please click here to download this File.](#)

Discussion

Local cellular laser ablation allows for temporal and spatial ablation with a high level of precision. However, its efficiency can be hampered by the non-accessibility of target cells; for example, all the cells are of a three-dimensional embryo. This protocol was developed on the embryo of the alga *Saccharina latissima*, which develops a monolayered lamina in which all cells can be easily distinguished and destroyed individually with a laser beam.

Laser power and wavelength

NIR fs-pulsed laser is commonly used in developmental studies on animals^{24,25}. However, in the case of brown algae such as *Saccharina*, the laser could not burst the cell without burning the whole embryo. This reaction may be related to the high activity of the chloroplast light harvesters.

Using the ns-pulsed UV laser for ablation, two approaches were tested: (1) using a high power pulse over a short period of time or (2) using a lower laser exposure over a longer period of time. The energy delivered by the laser, a combination of laser power and pulse duration, impacts the energy delivered to the irradiated cell. The delivered energy can also affect the surrounding cells by reflection and diffraction. Therefore, the lowest settings of the two parameters that gave reproducible results were selected to reduce any unwanted collateral effects. Laser power between 25-40 $\mu\text{W}\cdot\text{cm}^{-2}$ with a pulse of 1 ms appeared to be optimal. Using these parameters,

the effect of the UV laser was contained at a very local level with no visible bleaching in the surrounding cells but efficient enough to cause the target cell to burst. These parameters were repeatedly applied without any direct lethal effect on the embryos. Longer pulse times or higher laser power caused bleaching of the surrounding cells or even death of the embryo, whereas lower values were insufficient to break the cell wall.

Algal material and culture conditions

Although allowing for precise shooting at the subcellular level, this technique requires the experimenter to address four critical factors to allow reliable interpretation of the results. These points must be considered both before and after the laser ablation experiment.

The first factor to address is embryo population density. Negative crowding impacts the development rate of *S. latissima*²⁶. Low densities provide for (1) better pulse repeatability because the presence of other embryos in the laser path can decrease its power, and (2) easier monitoring of the embryos shot by the laser, which grow slightly slower than intact embryos; the latter quickly covering the shot embryos. The second critical factor of this protocol is the temperature at which the experiment is carried out. The laser beam itself heats the sample, but the temperature of the room and the local environment of the microscope add to the overall temperature conditions experienced by the sample, close to 18-22 °C. Here, the microscope's room was not refrigerated because this equipment is mainly used for animal cells that tolerate ambient temperatures. Fortunately, *Saccharina* embryos were able to withstand temperatures of 22 °C (9 °C higher than the optimal culture temperature of 13 °C) for up to 4 h. However, devices to help maintain a low ambient temperature, such as adequate ventilation or a cooling plate

holder, can help mitigate the risk of adverse effects on the survival and development of the algal embryos. Furthermore, slow pre-acclimation of gametophytes to 16 °C under red light can help the embryos withstand temperature spikes during the ablation process. Third, in addition to the increase in temperature, the embryos are deprived of a suitable light source for the duration of the experiment. Moreover, the chloroplasts may be partially bleached by the 561 nm laser. Using the lowest possible power on the 561 nm laser helps reduce this effect. Fourth, transport is also a critical factor to take into account because laser ablation equipment is not available in all laboratories. Temperature spikes and external movements or shocks should be avoided to prevent the algal material's dislodgement, loss, or death. Whenever possible, the transport boxes need to be refrigerated, vibration-resistant (e.g., shock-absorbing foam), and equipped with lights. Several transport boxes that meet these requirements are available commercially.

Even if all these factors are controlled as much as possible, weak but potentially significant environmental stress may still occur. This possibility must be considered in analyzing and interpreting the embryo response to laser ablation.

In addition to the environmental conditions that must be kept stable throughout the experiment, keeping track of the irradiated organisms throughout the monitoring step is also a challenge. The growth of the different embryos changes the original landscape over time. Unless an automated microscope can be dedicated to monitoring the experiment, following the embryo after laser ablation can easily become time-consuming and generate large amounts of data. Video recordings during the initial laser ablation pulse are highly recommended to track the embryo's immediate reaction to the pulse. This rapid monitoring of the pulse impact is of

significant importance because in some instances, the pulse, when targeted to the middle of the cell, caused the target cell to burst rapidly, most likely due to the difference of osmolarity between the interior of the cell and the medium (seawater). When the leakage was too fast, the neighboring cells also burst. Shooting at the most distal region of the targeted cell proved to be an efficient way of buffering the burst effect on any adjacent cells. Another efficient way to avoid violent bursts is to increase the osmolarity of the medium with sucrose²⁷. However, the difference in osmolarity is necessary to eliminate the targeted cell's contents. Thus, maintaining sufficient osmolarity potential is required. In a few cases, chloroplasts and other compounds obstructed the opening made by the laser ablation, which resulted in cells recovering from the laser shot, with growth resuming after a few days. Additional pulses directed at unclogging the opening proved sufficient to prevent obstruction.

Limitations

A trade-off must be struck between laser power, which should be high enough to make the cells empty their contents, and the survival of the neighboring cells, which in algal embryos are particularly sensitive to heat stress and photobleaching. Therefore, close monitoring of the cells after the laser shot is the key to controlling this step and ensuring that the target cells are dead. Otherwise, the interpretation of the targeted cells on the fate of the neighboring cells, and thus the subsequent development of the embryo, can be misleading.

Puncturing cells with a needle may seem to be an alternative in which the algal cells would not experience any heat or light stress. However, this approach would be challenging because brown algal embryo cells grow immersed in seawater and have no contact with any solid surface. The thick and elastic cell wall resists needle penetration even

when maintaining the embryo in contact with a solid, glass surface using a micromanipulator in a standard microinjection system.

In summary, this protocol describes the complete experimental procedure and settings for the laser ablation and monitoring of brown algal embryos and the critical steps for a successful experiment (**Supplementary Figure 1**). This unique approach is a promising method for studying cell interactions and cell fate in the early embryos of brown algae.

Disclosures

The authors have nothing to disclose.

Acknowledgments

S.B.'s PhD grant is funded by Region Bretagne (ARED grant Number COH20020) and Sorbonne Université. I.T.'s PhD grant is funded by Region Bretagne (ARED grant Number COH18020) and the Norwegian NMBU University. This project has received financial support from the CNRS through the MITI interdisciplinary programs. MRic is member of the national infrastructure France-BioImaging supported by the French National Research Agency (ANR-10-INBS-04).

References

1. Montell, D. J., Keshishian, H., Spradling, A. C. Laser ablation studies of the role of the *Drosophila* oocyte nucleus in pattern formation. *Science (New York, N.Y.)*. **254** (5029), 290-293 (1991).
2. Shivakumar, P. C, Lenne, P. F. Laser ablation to probe the epithelial mechanics in *drosophila*. *Methods In Molecular Biology*. **1478**, 241-251 (2016).
3. Bargmann, C. I., Avery, L. Laser killing of cells in *Caenorhabditis elegans*. *Modern Biological Analysis of an Organism*. **48**, 225-250 (1995).
4. Fouad, A. D., Liu, A., Du, A., Bhirgoo, P. D., Fang-Yen, C. Thermal laser ablation with tunable lesion size reveals multiple origins of seizure-like convulsions in *Caenorhabditis elegans*. *Scientific Reports*. **11** (1), 5084 (2021).
5. Johnson, C. S., Holzemer, N. F., Wingert, R. A. Laser ablation of the zebrafish pronephros to study renal epithelial regeneration. *Journal of Visualized Experiments*. **54**, e2845 (2011).
6. Mondia, J. P., Adams, D. S., Orendorff, R. D., Levin, M., Omenetto, F. G. Patterned femtosecond-laser ablation of *Xenopus laevis* melanocytes for studies of cell migration, wound repair, and developmental processes. *Biomedical Optics Express*. **2** (8), 2383-2391 (2011).
7. Reinhardt, D., Frenz, M., Mandel, T., Kuhlemeier, C. Microsurgical and laser ablation analysis of leaf positioning and dorsoventral patterning in tomato. *Development*. **132** (1), 15-26 (2005).
8. Berg, C. ; Hage, W.; Weisbeek, P.; Scheres, B. Laser ablation in *Arabidopsis* roots: a tool to study cell-to-cell communication. Cellular integration of signalling pathways in plant development. *Proceedings of the NATO Advanced Study Institute*. 237-250 (1998).
9. Berger, F., Taylor, A., Brownlee, C. Cell fate determination by the cell wall in early fucus development. *Science (New York, N.Y.)*. **263** (5152), 1421-1423 (1994).
10. Bouget, F. Y., Berger, F., Brownlee, C. Position dependent control of cell fate in the *Fucus* embryo: role

- of intercellular communication. *Development*. **125** (11), 1999-2008 (1998).
11. Bringloe, T. et al. Phylogeny and evolution of the brown algae. *Critical Reviews in Plant Sciences*. **39**(4), 281-321 (2020).
 12. Saifullah, S., Olsen, Y., Surilayani, D., Handå, A. Carbohydrate of the brown seaweed, saccharina latissima: a review. *Joint proceedings of the 2nd and the 3rd International Conference on Food Security Innovation (ICFSI 2018-2019)*. 180-182 (2021).
 13. Zhang, X., Thomsen, M. Techno-economic and environmental assessment of novel biorefinery designs for sequential extraction of high-value biomolecules from brown macroalgae *Laminaria digitata*, *Fucus vesiculosus*, and *Saccharina latissima*. *Algal Research*. **60**, 102499 (2021).
 14. Kanda, T. On the gametophytes of some Japanese species of laminariales. *Scientific papers of the Institute of Algological Research, Faculty of Science, Hokkaido Imperial University*. **1** (2), 221-260 (1936).
 15. Fritsch, F. E. *The structure and reproduction of the algae. Volume 2*. Cambridge University Press, Cambridge (1945).
 16. Bartsch, I. et al. The genus *Laminaria* sensu lato : recent insights and developments. *European Journal of Phycology*. **43** (1), 1-86 (2008).
 17. Theodorou, I., Charrier, B. Chapter 2: Brown algae: *ectocarpus* and *saccharina* as experimental models for developmental biology, In *Handbook of Marine Model Organisms in Experimental Biology - Established and Emerging*. (A. Boutet & B. Schierwater, eds). Francis & Taylor Group, CRC Press. ISBN 9780367444471, 485 pp. (2021).
 18. Drew, G. H. The reproduction and early development of *Laminaria digitata* and *Laminaria saccharina*. *Annals of Botany*. **os- 24** (1), 177-189 (1910).
 19. Yendo, K. The development of *Costaria*, *Undaria*, and *Laminaria*. *Annals of Botany*. **25** (99), 691-715 (1911).
 20. Forbord, S., Steinhovden, K., Rød, K., Handå, A., Skjermo, J. Cultivation protocol for *Saccharina latissima*. In *Protocols for Macroalgae Research*. (B. Charrier, T. Wichard & CRK Reddy, eds) CRC Press, Francis & Taylor Group. ISBN-10: 1498796427. ISBN-13: 978-1498796422, 37-59 (2018).
 21. Bartsch, I. Derivation of clonal stock cultures and hybridization of kelps. In *Protocols for Macroalgae Research*. (B. Charrier, T. Wichard & CRK Reddy, eds) CRC Press, Francis & Taylor Group. ISBN-10: 1498796427. ISBN-13: 978-1498796422, 61-78, (2018).
 22. Theodorou, I., Opsahl-Sorteberg, H.-G., Charrier, B. Preparation of zygotes and embryos of the kelp *saccharina latissima* for cell biology approaches. *Bio-protocol*. **101**, e4132 (2021).
 23. Lüning, K., Dring, M. J. Reproduction induced by blue light in female gametophytes of *Laminaria saccharina*. *Planta*. **104** (3), 252-256 (1972).
 24. de Medeiros, G. et al. Cell and tissue manipulation with ultrashort infrared laser pulses in light-sheet microscopy. *Scientific Reports*. **10** (1), 1942 (2020).
 25. Liang, X., Michael, M., Gomez, G. A. Measurement of mechanical tension at cell-cell junctions using two-photon laser ablation. *Bio-protocol*. **6** (24) e2068 (2016).
 26. Ebbing, A., Pierik, R., Bouma, T., Kromkamp, J. C., Timmermans, K. How light and biomass density influence the reproduction of delayed *Saccharina latissima*

gametophytes (Phaeophyceae). *Journal of Phycology*.

56 (3), 709-718 (2020).

27. Rabillé, H., Billoud, B., Tesson, B., Le Panse, S., Rolland, É., Charrier, B. The brown algal mode of tip growth: Keeping stress under control. *PLoS Biology*. **17** (1), e2005258 (2019).

Annexe 2: Growth and Labelling of Cell Wall Components of the Brown Alga Ectocarpus in Microfluidic Chips

[Supplementary Table 1: Growth of Ectocarpus in Microfluidic Chips](#)



Growth and Labelling of Cell Wall Components of the Brown Alga *Ectocarpus* in Microfluidic Chips

Bénédicte Charrier^{1*†}, Samuel Boscq¹, Bradley J. Nelson² and Nino F. Läubli^{2,3*†}

¹ Modeling and Morphogenesis of Macroalgae, UMR 8227, CNRS – Sorbonne University, Marine Biological Station, Roscoff, France, ² Multi-Scale Robotics Lab, ETH Zürich, Zurich, Switzerland, ³ Molecular Neuroscience Group, University of Cambridge, Cambridge, United Kingdom

OPEN ACCESS

Edited by:

Menghong Hu,
Shanghai Ocean University, China

Reviewed by:

Zhihua Feng,
Jiangsu Ocean University, China
Alejandra Moenne,
University of Santiago, Chile

*Correspondence:

Bénédicte Charrier
benedicte.charrier@sb-roscoff.fr
Nino F. Läubli
laeublin@ethz.ch

[†]These authors have contributed
equally to this work

Specialty section:

This article was submitted to
Marine Biology,
a section of the journal
Frontiers in Marine Science

Received: 22 July 2021

Accepted: 25 October 2021

Published: 15 November 2021

Citation:

Charrier B, Boscq S, Nelson BJ
and Läubli NF (2021) Growth
and Labelling of Cell Wall
Components of the Brown Alga
Ectocarpus in Microfluidic Chips.
Front. Mar. Sci. 8:745654.
doi: 10.3389/fmars.2021.745654

Polydimethylsiloxane (PDMS) chips have proven to be suitable environments for the growth of several filamentous organisms. However, depending on the specimen, the number of investigations concerning their growth and cell differentiation is limited. In this work, we monitored the developmental pattern of the brown alga *Ectocarpus* inside PDMS lab-on-chips. Two main methods of inoculation of the lab-on-chip were tested, i.e., *via* the direct injection of spores into the chamber as well as through the insertion of sporophyte filaments. The resulting growth rate, growth trajectory, cell differentiation, and cell branching were monitored and quantified for 20 days inside 25 or 40 μm parallel channels under standard light and temperature conditions. With growth rates of $2.8 \mu\text{m}\cdot\text{h}^{-1}$, normal growth trajectories and cell differentiation, as well as branching occurring inside the microfluidic environment, the main development steps were shown to be similar to those observed in non-constrained *in vitro* conditions. Additionally, the labelling of *Ectocarpus* cell wall polysaccharides using calcofluor for cellulose detection and immunolocalisation with monoclonal antibodies for alginates showed the expected patterns when compared to open space growth evaluated with either epifluorescence or confocal microscopy. Overall, this article describes the experimental conditions for observing and studying the basic unaltered processes of brown algal growth using microfluidic technology which provides the basis for future biochemical and biological researches.

Keywords: microfluidics, brown alga, tip growth, on-chip immunolocalisation, *Ectocarpus*, filaments, lab-on-chips

INTRODUCTION

Because of their highly polarised shape, filamentous organisms tend to raise many questions concerning their growth and differentiation, such as if their growth is restricted to the apical cell, which corresponds to a case of localised growth, or if it is shared by all the cells composing the filament as seen with diffuse growth patterns. Additionally, it is yet to be discovered how the complex intercellular transport of material and the correspondingly required communication in such polarised and uniaxial living structures occur. Furthermore, it is unclear what cues lead to the distribution of cell differentiations along such a linear tissue and how the repetition of all these functions is controlled when architectural complexity is increased through branching.

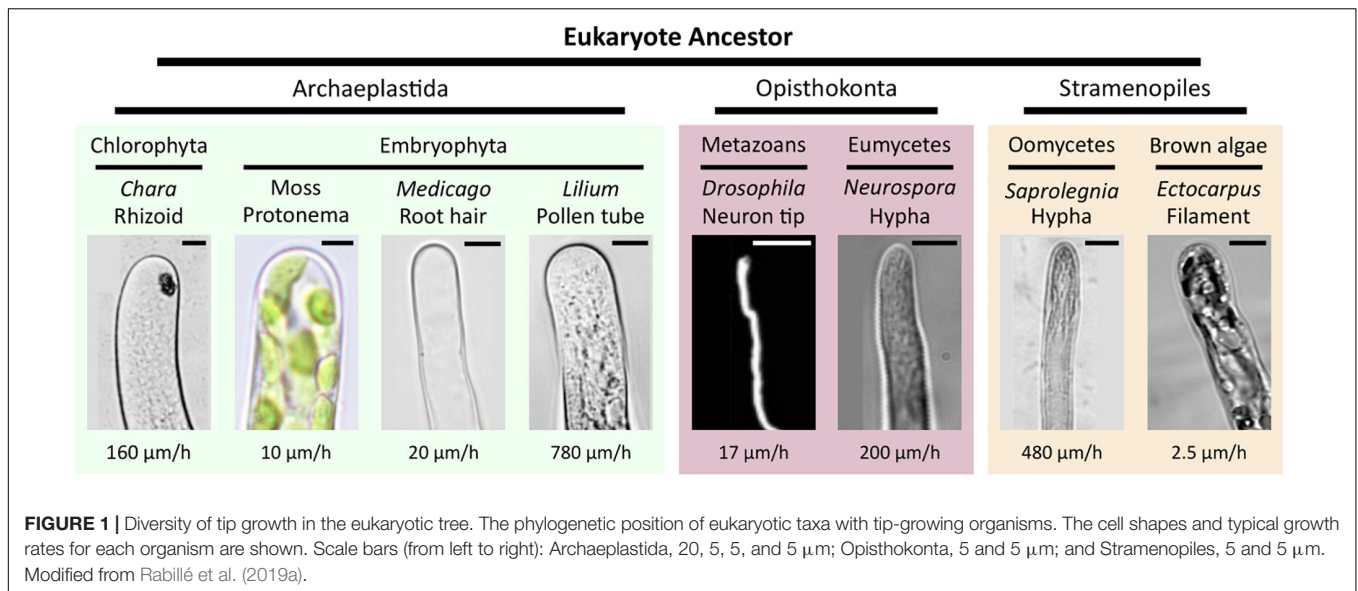
With advances in microtechnology driving the development of novel microelectromechanical systems (MEMS) and, consequently, the broader availability of corresponding fabrication facilities, the use of lab-on-chip devices has gained increasing interest in many research fields ranging from chemistry and biomedical engineering to biology (Azizpour et al., 2020; Bayareh et al., 2020; Pei et al., 2020; Zhu et al., 2020; Berlanda et al., 2021; Läubli et al., 2021a). As a subset of these technologies, microfluidic devices, i.e., structures containing fluid filled channels with dimensions in the μm to mm range, have been successfully established as a versatile tool that enables new avenues of research through the manipulation and handling of small organisms (Läubli et al., 2021b). In recent years, several pieces of work have relied on microfluidic technologies to study a wide range of organisms through the evolutionary tree including mammals and plants (Peyrin et al., 2011; Siddique and Thakor, 2013; Tong et al., 2015; Shamsudhin et al., 2016; Burri et al., 2018). The reasons for using microfluidic devices to study small specimens are numerous and reflect the need of investigations to spatially constrain these cultured materials, for example by limiting the height and width of the available environment in the chip path in order to simplify long-term monitoring and improve the resolution of microscopy-based observations (Shamsudhin et al., 2016; Kozgunova and Goshima, 2019; Zhou et al., 2021). It can also allow the separation of filaments which would otherwise grow too densely (Bascom et al., 2016) or guide them to grow perpendicular to a measuring device, such as a force sensor, positioned at the exit of the chip (Burri et al., 2018). Furthermore, depending on their design, constrained paths can also be utilised to evaluate the existence of directional memory of growing filaments (Held et al., 2011). Finally, in addition to the guidance of small organisms, microfluidic chips can be used for automated flows of controlled chemical compounds (Agudelo et al., 2013) as well as combined with microelectrodes to enable the generation of applied electrical pulses (Agudelo et al., 2016), both of which can be perceived as cues for the activation or repression of downstream signalling pathways in living specimens.

Nevertheless, the potential of microfluidic devices must first be evaluated for each biological model to avoid misinterpretations of subsequent results due to unidentified effects induced by the constraining environment. In the protonemata of the moss *Physcomitrium patens*, an initial study demonstrated that growth rate, cell differentiation, protoplast regeneration, and responses to drugs of specimens growing inside microchannels were all comparable to observations from samples under standard growth conditions (Bascom et al., 2016), thereby validating the use of polydimethylsiloxane (PDMS) chips for their study. However, the response to these conditions depends, to some extent, on the geometric parameters of the chip. The available height between the glass slide and the PDMS layer has been shown to impact certain cellular biological processes. When moss protonemata filaments with a diameter of $21 \mu\text{m}$ were constrained inside channels with a height of $4.5 \mu\text{m}$, their microtubule velocity was reduced while the viability and growth of the filaments were not impaired (Kozgunova and Goshima, 2019). On the other hand, growth in maze and grid PDMS meshworks was shown

to significantly impair both the growth rate and the branching pattern of the fungus *Neurospora crassa* (Held et al., 2011), although this effect was attributed to the design of the chip pathways rather than to the PDMS polymer which is generally known to be chemically compatible and non-toxic.

Here, we evaluated the ability of *Ectocarpus* sp. to grow within PDMS-based microfluidic devices and assessed the suitability of our approach for immunocytochemistry in the filamentous brown alga *Ectocarpus* sp. Brown algae (Phaeophyceae) are a class of photo-autotrophic organisms that evolved independently of animals and plants. The ancestor of this kingdom, Stramenopiles, diverged 1.6 billion years ago from the eukaryotic ancestor shared by the animal and plant lineages, i.e., the Opisthokonta and the Archaeplastida, respectively (Baldauf, 2003). Since the knowledge of the first genomic sequence of brown algae (Cock et al., 2010), metabolic, cellular, and developmental studies have confirmed their peculiar phylogenetic position, as they combine animal and plants characteristics (Bothwell et al., 2008; Cock et al., 2010; Michel et al., 2010; Popper et al., 2011; Bogaert et al., 2019; Rabillé et al., 2019a). While *Ectocarpus* was shown to grow on PDMS surfaces immersed in seawater (Evariste et al., 2012), we studied how its filaments cope with the restricted and constrained spatial environment provided by a microfluidic chip. We focused on the prostrate filament of the sporophyte because it grows immediately after mitospore or zygote germination. More importantly, this filament grows by tip growth, a mechanism that is shared by many organisms belonging to other phyla of the eukaryotic evolution tree, thereby, allowing macroevolutionary scale comparisons. In addition to the oomycetes belonging to the Stramenopiles like brown algae, tip growing cells include plant pollen tubes and plant root hairs, moss filaments (protonemata) and algal rhizoids of the Archaeplastida phylum, and fungal hyphae and neurons in the Opisthokonta phylum (Figure 1). Besides its different evolutionary history, *Ectocarpus* differs from other tip-growing organisms in many ways. Its sporophyte filaments are the slowest tip-growing organisms reported to date with a growth speed of $2.5 \mu\text{m}\cdot\text{h}^{-1}$ (Figure 1), i.e., 700 times slower than the pollen tube (Rabillé et al., 2019a), which highlights the necessity of evaluating lab-on-chip technology to simplify their long-term investigation in controlled environments. In addition, we showed that the mechanisms of tip growth selected by this alga relies on an adjustment of its cell wall thickness at the very tip of the apical cell, while most of the other tip growing cells, including the pollen tube, control their growth by varying the cell wall stiffness at this position (Rabillé et al., 2019a). Hence, further studies of tip growth mechanisms in *Ectocarpus*, namely those controlling the cell wall thickness during apical growth, require the development of technologies allowing to simultaneously monitor several filaments growing in similar conditions over a long period of time.

In this technical paper, we designed two PDMS-based lab-on-chips consisting of straight parallel channels to constrain filament growth and to guide them in a single, horizontal direction in contrast to their growth in all directions as observed in open space environments. The healthiness and growth performance of *Ectocarpus* filaments inside these microfluidic environments



were monitored for up to 20 days and their growth rates were, in addition to the qualitative evaluation of several development steps, quantitatively compared to open space growth conditions. Finally, the ability to label cytological markers, either by immunocytochemistry or directly with vital dyes, was tested to study the suitability of microfluidic environments for subsequent investigations of the tip growth in the brown alga *Ectocarpus*.

MATERIALS AND METHODS

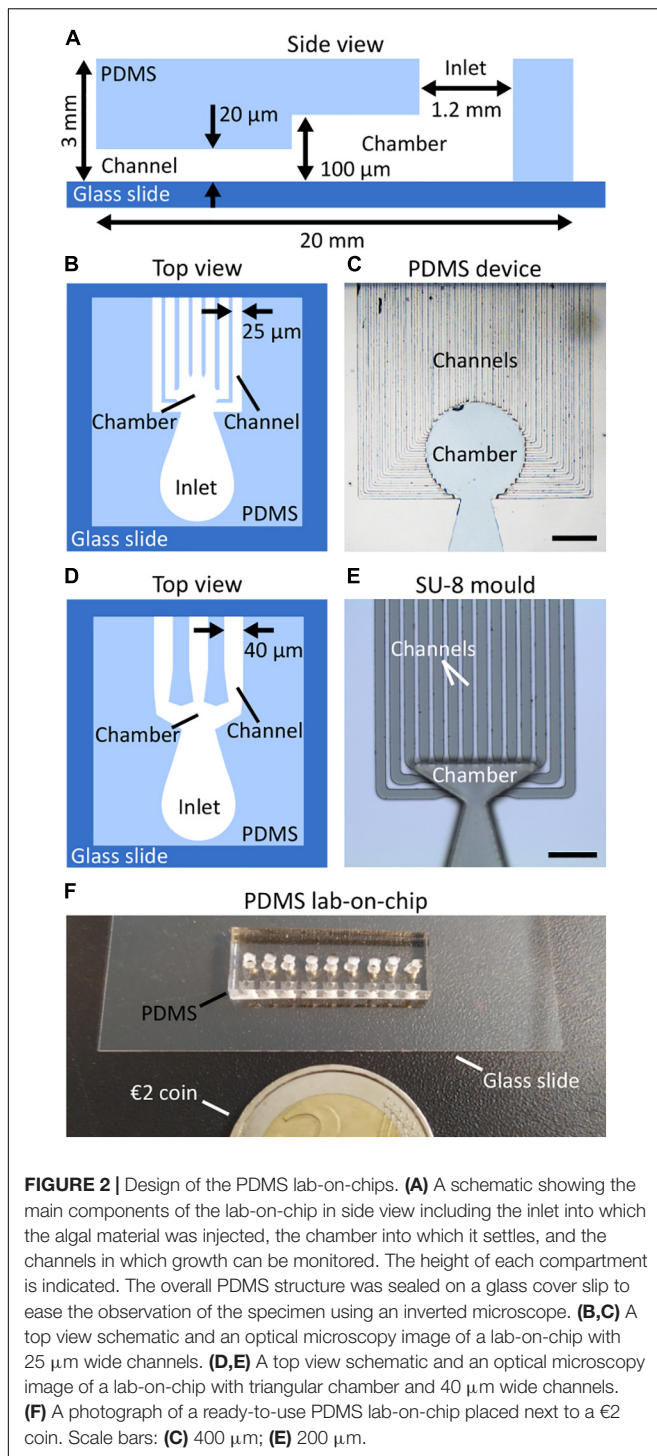
Chip Design

The transparent polymer PDMS, as often used for the fabrication of microfluidic environments, was shown to be not toxic for the brown alga *Ectocarpus* sp. (Evariste et al., 2012) as blended filaments inoculated on surfaces of different PDMS compositions grew as expected. **Figure 2A** shows a schematic of a PDMS device in side view. The key elements of the structure consist of the inlet, the main chamber, as well as the microchannels. The inlet has a diameter of 1.2 mm and enables filling of the chamber and loading of the samples. The height of the chamber is 100 µm to ensure sufficient availability of nutrients. Depending on the planned experiment, a design with a circular (**Figures 2B,C**) or triangular chamber (**Figures 2D,E**) can be chosen. The chamber is connected to numerous microchannels with a height of 20 µm. The reduction in height from the chamber to the channel constricts the specimen's growth direction and, by that, allows for long-term imaging within a stable focal plane. While circular chambers connect to 44 channels with a width of 25 µm and allow for multiplex observations of the specimens, triangular chambers connected to 14 channels with a width of 40 µm to enable the detailed investigation of specific growth trajectory, e.g., filament undulations. The channels are separated by PDMS walls with a width of 20 µm, which is necessary to ensure proper sealing and adhesion between the PDMS device and the glass substrate. **Figure 2D** shows a schematic of a

PDMS device with a triangular chamber. At the entrance of the channels, a small funnel guides filaments from the chamber into the channel, thereby enhancing the percentage of filaments growing into the channels. Once an entrance or channel is filled, a constriction at the end of the funnel should prevent an additional filament from entering the already occupied channel. Additionally, the constriction reduces the risk of specimens getting flushed through the channels during the initial filling of devices with wider structures.

The width chosen for the channels was a compromise of several criteria. On the one hand, narrower channels would increase the spatial constraints for *Ectocarpus*, which, despite being of broader interest concerning the resulting growth cell response, is not the focus of this initial investigation on the feasibility of lab-on-chip technology. Additionally, narrower channels would require a higher loading pressure, which could damage the samples or even separate the bond between the PDMS structure and the glass substrate. On the other hand, the use of wider channels bears the risk of samples passing through the microchannels rather than being collected in the chamber during loading. Overall, considering biological features as well as manufacturing constraints and technical challenges, we considered 25 µm to be a compromise that would allow the algae to have sufficient nutrients while ensuring a mechanically robust lab-on-chip device.

As to the chamber, its geometry was adjusted to allow a sufficiently large number of connected channels for each design while simultaneously limiting the volume available inside the chamber. Thus, it optimises the chance of obtaining filaments growing parallel to each other inside channels which is a crucial factor for the efficient study of slow-growing organisms like *Ectocarpus*. However, although no direct influence on the specimen's growth was observed in relation to changing the inlet geometry, future studies could examine the impact of additional design parameters, such as the height or diameter of the inlet, on the specimen's health and viability.



Fabrication

The lab-on-chips were fabricated by double-layer photolithography in clean room environments and by mould replication techniques. Silicon wafers were cleaned with acetone, isopropanol, and deionised water prior to mould fabrication. For the layer containing the microchannels, the photosensitive polymer SU-8 3025 (*Kayaku Advanced Materials*)

was spin-coated on the wafers using a three-step process with a maximum angular velocity of 4500 rpm to obtain a uniform photoresist layer of 20 μm . The corresponding design of the channel layer was transferred onto the photoresist using a mask aligner (MA6/BA6, *Süss MicroTec*). Finally, the wafers were developed (mr-Dev 600, *Micro Resist Technology GmbH*) and hard baked at 150°C for 5 min to improve the stability of the channels and their adhesion to the silicon substrate. The second layer of the lab-on-chip, i.e., the elevated section containing the inlets as well as the main chamber, was fabricated through an additional photolithography process using SU-8 100 (*Kayaku Advanced Materials*) and a maximum angular velocity of 3000 rpm to ensure a uniform 100 μm thick layer of photoresist. **Figure 2E** shows an optical microscopy image of a fabricated mould with a triangular chamber to be used for PDMS replication. The observed variation in the focal plane is based on the height difference between the channel layer and the triangular chamber layer.

Prior to PDMS casting, the fabricated structures were vapour coated with (tridecafluoro-1,1,2,2-tetrahydrooctyl) trichlorosilane (CAS 78560-45-9, *ABCR*) and heated to 120°C for 10 min to improve the reusability of the mould. PDMS (Sylgard 184, *Dow Corning*) with a weight ratio of 1:10 (curing agent to pre-polymer) was mixed sufficiently for 5 min, poured over the SU-8 mould, and degassed for 30 min in a vacuum chamber. To transfer the 3D pattern into the polymer, the PDMS was cured for 1 h in an oven at 80°C. Finally, the PDMS was cut and peeled off the mould and the inlets were punched using a biopsy punch with a diameter of 1.5 mm (BP15, *Vetlab*). To chemically bond the PDMS and the cover glass with a thickness of 0.17 μm , both surfaces were exposed to oxygen plasma (Femto Plasma Asher, *Diener Electronics*) for 30 s before being brought in contact. Slight pressure was manually applied to ensure proper contact between the entirety of the lab-on-chip and the cover glass to prevent future algal specimens from growing beyond the dimensions of the corresponding microchannels.

For size comparisons, **Figure 2F** shows a ready-to-use lab-on-chip with 25 μm wide channels next to a €2 coin.

Sterilisation of the Chips

The chips were sterilised by UV irradiation for 30 min in a sterile laminar flow hood. Then, they were used either dry or pre-filled with sterile seawater (see below).

Ectocarpus Cultivation

Ectocarpus strain CCAP 1310/4 (also named Ec32) from the Culture Collection of Algae and Protozoa was grown in natural seawater (approximately 550 mosmoles) supplemented by vitamins and microelements as described by Le Bail and Charrier (2013). Sporophyte filaments were produced from the germination of swimming mitospores (Charrier et al., 2008). Cultivation took place at 13°C under 12:12 light:dark conditions (light intensity of approximately 29 $\mu\text{E m}^{-2} \text{s}^{-1}$), usually on the main types of plastic and glassware. Seawater was renewed every 2 weeks when algae were grown in open space environments.

On-Chip Inoculation

Optimisation of the Loading Procedure

The 1.2 mm diameter inlet was filled with seawater by applying a constant pressure *via* a pipette mounted with a cut pipette tip to seal the 1.2 mm inlet.

As seawater is 1.3% more viscous and has a higher surface tension than pure water, filling the channels can be more difficult. Consequently, if the applied pressure is too low, the seawater introduced into the inlet only fills the chamber but not the channels (**Supplementary Figures 1A,B**). A solution of seawater stained with bromophenol blue was used to optimise the channel filling procedure with a micropipette. Once the protocol was established, algal material was introduced into the chamber.

Channel Filling

The algal material was introduced into the chamber by applying a steady pressure high enough to bring the algal material just at the entrance of the channels, yet low enough to prevent the algae from being flushed out of the chamber. After inoculation, the material was left still for 2 h to allow the spores to attach to the chamber surface and the glass substrate. If sporophytes were used instead of spores, they were removed after 2 h. The channels were then filled with seawater by applying a pipetting pressure high enough to allow the liquid to move from the chamber to the channels. Because we did not use a pump with standardised equipment (e.g., pipe diameter), the numerical value of the pressure is not known. However, pressure required to fill the channel when pressing on a micropipette has been experienced previously using blue seawater as a visible coloured marker to monitor channel filling (**Supplementary Figure 1C**). It is also worth noting that the required pressure varied slightly between each structure, as, due to their manual preparation, the final length of the microchannels showed minor variations. To confirm complete filling of the channels with clear seawater, the channels outlets were monitored under a microscope for the release of air bubbles. Channels in which air remained trapped after the first filling procedure (as shown in **Supplementary Figure 1D**) were flushed several times.

Once inoculated, the lab-on-chip was transferred to a Petri dish filled with seawater and kept fully submerged. It was cultured under standard conditions as described above, thereby, allowing for comparisons to open space cultivations. Seawater was renewed every 2 days. No salt crystals were observed inside the channels during at least 3 weeks.

This procedure was repeated on 7 independent experiments summing 12 slides containing a total of 108 lab-on-chip devices. Altogether, more than 500 filaments were observed.

It is important to highlight that the described on-chip inoculation has been tested with regards to the loading procedure and, consequently, to the optimum location for the loaded material to ensure successful germination and improved specimen health. The optimised method, as described above, relies on a two-step filling process for the microfluidic device in which loaded fertile sporophytes or released spores were initially prevented from entering the channels by the liquid/air interface formed between the chamber and the channel. The channels

were then made accessible to the germinating spores by flushing the full structure.

In contrast, filling the chamber as well as the channels with fertile sporophytes or spores in a single step did not only lead to partially blocked channels due to broken or small filament pieces (**Supplementary Figure 2A**) but further allowed the still swimming spores to enter the channels. This led to severely impaired filament growth behaviours with delayed spore germinations and qualitatively less asymmetrical cell divisions. Furthermore, some cases demonstrated growth directions perpendicular to the channel axis (**Supplementary Figure 2B**) as well as a general reduction in growth rate with less pronounced cell growth of the apical cells and shorter filaments (**Supplementary Figure 2C**). Finally, while cell rounding was still observed for filaments with normal apical growth (**Supplementary Figure 2D**), branching has not been detected for any spores that initially germinated inside the channels.

As a suitable alternative allowing many channels to be filled with branches at a similar stage of development (**Supplementary Figure 2E**), the loading of non-fertile sporophytes into fully flushed structures can be proposed. As *Ectocarpus* development is reiterative, subsequent branch growth followed the same developmental process as for primary filaments while the spore germination and initial asymmetrical divisions were skipped.

Image Acquisition

The Leica DMI-8 inverted microscope was used to observe calcofluor (Ex/Em: 380/475 nm) and fluorescein isothiocyanate (FITC; Ex/Em: 495/520 nm) labelling with the corresponding filters. Confocal microscopy (TCS SP5 AOBS inverted confocal microscope, *Leica, objective Plan-Apochromat 63×/1.4 Oil*) was used to increase the *z* spatial resolution compared to image acquisition by epifluorescence microscopy.

Labelling of Cellular Components

Cellulose was stained by incubating the lab-on-chip in 0.01% calcofluor white solution (fluorescent brightener 28, F-3543, *Sigma-Aldrich*) for 30 min at room temperature (RT) in the dark. The solution was injected into the channels by high pressure pipetting. Observation was performed under UV light using epifluorescence microscopy after flushing the channels with fresh seawater at least twice and after incubation for at least 15 min at RT between each rinsing step.

Immunolocalisation of cell wall polysaccharides in the lab-on-chip was developed by adapting the protocol from Rabillé et al. (2019b). The main modification consisted in fixing the algal material in 4% paraformaldehyde prepared in H₂O instead of seawater. All the solutions were rinsed by high pressure pipetting into the inlet which occasionally resulted in the loss of some filaments.

Statistical Evaluation

Statistical evaluations concerning the specimens' growth rates were performed as double-sided *t*-test with unequal variances for *n* = 15 specimens present in the free environment and *n* = 22 specimens in the microfluidic channels. The resulting

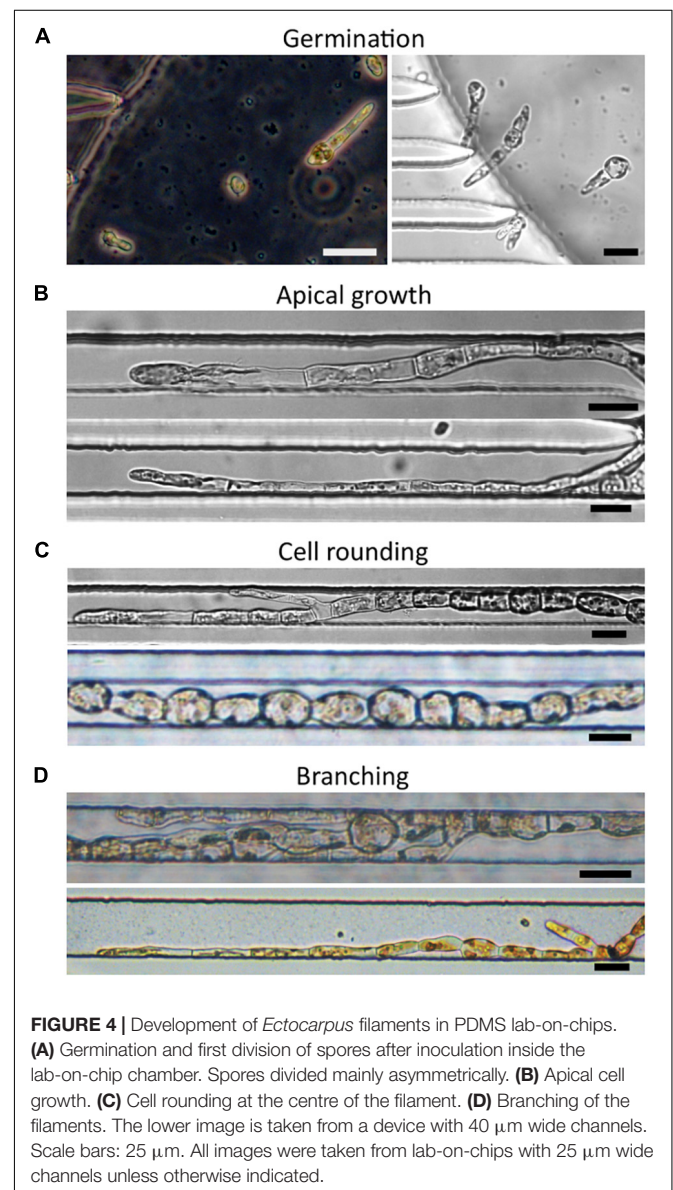
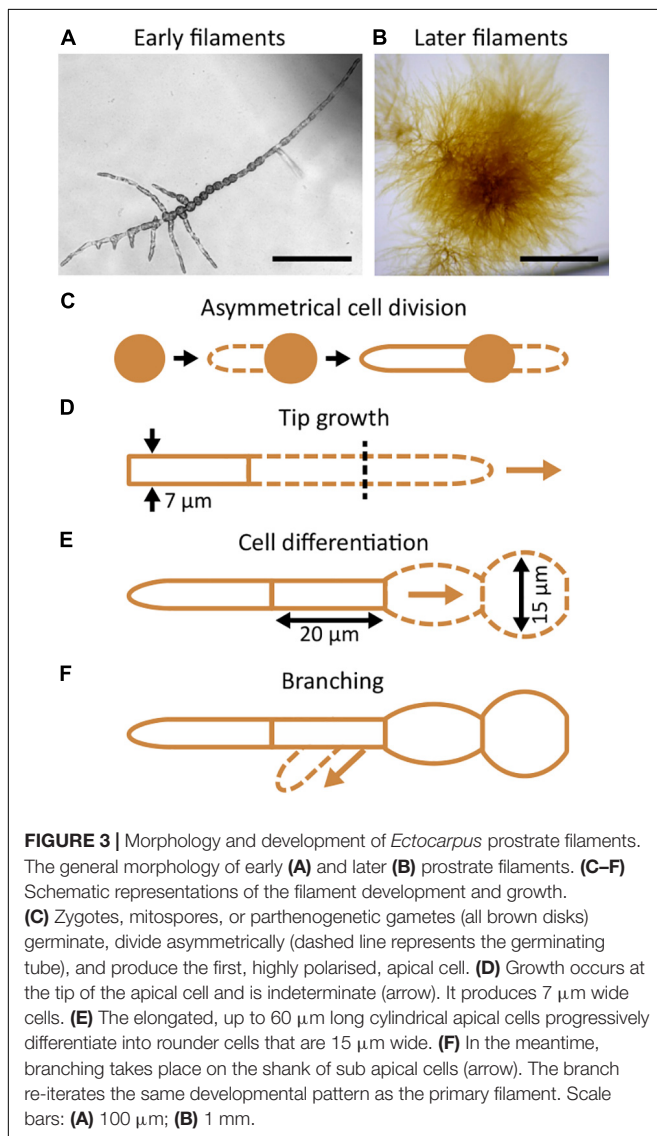
p -values are reported in the corresponding paragraph. Statistical significance was determined as $p \leq 0.05$.

RESULTS

Viability and Developmental Steps of *Ectocarpus* Filaments Within the Lab-on-Chip

The early development of the *Ectocarpus* sporophyte has been described in detail (Le Bail et al., 2008, 2010, 2011; Nehr et al., 2011; Rabillé et al., 2019a) and is summarised in **Figure 3**. When grown in open space environments, the *Ectocarpus* sporophyte is composed of microscopic, branched uniseriate filaments (**Figure 3A**) that form a visible tuft approximately 4 weeks after the very initial stages (**Figure 3B**). Sporophytic filaments growth is initiated by an asymmetrical cell division

of the zygote or mitospores (**Figure 3C**), forming the first apical cell that continues to grow indefinitely by tip growth (**Figure 3D**). A few hours later, the initial cell germinates again and gives rise to a second apical cell, which grows along the same axis as the first one but in the opposite direction. Over the span of several days, each first apical cell gradually differentiates into spherical cells. Apical growth and cell rounding generate a uniseriate filament which is composed of two main cell types, i.e., elongated cells with a width of approximately $7 \mu\text{m}$ located at both ends of the filaments and circular cells with a diameter of approximately $15 \mu\text{m}$ situated at the centre of the filaments (**Figure 3E**). After around 10 days, the sub-apical cells branch (**Figure 3F**) and the resulting branches continue to grow as the primary filaments do. This repeated developmental programme results in the overall morphology as shown in **Figure 3B**.



We investigated whether these developmental steps were preserved in the constrained environment of the lab-on-chip devices. *Ectocarpus* spores were introduced into the structures as described in section “Materials and Methods.” We monitored growth in the lab-on-chip with the goal of constraining the spores to germinate in the chamber. The spores successfully germinated inside the main chamber of the microfluidic device 5 days after inoculation (Figure 4A). The ratio of cell division asymmetry, i.e., the ratio of cell divisions producing unequally sized daughter cells as depicted in Figure 3C, was consistent with what was reported in open space germination, where about 80% of spores divide asymmetrically and approximately 20% symmetrically (Le Bail et al., 2011). When grown freely in water deprived of microelements, it has previously been observed that filaments tend to develop a cell sheet, meaning that *Ectocarpus* filaments shifted their development from uniaxial to bidirectional growth. This major change in body plan organisation is a sign that tip growth mechanisms have been severely impaired in the absence of microelements. However, in none of the lab-on-chips with 40 or 25 μm wide channels were such patterns observed and the filaments maintained an uniaxial growth throughout the experiment (Figure 4B) which indicates a sufficient supply of microelements even inside the confined regions of the lab-on-chip devices. Calcofluor staining further showed that filament growth took place in the dome of the apical cell (Figure 5I) as previously observed in open space environments (Le Bail et al., 2008). To monitor specimen health,

the growth rates of 22 filaments growing in 25 μm wide channels for 1 week were compared to the growth behaviour of filaments thriving in the open space environment of the same Petri dish (Figures 6A,B). Figures 6C,D showed that the overall growth dynamics were similar between the confined and free filaments, with filaments that grew inside the channels having an average growth rate of $2.8 \mu\text{m}\cdot\text{h}^{-1}$ compared to $2.41 \mu\text{m}\cdot\text{h}^{-1}$ for filaments growing in the open space (Supplementary Table 1; *t*-test *p*-value = 0.39). While the growth rates appeared to decrease with time independently of the environment (e.g., from 3.13 to $2.60 \mu\text{m}\cdot\text{h}^{-1}$ inside the microchannels), this reduction in growth speed did not reach statistical significance (*t*-test *p*-value = 0.15). For direct comparisons, Supplementary Figure 3 displays the average growth rate over time for both environments in a single graph. Overall, the observed growth rates occur with the same dynamic as previously reported, i.e., $2.5 \mu\text{m}\cdot\text{h}^{-1}$ (Rabillé et al., 2019a).

The rounding of the cells is a function of their maturation stage and their position along the filament. It is, therefore, an excellent qualitative parameter reflecting the fitness of *Ectocarpus*. Rounding of elongated sub-apical cells (Figure 3E) was observed as expected, so that spherical cells were located only in the most proximal parts of the filaments (Figure 4C). Additionally, branching, which is an additional cellular event reflecting the canonical developmental pattern as described in Figure 3, also occurred in the filaments developed within the channels (Figures 4C,D). Furthermore, we did not notice any

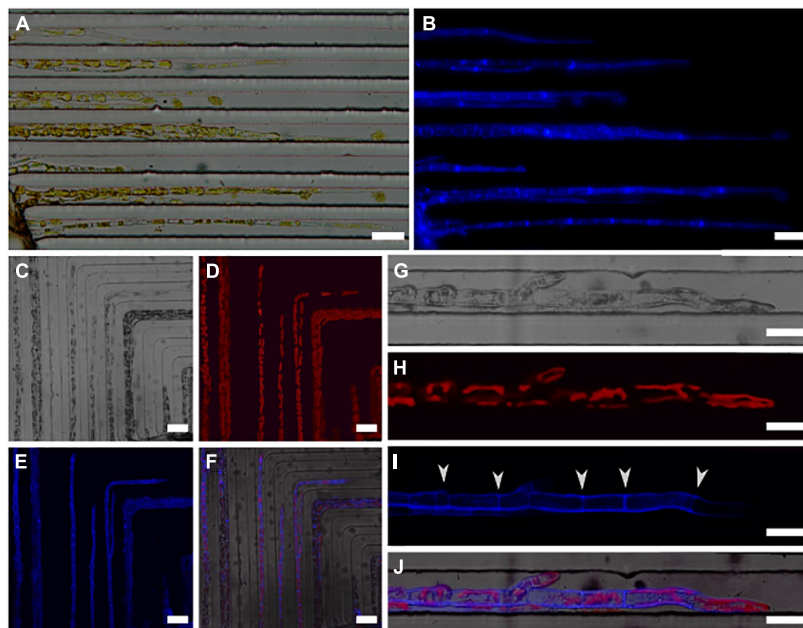
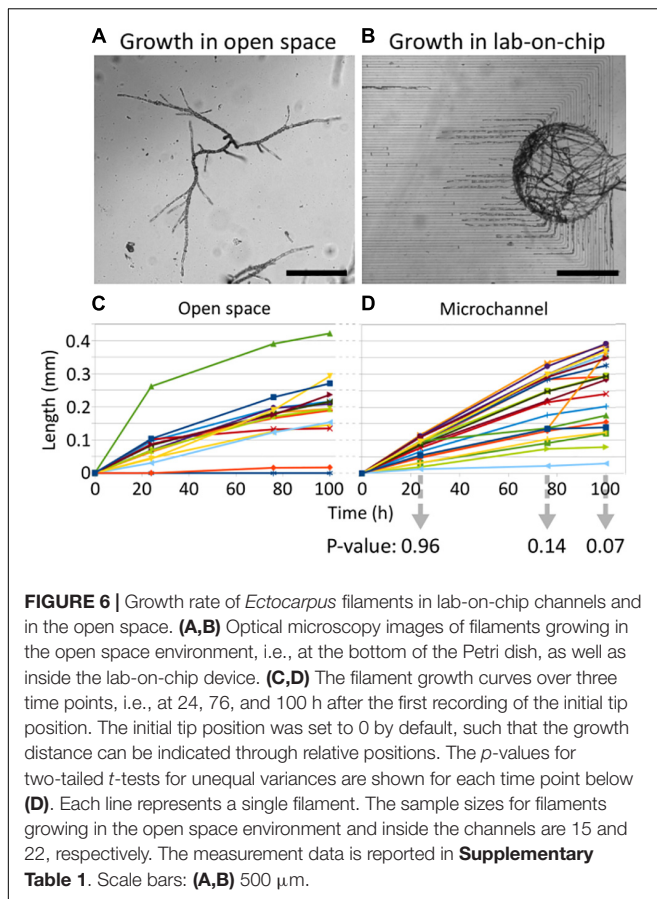


FIGURE 5 | Labelling of cellulose in the cell wall of filaments growing in 25 μm wide channels. (A,B) Two images obtained using epifluorescence microscopy. (A) A bright field microscopy image of the filaments and (B) a UV image showing the labelled cellulose (blue) present in the external cell wall. A stronger signal has been observed in the transversal walls. (C–J) A series of confocal microscopy images. (C) A bright field image of growing filaments, (D) chloroplast autofluorescence (red), (E) calcofluor fluorescence (blue), and (F) a merged image of all three channels. (G,H) A close-up of filaments labelled with calcofluor and imaged after growing for 24 h following the post-labelling rinsing of the channels. (G) The bright field image, (H) chloroplast fluorescence (red), (I) calcofluor fluorescence (blue), and (J) the three merged channels. The transverse cell walls (white arrowheads) are clearly distinguishable. The tip of the filament is not fluorescent, and as such, displays the newly grown cell wall. Scale bars: (A–F) 50 μm ; (G–J) 25 μm .



colour changes from brown to green in the chloroplasts of cells growing inside the microfluidic chip, which is typically observed in correlation with filament death. Finally, under UV exposure, the intensity of the auto-fluorescence emitted by the chloroplasts was detected at a level similar to that of filaments growing in the open space environment (see **Figures 5D,H**).

Therefore, for spores germinating inside the chamber, neither the presence of the PDMS nor the enforced space limitations demonstrated a negative effect on the filament development and growth pattern, e.g., by impairing the quality of the seawater inside the confined environment or through a possible increase in mechanical stress. Altogether, the developmental pattern of the filaments growing inside the channels, i.e., apical cell polarisation, growth rate, and cell shape changes, was consistent with the pattern observed in filaments growing in an open environment.

Display of Cellular Components of *Ectocarpus* Within the Lab-on-Chip

Despite the recent advances of editing approaches of *Ectocarpus* (Badis et al., 2021), the expression of fluorescent reporter genes is not yet feasible. Therefore, the study of *Ectocarpus* cell biology requires the use of classical cytological approaches, like vital staining and immunolocalisation that are the only available non-invasive techniques allowing for the labelling of specific components in or at the surface of the algal cells. Cellulose,

i.e., a rigid polymer of $\beta(1-4)$ glucose present in *Ectocarpus* cell walls at a level of approximately 10% (Charrier et al., 2019), was uniformly labelled throughout filaments growing inside the 25 μm wide channels on both the outer and transverse cell walls (**Figures 5A,B**). This observation is in great agreement with previous studies for filaments grown in open space environment (Le Bail et al., 2008; Simeon et al., 2020). Similar results were also obtained for filaments in devices with 40 μm wide channels. Using confocal microscopy, the more focused images shown in **Figures 5C-F** confirmed the overall and homogeneous labelling of all filaments present inside channels. Both the shape of the chloroplasts highlighted by autofluorescence (**Figures 5G,H**) and the apical growth indicated by the new dark area at the filament tip (**Figures 5I,J**) confirmed that the filaments were thriving in this confined environment and, hence, supported the value of the previously derived growth rate measurements.

In a second step, we labelled alginates, i.e., a polysaccharide consisting of a mixture of guluronic and mannuronic acids linked by $\beta(1-4)$ bond, which is present in brown algal cell walls at a ratio of up to 40% (reviewed in Charrier et al., 2019). The monoclonal BAM6, that recognises mannuronan-rich alginates, was used in combination with a secondary antibody coupled to the green fluorochrome FITC. The immunolocalisation protocol was applied in the lab-on-chip, aiming to label several filaments growing in parallel in separate channels. Simultaneously, free organisms present in the same Petri dish were labelled and used as positive controls. In contrast to the negative control without primary antibody (**Figures 7A-C**), the cell wall of both apical (**Figures 7D,E**) and rounding cells (**Figure 7F**) of labelled free-growing organisms displayed a specific signal similar to that reported in Rabillé et al. (2019b). In the 25 μm channels, *Ectocarpus* filaments also showed a strong signal in the dome of apical cells (**Figures 7G-J**) and on the flanks of rounding cells (**Figure 7K**). This pattern was as strong and specific as in the internal positive controls. The remaining cell walls of an empty plurilocular sporangium incidentally present within one of the channels also displayed significant labelling (**Figure 7L**). The red autofluorescence signal emitted by the chloroplasts further demonstrated the healthiness of the filaments prior to the formaldehyde fixation step of the immunolocalisation protocol (**Figures 7A-J**).

Overall, both cell biology protocols successfully labelled cellulose and alginate cell wall polysaccharides, either homogeneously (cellulose) or in specific locations (alginates) along the filaments. The labelling of the filaments was independent of the position of the specimen inside the lab-on-chip, e.g., at the entrance or exit of the channels, and displayed expected results even for samples located far away from the main chamber (**Figure 7G**).

DISCUSSION

Ectocarpus early development is accompanied by a significant number of cellular events while its morphological complexity is low. Initially, it leads to the formation of uniseriate filaments, which grow by elongation and division of apical cells, and

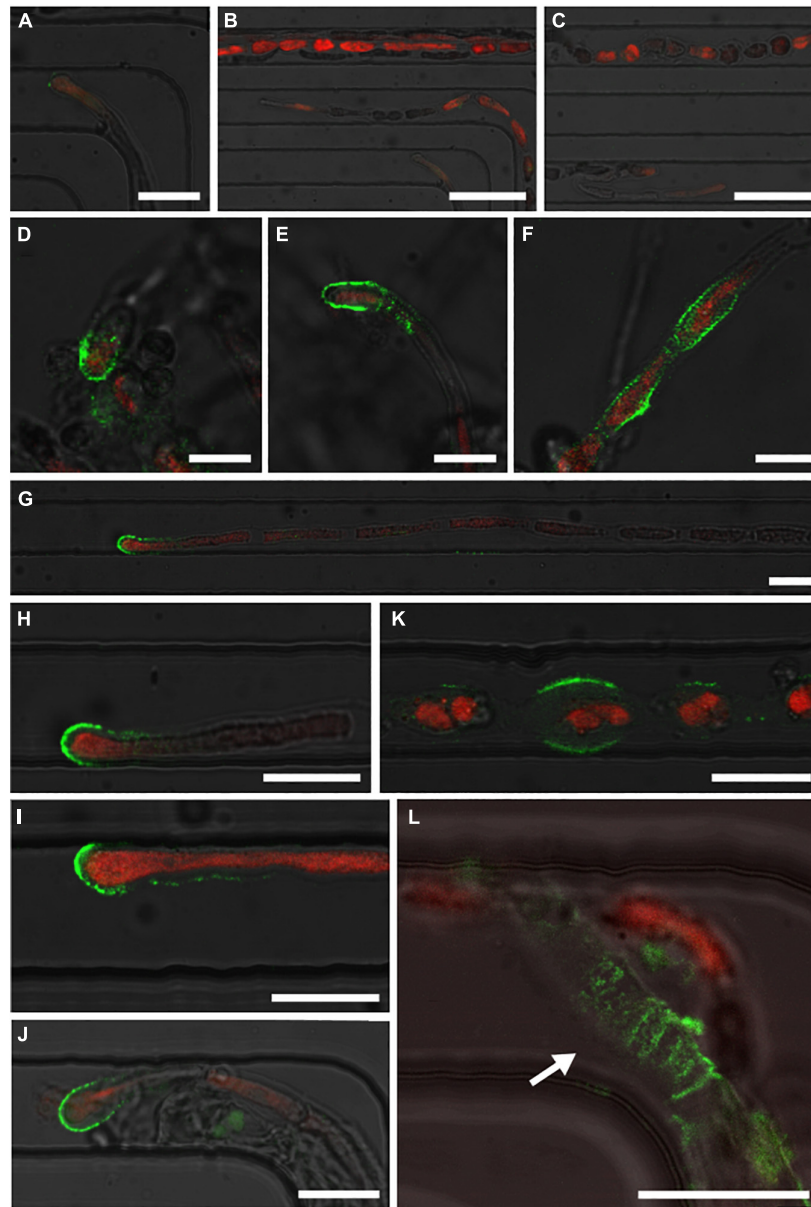


FIGURE 7 | Immunolocalisation of alginate polysaccharides in *Ectocarpus* filaments using monoclonal antibody BAM6. Labelled sections were observed through confocal microscopy. **(A–C)** Optical microscopy images demonstrating the negative controls for filaments without primary anti-alginate antibody. Both the apical parts and central parts of several filaments are shown without any signal from BAM6 (green fluorescent signal from the secondary FITC-conjugated antibody). Only autofluorescence (red) emitted by the chloroplasts was detected. **(D–F)** Optical images presenting freely growing filaments in the same Petri dish. With the same image capture parameters such as laser power and selective bands of the photomultiplier tubes, BAM6 labelling was observed in the dome of apical cells and in the flanks of rounded cells. **(G–L)** Image series showing the results on filaments grown in 25 μm wide channels. **(G–J)** Fluorescent images of the domes of apical cells, **(K)** rounding cells, and **(L)** empty plurilocular sporangium (white arrow). The autofluorescence of chloroplasts of BAM6 labelled filaments was observed, except in **L**, as the cavities of the plurilocular sporangium no longer contained spores. Scale bars: **(A)** 25 μm ; **(B,C)** 50 μm ; **(D–F)** 10 μm ; **(G–L)** 20 μm . The specific green BAM6 signal and the red chloroplast autofluorescence signals are superimposed with the bright field signal.

the progressive rounding of cells acting as the main cell differentiation process. Recently, it has been demonstrated that *Ectocarpus* tip growth relies on a different biophysical mechanism than that reported in most of the other tip growing cells, including the pollen tube. In the former, the cell wall stiffness controls growth (Rabillé et al., 2019a), while in the latter, this

is the cell wall thickness. This further illustrated that brown algae are promising model organisms to display alternative growth mechanisms.

To study the tip growth behaviour of *Ectocarpus*, we tested the use of lab-on-chips as a microfluidic device aimed for the long-term monitoring of filaments. The possibility of delivering

chemicals at a specific time and simultaneously to several filaments growing in a single focal plane while being guided through parallel channels is particularly attractive for slow growing specimens such as the *Ectocarpus* filaments. Here, we have shown that microfluidic chips with 44 parallel channels as narrow as 25 μm are suitable for studying *Ectocarpus* tip growth and dynamics of cell rounding. The inoculation procedure and cell wall labelling experiments were developed such that more than 50% of the lab-on-chip channels were filled with healthy filaments growing in-plane over more than 3 weeks, which is a duration that significantly exceeds the typical use of such technology for other samples (Agudelo et al., 2013; Shamsudhin et al., 2016; Burri et al., 2018). Furthermore, the presented designs allowed for the incorporation of specimen studies using standard cytology protocols. Our observations are consistent with previous conclusions drawn for the protonemata of the moss *P. patens*, where the growth rate and cell differentiation, with some impairments (Kozgunova and Goshima, 2019), proceeded as expected (Bascom et al., 2016). In contrast, different results were obtained with the hyphae of the fungi *N. crassa* growing in grid or maze chips, where the velocity of the apical extension was drastically reduced and their branching pattern impaired (Held et al., 2011).

In our case, possible limitations depended on the applied loading procedure and the inoculation of the mitospores. While the filaments successfully entered and grew along the microchannels if the mitospores were germinated in the main chamber, mitospores loaded inside the channels were severely hindered in their germination. However, by optimising the inoculation procedure, we were able to prevent these drawbacks. Furthermore, the study of germination and especially of the first asymmetric cell division did not rely on a specific device geometry as both major cellular events could be observed in all spatial directions. Altogether, this study validates the use of microfluidic devices for the study of the development and of the physiology of *Ectocarpus* in a confined microenvironment. Hence, it represents a first step in the subsequent characterisation of tip growing mutants (Le Bail et al., 2011) and potentially life cycle mutants of this species (Coelho et al., 2011; Macaisne et al., 2017), as it has previously been performed with *Physcomitrium* (Bascom et al., 2016) and *Neurospora* (Held et al., 2011). It also paves the way for the study of other brown algae, especially those which develop filaments in one or both phases of their life cycle, such as *Sphacelaria* and filamentous gametophytes of many brown algae including the Laminariales, the Desmarestiales, and the Sporochnales (Fritsch, 1954).

CONCLUSION

In recent years, microfluidic devices have proven suitable for the investigation and manipulation of numerous small organisms and, by that, enabled novel possibilities and pathways for biological research. However, prior to their application, lab-on-chips must first be evaluated for each potential biological model to avoid misinterpretations of newly gained observations and of the corresponding results. In this work, the healthiness

and performance of *Ectocarpus* filaments growing in confined microfluidic environments were monitored under controlled conditions for several days and the development steps were quantitatively and qualitatively compared to *in vitro* open space growth. Additionally, the ability to label cytological markers, either by immunochemistry or directly with vital dyes, was investigated to ensure the suitability of microfluidic devices for the in-depth study of the brown alga *Ectocarpus*. The results demonstrated that, following an optimised loading procedure, all the developmental steps of *Ectocarpus* filament growth inside PDMS channels were similar to those observed in unconstrained conditions and as described in previous reports. Therefore, PDMS lab-on-chips are suitable experimental devices to further study apical growth, cell differentiation, and branching and enable simplified investigations by allowing for chemically controlled environments in combination with high-resolution microscopy techniques.

DATA AVAILABILITY STATEMENT

The raw data supporting the conclusions of this article will be made available by the authors, without undue reservation.

AUTHOR CONTRIBUTIONS

BC and NL conceived the initial idea and wrote the manuscript. BC and BN supervised the project. BC, BN, and NL raised the funding. NL designed and fabricated the microfluidic devices. BC adjusted the culture conditions and monitored growth. SB performed the cell wall staining experiments. All authors reviewed and commented on the manuscript.

FUNDING

This work was supported by ETH Zürich, the University of Cambridge, and, in part, by an interdisciplinary grant from the Swiss National Science Foundation (Grant Number CR22I2_166110) to BN as well as a career grant from the Swiss National Science Foundation (Grant Number P2EZP2_199843) to NL. SB's Ph.D. grant is funded by the ARED Région Bretagne (Grant Number COH20020) and the Sorbonne Université. The authors acknowledge open access funding by ETH Zürich.

ACKNOWLEDGMENTS

We thank Naveen Shamsudhin for the discussions about the experimental setup at the onset of this project.

SUPPLEMENTARY MATERIAL

The Supplementary Material for this article can be found online at: <https://www.frontiersin.org/articles/10.3389/fmars.2021.745654/full#supplementary-material>

REFERENCES

- Agudelo, C., Packirisamy, M., and Geitmann, A. (2016). Influence of electric fields and conductivity on pollen tube growth assessed via electrical lab-on-chip. *Sci. Rep.* 6:19812. doi: 10.1038/srep19812
- Agudelo, C. G., Nezhad, A. S., Ghanbari, M., Naghavi, M., Packirisamy, M., and Geitmann, A. (2013). TipChip: a modular, MEMS-based platform for experimentation and phenotyping of tip-growing cells. *Plant J.* 73, 1057–1068. doi: 10.1111/tpj.12093
- Azizpour, N., Avazpour, R., Rosenzweig, D. H., Sawan, M., and Aji, A. (2020). Evolution of biochip technology: a review from lab-on-a-chip to organ-on-a-chip. *Micromachines* 11:599. doi: 10.3390/mi11060599
- Badis, Y., Scornet, D., Harada, M., Caillard, C., Godfroy, O., Raphalen, M., et al. (2021). Targeted CRISPR-Cas9-based gene knockouts in the model brown alga *Ectocarpus*. *New Phytol.* 231, 2077–2091. doi: 10.1111/nph.17525
- Baldauf, S. L. (2003). The deep roots of eukaryotes. *Science* 300, 1703–1706. doi: 10.1126/science.1085544
- Bascom, C. S., Wu, S.-Z., Nelson, K., Oakey, J., and Bezanilla, M. (2016). Long-term growth of moss in microfluidic devices enables subcellular studies in development. *Plant Physiol.* 172, 28–37. doi: 10.1104/pp.16.00879
- Bayareh, M., Ashani, M. N., and Usefian, A. (2020). Active and passive micromixers: a comprehensive review. *Chem. Eng. Process. Process Intensification* 147:107771. doi: 10.1016/j.cep.2019.107771
- Berland, S. F., Breithfeld, M., Dietsche, C. L., and Dittrich, P. S. (2021). Recent advances in microfluidic technology for bioanalysis and diagnostics. *Anal. Chem.* 93, 311–331. doi: 10.1021/acs.analchem.0c04366
- Bogaert, K. A., Blommaert, L., Ljung, K., Beeckman, T., and De Clerck, O. (2019). Auxin function in the brown alga *Dictyota dichotoma*. *Plant Physiol.* 179, 280–299. doi: 10.1104/pp.18.01041
- Bothwell, J. H. F., Kisieleska, J., Gennner, M. J., McAinsh, M. R., and Brownlee, C. (2008). Ca²⁺ signals coordinate zygotic polarization and cell cycle progression in the brown alga *Fucus serratus*. *Dev. Camb. Engl.* 135, 2173–2181. doi: 10.1242/dev.017558
- Burri, J. T., Vogler, H., Läubli, N. F., Hu, C., Grossniklaus, U., and Nelson, B. J. (2018). Feeling the force: how pollen tubes deal with obstacles. *New Phytol.* 220, 187–195. doi: 10.1111/nph.15260
- Charrier, B., Coelho, S. M., Le Bail, A., Tonon, T., Michel, G., Potin, P., et al. (2008). Development and physiology of the brown alga *Ectocarpus siliculosus*: two centuries of research. *New Phytol.* 177, 319–332. doi: 10.1111/j.1469-8137.2007.02304.x
- Charrier, B., Rabillé, H., and Billoud, B. (2019). Gazing at cell wall expansion under a golden light. *Trends Plant Sci.* 24, 130–141. doi: 10.1016/j.tplants.2018.10.013
- Cock, J. M., Sterck, L., Rouzéé, P., Scornet, D., Allen, A. E., Amoutzias, G., et al. (2010). The *Ectocarpus* genome and the independent evolution of multicellularity in brown algae. *Nature* 465, 617–621. doi: 10.1038/nature09016
- Coelho, S. M., Godfroy, O., Arun, A., Le Corguill, G., Peters, A. F., and Cock, J. M. (2011). OUROBOROS is a master regulator of the gametophyte to sporophyte life cycle transition in the brown alga *Ectocarpus*. *Proc. Natl. Acad. Sci. U.S.A.* 108, 11518–11523. doi: 10.1073/pnas.1102274108
- Evariste, E., Gachon, C. M. M., Callow, M. E., and Callow, J. A. (2012). Development and characteristics of an adhesion bioassay for ectocarpoid algae. *Biofouling* 28, 15–27. doi: 10.1080/08927014.2011.643466
- Fritsch, F. E. (1954). *The Structure and Reproduction of the Algae*, Vol. II. Cambridge: Cambridge University Press.
- Held, M., Edwards, C., and Nicolau, D. V. (2011). Probing the growth dynamics of *Neurospora crassa* with microfluidic structures. *Fungal Biol.* 115, 493–505. doi: 10.1016/j.funbio.2011.02.003
- Kozgunova, E., and Goshima, G. (2019). A versatile microfluidic device for highly inclined thin illumination microscopy in the moss *Physcomitrella patens*. *Sci. Rep.* 9:15182. doi: 10.1038/s41598-019-51624-9
- Läubli, N. F., Burri, J. T., Marquard, J., Vogler, H., Mosca, G., Vertti-Quintero, N., et al. (2021a). 3D mechanical characterization of single cells and small organisms using acoustic manipulation and force microscopy. *Nat. Commun.* 12:2583. doi: 10.1038/s41467-021-22718-8
- Läubli, N. F., Gerlt, M. S., Wüthrich, A., Lewis, R. T. M., Shamsudhin, N., Kutay, U., et al. (2021b). Embedded microbubbles for acoustic manipulation of single cells and microfluidic applications. *Anal. Chem.* 93, 9760–9770. doi: 10.1021/acs.analchem.1c01209
- Le Bail, A., Billoud, B., Kowalczyk, N., Kowalczyk, M., Gicquel, M., Le Panse, S., et al. (2010). Auxin metabolism and function in the multicellular brown alga *Ectocarpus siliculosus*. *Plant Physiol.* 153, 128–144. doi: 10.1104/pp.109.149708
- Le Bail, A., Billoud, B., Le Panse, S., Chenivesse, S., and Charrier, B. (2011). ETOILE regulates developmental patterning in the filamentous brown alga *Ectocarpus siliculosus*. *Plant Cell* 23, 1666–1678. doi: 10.1105/tpc.110.081919
- Le Bail, A., Billoud, B., Maisonneuve, C., Peters, A., Cock, J. M., and Charrier, B. (2008). Initial pattern of development of the brown alga *Ectocarpus siliculosus* (Ectocarpales: Phaeophyceae) sporophyte. *J. Phycol.* 44, 1269–1281.
- Le Bail, A., and Charrier, B. (2013). “Culture methods and mutant generation in the filamentous brown algae *Ectocarpus siliculosus*,” in *Plant Organogenesis Methods in Molecular Biology*, ed. I. De Smet (Totowa, NJ: Humana Press), 323–332. doi: 10.1007/978-1-62703-221-6_22
- Macaisne, N., Liu, F., Scornet, D., Peters, A. F., Lipinska, A., Perrineau, M.-M., et al. (2017). The *Ectocarpus* immediate upright gene encodes a member of a novel family of cysteine-rich proteins with an unusual distribution across the eukaryotes. *Development* 144, 409–418. doi: 10.1242/dev.141523
- Michel, G., Tonon, T., Scornet, D., Cock, J. M., and Kloareg, B. (2010). Central and storage carbon metabolism of the brown alga *Ectocarpus siliculosus*: insights into the origin and evolution of storage carbohydrates in eukaryotes. *New Phytol.* 188, 67–81. doi: 10.1111/j.1469-8137.2010.03345.x
- Nehr, Z., Billoud, B., Le Bail, A., and Charrier, B. (2011). Space-time decoupling in the branching process in the mutant étoile of the filamentous brown alga *Ectocarpus siliculosus*. *Plant Signal. Behav.* 6, 1889–1892.
- Pei, H., Li, L., Han, Z., Wang, Y., and Tang, B. (2020). Recent advances in microfluidic technologies for circulating tumor cells: enrichment, single-cell analysis, and liquid biopsy for clinical applications. *Lab Chip* 20, 3854–3875. doi: 10.1039/d0lc00577k
- Peyrin, J. M., Deleglise, B., Saias, L., Vignes, M., Gougis, P., Magnifico, S., et al. (2011). Axon diodes for the reconstruction of oriented neuronal networks in microfluidic chambers. *Lab Chip* 11, 3663–3673. doi: 10.1039/c1lc20014c
- Popper, Z. A., Michel, G., Hervé, C., Domozych, D. S., Willats, W. G. T., Tuohy, M. G., et al. (2011). Evolution and diversity of plant cell walls: from algae to flowering plants. *Annu. Rev. Plant Biol.* 62, 567–590. doi: 10.1146/annurev-arplant-042110-103809
- Rabillé, H., Billoud, B., Tesson, B., Le Panse, S., Rolland, É., and Charrier, B. (2019a). The brown algal mode of tip growth: keeping stress under control. *PLoS Biol.* 17:e2005258. doi: 10.1371/journal.pbio.2005258
- Rabillé, H., Torode, T. A., Tesson, B., Le Bail, A., Billoud, B., Rolland, E., et al. (2019b). Alginates along the filament of the brown alga *Ectocarpus* help cells cope with stress. *Sci. Rep.* 9:12956. doi: 10.1038/s41598-019-49427-z
- Shamsudhin, N., Laeubli, N., Atakan, H. B., Vogler, H., Hu, C., Haerberle, W., et al. (2016). Massively parallelized pollen tube guidance and mechanical measurements on a lab-on-a-chip platform. *PLoS One* 11:e0168138. doi: 10.1371/journal.pone.0168138
- Siddique, R., and Thakor, N. (2013). Investigation of nerve injury through microfluidic devices. *J. R. Soc. Interface* 11:20130676. doi: 10.1098/rsif.2013.0676
- Simeon, A., Kridi, S., Kloareg, B., and Herve, C. (2020). Presence of exogenous sulfate is mandatory for tip growth in the brown alga *Ectocarpus subulatus*. *Front. Plant Sci.* 11:1277. doi: 10.3389/fpls.2020.01277
- Tong, Z., Segura-Feliu, M., Seira, O., Homs-Corbera, A., Del Rio, J. A., and Samitier, J. (2015). A microfluidic neuronal platform for neuron axotomy and controlled regenerative studies. *RSC Adv.* 5, 73457–73466. doi: 10.1039/c5ra11522a

- Zhou, X., Lu, J., Zhang, Y., Guo, J., Lin, W., Norman, J. M. V., et al. (2021). Membrane receptor-mediated mechano-transduction maintains cell integrity during pollen tube growth within the pistil. *Dev. Cell* 56, 1030–1042.e6. doi: 10.1016/j.devcel.2021.02.030
- Zhu, H., Fohlerova, Z., Pekarek, J., Basova, E., and Neuzil, P. (2020). Recent advances in lab-on-a-chip technologies for viral diagnosis. *Biosens. Bioelectron.* 153:112041. doi: 10.1016/j.bios.2020.112041

Conflict of Interest: The authors declare that the research was conducted in the absence of any commercial or financial relationships that could be construed as a potential conflict of interest.

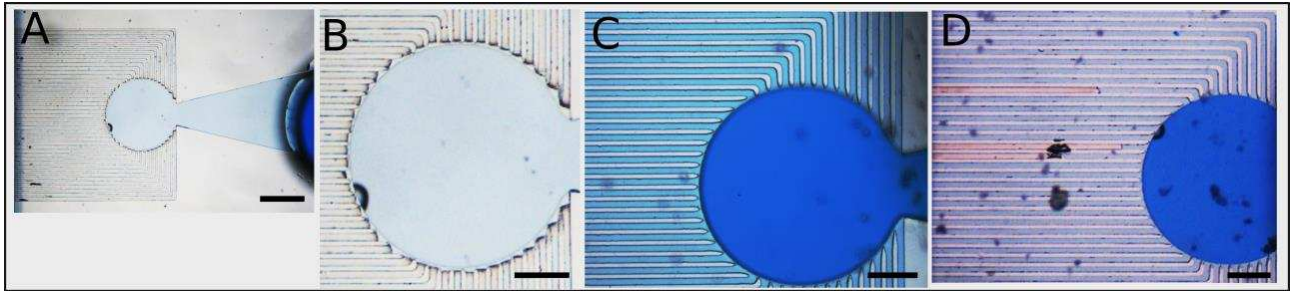
Publisher's Note: All claims expressed in this article are solely those of the authors and do not necessarily represent those of their affiliated organizations, or those of the publisher, the editors and the reviewers. Any product that may be evaluated in this article, or claim that may be made by its manufacturer, is not guaranteed or endorsed by the publisher.

Copyright © 2021 Charrier, Bosca, Nelson and Läubli. This is an open-access article distributed under the terms of the Creative Commons Attribution License (CC BY). The use, distribution or reproduction in other forums is permitted, provided the original author(s) and the copyright owner(s) are credited and that the original publication in this journal is cited, in accordance with accepted academic practice. No use, distribution or reproduction is permitted which does not comply with these terms.

Supplementary Material

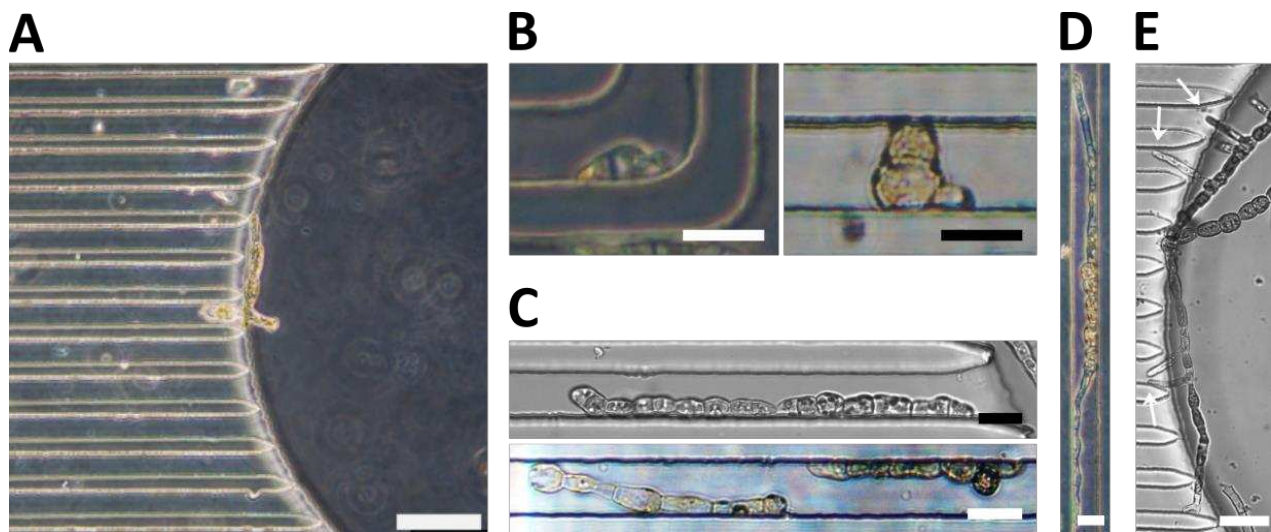
Growth and labelling of cell wall components of the brown alga *Ectocarpus* in microfluidic chips

Bénédicte Charrier, Samuel Boscq, Bradley J. Nelson, Nino F. Läubli



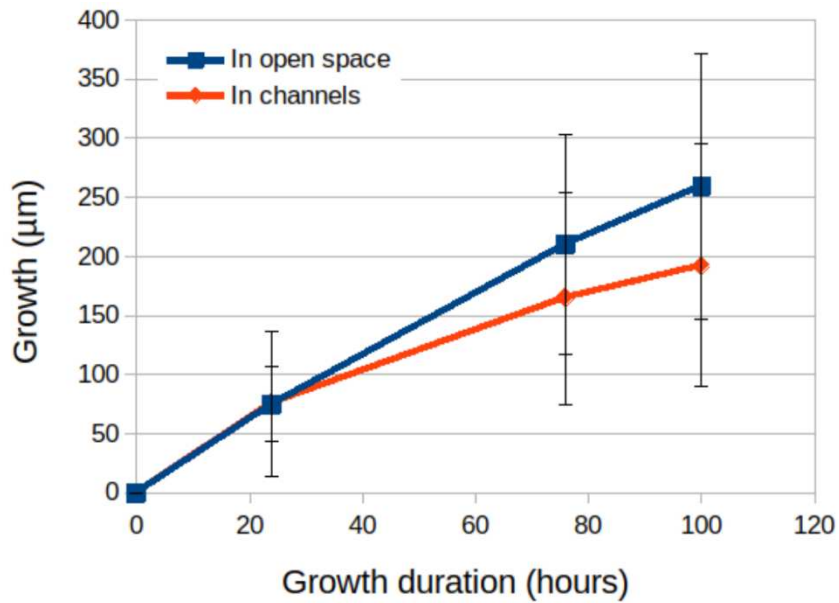
Supplementary Figure 1: Filling in the chips.

A solution of sea water with bromophenol blue was used to monitor the filling of the lab-on-chip device. (A) If pipetting pressure was too low, the solution did not fill the channels and remained in the chamber (the inlet is on the right of the photo). (B) Zoom-in on the channels entrance showing that the liquid did not get in. (C) Fully filled channels. (D) Partially filled channels where air remains trapped inside some channels. Scale bar: (A) = 500 μm , (B – D) = 200 μm .



Supplementary Figure 2: Pieces of *Ectocarpus* filaments stuck in the chamber and spore germination inside microchannels.

(A) A piece of fertile sporophytes blocked at the entrance of the channels. (B) Impaired spore germination inside microchannels: germination was delayed and occurred perpendicularly to the main channel orientation. (C) Apical growth for spores germinated inside microchannels was impaired, with shorter and less anisotropic apical cells and a slower growth rate. (D) Despite germination inside microchannels, cell differentiation through cell rounding occurred in some filaments. (E) A piece of a non-fertile sporophyte from which branches (white arrows) emerge and grow into the channels. Scale bar: (A) = 100 μm , (B - D) = 25 μm , (E) = 50 μm . All images were taken from devices with 25 μm wide channels.



Supplementary Figure 3: Comparison of specimen growth behaviour for different environments.




A graph comparing the growth between Ectocarpus filaments in open space environments (blue) and filaments growing inside microfluidic channels (red). The lengths of the filaments were characterised after 24, 76, and 100 hours with the initial length at the start of the measurement being set to 0 to allow for direct comparison of the growth behaviour. No statistical significance has been found between the growth rate in the open space and the confined environment with 15 and 22 samples, respectively.

Annexe 3: Cultivation and Imaging of *S. latissima* Embryo Monolayered Cell Sheets Inside Microfluidic Devices

[Supplementary Table 1](#)

Article

Cultivation and Imaging of *S. latissima* Embryo Monolayered Cell Sheets Inside Microfluidic Devices

Thomas Clerc ^{1,†} , Samuel Boscq ^{1,†}, Rafaele Attia ², Gabriele S. Kaminski Schierle ³, Bénédicte Charrier ^{1,*} 
and Nino F. Läubli ^{3,*} 

¹ Morphogenesis of Macroalgae, Laboratory of Integrative Biology of Marine Models, Station Biologique de Roscoff, CNRS, Sorbonne University, 29680 Roscoff, France

² Ecology of Marine Plankton, Laboratory of Adaptation and Diversity in the Marine Environment, Station Biologique de Roscoff, CNRS, Sorbonne University, 29680 Roscoff, France

³ Molecular Neuroscience Group, Department of Chemical Engineering and Biotechnology, University of Cambridge, Cambridge CB3 0AS, UK

* Correspondence: benedicte.charrier@cnrs.fr (B.C.); nl431@cam.ac.uk (N.F.L.)

† These authors contributed equally to this work.

Abstract: The culturing and investigation of individual marine specimens in lab environments is crucial to further our understanding of this highly complex ecosystem. However, the obtained results and their relevance are often limited by a lack of suitable experimental setups enabling controlled specimen growth in a natural environment while allowing for precise monitoring and in-depth observations. In this work, we explore the viability of a microfluidic device for the investigation of the growth of the alga *Saccharina latissima* to enable high-resolution imaging by confining the samples, which usually grow in 3D, to a single 2D plane. We evaluate the specimen's health based on various factors such as its growth rate, cell shape, and major developmental steps with regard to the device's operating parameters and flow conditions before demonstrating its compatibility with state-of-the-art microscopy imaging technologies such as the skeletonisation of the specimen through calcofluor white-based vital staining of its cell contours as well as the immunolocalisation of the specimen's cell wall. Furthermore, by making use of the on-chip characterisation capabilities, we investigate the influence of altered environmental illuminations on the embryonic development using blue and red light. Finally, live tracking of fluorescent microspheres deposited on the surface of the embryo permits the quantitative characterisation of growth at various locations of the organism.

Keywords: microfluidics; microfluidic cultivation; brown alga; *Saccharina*; embryogenesis; lab-on-a-chip; microsphere tracking; kelp; laminariales; blue light; immunocytochemistry; time-lapse microscopy



Citation: Clerc, T.; Boscq, S.; Attia, R.; Kaminski Schierle, G.S.; Charrier, B.; Läubli, N.F. Cultivation and Imaging of *S. latissima* Embryo Monolayered Cell Sheets Inside Microfluidic Devices. *Bioengineering* **2022**, *9*, 718. <https://doi.org/10.3390/bioengineering9110718>

Academic Editors: Janina Bahnemann and Sofia Arshavsky-Graham

Received: 30 September 2022

Accepted: 17 November 2022

Published: 21 November 2022

Publisher's Note: MDPI stays neutral with regard to jurisdictional claims in published maps and institutional affiliations.



Copyright: © 2022 by the authors. Licensee MDPI, Basel, Switzerland. This article is an open access article distributed under the terms and conditions of the Creative Commons Attribution (CC BY) license (<https://creativecommons.org/licenses/by/4.0/>).

1. Introduction

While the level of knowledge about the biology of marine organisms lags far behind that of terrestrial organisms, climate change accentuates the need to shift gears to fill these gaps. Indeed, a large number of marine organisms are under increasing threat [1,2] and further insights into how these organisms reproduce, develop, and grow are necessary to develop appropriate protection strategies [3]. Algae are one of these organisms, as they are the oceans' primary producer and are especially sensitive to increasing temperatures [4]. Multicellular algae thrive along all coastlines of our planet from the tropics to the polar circles, where they are at the top of the local trophic chain [5]. The kelp, a group of brown algae, grow to lengths of several metres within a few months, which makes them the most conspicuous seaweeds. Furthermore, several kelp species, such as *Saccharina species pluralis*, are widely cultivated in Asia and western Europe for their economic value as a source of food and of hydrocolloids useful in industry [6]. Yet, how they develop is only scarcely known and, especially, the mechanisms that regulate the early steps of their embryogenesis, which are essential for both our understanding of the developmental processes and initial

advances towards aquacultures, are a scientific black box [7]. One of the main reasons for this lack of insight is the difficulty of imaging developing organisms in a dynamic way that permits us to obtain accurate and quantitative information at the tissue and cellular levels. While the early embryo is a monolayered cell sheet [8], its upward growth prevents the acquisition of focused images of the entire embryo structure. Therefore, we introduce an experimental protocol enabling the cultivation of the embryos of the kelp *Saccharina latissima*, also known as sugar kelp, in horizontal confinement. Eggs and zygotes were loaded into the microfluidic chip forcing further growth into only two spatial dimensions. Coupled to time-lapse brightfield and fluorescence microscopy, this approach permitted us to quantitatively monitor each step of the development of the embryos in a dynamic way and in different culture conditions, including the influence of liquid renewal for on-chip cultures. We evaluated the usability of microfluidic growth chambers through the study of the specimens' developmental stages and compared their performance to samples cultured in standard open-space in vitro environments using lab Petri dishes. Furthermore, by building on the improved optical monitoring capabilities, we quantify the effect of varying environmental illumination by analysing changes in the embryonic development induced through the application of blue and red light. Finally, we demonstrate the amenability of microfluidic devices to monitor local variations in growth through confocal microscopy of on-chip calcofluor staining, the tracking of fluorescent microspheres on the surface of the embryos, as well as the immunolocalisation of the specimen's cell wall. Altogether, these tools demonstrate the suitability of microfluidic environments for the detailed investigation of embryonic growth, cell growth, and cell division patterns within the monolayered cell sheet of the embryo of the kelp *Saccharina latissima*.

2. Results and Discussion

2.1. Characteristics of *S. latissima* Development and Growth

Saccharina latissima is a prominent marine model organism of interest for developmental studies due to its heteromorphic diplophasic life cycle, as shown in Figure 1a [9]. Its diploid sporophyte grows following the successful fertilisation of the egg via a sperm cell. Several parallel cell divisions of the zygote produce an embryo that first consists of a stack of cells, before widening by perpendicular cell divisions to form a two-dimensional monolayered cell sheet called a lamina or blade. This morphology persists for several days until the embryo reaches a size of about one thousand cells, after which the cells start differentiating and initiate the thickening of the lamina by tilting their cell division plane into the third spatial axis.

This noteworthy sequential and tiered growth, further enhanced by the morphological simplicity of *S. latissima*, makes it a suitable model to investigate the development of brown algae. Additionally, the cell arrangement of the embryo is particularly original, as it depicts a grid in which cells are in contact with their neighbours by means of "four-cell junctions" [10]. This grid or "chocolate bar"-type of cell organisation is not observed in plants and animals under normal conditions as intrinsic mechanisms prevent their formation [11,12].

Given the repeated change in its dimensional growth, the detailed study of *S. latissima* embryos relies on the availability of methods suitable to assess the whole embryonic development in a single plane. However, *S. latissima* embryos, when cultured in open environments such as the sea or in vitro Petri dishes, grow mainly upright—including twisted and curved specimens—with only 9.7% of embryos growing parallel or nearly parallel to the bottom of the Petri dish. This makes optical microscopy-based observations of the whole embryo, especially in combination with time-lapse imaging, almost impossible and prevents accurate assessments of their growth rates or the mapping of cellular features within living embryos. Figure 1b shows an embryo growing in 3D while being attached to the glass bottom of a Petri dish with neither its stipe nor its lamina being fully in focus, demonstrating the limited accessibility for optical evaluations. Hence, the development of novel protocols permitting the detailed observation of the whole embryo by restricting

growth to a single focal plane is crucial to further our understanding of the organism's development and growth behaviour.

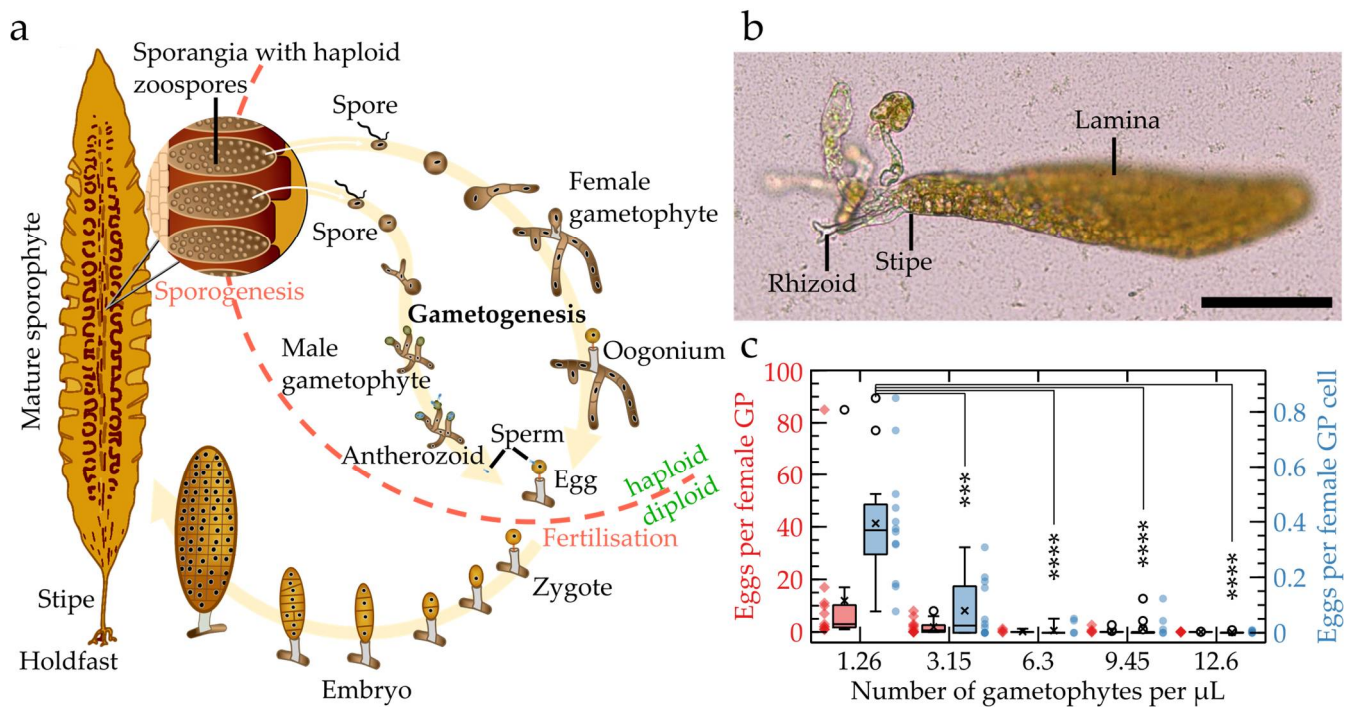


Figure 1. Biological specimen and density impact on culture. (a) Sketched life cycle of *S. latissima*. The mature sporophyte produces mobile zoospores that will develop into female and male filamentous gametophytes. Eggs hatched by the female gametophyte are then fertilised by swimming sperm cells released by the male gametophyte. Upon a series of parallel cell divisions, the resulting zygote develops into a multicellular embryo still attached to the female gametophyte before it develops its own attachment system first made of rhizoids (shown in 1b) and then a holdfast. (b) Optical microscopy image of a ~150-cell *S. latissima* embryo growing in a glass bottom Petri dish. Only the base, which is attached to the bottom of the Petri dish by the rhizoids, is in focus. The lamina is blurred as it is growing vertically within the water column. (c) Influence of culture density on egg release in open space expressed as the number of eggs per female gametophyte (GP, red) and number of eggs per total number of female gametophyte cells (blue). The number of eggs released by the female gametophytes is drastically reduced at higher densities of both female gametophytes and number of cells of female gametophytes. Asterisks indicate statistically significant differences relative to 10 μL of stock gametophytes analysed using one-way ANOVAs (see detailed protocol in Materials and Methods). No significant differences were detected for eggs per female gametophyte (red). Scale bar: 100 μm .

In addition, the in vitro cultivation of *S. latissima* embryos is further complicated due to the release of cues by the algae which reduce the reproduction success, as reported in [13]. Given the reduction in the liquid volume within microfluidic growth chambers compared to open-space cultivation, we, therefore, investigated how the density of *S. latissima* cultures impacts the production of eggs. We inoculated Petri dishes with five different concentrations of a mixture of short male and female gametophyte filaments (10, 25, 50, 75, and 100 μL in 2 mL of sea water, which relate to concentrations ranging from 1.26 to 12.6 gametophytes per μL). Figure 1c and Supplementary Figure S1 show that, while the number of eggs per gametophyte did not significantly change (red), increasing the density of gametophytes (to more than 1.26 gametophytes per μL) significantly reduced the rate of egg releases per total number of female gametophytes cells. Additionally, while no egg releases were observed at higher concentrations, ongoing maturations of gametophytic cells into oogonia were still monitored for all concentrations. In fact, oogonium differentiation was reverted into

vegetative cells, as the cells started to divide and produce additional vegetative filaments (Supplementary Figure S1f). Altogether, this suggests that *Saccharina latissima* gametophytes negatively control egg differentiation and release in high culture densities, which is potentially caused through the secretion of growth-inhibitory molecules in agreement with [13]. Hence, this result highlights that the number of gametophytes doomed to be inoculated inside the chips must be small enough to ensure the production of a sufficient number of embryos available for observation.

2.2. Microfluidic Cultivation of *S. latissima* Embryos

Due to its ease of fabrication and its biocompatible properties, polydimethylsiloxane (PDMS)-based microfluidics is of increasing relevance for developmental biology [14] and has been widely applied for the investigation of various small organisms ranging from plant specimens [15–17] to animal models [18–22]. Furthermore, microfluidic-based cultivation has recently been reported as a suitable tool for the study of the filamentous growth of the brown alga *Ectocarpus silicosus* [23].

Here, we propose a PDMS-based microfluidic device capable of limiting the specimen's growth to a single focal plane while minimising the potential limitations induced by nearby channel walls or similar constrictions (Figure 2a,b). As detailed in the Materials and Methods section, the device consists of a single-layer microfluidic chamber with a height of 25 μm to accommodate *Saccharina* embryos with an average thickness of approximately 15 μm . Given the chamber's large in-plane dimensions, a grid of micropillars is used to prevent the chamber from collapsing, while also simplifying the loading procedure through the increased availability of surface area to which the specimens can attach. The PDMS structures are fixed to glass bottom Petri dishes before being filled and submerged in sea water. The application of Petri dishes reduces the chance of contaminations through the additional cover of the sample via a lid and allows for the simplified transfer of the specimens between incubation chambers and microscopy setups, such as those used for extended time-lapse imaging under controlled environmental conditions (Supplementary Figure S2).

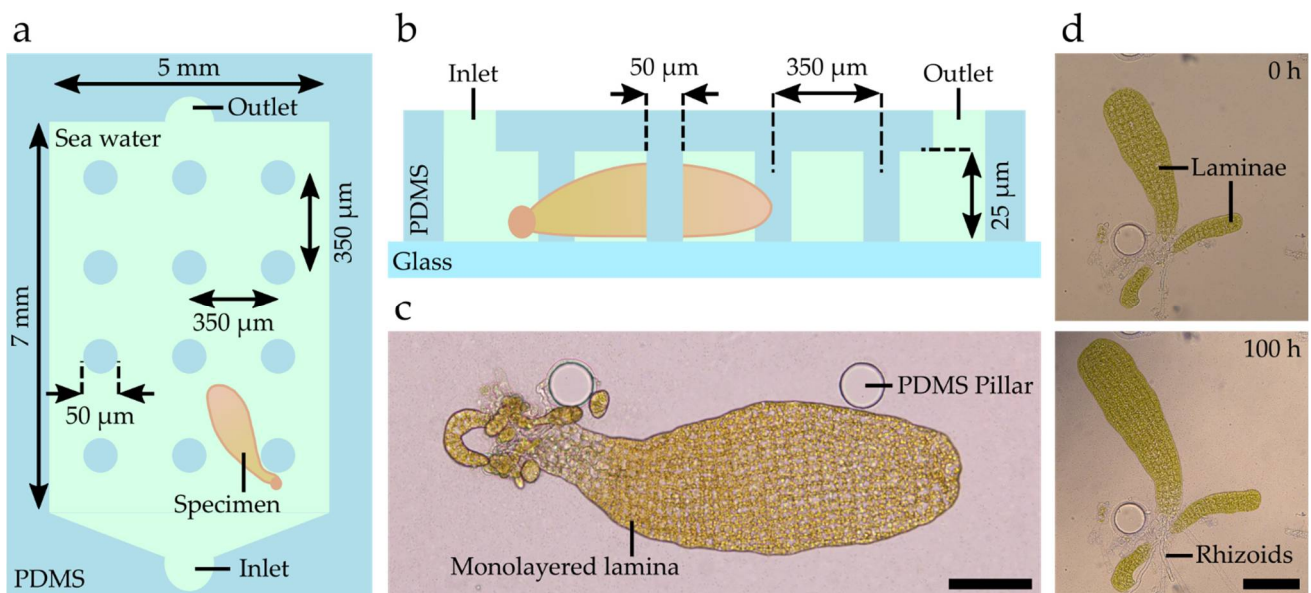


Figure 2. Microfluidic device enabling horizontally constrained growth of *Saccharina* culture. (a) Sketch of the microfluidic device (top view) showing the main chamber containing a grid of PDMS pillars as well as the inlet and outlet of the device. (b) Sketch of the side view of the microfluidic device with a constant chamber height of 25 μm and PDMS pillars with a diameter of 50 μm and a separation of 350 μm . (c) Brightfield image of a *Saccharina* monolayered lamina growing inside the device. This embryo was grown in a Petri dish before inoculation. All cells of the lamina are within a single focal plane. (d) Comparison of the same embryo growing inside the chip over a period of 100 h. Scale bars: 100 μm .

To assess the suitability of microfluidic cultivation, the chips were inoculated with different types of algal material, i.e., (i) unfertile and (ii) fertile female and male gametophytes, as well as (iii) female gametophytes with zygotes. When inoculated with gametophytes previously induced under white light for one week, the differentiation of eggs and sperm cells took place as early as 1 day after inoculation (see egg release in Supplementary Movie M1), which is similar to what has been observed when the material was cultured in open environments [24]. In contrast, when fertile gametophytes were inoculated, the first zygotes were observed 1 to 2 days after inoculation. Finally, inoculated zygotes initiated embryogenesis immediately after inoculation. Imaging the embryo's contour and the cell arrangement was easy as the lamina was located horizontally (Figure 2c). Time-lapse microscopy further showed that the cell division pattern within the embryo lamina and the formation of rhizoids from the base of the embryo took place as observed in open environments (Figure 2d and Supplementary Movie M2).

We further assessed the maximum duration of living embryos inside the chip. Although the embryos remained alive during the whole 12-day monitoring period, a decrease in pigmentation was observed after 9 days (data not shown). Hence, it is worth noting that the monitoring of *S. latissima* growth within these chips should not be extended beyond 9 days, which, however, is sufficient for the detailed evaluation of its embryonic development.

Additionally, to prevent a lack of nutrients caused by an increase in culture density while simultaneously diluting potential growth-inhibitory molecules released by the neighbouring specimens as described previously (see Figure 1c and Supplementary Figure S1), the use of a continuous flow or periodic liquid renewal was investigated. As the application of a continuous liquid exchange via a hydrostatic pressure difference has been found practically unfeasible (see Materials and Methods), the use of a pump is recommended. While the presented work relied on a pressure controller, in contrast to a passive solution, pumps have the advantage of permitting periodic actuations, which enables the use of a broad range of affordable, non-task-specific equipment, such as peristaltic pumps, even for microfluidic applications. To allow for continuous liquid exchange while preventing potentially damaging hydrodynamic forces, the pressure controller was set up to renew the volume of the medium inside the chip roughly 100 times per day.

We demonstrated that the proposed microfluidic chips are capable of providing environmental conditions suitable for the growth of *Saccharina* embryos in vitro, including cell growth, differentiation, e.g., for rhizoid formations, and growth of the laminae. However, it is worth highlighting that the current flow control and system performance could be further enhanced by replacing the applied system with higher-end options such as dedicated microfluidic syringe pumps. In the following sections, we assess whether the conditions produced by the confined environment of the microfluidic device allow for the maintenance of the early developmental transitions from the egg to the formation of an early embryo and, hence, their study using state-of-the-art microscopy techniques.

2.3. Assessment of *Saccharina* Developmental Steps inside Microfluidic Devices

The growth of *Saccharina* starts with several identified embryogenetic steps [8]. These steps are essential for the specimen's development as they ensure the establishment of the two main body planes of the adult algae, i.e., the apico-basal and the medio-lateral axes. However, thus far, the effect of increasing temperatures and lower pH conditions induced by climate change or the impact of chemicals and drugs on the specimen's development are unknown. Hence, the interest of these chips for further studies aiming to explore the possible consequences for the embryogenesis of *Saccharina latissima* depends on the chip's amenability to allow *Saccharina* to undertake and achieve these embryogenetic steps. Therefore, we performed a comparison of the main developmental steps observed between the algal specimens growing inside microfluidic devices and outside the PDMS structure, i.e., in the same glass bottom Petri dishes. The embryogenetic steps of *S. latissima*, as introduced in Figure 1a, are 1. the egg release, 2. the fertilisation of the egg by the sperm cells, 3. the first, parallel cell divisions of the zygote leading to a stack of ~8 cells, and 4.

the widening of the embryo by changing the planes of the cell division to 90° from the initial orientation.

Figure 3 shows that all of the abovementioned steps were successfully conserved within the device. The release of eggs inside microfluidic chips has been observed repeatedly (Figure 3a) and the eggs were successfully fertilised (Figure 3b). However, the very first cell division of the zygote was rarely observed for on-chip cultures as several eggs struggled to pass this developmental stage. This can be explained by the weak attachment of the eggs to the female gametophytes, which only consists of their flagella [25], in combination with substantial shear forces and high peak flow rates (estimated at 10^1 – 10^2 mm s⁻¹) inside the chip during the inoculation. To circumvent this issue, vegetative gametophytes can be loaded to have eggs differentiated and released into the device long after the inoculation. Another observation is that zygotes managing to induce the first cell division often fail to elongate and, hence, to break the initial radial symmetry of the eggs.

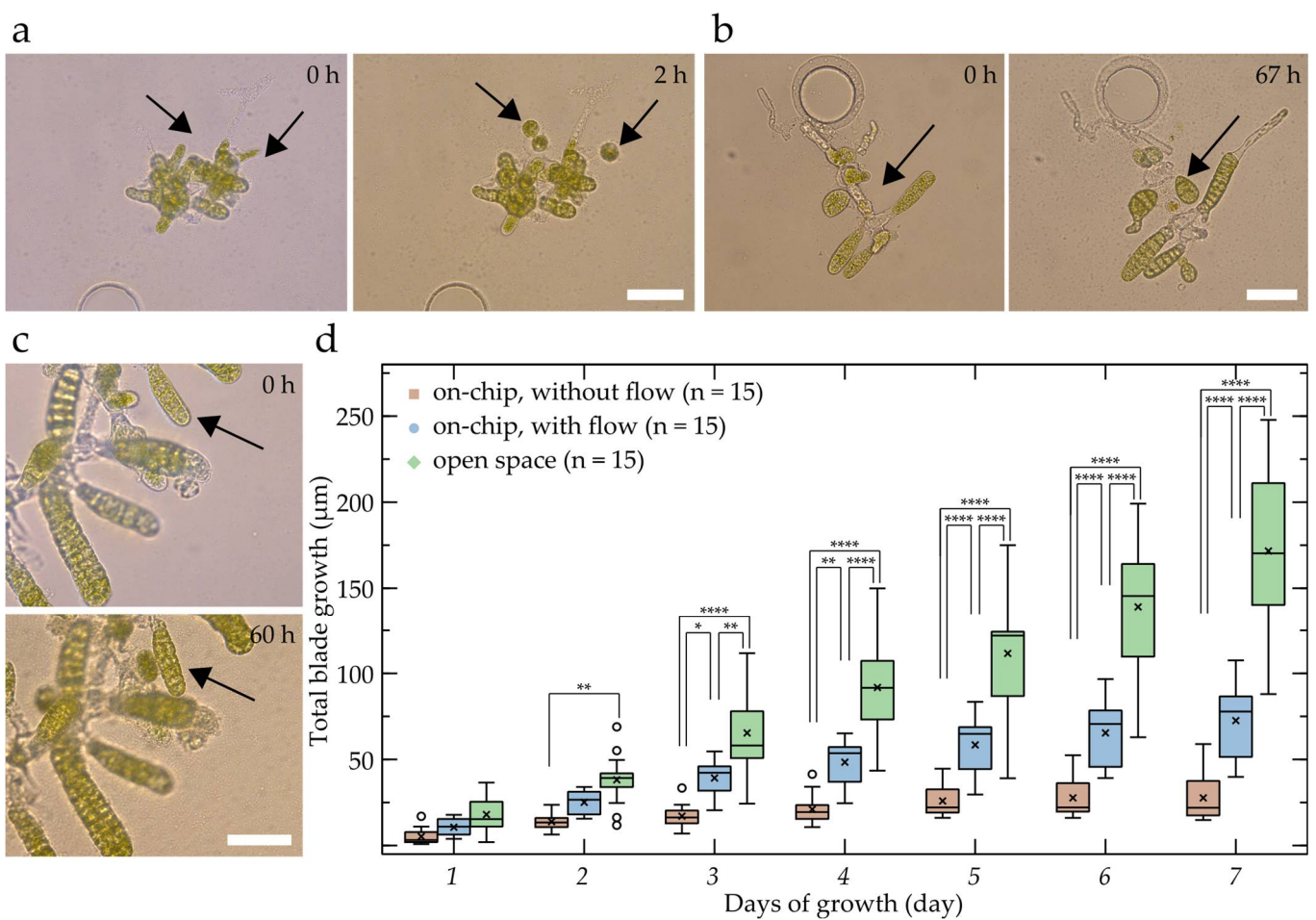


Figure 3. Assessment of the normal growth in the microfluidic device. Different developmental stages of *S. latissima* embryos observed while growing inside the chip: (a) induction of gametogenesis through egg release (three eggs have been released), (b) zygote formation after fertilisation and early embryo development (two cell divisions took place (arrow)), (c) first longitudinal cell division allowing growth and embryo expansion in the medio–lateral axis (arrow). (d) Growth rate comparison between embryos growing inside, with and without flow, as well as outside the chip. Statistically significant differences between the blade lengths of the different conditions within each day are indicated by the asterisks and were analysed using a two-way ANOVA (see Materials and Methods section). Scale bars: 50 µm.

For the abovementioned reasons and if the devices are only intended to allow for the detailed investigation and imaging of laminae, it is recommended to inoculate either elongated zygotes or embryos, which were shown to thrive within the device and consistently developed into large 2D monolayer laminae (Figure 3c and Supplementary Movie M2).

In addition to the evaluation of the different developmental stages, the impact of the microfluidic device on the specimen's growth behaviour has been investigated. Comparing the growth rate inside the device with and without liquid renewal as well as outside the device, i.e., in the same Petri dish next to the PDMS structure, provided us with clues about the general health of the specimens growing inside the device and allowed for the detection of possible drawbacks, e.g., in terms of access to nutrients. To quantify the effect of the device onto the growth of the embryo, we measured the apico-basal growth rate, i.e., the daily change in distance between the stipe and the apex of the lamina in both the specimens growing inside the chips and specimens growing in an open environment. For the latter condition, only specimens with a horizontal or near-horizontal orientation were considered to reduce measurement errors induced by the out-of-plane growth.

As shown in Figure 3d, the embryos inside the microfluidic devices with liquid renewal (blue, $n = 15$) kept growing qualitatively similar to the specimens outside the chip (green, $n = 15$), although, due to the low growth rates, no significant differences in the total blade growth between consecutive days were detected for specimens with liquid renewal following day 3 (or throughout the experiment for specimens without liquid renewal). Additionally, the growth dynamics of the specimens in devices with liquid renewal were similar to those of specimens growing in open space (Supplementary Figure S3a), with no significant differences in growth rates being observed within individual conditions for consecutive days. However, as indicated, the overall growth rate inside the device was, even with liquid renewal, substantially lower throughout the growth period and the differences in growth rate became significant after day 2, which further led to significant differences in the total blade growth from day 3 onwards. Interestingly, the length-width ratio (Supplementary Figure S3b) of the on-chip specimens with liquid renewal and samples growing in open space were not significantly different, while the outliers with higher ratios in the open environment can be accounted for by occasional twistings of the blades which reduce their width. The generally observed lower growth rates inside the chip could be caused by a reduction in light intensity due to absorption by the PDMS layer [26]; however, additional effects caused by the spatial confinement cannot be excluded. Furthermore, it is important to note that the on-chip growth rates and growth behaviours were only compared to specimens growing (near-)horizontally within the same Petri dishes, which suggests that variations between the observed conditions caused by gravitational effects can be neglected. However, gravimetric factors, such as gravitropism, which have been argued to influence growth hormones, e.g., auxin, in algal development need to be considered when comparing developmental data obtained via horizontally constricting devices, such as our microfluidic setup, to other literature [27,28]. Additionally, while our approach might be suitable for gravimetric investigations by mounting the chip vertically onto an appropriate microscopy setup, further design adjustment might be required, such as the re-orientation of the chamber axis to enable horizontal liquid renewal and prevent hydrostatic pressure differences or a reduction in chamber width to ensure equal distribution of nutrients and reliable medium exchange.

Finally, the applicability of the chip for physiological studies has been tested. Sea water filters longer wavelengths more than shorter ones, resulting in red light being unable to penetrate water columns deeper than 2 metres, while blue light is present up to 200 metres deep depending on the turbidity of the water. Brown algae live attached to the bottom of the sea at depths of 1 to 40 metres along coastal regions and several studies have already shown the developmental response of *Saccharina* to blue light at different stages of its life cycle and especially for the growth of the gametophytes and the induction of fertility [29,30]. Here, we tested the suitability of the chip to investigate the impact of blue and red lights on the development of the early embryos of *Saccharina*. *Saccharina* embryos

were grown in the chip exposed to either red or blue light (Supplementary Figure S4) for five days. Figure 4a,b,g,h highlights the difficulties concerning the evaluation and imaging of embryos growing outside the chip, as illustrated by the slices of strong red fluorescence (chloroplast autofluorescence) cutting through the embryos. Embryos within the chip displayed different morphologies depending on whether they were growing under blue (Figure 4c–f) or red (Figure 4i–l) light. Embryos under blue light displayed distorted morphologies characterised by a higher length/width ratio (Figure 4d–f) and several growth axes (Figure 4d). In contrast, embryos grown under red light (Figure 4i–l) displayed a morphology similar to the one under white light (see Figure 2c,d). These results not only strengthened the conclusion by Wang et al. based on experiments with embryos grown in open environments (glass slides in a flask or Petri dish), which reported higher length-to-width ratios under blue light [31], but also showed that our device provides images permitting accurate measurements by forcing the *Saccharina* blades to grow horizontally within the chip. The amenability of the chip design for confocal microscopy will also open the way for deeper studies concerning the role of the blue light receptor Aureochrome [32] during *Saccharina* embryogenesis.

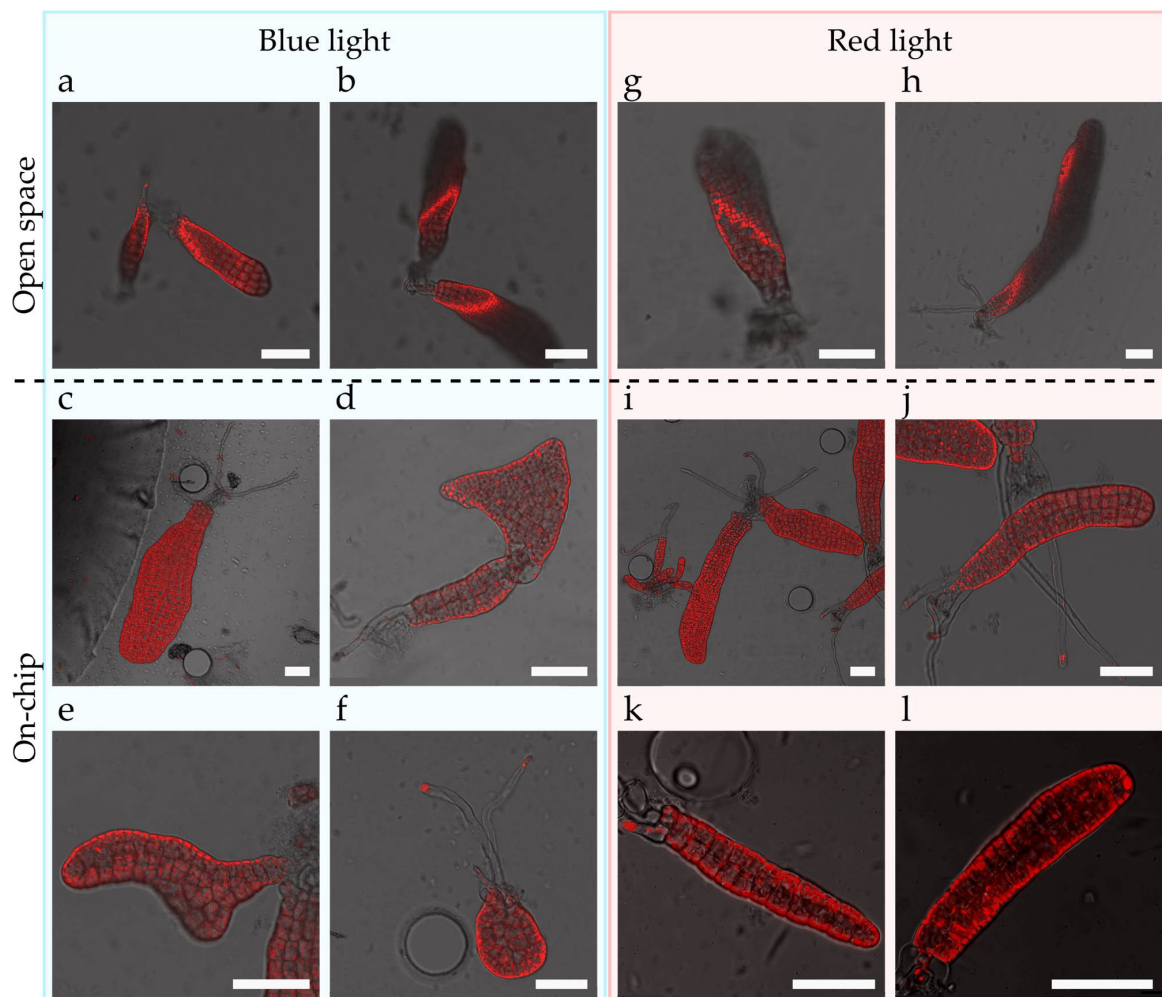


Figure 4. Morphogenetic impact of blue and red lights in the embryogenesis of *Saccharina*. (a,b,g,h) Confocal microscopy images of embryos grown outside the chips. (c–f, i–l) Confocal microscopy images of embryos growing inside the chips. (a–f) Embryos growing under blue light. (g–l) Embryos growing under red light. The embryos grown under blue light display distorted morphologies. Note that embryos with distorted shapes were also present outside the chip under blue light. Red: autofluorescence of the chloroplasts. Scale bars: 50 μm .

2.4. Cell Biology Protocols to Accurately Image the Cells of the Kelp Embryos

Increasing our knowledge of the mechanisms involved in the embryogenesis of kelp requires not only quantitative values of the growth rate, such as those obtained by time-lapse brightfield microscopy, but also cell characterisations at the sub-cellular level. The use of transgenic lines expressing fluorescent proteins would be the ideal approach, as they permit us to monitor the localisation of proteins over time in living algae. However, while the expression of reporter genes was reported in *S. japonica* via a biolistic approach [33], it has never been repeated and, since, doubts about this approach in *Saccharina* were raised [34]. Therefore, we assessed the efficiency of several cell biology protocols that were previously developed for the filamentous brown alga *Ectocarpus* [35,36].

First, the cell wall was labelled with calcofluor white. Cellulose, a rigid polymer of $\beta(1-4)$ glucose reported in brown algae's cell walls at a level of approximately 10% [37], can be stained by calcofluor white, that is a vital fluorescent probe that binds to β -glucans [38]. We used it to stain *S. latissima* gametophytes and embryos inside the chip. Figure 5a,b displays a uniformly labelled embryo, as a representative of the whole population inside the chip. In addition, we did not observe any loss of specimen during this experimental procedure, supporting the fact that the gentle washing steps were compatible with this protocol. Interestingly, as calcofluor white is a vital stain, monitoring the fluorescent signal over time makes studies of the growth dynamics within the chip possible.

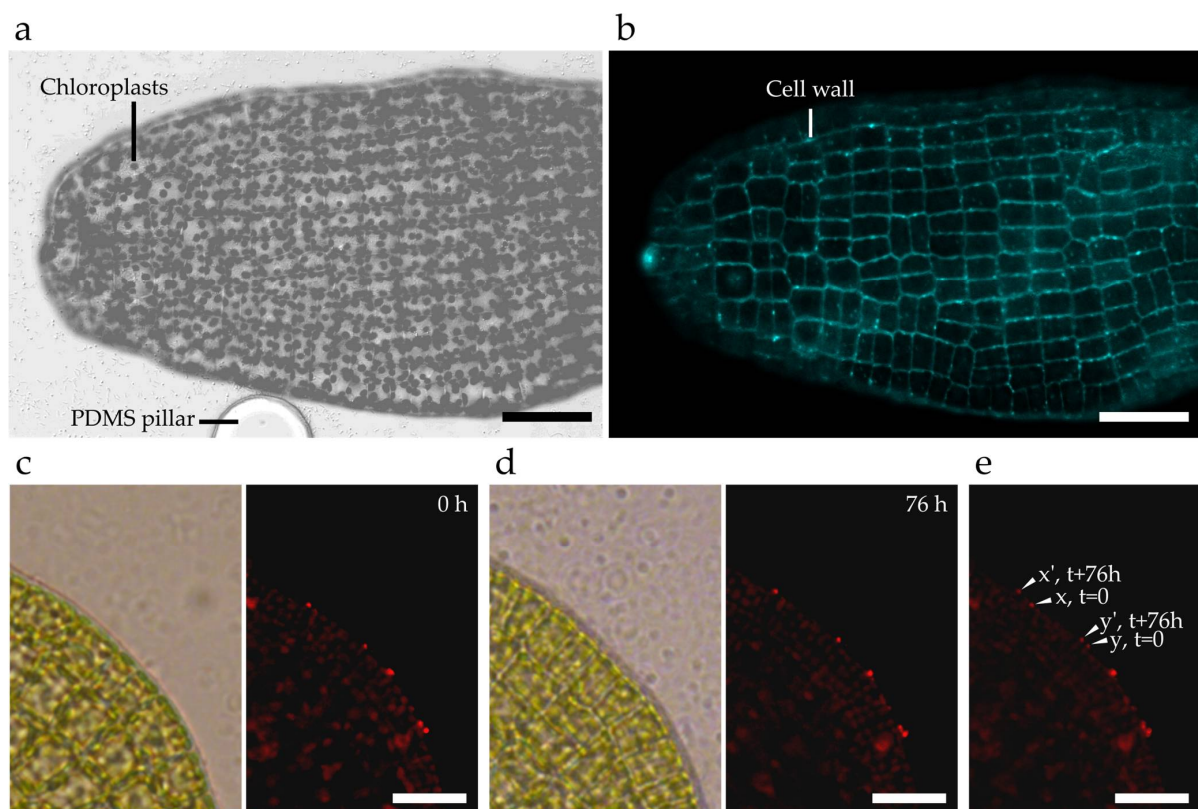


Figure 5. Microscopy-based imaging using on-chip cultures to track localised specimen growth. (a) Brightfield confocal microscopy image of an embryo blade with the auto-fluorescent chloroplasts (displayed here as grey dots). (b) Calcofluor white imaging of the same *Saccharina* blade. (c–e) Time-lapse tracking of fluorescent microspheres. (c) Brightfield and fluorescence microscopy images of functionalised red-fluorescent microspheres with a diameter of 200 nm were attached to the side of a monolayered cell sheet inside a microfluidic device on day 0. (d) The same location of the *S. latissima* lamina 76 h later. (e) Overlap of the two fluorescence microscopy images aligned. The time-lapse tracking highlights the difference in growth between the location of microsphere x (to x') and microsphere y (to y') for a growth period of 76 h. Scale bars: (a,b) 50 μm , (c–e) 25 μm .

As the microfluidic device restrains growth to a 2D plane, it further allows us to obtain accurate outlines of the embryo shape and the precise contour of cells with calcofluor labelling. To add temporal and spatial precision to the growth mode of the algal specimen, we used fluorescent microspheres that stick to the cell surface. Microsphere-based tracking has previously been proven suitable to study growth in microfluidic environments, e.g., by Shaw et al. for the investigation of *Medicago truncatula* root hairs [39]. Additionally, the same beads have successfully been applied for the study of the brown alga *Ectocarpus* [36]. Hence, measuring the relative displacement of a microsphere over time in the same focal plane permits us to obtain quantitative data about the rate and direction of growth. The precision of the measurements directly depends on the size of the beads (down to 200 nm in the present study; see below) and on the parameters of the image acquisition (resolution down to ~200 nm in confocal microscopy). This high level of spatial accuracy should permit monitoring the trajectory of the beads, a necessary insight to further characterise the mode of cell growth [40].

Given the limited amount of detail currently known about the various developmental stages of the specimen and the cell wall of brown algae in general, different types of microspheres were tested, i.e., green-fluorescent carboxylate-coated spheres with a diameter of 500 nm and red-fluorescent amine-coated spheres with a diameter of 200 nm. Although the amine-coated red-fluorescent microspheres seemed to be adsorbed onto both gametophytes and sporophytic embryos, the carboxylate-coated green-fluorescent microspheres attached almost exclusively to gametophytes. This further demonstrates that *Saccharina*'s outer cell wall composition differs in gametophytes and sporophytes and that the type of beads has to be carefully chosen.

Using the derived parameters, we observed that the microspheres (pink dots) successfully attached to the outline of the embryos as shown in Supplementary Figure S5. While the majority of particles were present around the blade, additional microspheres were present in other focal planes. Furthermore, both the shapes and the autofluorescence wavelength of the chloroplasts (Supplementary Figure S5) show that the embryo is in good health. This latter observation further supports our conclusions based on the on-chip growth rates.

The resulting time-lapse monitoring of a growing embryo coated with red-fluorescent microspheres is shown in Figure 5c–e. The overlay of the two fluorescence microscopy images recorded at $t = 0$ h and $t = 76$ h display the rate of growth.

Finally, to assess the possibility to perform experiments of immunolocalisations within the chip, we used the BAM10 monoclonal antibody that recognises guluronates present in the cell wall of brown algae [37]. Figure 6 shows that, similar to embryos growing outside the chip (Figure 6a), BAM10 successfully labels the surface of early (Figure 6b) and late (Figure 6c) embryos within the device. In addition, in both conditions, BAM10 antibodies label the dome of tip-growing gametophytic cells (Figure 6a, right side) as well as rhizoids (Figure 6d, inside the device)—a pattern that is reminiscent of the BAM10 labelling of the apical cell of the filament of the brown alga *Ectocarpus* [41]. Hence, this work demonstrates that immunolocalisation experiments aiming at localising cell wall components in both embryo and gametophyte tissues of *Saccharina* are achievable inside the microfluidic chip. This opens avenues for the study of spatial distributions of molecular factors at the tissue and even organism scale, made possible thanks to the in-plane imaging conditions provided by the chip.

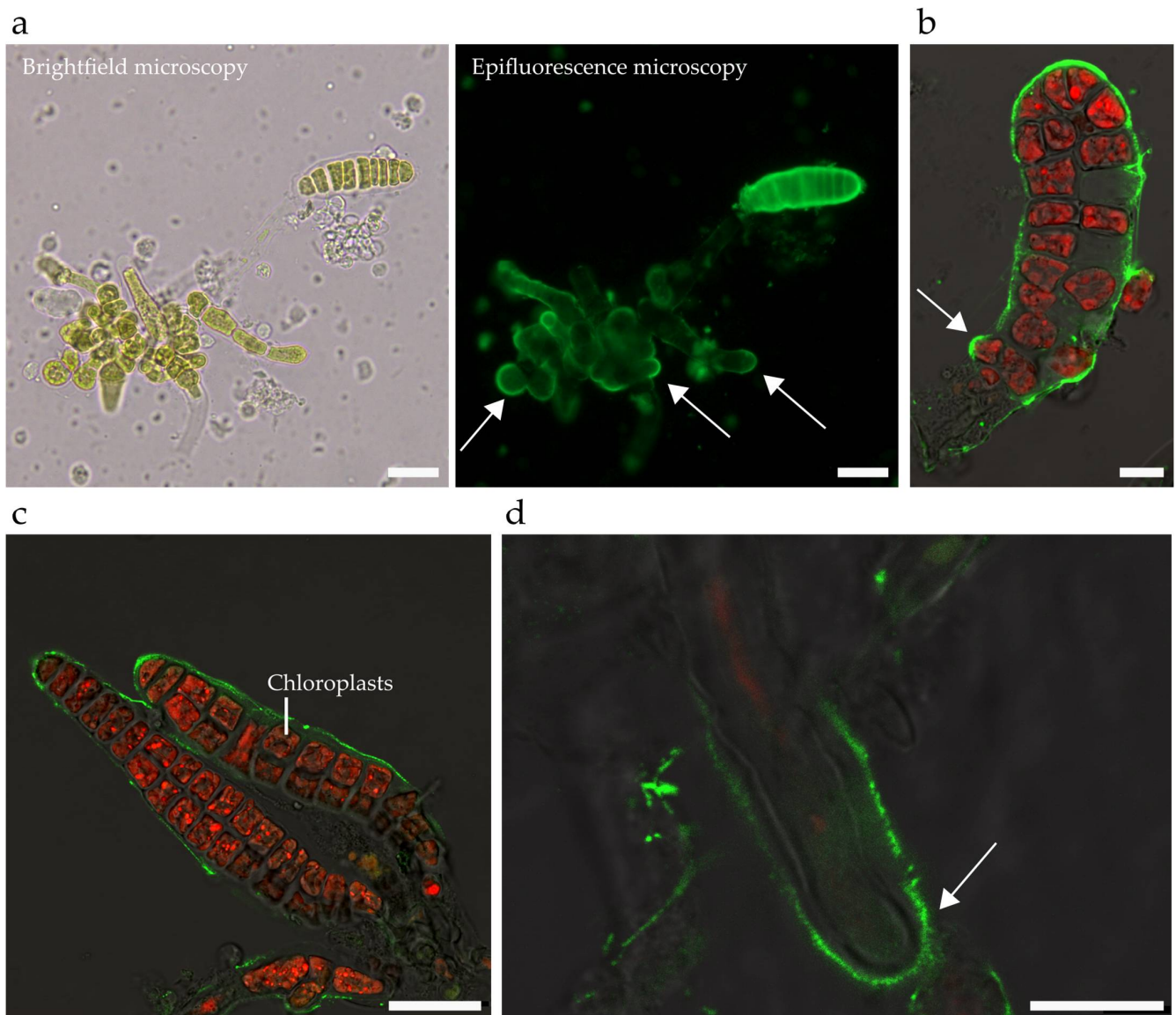


Figure 6. Immunolocalisation of guluronate alginates in the cell wall of *Saccharina* embryos. Different stages and tissues of *Saccharina* embryos are shown, from the zygote stage to the ~25-cell stage. (a) Labelled embryos grown in a Petri dish. An eight-cell-stage embryo showing a strong labelling in the outer cell wall is displayed (left: brightfield; right: epifluorescence), in addition to eggs, zygotes, and cells of the gametophytes showing labelling at the tip (white arrows). (b–d) Embryos growing within the microfluidic chip. (b) A ~15-cell-stage embryo labelled in the outer cell wall. Note the emerging rhizoid, which is strongly labelled (white arrow). (c) ~25-cell embryos showing a labelled outer cell wall. (d) Rhizoid showing an accumulation of guluronates in its dome (white arrow) and distal shanks. Green: Alexa-488 secondary antibody recognising the BAM10 primary antibody. Red: Autofluorescence of the chloroplast (displayed only in b, c, and d. Note that rhizoids have very few chloroplasts, which explains why the red autofluorescence signal is weak). The contrast has been enhanced linearly in b and c. Scale bars: (a,c) 25 µm, (b,d) 10 µm.

3. Conclusions

The in vitro investigation of marine specimens is crucial to further our understanding of their development and their interaction with these complex environments. Here, we report the first use of microfluidic chips for the study of kelp, specifically *Saccharina latissima*. While these algae are usually large-sized organisms growing upwards in the sea, we successfully demonstrated the suitability of microfluidic devices to monitor the initial steps of

their embryogenesis within a chip restricting their amplitude of growth to 25 μm in height. This was made possible due to the specimen's early-stage embryogenetic development, which leads to the formation of a monolayered cell sheet of only 15 μm thickness. We showed that, in this confined environment, *Saccharina* realises the main embryogenetic steps in conformity with the observations made in open environments. Furthermore, building on the investigation capabilities enabled by the microfluidic device, we qualitatively analysed the influence of varying illumination conditions, i.e., blue and red light, onto the specimen's embryonic development. Finally, together with the in vivo labelling of the cell surface and on-chip immunolocalisation of cell wall components, this chip enables accurate observations of the specimen's development over time, which provides new possibilities to study the embryogenesis of this organism in more detail and will help boost further knowledge increase for this important class of marine organisms.

4. Materials and Methods

4.1. Production of *Saccharina* Embryos: General Conditions (Genotype, Storage of the Gametophytes)

The *Saccharina latissima* embryos were produced from one isolated female gametophyte and one isolated male gametophyte, which were both derived from the same sporophyte, as described in [24]. In brief, female and male gametophytes were cultivated in PES1X (Provasoli-Enriched Seawater, see [42]) medium at 13 °C under red light, with a light intensity of about 16 $\mu\text{E s}^{-1} \text{m}^{-2}$ (lower than 30 $\mu\text{E s}^{-1} \text{m}^{-2}$ in all cases) with a long photoperiod of 14:10 (L:D). This maintained the gametophytes in a vegetative state. Gametogenesis was induced by transferring the gametophytes to white light with the same conditions of temperature and light intensity as indicated above. Five to ten days later, the gametes were released and fertilisation occurred. PES medium was made with natural sea water pumped at ~30 m under the sea level, filtered at 100–101 μm to remove debris, and autoclaved. Provasoli's solution (see concentration below) was then added to this sea water to make different PES media. A concentration of PES1X (300 μL of PES in 1 L of natural sea water) was used for the culture of the gametophytes, while PES2X (600 μL of PES in 1 L of natural sea water) was used for the culture of the sporophytes (embryos and adults).

4.2. Design and Fabrication of the Microfluidic Device

The microfluidic design consists of a single chamber with a length and width of 7 mm and 5 mm, respectively, with an inlet and an outlet with diameters of 1.2 mm. The inlet is connected to the chamber via a funnel to ensure the uniform distribution of sea water and nutrients and to prevent the trapping of air bubbles. Additionally, to increase chamber stability as well as to simplify the trapping of specimens during the loading procedure, the chamber is filled with a grid of pillars with a diameter of 50 μm and a spacing of 350 μm . To allow the devices to be submerged in sea water inside small glass bottom Petri dishes with diameters of 2 cm (Model No. 801001, Wuxi NEST Biotechnology Co. Ltd., Wuxi, China), the outside dimensions of the polydimethyl-siloxane (Sylgard 184, Dow Corning, Midland, MI, USA) structures are 7 mm by 11.5 mm. The mould used for PDMS replication was fabricated using single-layer photolithography. A silicon wafer was prebaked at 200 °C for 10 min before being cooled down to room temperature and used as a substrate. Photoresist (SU-8 25, MicroChem Corp., Newton, MA, USA) was applied with a maximum speed of 2000 rpm to achieve a thickness of 25 μm and soft baked at 65 °C and 95 °C for 3 min and 15 min, respectively, before being cooled down to room temperature on the hotplate. An exposure dose of 170 mJ/cm^2 was applied to transfer the design pattern (Film Photomask, JD Photodata, Hitchin, UK) into the photoresist. The wafer was post exposure baked for 1 min at 65 °C and 3 min at 95 °C before being developed for 3 min 30 s (SU-8 Developer, MicroChem Corp.) and hard baked for 10 min at 150 °C. PDMS with a ratio of 1:10 was poured onto the mould and cured under vacuum at room temperature overnight before being cut into individual chips and punching the inlet and outlet with a 2 mm diameter sterile biopsy punch. The PDMS chips were then dusted with compressed air and Scotch tape (Model 7100069922, 3M, Saint Paul, MI, USA) before being exposed to oxygen plasma

in a plasma cleaner (Model PDC-32G-2, Harrick Plasma, Ithaca, NY, USA) for 45 s together with the Petri dishes and being brought into contact to seal the chambers chemically. These chips in dishes were then filled and submerged with PES2X and sterilised overnight under UV lights before hosting embryos.

4.3. Chip Inoculation

The chips were inoculated with different types of algal material, which differed in their position in the life cycle. It was (i) a mix of unfertile female and male gametophytes, (ii) a mix of fertile female and male gametophytes, or (iii) a mix of gametophytes with early-stage embryos. However, for most of the lab-on-chip experiments presented in this article, early-stage embryos growing on female gametophytes were used. For all cases, after quickly and gently replacing the culture medium with 1 mL of PES2X, the bottom of a Petri dish containing embryos with fewer than 10 cells was softly scraped with a cell scraper (Model No 83.3950, Sarstedt AG & Co. KG, Nümbrecht, Germany). The embryos were then resuspended in the medium by gently shaking the Petri dish, and then carefully sucked with a 1000 μL pipette with disposable tips large enough to allow for a continuous flow of embryos. The specimens were directly injected in the inlet of the chip (punctured with a biopsy punch of 2 mm diameter) and introduced into the chip by a gentle flow. Slowly emptying the tip into the chip took up to 30 s and a gentle up and down movement—using the flexibility of the PDMS—helped the embryos flow further into the device. This operation was easier when assisted with a stereomicroscope. The inoculated chip was then submerged with PES2X and transferred back to a 13 $^{\circ}\text{C}$ culture chamber with a long day schedule (14:10) of white lighting of around $16 \mu\text{E s}^{-1} \text{m}^{-2}$, along with other embryos.

4.4. Hydrostatic Pressure-Based Liquid Renewal

The volume flow resulting from a constant height difference can be simplified as follows:

$$Q = \Delta P / R_h \quad (1)$$

where R_h is the hydraulic resistance and the pressure difference ΔP can be expressed as $\Delta P = -\rho g \Delta h$ with ρ , g , and Δh being the volumetric mass, the gravitational constant, and the height difference, respectively. Additionally, the hydraulic resistance induced by the microfluidic device and the tubing with an inner diameter of 500 μm and a length of 30 cm can be approximated with $1012 \text{ kg m}^{-4} \text{ s}^{-1}$ and $2.5 \times 1011 \text{ kg m}^{-4} \text{ s}^{-1}$, respectively. Hence, the resulting height difference needed for a sufficiently slow liquid exchange, e.g., suitable to renew the internal chip volume about once a day, is located in the μm scale.

4.5. Pump-Based Liquid Renewal

A modular pressure controller (Flow EZ, Fluigent, Le Kremlin-Bicêtre, France) was used to allow for continuous medium renewal inside the microfluidic devices. Given the extended duration of the culture and to reduce the risk of contaminations, the pump was connected to the chip via platinum-cured silicone tubing with an internal diameter of 0.5 mm (Model No SHE-TUB-SIL-0.5*0.8, Darwin Microfluidics, Paris, France). The liquid renewal rate was estimated based on the excess media in the dish.

4.6. Setting Up the Protocol for Time-Lapse Monitoring

The acquisition of images and time-lapse monitoring was performed using an inverted epifluorescence microscope (microscope: Leica DMI6000B, objective: Leica Microsystems HC PL APO 40x/0.85 CORR, camera: Leica DFC450C, software: LAS X 3.7) and an inverted confocal microscope (TCS SP5 AOBS, Leica Microsystems, camera: Leica DFC450C). The observations were made in the same lighting and temperature conditions as in the regular culture room. For this purpose, the microscope was placed in a room cooled to 17 $^{\circ}\text{C}$ and framed by a carbonate-glass chamber fitted to a thermostatically controlled air flow system (Model: CUBE & BOX, Life Imaging Services GmbH) to further cool the sample down to

13 °C. Two LED lamps were placed inside the chamber to provide adapted lighting (see Section 4.3 for detailed conditions).

4.7. Growth Rate Measurements

The growth was calculated by measuring the length and the width of the embryo, respectively the distance between the apex and the base of the embryo, and largest width, every 24 h in embryos growing (i) within the chips with flow, (ii) within the chip without flow, and (iii) in the Petri dish outside the chip. All conditions were applied in a single Petri dish, and 15 marked specimens for each condition were monitored for 7 days by time-lapse microscopy as described in 4.6. For long-term measurements outside the microfluidic device, only embryos growing horizontally were selected. Measurements were performed using the Fiji distribution of ImageJ2 [43], from which the total length (L), the length/width ratio, and the growth rate $(L_{n+1} - L_n)/(t_{n+1} - t_n)$ were plotted as a function of time (t).

4.8. Duration of Embryos Viability in Microfluidic Devices

We assessed how long the embryos could stay alive in the microfluidic device by using four inoculated microfluidic devices loaded with 5 to 10 specimens each. These devices were placed in a 13 °C culture chamber with long day illumination (14:10). After opening the Petri dishes in a laminar flow hood, the devices were flushed manually every day with approx. 101–102 µL of PES2X using a 1 mL pipette. Embryo viability was evaluated for up to 12 days and viability was monitored through growth (or stagnation) as well as the colour of the embryos' pigments.

4.9. Cultures and Assessment of the Impact of Culture Density

To assess the effect of the density of female gametophytes in the formation of eggs, a stock of female and male gametophytes was crushed into ~5- to 10-cell gametophyte filaments, mounted and optically inspected to ensure the required filament length, and 10, 25, 50, 75, and 100 µL of this mixture diluted in 2 mL PES1X (roughly 0.6 µL of PES per dish) were transferred to Petri dishes. After 2 weeks, the emerging eggs were imaged using an inverted microscope (Leica DMI-8). Each condition was observed in three Petri dishes and from two independent stock cultures. Counting was conducted from two snapshots taken on two different positions in the dishes. The number of eggs released was counted relative to the sum of dead + alive gametophytes as organisms and as their total cell number. The concentration of gametophytes per µL was derived as 252 (124 female GP and 128 male GP) using Malassez counting.

4.10. Assessment of the Embryonic Developmental Stages

The algal material was loaded in the chips and observed as described in Sections 4.3 and 4.6. No flow was applied to the system for the duration of the observation. Time-lapse monitoring for 5 days allowed the observation of different transitions of the life cycle, especially those involved in the formation and development of *Saccharina* embryos.

4.11. Impact of Blue and Red Lights in Embryogenesis

Three-week-old embryos of *Saccharina* were inoculated in the chip with PES2X and cultivated for 5 days under red ($9.2 \mu\text{E}\cdot\text{m}^{-2}\cdot\text{s}^{-1}$) or blue ($5.1 \mu\text{E}\cdot\text{m}^{-2}\cdot\text{s}^{-1}$) light with a 16:8 (L:D) photoperiod. The light spectra are shown in Supplementary Figure S4. Brightfield and autofluorescent embryos were observed in confocal microscopy (Argon laser, SP5, Leica Microsystems, Wetzlar, Germany). The autofluorescence of the chlorophyll was observed through a PMT with a 675–745 nm passing band.

4.12. Staining the Embryos with Calcofluor

Cellulose was stained by filling the microfluidic device with 20 µM calcofluor white solution (fluorescent brightener 28, F-3543, Sigma-Aldrich, St. Louis, MI, USA) diluted in PES2X. The incubation lasted 45 min at 13 °C (RT) in the dark. The solution was injected

into the inlet of the device by pipetting. Observation was performed under UV light (excitation wavelength: 380 nm, emission wavelength: 475 nm) using epifluorescence (DMI8, Leica Microsystems) and confocal microscopy (405 nm emission laser, PMT band of 450–500 nm; SP5, Leica Microsystems) after flushing the channels with fresh PES2X at least twice and after incubation for at least 15 min at 13 °C between each rinsing step. No major bleaching effects, induced by the white light illumination needed for the cultivation of the specimen, were observed.

4.13. Marking the Embryo Surface with Fluorescent Beads

The embryos were marked with amine-coated 0.2 µm red-fluorescent microspheres (FluoSpheres™ ref. F8763, Invitrogen™, 580/605, Waltham, MA, USA). The concentration of the microspheres was found to be an important parameter for successful labelling, as the beads should uniformly label the specimens while still being distinguishable. Working solutions were prepared by diluting the beads to 0.05% in 500 µL of PES2X (*w/v*) in a 1.5 mL Eppendorf tube. Before dilution, the beads were scattered by 1 min of fast vortexing and 1 min of sonication (50 Hz, amplitude 40 Pa) with a probe cleaned with 70% ethanol. These working solutions were used to mark the surface of embryos grown in Petri dishes with diameters of 20–35 mm, as described below. Under a sterile laminar hood, the working solution was poured onto the embryo cultures previously emptied of sea water. In order to help the beads to attach to the embryos, the Petri dishes were carefully shaken in a circular motion for 1 min. The solution was then discarded and 1 mL of PES2X was added to wash off excessive beads during 1 min of circular motion. After five similar washing cycles, the dish was refilled with culture medium. These marked embryos were directly transferred into a chip for observation. Alternatively, they were placed back to the culture room.

Carboxylate-coated 0.5 µm green-fluorescent microspheres (FluoSpheres™ ref. F8813, Invitrogen™) were also tested, but they were only faintly attached to gametophytes and embryos.

4.14. On-Chip Immunolocalisation

The protocol was adapted from Charrier et al. [23]. The algal material in the chip was fixed for 2 1/2 hours with 2% PFA prepared in H2O. PFA was added as gently as possible to avoid too high pressures and distortions of the embryos inside the chip. Similarly, all mechanical pressures, e.g., applied manually directly onto chip, were avoided. All solutions were passed through the chip at least three times to ensure complete and homogeneous flooding of the chip volume. Primary and secondary antibodies were incubated for at least 2 h at 4 °C in the dark. The secondary antibody was coupled to Alexa488 and the signal was observed either in epifluorescence microscopy (DMI8, Leica Microsystems) with an FITC filter or with a SP5 confocal microscope (Leica Microsystems) with an Argon laser at 488 nm for excitation and through PMT with a band of 500–530 nm for emission.

4.15. Statistical Evaluation

Statistical evaluations were performed in Prism 6 (GraphPad). The culture concentrations (Figure 1c) were analysed using a one-way ANOVA in combination with Tukey's multiple comparisons test to detect differences between individual culturing conditions. Blade growth (Figure 3d), growth rate (Supplementary Figure S3a), and blade length–width ratios (Supplementary Figure S3b) were analysed using two-way ANOVAs, while Tukey's multiple comparisons tests were applied to detect significant differences between the experimental conditions within days as well as between consecutive growth days within individual experimental conditions. Asterisks indicate the results (adjusted *p*-values) of the corresponding tests: * < 0.05, ** < 0.01, *** < 0.001, and **** < 0.0001.

Supplementary Materials: The following supporting information can be downloaded at: <https://www.mdpi.com/article/10.3390/bioengineering9110718/s1>, Supplementary Information I1 containing Figure S1: Effect of sample density on growth behaviour, Figure S2: Microscopy setup with controlled environmental conditions, Figure S3: Comparison of daily growth rates and blade shapes between on-chip cultures with and without liquid renewal and open space, Figure S4: Blue and red

light spectra for physiological investigation, Figure S5: Time-lapse growth tracking using microspheres, Caption for Movie M1, Caption for Movie M2; Supplementary Movie M1: Transition from oogonium to egg; Supplementary Movie M2: Growth of mature embryos; Supplementary Data D1: Data used for the production of the presented graphs.

Author Contributions: Conceptualization, B.C. and N.F.L.; methodology, S.B., R.A., B.C. and N.F.L.; validation, T.C., S.B. and B.C.; formal analysis, T.C., S.B. and N.F.L.; investigation, T.C., S.B. and B.C.; resources, R.A., G.S.K.S., B.C. and N.F.L.; data curation, T.C., S.B. and N.F.L.; writing—original draft preparation, T.C., B.C. and N.F.L.; writing—review and editing, B.C. and N.F.L.; visualization, T.C., S.B., B.C. and N.F.L.; supervision, G.S.K.S., B.C. and N.F.L.; project administration, B.C. and N.F.L.; funding acquisition, R.A., G.S.K.S., B.C. and N.F.L. All authors have read and agreed to the published version of the manuscript.

Funding: This work was supported by the CNRS, Sorbonne Université, the University of Cambridge, and, in part, by a grant from the Infinitus (China) Company Ltd (Contract Number RG82367) to G.S.K.S., by a career grant from the Swiss National Science Foundation (Grant Number P2EZP2_199843) to N.F.L., a project grant from the ARED Région Bretagne (Grant Number COH20020) to S.B., a CNRS grant (MITI “Lame Brune”) to B.C., and a project grant from the Gordon and Betty Moore Foundation (Symbiochip, Grant Number GBMF9333) to R.A. The authors acknowledge open access funding by the Swiss National Science Foundation.

Institutional Review Board Statement: Not applicable.

Informed Consent Statement: Not applicable.

Data Availability Statement: The data presented in this study are available in the article and the Supplementary Materials.

Acknowledgments: The authors thank Roman Milstein for providing an image of embryos labelled with BAM10 outside the chip as well as Fabrice Not for his support with the microfluidic equipment.

Conflicts of Interest: The authors declare no conflict of interest.

References

- Babcock, R.C.; Bustamante, R.H.; Fulton, E.A.; Fulton, D.J.; Haywood, M.D.E.; Hobday, A.J.; Kenyon, R.; Matear, R.J.; Plagányi, E.E.; Richardson, A.J.; et al. Severe Continental-Scale Impacts of Climate Change Are Happening Now: Extreme Climate Events Impact Marine Habitat Forming Communities Along 45% of Australia’s Coast. *Front. Mar. Sci.* **2019**, *6*, 411. [[CrossRef](#)]
- Lotze, H.K.; Tittensor, D.P.; Bryndum-Buchholz, A.; Eddy, T.D.; Cheung, W.W.L.; Galbraith, E.D.; Barange, M.; Barrier, N.; Bianchi, D.; Blanchard, J.L.; et al. Global Ensemble Projections Reveal Trophic Amplification of Ocean Biomass Declines with Climate Change. *Proc. Natl. Acad. Sci. USA* **2019**, *116*, 12907–12912. [[CrossRef](#)] [[PubMed](#)]
- Miller, D.D.; Ota, Y.; Sumaila, U.R.; Cisneros-Montemayor, A.M.; Cheung, W.W.L. Adaptation Strategies to Climate Change in Marine Systems. *Glob. Chang. Biol.* **2018**, *24*, e1–e14. [[CrossRef](#)] [[PubMed](#)]
- Henson, S.A.; Cael, B.B.; Allen, S.R.; Dutkiewicz, S. Future Phytoplankton Diversity in a Changing Climate. *Nat. Commun.* **2021**, *12*, 5372. [[CrossRef](#)]
- Pessarrodona, A.; Assis, J.; Filbee-Dexter, K.; Burrows, M.T.; Gattuso, J.-P.; Duarte, C.M.; Krause-Jensen, D.; Moore, P.J.; Smale, D.A.; Wernberg, T. Global Seaweed Productivity. *Sci. Adv.* **2022**, *8*, eabn2465. [[CrossRef](#)]
- Barbier, M.; Charrier, B.; Araujo, R.; Holdt, S.L.; Jacquemin, B.; Rebours, C. *Pegasus-Phycomorph European Guidelines for a Sustainable Aquaculture of Seaweeds*; COST Action: Brussels, Belgium, 2019.
- Charrier, B.; Abreu, M.H.; Araujo, R.; Bruhn, A.; Coates, J.C.; de Clerck, O.; Katsaros, C.; Robaina, R.R.; Wichard, T. Furthering Knowledge of Seaweed Growth and Development to Facilitate Sustainable Aquaculture. *New Phytol.* **2017**, *216*, 967–975. [[CrossRef](#)]
- Fritsch, F.E. *The Structure and Reproduction of the Algae*; Cambridge University Press: Cambridge, UK, 1945.
- Theodorou, I.; Charrier, B. Brown Algae. In *Handbook of Marine Model Organisms in Experimental Biology*; CRC Press: Boca Raton, FL, USA, 2021; pp. 27–47.
- Lloyd, C.W. How Does the Cytoskeleton Read the Laws of Geometry in Aligning the Division Plane of Plant Cells? *Development* **1991**, *113*, 55–65. [[CrossRef](#)]
- Flanders, D.J.; Rawlins, D.J.; Shaw, P.J.; Lloyd, C.W. Nucleus-Associated Microtubules Help Determine the Division Plane of Plant Epidermal Cells: Avoidance of Four-Way Junctions and the Role of Cell Geometry. *J. Cell Biol.* **1990**, *110*, 1111–1122. [[CrossRef](#)]
- Bardet, P.-L.; Guirao, B.; Paoletti, C.; Serman, F.; Léopold, V.; Bosveld, F.; Goya, Y.; Mirouse, V.; Graner, F.; Bellaïche, Y. PTEN Controls Junction Lengthening and Stability during Cell Rearrangement in Epithelial Tissue. *Dev. Cell* **2013**, *25*, 534–546. [[CrossRef](#)]

13. Ebbing, A.; Pierik, R.; Bouma, T.; Kromkamp, J.C.; Timmermans, K. How Light and Biomass Density Influence the Reproduction of Delayed *Saccharina latissima* Gametophytes (Phaeophyceae). *J. Phycol.* **2020**, *56*, 709–718. [[CrossRef](#)]
14. Täuber, S.; Schmitz, J.; Blöbaum, L.; Fante, N.; Steinhoff, H.; Grünberger, A. How to Perform a Microfluidic Cultivation Experiment—A Guideline to Success. *Biosensors* **2021**, *11*, 485. [[CrossRef](#)] [[PubMed](#)]
15. Sanati Nezhad, A.; Naghavi, M.; Packirisamy, M.; Bhat, R.; Geitmann, A. Quantification of Cellular Penetrative Forces Using Lab-on-a-Chip Technology and Finite Element Modeling. *Proc. Natl. Acad. Sci. USA* **2013**, *110*, 8093–8098. [[CrossRef](#)] [[PubMed](#)]
16. Shamsudhin, N.; Laebli, N.; Atakan, H.B.; Vogler, H.; Hu, C.; Haeberle, W.; Sebastian, A.; Grossniklaus, U.; Nelson, B.J. Massively Parallelized Pollen Tube Guidance and Mechanical Measurements on a Lab-Ona-Chip Platform. *PLoS ONE* **2016**, *11*, e0168138. [[CrossRef](#)] [[PubMed](#)]
17. Burri, J.T.; Vogler, H.; Läubli, N.F.; Hu, C.; Grossniklaus, U.; Nelson, B.J. Feeling the Force: How Pollen Tubes Deal with Obstacles. *New Phytol.* **2018**, *220*, 187–195. [[CrossRef](#)]
18. Gladkov, A.; Pigareva, Y.; Kutyna, D.; Kolpakov, V.; Bukatin, A.; Mukhina, I.; Kazantsev, V.; Pimashkin, A. Design of Cultured Neuron Networks in Vitro with Predefined Connectivity Using Asymmetric Microfluidic Channels. *Sci. Rep.* **2017**, *7*, 15625. [[CrossRef](#)]
19. Gupta, P.; Shinde, A.; Illath, K.; Kar, S.; Nagai, M.; Tseng, F.-G.; Santra, T.S. Microfluidic Platforms for Single Neuron Analysis. *Mater. Today Bio.* **2022**, *13*, 100222. [[CrossRef](#)]
20. Läubli, N.F.; Gerlt, M.S.; Wüthrich, A.; Lewis, R.T.M.; Shamsudhin, N.; Kutay, U.; Ahmed, D.; Dual, J.; Nelson, B.J. Embedded Microbubbles for Acoustic Manipulation of Single Cells and Microfluidic Applications. *Anal. Chem.* **2021**, *93*, 9760–9770. [[CrossRef](#)]
21. Deleglise, B.; Lassus, B.; Soubeyre, V.; Alleaume-Butaux, A.; Hjorth, J.J.; Vignes, M.; Schneider, B.; Brugg, B.; Viovy, J.-L.; Peyrin, J.-M. Synapto-Protective Drugs Evaluation in Reconstructed Neuronal Network. *PLoS ONE* **2013**, *8*, e71103. [[CrossRef](#)]
22. Läubli, N.F.; Burri, J.T.; Marquard, J.; Vogler, H.; Mosca, G.; Vertti-Quintero, N.; Shamsudhin, N.; DeMello, A.; Grossniklaus, U.; Ahmed, D.; et al. 3D Mechanical Characterization of Single Cells and Small Organisms Using Acoustic Manipulation and Force Microscopy. *Nat. Commun.* **2021**, *12*, 2583. [[CrossRef](#)]
23. Charrier, B.; Boscq, S.; Nelson, B.J.; Läubli, N.F. Growth and Labelling of Cell Wall Components of the Brown Alga *Ectocarpus* in Microfluidic Chips. *Front. Mar. Sci.* **2021**, *8*. [[CrossRef](#)]
24. Theodorou, I.; Opsahl-Sorteberg, H.-G.; Charrier, B. Preparation of Zygotes and Embryos of the Kelp *Saccharina latissima* for Cell Biology Approaches. *Bio. Protoc.* **2021**, *11*. [[CrossRef](#)]
25. Klochkova, T.A.; Motomura, T.; Nagasato, C.; Klimova, A.V.; Kim, G.H. The Role of Egg Flagella in the Settlement and Development of Zygotes in Two *Saccharina* Species. *Phycologia* **2019**, *58*, 145–153. [[CrossRef](#)]
26. Wu, M.-H.; Paul, K.E.; Whitesides, G.M. Patterning Flood Illumination with Microlens Arrays. *Appl. Opt.* **2002**, *41*, 2575. [[CrossRef](#)] [[PubMed](#)]
27. Davidson, F.F. The Effects of Auxins on the Growth of Marine Algae. *Am. J. Bot.* **1950**, *37*, 502. [[CrossRef](#)]
28. Sun, H.; Basu, S.; Brady, S.R.; Luciano, R.L.; Muday, G.K. Interactions between Auxin Transport and the Actin Cytoskeleton in Developmental Polarity of *Fucus distichus* Embryos in Response to Light and Gravity. *Plant. Physiol.* **2004**, *135*, 266–278. [[CrossRef](#)]
29. Lüning, K.; Dring, M.J. Reproduction Induced by Blue Light in Female Gametophytes of *Laminaria saccharina*. *Planta* **1972**, *104*, 252–256. [[CrossRef](#)]
30. Lüning, K.; Dring, M.J. Reproduction, Growth and Photosynthesis of Gametophytes of *Laminaria saccharina* Grown in Blue and Red Light. *Mar. Biol.* **1975**, *29*, 195–200. [[CrossRef](#)]
31. Wang, W.-J.; Sun, X.-T.; Wang, G.-C.; Xu, P.; Wang, X.-Y.; Lin, Z.-L.; Wang, F.-J. Effect of Blue Light on Indoor Seedling Culture of *Saccharina japonica* (Phaeophyta). *J. Appl. Phycol.* **2010**, *22*, 737–744. [[CrossRef](#)]
32. Deng, Y.; Yao, J.; Fu, G.; Guo, H.; Duan, D. Isolation, Expression, and Characterization of Blue Light Receptor AUREOCHROME Gene From *Saccharina japonica* (Laminariales, Phaeophyceae). *Mar. Biotechnol.* **2014**, *16*, 135–143. [[CrossRef](#)]
33. Jiang, P.; Qin, S.; Tseng, C.K. Expression of the LacZ Reporter Gene in Sporophytes of the Seaweed *Laminaria japonica* (Phaeophyceae) by Gametophyte-Targeted Transformation. *Plant Cell Rep.* **2003**, *21*, 1211–1216. [[CrossRef](#)]
34. Badis, Y.; Scornet, D.; Harada, M.; Caillard, C.; Godfroy, O.; Raphalen, M.; Gachon, C.M.M.; Coelho, S.M.; Motomura, T.; Nagasato, C.; et al. Targeted CRISPR-Cas9-based Gene Knockouts in the Model Brown Alga *Ectocarpus*. *New Phytol.* **2021**, *231*, 2077–2091. [[CrossRef](#)] [[PubMed](#)]
35. le Bail, A.; Billoud, B.; Maisonneuve, C.; Peters, A.F.; Mark Cock, J.; Charrier, B. Early Development Pattern of the Brown Alga *Ectocarpus siliculosus* (Ectocarpales, Phaeophyceae) Sporophyte 1. *J. Phycol.* **2008**, *44*, 1269–1281. [[CrossRef](#)] [[PubMed](#)]
36. Rabillé, H.; Billoud, B.; Rolland, E.; Charrier, B. Dynamic and Microscale Mapping of Cell Growth. In *Protocols for Macroalgae Research*; CRC Press: Boca Raton, FL, USA; Taylor & Francis: Oxfordshire, UK, 2018; pp. 349–364.
37. Charrier, B.; Rabillé, H.; Billoud, B. Gazing at Cell Wall Expansion under a Golden Light. *Trends Plant Sci.* **2019**, *24*, 130–141. [[CrossRef](#)] [[PubMed](#)]
38. Bidhendi, A.J.; Chebli, Y.; Geitmann, A. Fluorescence Visualization of Cellulose and Pectin in the Primary Plant Cell Wall. *J. Microsc.* **2020**, *278*, 164–181. [[CrossRef](#)]
39. Shaw, S.L.; Dumais, J.; Long, S.R. Cell Surface Expansion in Polarly Growing Root Hairs of *Medicago truncatula*. *Plant Physiol.* **2000**, *124*, 959–970. [[CrossRef](#)] [[PubMed](#)]

40. Rabillé, H.; Billoud, B.; Tesson, B.; le Panse, S.; Rolland, É.; Charrier, B. The Brown Algal Mode of Tip Growth: Keeping Stress under Control. *PLoS Biol.* **2019**, *17*, e2005258. [[CrossRef](#)] [[PubMed](#)]
41. Rabillé, H.; Torode, T.A.; Tesson, B.; le Bail, A.; Billoud, B.; Rolland, E.; le Panse, S.; Jam, M.; Charrier, B. Alginates along the Filament of the Brown Alga *Ectocarpus* Help Cells Cope with Stress. *Sci. Rep.* **2019**, *9*, 12956. [[CrossRef](#)]
42. le Bail, A.; Charrier, B. Culture Methods and Mutant Generation in the Filamentous Brown Algae *Ectocarpus Siliculosus*. *Methods Mol. Biol.* **2013**, *959*, 323–332.
43. Schindelin, J.; Arganda-Carreras, I.; Frise, E.; Kaynig, V.; Longair, M.; Pietzsch, T.; Preibisch, S.; Rueden, C.; Saalfeld, S.; Schmid, B.; et al. Fiji: An Open-Source Platform for Biological-Image Analysis. *Nat. Methods* **2012**, *9*, 676–682. [[CrossRef](#)]

Supplementary Information:

Cultivation and imaging of *S. latissima* embryo monolayered cell sheets inside microfluidic devices

Thomas Clerc, Samuel Boscq, Rafaele Attia, Gabriele S. Kaminski Schierle, Bénédicte Charrier, and Nino F. Lübli

Content:

Supplementary Figures:

Figure S1: Effect of sample density on egg release and growth behaviour

Figure S2: Microscopy setup with controlled environmental conditions

Figure S3: Comparison of daily growth rates and blade shapes between on-chip cultures with and without liquid renewal and open space

Figure S4: Blue and red light spectra for physiological investigation

Figure S4: Time-lapse growth tracking using microspheres

Captions for Supplementary Movies:

Movie M1: Transition from oogonium to egg

Movie M2: Growth of mature embryos

Supplementary Data:

Data D1: Data used for the production of the presented graphs (see separate file)

Supplementary Figures

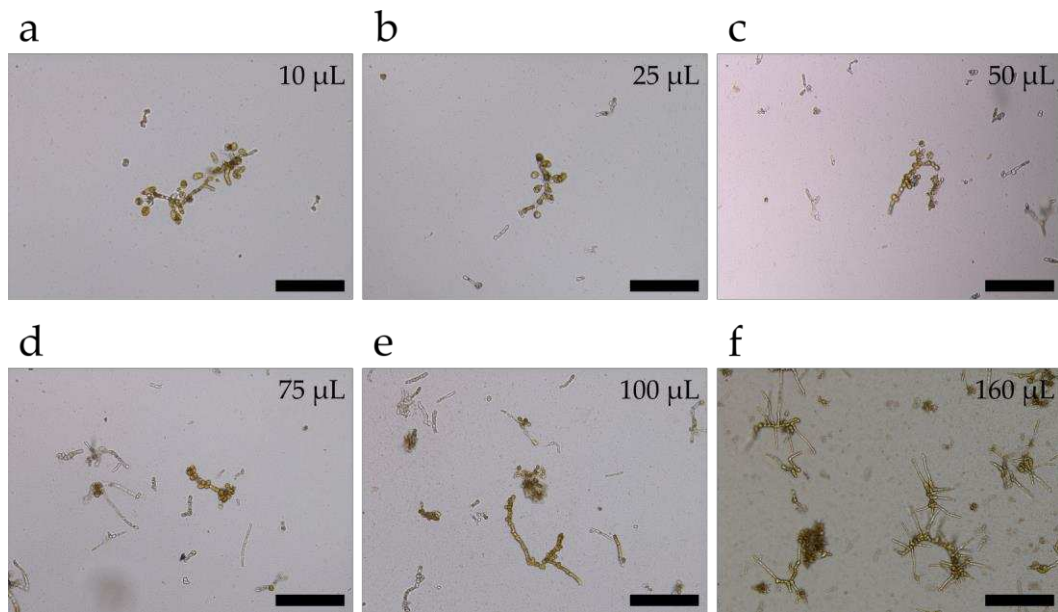


Figure S1. Different concentrations of *Saccharina latissima* gametophytes left to induce gamete release and embryo growth. From the initial crushed gametophyte stock culture, (a) 10, (b) 25, (c) 50, (d) 75, or (e) 100 µL were taken and diluted with 2 mL of natural sea water inside Petri dishes. Egg release was drastically reduced at higher density of gametophytes even though the stage of the gametophyte should still allow oogenesis. (f) If left to grow in unfavourable conditions, the cells (that normally differentiate into an egg-producing oogonium) form more gametophyte cells instead of eggs. Specimens were cultured under white light for (a) – (e) 2 weeks or (f) 3.5 weeks. Scale bars: 250 µm.

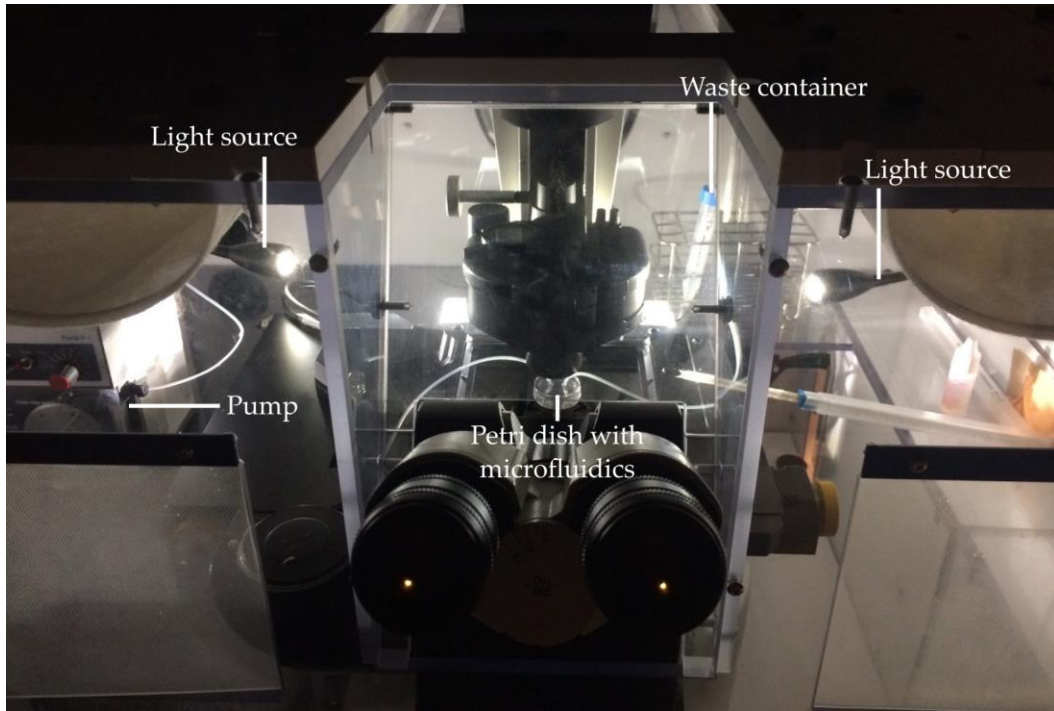


Figure S2. Microscopy setup with controlled environmental conditions. The setup consists of an inverted microscope incubation chamber. Light intensity equal to standard culturing conditions is provided *via* two lateral LEDs. The glass-bottom Petri dish containing either the samples directly or the microfluidic device with the specimens is highlighted at the centre of the image. For experiments requiring automatic liquid renewal, the microfluidic device was connected to a pump (left side) while the liquid waste was collected on the right side through tubing connected to the device's outlet.

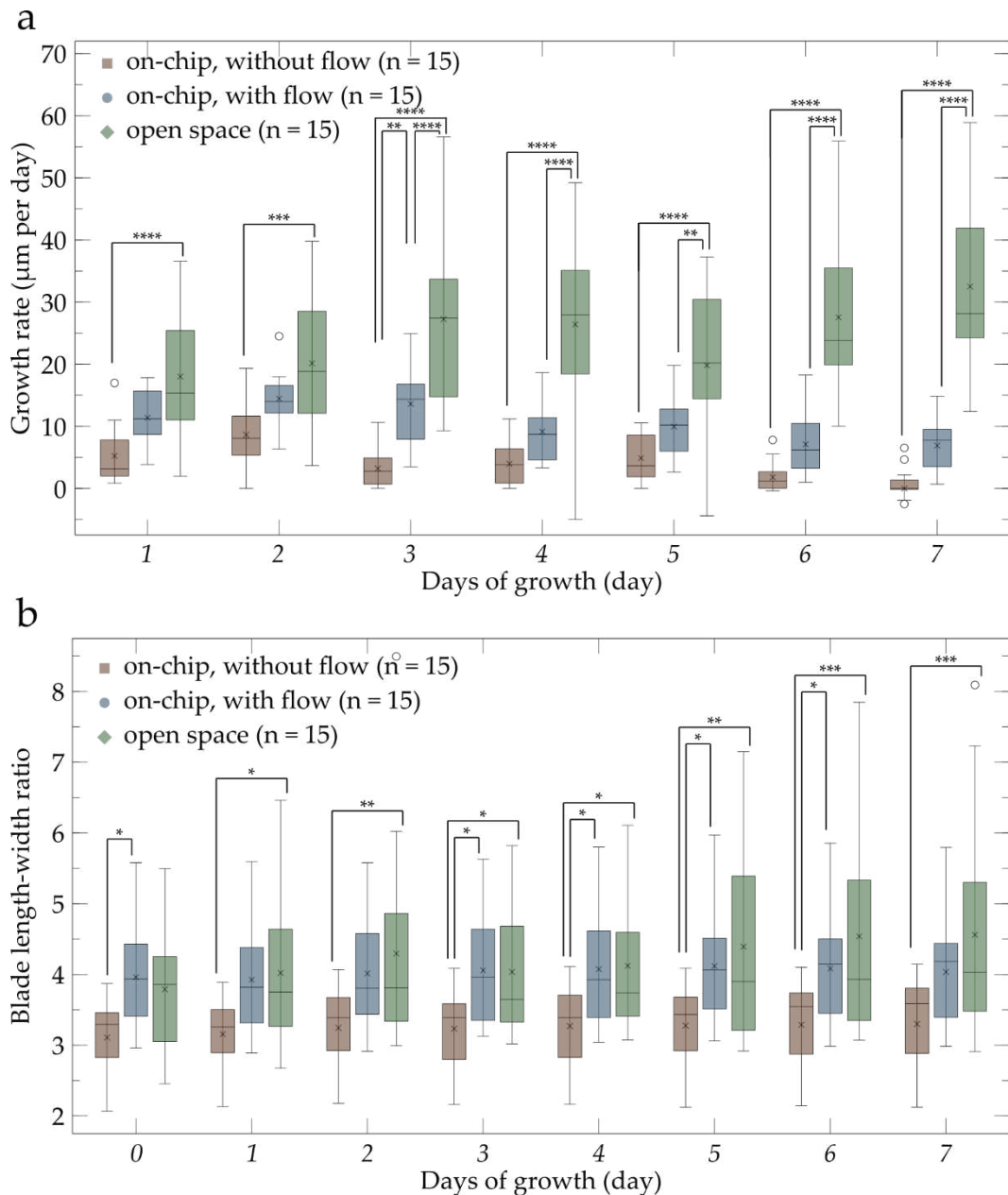


Figure S3. Comparison of daily growth rates and blade shapes between on-chip cultures with and without liquid renewal and open space. (a) Growth rates of specimens cultured in open space, *i.e.*, in glass bottom Petri dishes, are on most days significantly higher than for specimens growing inside microfluidic devices with and without liquid renewal. (b) Specimens growing inside the device with liquid renewal show similar blade shapes with regard to their length-width ratio as samples growing outside the device, while specimens inside the chips without liquid renewal are less elongated. Asterisks indicate statistically significant differences in growth rate and blade length-width ratio between the culturing conditions on specific days as analysed using with two-way ANOVAs (see Materials and Methods).

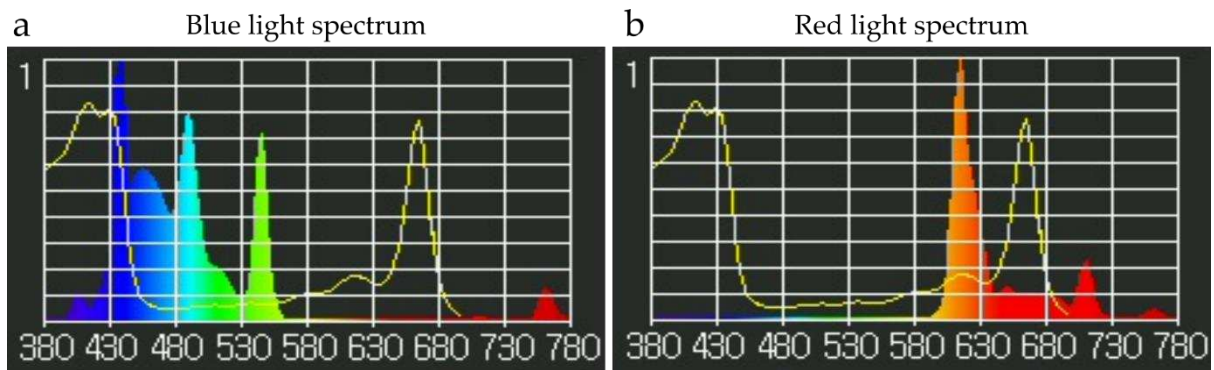


Figure S4. Blue and red light spectra for physiological investigation.

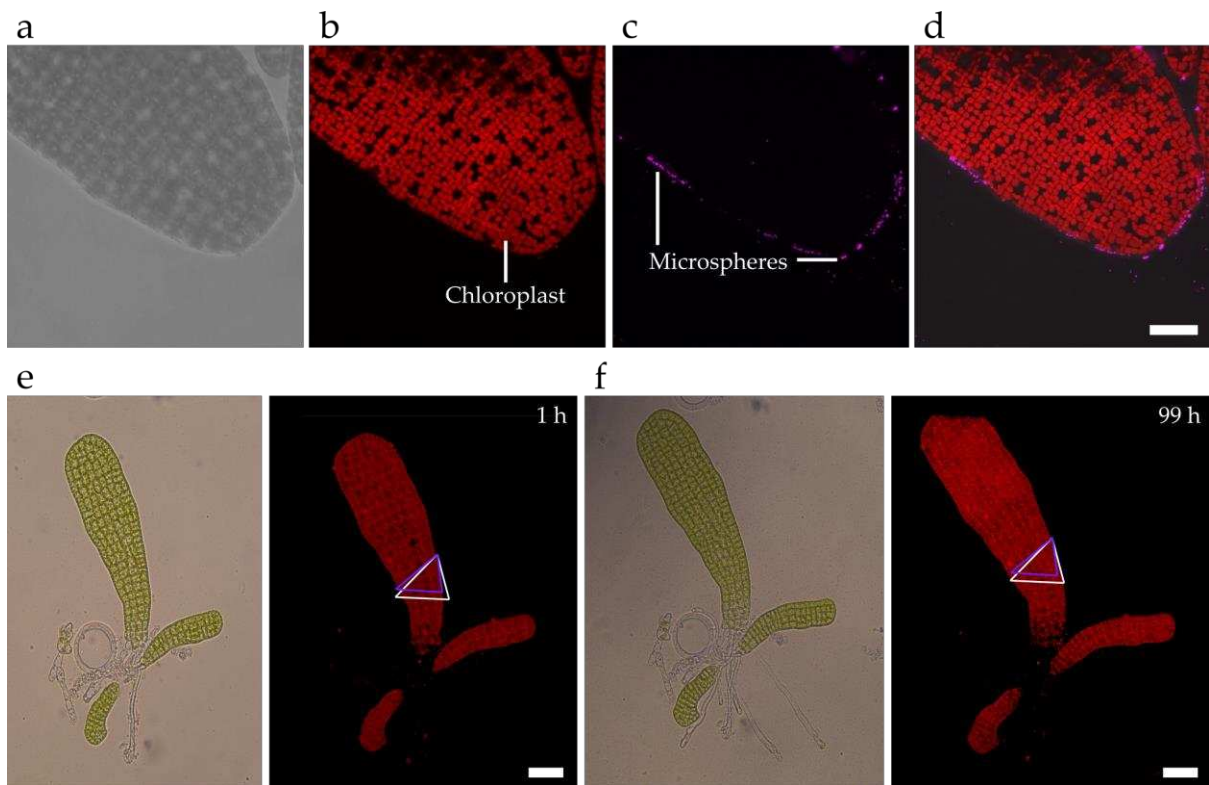


Figure S5. Confocal microscopy image of a monolayered lamina labelled with fluorescent beads for live tracking. (a) Brightfield image of the monolayered lamina. (b) Autofluorescence of the chloroplasts. (c) 200 nm red fluorescent microspheres attached to the lamina. Only the beads stuck at the outline of the lamina were imaged, thereby making sure that they are in the same focal plane. (d) Merged microscopy image of the fluorescence channels showing the chloroplasts (red) and the functionalised microspheres (purple). (e, f) Brightfield and fluorescence images of a monolayered lamina labelled with fluorescent microspheres growing over ~ 4 days. The triangle joins 3 red beads at 1 h (blue) and 99 h (white). The larger white triangle illustrates the higher distance between the beads and, therefore, growth of the embryo in this area. Scale bars: (a-d) = 25 μm ; (e, f) = 50 μm .

Supplementary Movie Captions:

Movie characteristics: Movie duration: 20 sec, with 5 image acquisitions per sec (total 100 images). Each image acquisition corresponds to one hour of time-lapse microscopy (one image every hour). Total duration in real-time is approximately 4 days.

Movie S1. Time-lapse movie showing a growing monolayered sheet of a *Saccharina* embryo and a maturing gametophyte. Note the hatching of 3 eggs over time, each in less than one hour.

Movie S2. Time-lapse movie showing a growing monolayered sheet of a *Saccharina* embryo differentiating rhizoids. Note one of the rhizoids pushing the small embryo lamina in the bottom left side of the movie, thereby showing that all the algal material grows in a single plane.

Annexe 4: List of publications.

Charrier, B., **Boscq, S.**, Nelson, B. J. and Läubli, N. F. (2021). Growth and Labelling of Cell Wall Components of the Brown Alga *Ectocarpus* in Microfluidic Chips. *Frontiers in Marine Science* 8: 745654. Doi: 10.3389/fmars.2021.745654.

Boscq, S., Dutertre, S., Theodorou, I., Charrier, B. Targeted Laser Ablation in the Embryo of *Saccharina latissima*. *JoVE* 181: e63518. Doi: 10.3791/63518.

Clerc, T., **Boscq, S.**, Attia, R., Kaminski Schierle, G.S., Charrier, B., and Läubli, N.F. (2022). Cultivation and Imaging of *S. latissima* Embryo Monolayered Cell Sheets Inside Microfluidic Devices. *Bioengineering* 9.11: 718. Doi: 10.3390/bioengineering9110718.

Annexe 5: List of oral communications and poster in congress and workshops.

Oral presentations

- 2023 **Boscq S.**, Billoud B., Theodorou I., Joemmanbacks T., Charrier B., Quantitative study of the role of the maternal tissue in body shape and tissue patterning in the early embryo of the brown alga *Saccharina latissima*. *IRN France-Japan Frontiers in plant biology (FJFPB) Symposium*. Kyoto, JAPAN.
- 2023 **Boscq S.**, Billoud B., Joemmanbacks T., Theodorou I., Charrier B., Role of the maternal tissue in the establishment of polarity axes in the early embryo of the brown alga *Saccharina latissima*. *8th European Phycological congress*. Brest, FRANCE.
- 2023 **Boscq S.**, Billoud B., Joemmanbacks T., Theodorou I., Charrier B., Role of the maternal tissue in the establishment of polarity axes in the early embryo of the brown alga *Saccharina latissima*. *Journées du réseau André Picard*. Paris, FRANCE.
- 2022 **Boscq S.**, Näubli N., Dutertre S., Charrier B., First steps toward the development of cytology tools in brown algae: microfluidics and laser ablation. *Bio-Imaging GDR*. Sophia Antipolis, FRANCE.
- 2022 **Boscq S.**, Billoud B., Dutertre S., Lèpanse S., Milstein R., Näubli N, Charrier B., Role of the maternal tissue in the establishment of polarity axes in the early embryo of the brown alga *Saccharina latissima*. *Euro Evo Devo 2022*. Naples, ITALY.
- 2022 **Boscq S.**, Billoud B., Dutertre S., Lèpanse S., Milstein R., Näubli N, Charrier B., Role of the maternal tissue in the establishment of polarity axes in the early embryo of the brown alga *Saccharina latissima*. *Journées Boris Ephrussi*. Paris, FRANCE.
- 2021 Charrier B., Theodorou I., Billoud B., **Boscq S.**, Opsahl-Sorteberg H-G., Embryo patterning in the brown alga *Saccharina*. *Laboratory Plant Reproduction & Development* (webinar ENS-Lyon).
- 2021 Theodorou I., Billoud B., **Boscq S.**, Le Panse S., Opsahl Sorteberg H-G., Charrier B., Grid patterning on the embryonic lamina of the brown alga *Saccharina latissima*. *Journées Réseau André Picard* (webinar).

2021 **Boscq S.**, Theodorou I., Billoud B., Le Panse S., Dutertre S., Charrier B., Establishment of the Apico-Basal axis in the early embryo of the brown alga *Saccharina latissima*. *Journées Réseau André Picard* (webinar).

Posters

2022 Theodorou I., Billoud B., **Boscq S.**, Opsahl-Sorteberg H-G., Charrier B., Key cell and tissue features during embryogenesis in brown alga *Saccharina latissima*. *29th Scandinavian Plant Physiology Society Conference*. Longyearbyen, Svalbard, NORWAY.

2022 Theodorou I., Milstein R., **Boscq S.**, Charrier B., Cell structure during grid morphogenesis in the brown alga species *Saccharina latissima*. 2nd International Symposium on quantitative Plant Morphodynamics Plant Growth & Form. Heidelberg, GERMANY.

2022 Billoud B., Theodorou I., **Boscq S.**, Sellin G., Godin C., Charrier B., Modelling the force-driven early morphogenesis in the brown alga *Saccharina latissima*. *Journées du réseau André Picard*. Villefrance-sur-Mer, FRANCE.

2021 **Boscq S.**, Billoud B., Gonneau Y., Dutertre S., Charrier B., Establishment of growth and polarity axes in the early embryo of the brown algae *Saccharina latissima*. *FASEB* (webinar).

2021 **Boscq S.**, Theodorou I., Billoud B., Le Panse S., Dutertre S., Charrier B., Mechanisms controlling the establishment of the apico-basal axis in the brown alga *Saccharina latissima*. *Shaping Life 2* (webinar).